Effects of cerebral small vessel disease in the brain beyond the visible lesions

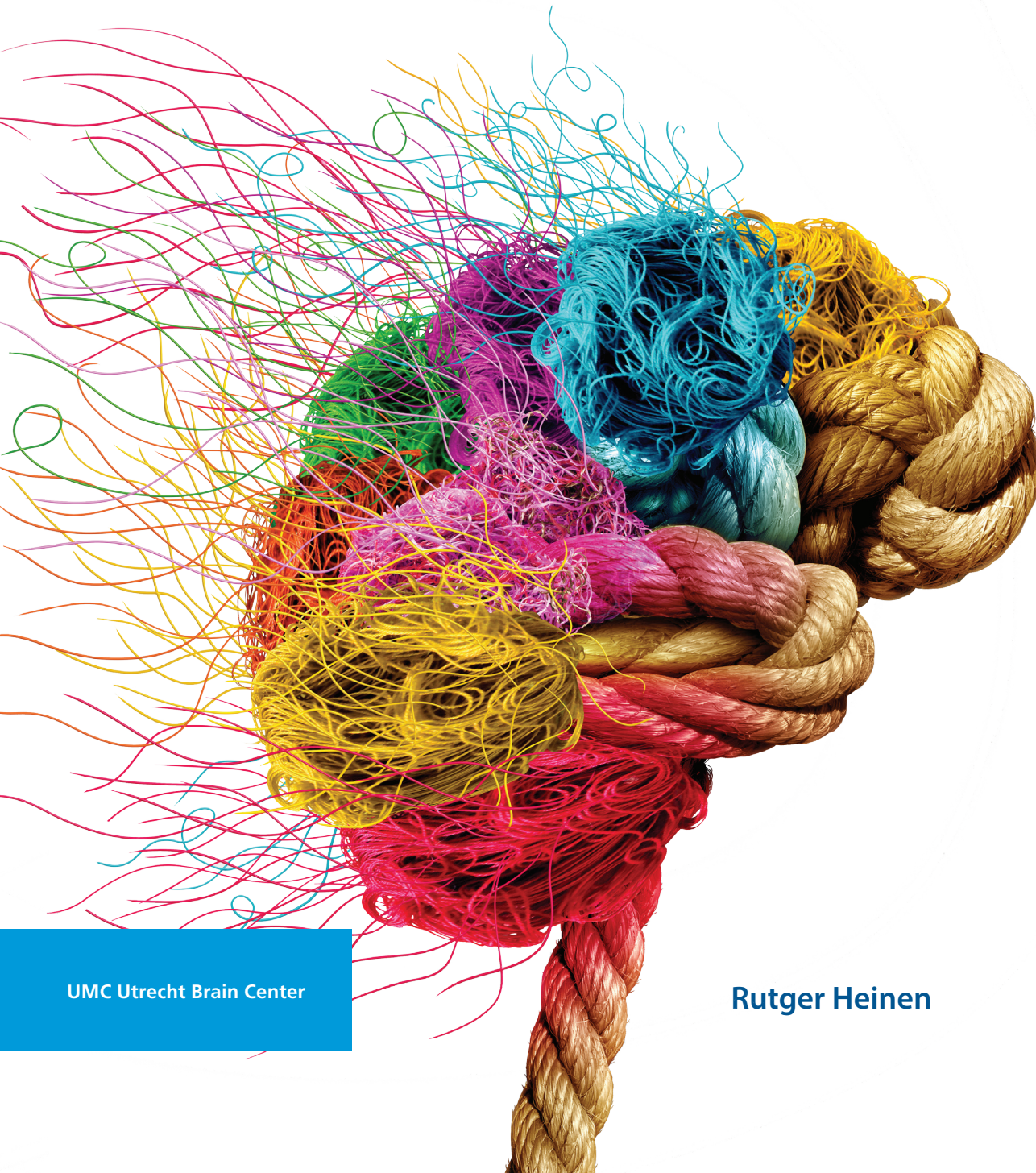

UMC Utrecht Brain Center

Rutger Heinen

Effects of cerebral small vessel disease in the brain beyond the visible lesions

Rutger Heinen

Cover image Shutterstock
Layout Renate Siebes | Proefschrift.nu
Printed by Proefschriftmaken.nl
ISBN 978-90-393-7191-6

Effects of cerebral small vessel disease in the brain beyond the visible lesions

Gevolgen van microvasculaire schade in de hersenen
die verder gaan dan de zichtbare laesies

(met een samenvatting in het Nederlands)

Proefschrift

ter verkrijging van de graad van doctor aan de
Universiteit Utrecht op gezag van de rector magnificus,
prof.dr. H.R.B.M. Kummeling, ingevolge het besluit van het
college voor promoties in het openbaar te verdedigen
op donderdag 19 december 2019 des middags te 2.30 uur

door

Rutger Heinen

geboren op 29 augustus 1988
te Hilvarenbeek

Promotor:	Prof.dr. G.J. Biessels
Copromotoren:	Dr. Y.D. Reijmer Dr. J.H.J.M. de Bresser

The research described in this thesis was supported by a grant of the Dutch Heart Foundation (DHF 2010T073).

We gratefully acknowledge Alzheimer Nederland, ChipSoft and the Dutch Heart Foundation for providing financial support for the publication of this thesis.

If you can't fly, then run,
if you can't run, then walk,
if you can't walk, then crawl,
but whatever you do,
you have to keep *moving forward*

Martin Luther King Jr.

Contents

Chapter 1	General introduction	**9**
PART ONE | Challenges when measuring cerebral small vessel disease-related brain changes		
Chapter 2	Robustness of automated methods for brain volume measurements across different MRI field strengths	**21**
Chapter 3	Performance of five automated white matter hyperintensity segmentation methods in a multicenter dataset	**49**
PART TWO | Effects of cerebral small vessel disease beyond the visible lesions and the interplay with Alzheimer's disease		
Chapter 4	Cortical microinfarcts and white matter connectivity in memory clinic patients	**79**
Chapter 5	The cumulative effect of small vessel disease lesions is reflected in structural brain networks of memory clinic patients	**101**
Chapter 6	Amyloid status modifies the relation between small vessel disease lesion type and brain atrophy	**119**
Chapter 7	Pattern of impaired white matter connectivity in Alzheimer's disease versus small vessel disease	**151**
Chapter 8	General discussion	**171**
Appendices	Summary	**184**
	Nederlandse samenvatting (summary in Dutch)	**190**
	About the author	**198**
	Publications	**199**
	Dankwoord	**201**

Chapter 1

General introduction

Cerebral small vessel disease (SVD) is an umbrella term describing different pathological processes that affect the smallest blood vessels of the brain, including the perforating arterioles, capillaries, and venules. The most common types are arteriolosclerosis and cerebral amyloid angiopathy (CAA).[1] Arteriolosclerosis is characterized by thickening of the wall and narrowing of the lumen of perforating vessels in subcortical brain regions, and is related with ageing and several cardiovascular risk factors, especially hypertension.[1] Therefore, it is often referred to as age-related or hypertensive small vessel disease. CAA is characterized by the accumulation of amyloid-β in the walls of predominantly posteriorly located arterioles and capillaries in the cerebral cortex and overlying leptomeninges.[2] It is related with ageing and an APOE genotype, but not with hypertension. CAA is common in the elderly population and is often accompanied by Alzheimer's disease pathology.[2]

SVD is a major cause of cognitive decline, dementia and stroke.[3] Worldwide, over 40 million people suffer from dementia and this is expected to almost double every 20 years.[4] SVD contributes to up to 45% of all dementias and is as such the second most common cause of dementia after Alzheimer's disease.[5,6] Stroke is currently the second leading cause of death worldwide and one of the leading causes of long-term disability. SVD accounts for approximately 25% of all ischemic strokes and the majority of spontaneous hemorrhagic strokes (either due to arteriolosclerosis [more often in the basal ganglia, thalamus and brainstem; "hypertensive" hemorrhages] or CAA [more often lobar]).[7,8] Despite its high prevalence and impact, limited SVD specific therapeutic options are currently available, and primarily consist of general management of cardiovascular risk factors and antiplatelet therapy in patients with ischemic stroke due to SVD. Furthermore, the available treatment strategies have been developed primarily for large vessel disease (i.e. atherosclerosis) affecting large blood vessels elsewhere in the body (e.g. coronary arteries, aorta). This lack of treatment options can be partly explained by the limited understanding of the pathophysiology of SVD. Brain Magnetic Resonance Imaging (MRI) has proven to be an important technique in the research field aiming to clarify the pathophysiology of SVD.

Detecting SVD lesions on MRI

Several lesions can be detected as manifestations of SVD on conventional brain MRI, including white matter hyperintensities of presumed vascular origin (WMHs), lacunes of presumed vascular origin, cerebral microbleeds, recent small subcortical infarcts and perivascular spaces (Figure 1.1). Cortical microinfarcts can be a manifestation of both SVD and large vessel disease (Figure 1.1).

Both presence and severity of these lesions can be quantified using established criteria.[9,10] These different lesion types can reflect different disease processes affecting different vessels,

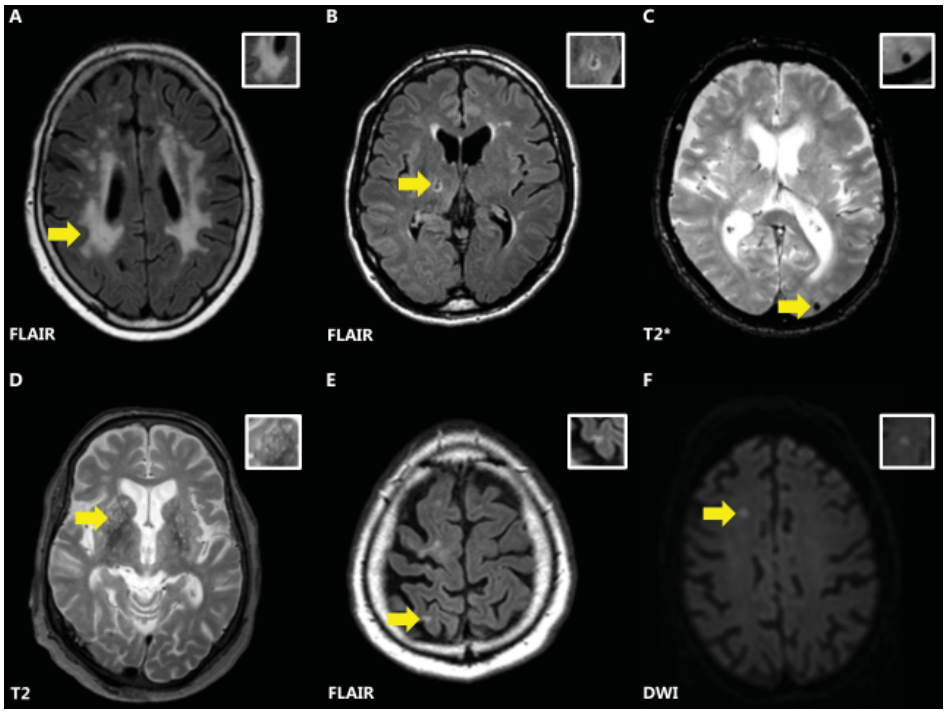

Figure 1.1 | Examples of different SVD lesion types on conventional brain MRI. Depicted with yellow arrows are WMHs (A), a lacune of presumed vascular origin (B), a cerebral microbleed (C), perivascular spaces (D), a cortical microinfarct (E) and a recent small subcortical infarct (F).

in different parts of the brain. For instance, in arteriolosclerosis WMHs occur throughout the brain, cerebral microbleeds predominantly occur in the deep areas of the brain and lacunes are common, particularly in the basal ganglia or deep white matter. By contrast, in CAA WMHs predominantly occur in posterior brain regions, cerebral microbleeds occur strictly in lobar brain regions and lacunes are not typically present.[2] As such, these different lesion types and distributions can be used to study the effects of different types of SVD in the brain.

Effects of SVD beyond the visible lesions – looking beyond the obvious

In the past years, increasing evidence suggests that visible SVD lesions on conventional structural MRI do not fully capture the burden of SVD-related brain injury.[11] Previous studies have suggested that focal SVD lesions represent only the tip of the iceberg and that SVD-related changes seem to occur in the brain's gray and white matter beyond the visible lesions.[12-14] It is thought that these changes can occur directly surrounding the visible SVD lesions (i.e. 'perilesional effects') or more distant to the visible SVD lesions (i.e. 'distant

effects').[11] An example of a perilesional effect are abnormalities that can be found in the 'normal appearing' white matter surrounding WMHs (the so called 'lesion penumbra').[12–14] An example of a distant effect is the cortical thinning that can occur distant to new subcortical infarcts in cortical areas connected to the lesioned area by white matter tracts.[15]

When considering SVD-related brain changes it is also important to take a more global view by looking at the brain as a complex network.[11] This complex network is often referred to as the human connectome, in which white matter fibers are vital in transferring information by connecting different brain regions with each other. Disconnection of the network (either structural, functional or both) can subsequently lead to clinical symptoms. The network can be disconnected as the direct result of visible SVD lesions, but disconnections can also occur due to tissue injury directly surrounding the visible SVD lesions,[13] as well as more diffuse or distant injury partially independent of SVD lesions.[14]

Effects of SVD that occur beyond the visible lesions provide a new framework to look at the impact of SVD. These effects can be used to better understand the functional impact of SVD than visible SVD lesions alone, as they have been shown to relate to cognitive decline and dementia.[14-20] However, there are still some open questions regarding effects of SVD beyond the visible lesions. For instance, are these effects similar for different types and manifestations of SVD? Do these effects also occur in patients with cortical cerebral microinfarcts (a relatively new MRI marker of SVD)? Do these effects have specific patterns? Is there an interplay with Alzheimer's disease, a common co-morbidity of SVD.

- *The overarching aim of the work described in this thesis was to examine changes in the gray and white matter of the brain that extend beyond the visible lesions in patients with SVD.*

Until now, changes in the gray and white matter of the brain that extend beyond the visible lesions have not been systematically investigated in memory clinic patients with both SVD and co-occurring Alzheimer's disease pathology. As such, I chose to measure brain volumes (using structural brain MRI) as well as white matter connectivity (using diffusion tensor imaging) and investigate the severity and pattern of changes in both the gray and white matter of the brain in memory clinic patients, how these changes relate to visible SVD lesions and whether this differed between lesion types, the impact of these changes on cognition, and the interplay with co-occurring Alzheimer's disease pathology.

Challenges when measuring SVD-related changes in the brain on MRI

When measuring SVD-related changes in the brain, it is important that measurements are reliable. Reliability of measurements can be defined in several ways.[21] For instance,

robustness refers to whether measurements are constant under different circumstances (e.g. different MRI field strength). Accuracy refers to how well a measurement actually measures what it is supposed to measure, or in other words whether it is correct. Measurements of SVD-related changes on MRI can be obtained using various qualitative and (semi) quantitative techniques, where the quantitative techniques in particular depend on brain segmentation. Brain segmentation refers to techniques that partition a digital image (e.g. MRI) into multiple segments (e.g. gray and white matter). Several automated methods have been developed using various algorithms to classify each voxel on MRI and subsequently measuring a volume or SVD lesion of interest, such as WMHs.[22,23] Segmentation results can be influenced by several factors, such as the burden of pathology, including presence of SVD lesions, motion artifacts, and technical issues (e.g. field strength or scan protocol).[24]

Dealing with technical issues is of great importance, since pooling of multicenter brain MRI data has become a trend in various research fields, for example in studies on age-related brain diseases.[25] Pooling has the advantage that it increases sample sizes (and thus statistical power), and can support a faster patient inclusion. Moreover, findings of multicenter studies may have larger external validity and are more readily translatable to a clinical setting. However, pooling of multicenter data poses challenges for brain and WMH segmentation by introducing variation in measurements due to different MRI acquisition techniques. Therefore, as a first step in my thesis I dealt with some of these technical issues that needed to be resolved for the analysis of our multicenter data. **Part 1** of this thesis describes two studies in which I compare the performance of several automated segmentation methods to support segmentation in a multicenter setting.

Key objectives were to:

- *compare the performance of automated brain segmentation methods across different MRI field strengths* (**chapter 2**).
- *compare the performance of automated WMH segmentation methods in a multicenter setting* (**chapter 3**).

The relation between visible SVD lesions and changes occurring beyond these lesions

While effects of SVD on the brain beyond the visible lesions have been demonstrated in patients with several manifestations of SVD (e.g. WMHs, lacunes), this is not clear for cortical microinfarcts (CMIs). CMIs are small (< 5 mm) ischemic lesions that can be detected in vivo on MRI.[10] Therefore, in **part 2** of this thesis I look at possible effects of SVD on white matter connectivity in patients with CMIs.

- *A key objective was to determine the distribution of CMIs in the brain and whether their presence relates with impaired white matter connectivity* (**chapter 4**).

Another important issue is the question whether to 'lump' or 'split' SVD lesions when investigating their causes and consequences. This also applies when investigating effects of SVD on the brain beyond visible SVD lesions. In recent years, it has become a trend in SVD research to use a SVD burden score to capture multiple types of vascular brain injury in a single measure.[26] The rationale behind this "lumping" is creating a single measure of vascular brain injury that relies on more than just a single SVD lesion, is easy to use and could serve as a surrogate endpoint in clinical research. Therefore, in **part 2** of this thesis, I investigate the effects of SVD on white matter connectivity by using a SVD burden score.

- *A key objective was to assess the relation between total SVD burden on MRI, global brain network efficiency and cognition* (**chapter 5**).

Splitting SVD lesion types is the preferred method when investigating specific disease mechanisms underlying effects of SVD, since different lesion types can reflect different underlying pathological processes, affecting different vessels, in different parts of the brain.[27] Therefore, in **part 2** of this thesis, I also investigate the effects of SVD on gray matter atrophy by looking at different SVD lesion types.

- *A key objective was to investigate whether different SVD lesion types differentially affect brain atrophy* (**chapter 6**).

Interplay between SVD and Alzheimer's disease

When investigating SVD-related brain changes, it is important to consider the possible confounding effect of common co-occurring pathologic processes that can also lead to changes in the gray and white matter, such as Alzheimer's disease. Alzheimer's disease, a neurodegenerative disease characterized microscopically by the presence of aggregations of amyloid-β and tau, is the most common cause of cognitive dysfunction and dementia.[28] It has been shown to damage both the gray and white matter of the brain.[29]

SVD and Alzheimer's disease often co-occur, especially with increasing age.[30] Post-mortem studies have shown that in patients with Alzheimer's disease histopathological evidence of arteriolosclerosis can be found in up to 41% of cases and of CAA in 78–98% of cases.[2,31] The relation between SVD, Alzheimer's disease and brain changes has gained increasing attention in the past decade.[32] However, whether SVD and Alzheimer's disease have independent, additive or interactive effects on the brain remains unclear. Therefore, **part 2** of this thesis also focusses on investigating the effects of both SVD and Alzheimer's

disease on gray matter atrophy as well as the independent effect of each disease on white matter connectivity.

Key objectives were to:

- *investigate whether co-occurring amyloid-β pathology modifies the relation between SVD lesion type and brain atrophy* (**chapter 6**).
- *determine whether the pattern of impaired white matter connectivity differed between patients with primarily SVD and patients with primarily Alzheimer's disease* (**chapter 7**).

I conclude this thesis with a general discussion of the results (**chapter 8**).

REFERENCES

1. Pantoni L. Cerebral small vessel disease: from pathogenesis and clinical characteristics to therapeutic challenges. Lancet Neurol. 2010;9:689–701.
2. Charidimou A, Boulouis G, Gurol ME, Ayata C, Bacskai BJ, Frosch MP, et al. Emerging concepts in sporadic cerebral amyloid angiopathy. Brain. 2017;140:1829-50.
3. Rensma SP, van Sloten TT, Launer LJ, Stehouwer CDA. Cerebral small vessel disease and risk of incident stroke, dementia and depression, and all-cause mortality: A systematic review and meta-analysis. Neurosci Biobehav Rev. 2018;90:164–73.
4. World Alzheimer Report 2015, Prince M, Wimo A, Guerchet M, Gemma-Claire A, Wu Y-T, Prina M. World Alzheimer Report 2015: The Global Impact of Dementia - An analysis of prevalence, incidence, cost and trends. Alzheimer's Dis Int. Epub 2015:1–84.
5. Rizzi L, Rosset I, Roriz-Cruz M. Global epidemiology of dementia: Alzheimer's and vascular types. Biomed Res Int. 2014;908915:1–8.
6. Shi Y, Wardlaw JM. Update on cerebral small vessel disease: A dynamic whole-brain disease. Stroke Vasc. Neurol. 2016;183–92.
7. Katan M, Luft A. Global Burden of Stroke. Semin Neurol. 2018;38:208–11.
8. Cordonnier C, Demchuk A, Ziai W, Anderson CS. Intracerebral haemorrhage: current approaches to acute management. Lancet. 2018;392:1257–68.
9. Wardlaw JM, Smith EE, Biessels GJ, et al. Neuroimaging standards for research into small vessel disease and its contribution to ageing and neurodegeneration. Lancet Neurol. 2013;12: 822–38.
10. van Veluw SJ, Shih AY, Smith EE, et al. Detection, risk factors, and functional consequences of cerebral microinfarcts. Lancet Neurol. 2017;16:730–40.
11. Ter Telgte A, Van Leijsen EMC, Wiegertjes K, Klijn CJM, Tuladhar AM, De Leeuw FE. Cerebral small vessel disease: From a focal to a global perspective. Nat Rev Neurol. 2018;14: 387–98.
12. Maillard P, Fletcher E, Harvey D, Carmichael O, Reed B, et al. White matter hyperintensity penumbra. Stroke. 2011;42:1917–22.
13. Maniega SM, Valdés Hernández MC, Clayden JD, Royle NA, Murray C, et al. White matter hyperintensities and normal- appearing white matter integrity in the aging brain. Neurobiol Aging. 2015;36:909–18.
14. Lawrence AJ, Chung AW, Morris RG, Markus HS, Barrick TR. Structural network efficiency is associated with cognitive impairment in small-vessel disease. Neurology. 2014;83:304–11.
15. Kim HJ, Im K, Kwon H, Lee JM, Kim C, Jung NY, et al. Clinical effect of white matter network disruption related to amyloid and small vessel disease. Neurology. 2015;85:63–70.
16. Tuladhar AM, van Dijk E, Zwiers MP, van Norden AG, de Laat KF, Shumskaya E, et al. Structural network connectivity and cognition in cerebral small vessel disease. Hum Brain Mapp. 2016;37:300–10.
17. Duering M, Righart R, Csanadi E, Jouvent E, Herve D, Chabriat H, et al. Incident subcortical infarcts induce focal thinning in connected cortical regions. Neurology. 2012;79:2025–28.
18. Banerjee G, Jang H, Kim HJ, Kim ST, Kim JS, Lee JH, et al. Total MRI Small Vessel Disease Burden Correlates with Cognitive Performance, Cortical Atrophy, and Network Measures in a Memory Clinic Population. J Alzheimer's Dis. 2018;63:1485–97.
19. Lambert C, Sam Narean J, Benjamin P, Zeestraten E, Barrick TR, Markus HS. Characterising the grey matter correlates of leukoaraiosis in cerebral small vessel disease. NeuroImage Clin. 2015;9:194–205.
20. Lambert C, Benjamin P, Zeestraten E, Lawrence AJ, Barrick TR, Markus HS. Longitudinal patterns of leukoaraiosis and brain atrophy in symptomatic small vessel disease. Brain. 2016; 139:1136–51.

21. International Bureau of Weights and Measures (BIPM). International Standardization Organization: International Vocabulary of Basic and General Terms in Metrology. 3. Ed. 2012.
22. Despotović I, Goossens B, Philips W. MRI segmentation of the human brain: Challenges, methods, and applications. Comput Math Methods Med. 2015;2015:450341.
23. Caligiuri ME, Perrotta P, Augimeri A, Rocca F, Quattrone A, Cherubini A. Automatic Detection of White Matter Hyperintensities in Healthy Aging and Pathology Using Magnetic Resonance Imaging: A Review. Neuroinformatics. 2015;13:261–76.
24. Jovicich J, Czanner S, Han X, Salat D, van der Kouwe A, Quinn B, et al. MRI-derived measurements of human subcortical, ventricular and intracranial brain volumes: Reliability effects of scan sessions, acquisition sequences, data analyses, scanner upgrade, scanner vendors and field strengths. Neuroimage. 2009;46:177–92.
25. Mueller SG, Weiner MW, Thal LJ, Petersen RC, Jack CR, Jagust W, et al. Ways toward an early diagnosis in Alzheimer's disease: The Alzheimer's Disease Neuroimaging Initiative (ADNI). Alzheimer's Dement. 2005;1:55–66.
26. Staals J, Booth T, Morris Z, Bastin ME, Gow AJ, Corley J, et al. Total MRI load of cerebral small vessel disease and cognitive ability in older people. Neurobiol Aging. 2015;36:2806–11.
27. Gouw AA, Seewann A, Van Der Flier WM, et al. Heterogeneity of small vessel disease: A systematic review of MRI and histopathology correlations. J Neurol Neurosurg Psychiatry. 2011;82:126–35.
28. Jack CR, Bennett DA, Blennow K, Carrillo MC, Dunn B, Haeberlein SB, et al. NIA-AA Research Framework: Toward a biological definition of Alzheimer's disease. Alzheimer's Dement. 2018;14:535–62.
29. Mak E, Gabel S, Mirette H, Su L, Williams GB, Waldman A, et al. Structural neuroimaging in preclinical dementia: From microstructural deficits and grey matter atrophy to macroscale connectomic changes. Ageing Res Rev. 2017;35:250–64.
30. Toledo JB, Arnold SE, Raible K, Brettschneider J, Xie SX, Grossman M, et al. Contribution of cerebrovascular disease in autopsy confirmed neurodegenerative disease cases in the National Alzheimer's Coordinating Centre. Brain. 2013;136:2697–706.
31. Arvanitakis Z, Capuano AW, Leurgans SE, Bennett DA, Schneider JA. Relation of cerebral vessel disease to Alzheimer's disease dementia and cognitive function in elderly people: a cross-sectional study. Lancet Neurol. 2016;15:934–43.
32. Koncz R, Sachdev PS. Are the brain's vascular and Alzheimer pathologies additive or interactive? Curr. Opin. Psychiatry. 2018;31:147–52.

PART ONE

Challenges when measuring cerebral small vessel disease-related brain changes

Chapter 2

Robustness of automated methods for brain volume measurements across different MRI field strengths

Rutger Heinen
Willem H. Bouvy
Adrienne M. Mendrik
Max A. Viergever
Geert Jan Biessels
Jeroen de Bresser

PLoS One. 2016;11(10):e0165719

ABSTRACT

Pooling of multicenter brain imaging data is a trend in studies on ageing related brain diseases. This poses challenges to MR-based brain segmentation. The performance across different field strengths of three widely used automated methods for brain volume measurements was assessed in the present study.

Ten subjects (mean age: 64 years) were scanned on 1.5T and 3T MRI on the same day. We determined robustness across field strength (i.e., whether measured volumes between 3T and 1.5T scans in the same subjects were similar) for SPM12, Freesurfer 5.3.0 and FSL 5.0.7. As a frame of reference, 3T MRI scans from 20 additional subjects (mean age: 71 years) were segmented manually to determine accuracy of the methods (i.e., whether measured volumes corresponded with expert-defined volumes).

Total brain volume (TBV) measurements were robust across field strength for Freesurfer and FSL (mean absolute difference as % of mean volume ≤ 1%), but less so for SPM (4%). Gray matter (GM) and white matter (WM) volume measurements were robust for Freesurfer (1%; 2%) and FSL (2%; 3%) but less so for SPM (5%; 4%). For intracranial volume (ICV), SPM was more robust (2%) than FSL (3%) and Freesurfer (9%). TBV measurements were accurate for SPM and FSL, but less so for Freesurfer. For GM volume, SPM was accurate, but accuracy was lower for Freesurfer and FSL. For WM volume, Freesurfer was accurate, but SPM and FSL were less accurate. For ICV, FSL was accurate, while SPM and Freesurfer were less accurate.

Brain volumes and ICV could be measured quite robustly in scans acquired at different field strengths, but performance of the methods varied depending on the assessed compartment (e.g., TBV or ICV). Selection of an appropriate method in multicenter brain imaging studies therefore depends on the compartment of interest.

INTRODUCTION

Pooling of multicenter brain MRI data is a trend in various research fields, for example in studies on ageing related brain diseases.[1–3] Pooling of multicenter data increases sample size (and thus statistical power) and can support a faster patient inclusion. Moreover, findings of multicenter studies may have larger external validity and are more readily translatable to a clinical setting. However, use of different MRI acquisition techniques, for example with regard to scanner types or field strength,[4–6] across centers could introduce variation in results of frequently used MR-based automated brain segmentation methods.[6] This variation could potentially even be larger than the actual effect size of the brain changes studied.[7,8]

To date, the performance of the most recent versions of Statistical Parametric Mapping (SPM),[9] Freesurfer[10] and FMRIB Software Library (FSL)[11] in datasets with different MRI acquisition techniques (such as different field strengths) is not well studied. Performance of these methods can be assessed in terms of robustness (i.e., whether measured volumes on scans with different acquisitions techniques in the same subjects are similar) and accuracy (i.e., whether measured volumes correspond with expert-defined reference volumes). It is important to consider both measures of performance together, since neither a robust, inaccurate method nor an accurate, non-robust method will lead to valid results in a multicenter study.

In the present study, we evaluated the performance of three widely used automated methods for brain volume measurements (SPM, Freesurfer and FSL). Robustness was assessed in subjects that were scanned on 1.5T and 3T MRI on the same day. Accuracy was determined by comparing the measurements of the methods with manual segmentations on 3T MRI scans of additional subjects.

MATERIALS AND METHODS

Automated methods for brain volume measurements and image processing

SPM (version 12), Freesurfer (version 5.3.0) and FSL (version 5.0.7 with use of SIENAX, version 2.6) were used to calculate brain volumes and intracranial volume (ICV) on T1-weighted MRI images.

SPM12. SPM (Wellcome Department of Cognitive Neurology, Institute of Neurology, Queen Square, London; available at http://www.fil.ion.ucl.ac.uk/spm/) uses the unified segmentation (US) algorithm, which combines tissue classification, bias correction and

image registration in the same generative model.[9] It produces partial volume segmentation results for each tissue compartment, using tissue prior probability maps based on intensity values. From these results absolute volumes of gray matter (GM), white matter (WM) and cerebrospinal fluid (CSF) are calculated. Additional tissue maps for soft tissue, bone and air/background were included in SPM8 and are now part of standard segmentation.[12] This reduces the possibility of misclassification of non-brain tissue. In our study, segmentation was performed using the advised default settings. Partial volume segmentation results for each of the three tissue compartments (GM, WM and CSF) were obtained and extracted by using the 'Tissue Volumes' utility in SPM. Total brain volume (TBV) was calculated by summing up GM and WM volumes. ICV was determined by summing up TBV and CSF volumes.

Freesurfer. Freesurfer (Martinos Center for Biomedical Imaging, Harvard-MIT, Boston; available at http://surfer.nmr.mgh.harvard.edu/) consists of surface based analysis[13] and volumetric segmentation.[10,14] It involves intensity non-uniformity correction,[15] affine transformation to a MNI305 template, intensity normalization, removal of non-brain tissue,[16] linear and non-linear transformations to a probabilistic brain atlas and labeling of cortical and subcortical structures.[10,14] It uses a Markov Random Field model for each structure for each point in space. Spatial localization priors are used in determining the right label per voxel.[17] Since Freesurfer version 5.2, surface-based calculations are used to calculate various brain volumes to get better accuracy. In our study, segmentation was performed using default settings (i.e. using the command: 'recon-all'). For our study, we used the compartment measurements reported by Freesurfer. All volumes were extracted from the stat files that Freesurfer produces using the 'asegstats2table' command. Since Freesurfer estimates ICV and does not perform segmentation of extracerebral CSF, we obtained the CSF volume by subtracting TBV from the estimated ICV.

FSL. FSL (Analysis Group, FMRIB, Oxford, United Kingdom; available at http://fsl.fmrib.ox.ac.uk/fsl/fslwiki/) uses the SIENAX package for estimating brain tissue volumes from a single image.[11,18,19] SIENAX starts by extracting brain and skull images from the single whole-head input data.[20] The brain image is then affine-registered to MNI152 space.[21,22] Next, tissue-type segmentation with partial volume estimation is carried out.[23] From these estimations, GM, WM and ventricular CSF volumes were calculated. In our study, we stripped excessive slices at the level of the neck to allow accurate skull stripping, which in an earlier study yielded optimal results with various scan protocols.[24] In concordance with a previous study investigating the optimal settings for the brain extraction tool (BET) we used the following settings: a fraction intensity threshold value of 0.1 and use of the B-option (bias field and neck clean up).[24] Partial volume segmentation results for each of the three tissue compartments (GM, WM and CSF) were obtained. TBV was calculated

by summing up GM and WM volumes (as reported by FSL). We used MeVisLab (MeVis Medical Solutions AG, Bremen, Germany, version 2.5) to obtain CSF measurements from the FSL partial volume segmentation (since FSL only reports ventricular CSF volume). ICV was calculated by summing up GM, WM and (total) CSF volumes.

Robustness analysis

Study population. To determine the robustness across field strengths, subjects were scanned on 1.5T and 3T MRI on the same day. The intention was to recruit a group of patients with ageing related brain changes, but without a known primary cerebral disease. Therefore, patients, aged 50–80 years, with chronic idiopathic axonal polyneuropathy (CIAP) were recruited from an ongoing cohort study at the University Medical Center Utrecht, Utrecht, the Netherlands between September 2012 and October 2013.[25] Exclusion criteria were a history of brain disease, not living independently and/or a contra-indication for MRI. Written informed consent was provided by all participants. The study was approved by the local medical ethics committee.

MRI data acquisition. The 1.5T MRI (Achieva; Philips, Best, the Netherlands) protocol consisted of the following sequences covering the entire brain: a sagittal 3D T1-weighted sequence (170 continuous slices, voxel size: 0.94 × 0.94 × 1.00 mm, repetition time (TR)/echo time (TE): 7.0/3.2 ms) and an axial 2D fluid attenuated inversion recovery (FLAIR) sequence (38 continuous slices, voxel size: 0.90 × 0.90 × 4.0 mm, TR/TE/inversion time (TI): 6.000/100/2000 ms). The 3T MRI (Achieva; Philips, Best, the Netherlands) protocol consisted of the following sequences: a sagittal 3D T1-weighted sequence (192 continuous slices, voxel size: 1.00 × 1.00 × 1.00 mm, TR/TE: 7.9/4.5 ms) and an axial 2D FLAIR sequence (48 continuous slices, voxel size: 0.96 × 0.95 × 3.00 mm, TR/TE/TI: 11000/125/2800 ms). Additionally, to evaluate robustness across different spatial resolutions (high versus low), the 3D T1 images of the 1.5T and 3T MRI scans were downsampled to a voxel size of 0.96 × 0.96 × 3.00 mm.

Statistical analysis. Non-parametric statistical tests were used because of the limited number of subjects. Robustness was assessed in two ways. First, we assessed potential systematic bias across field strength for each method with a Wilcoxon signed rank test. Next, the amount of variation/bias between 3T and 1.5T measurements was assessed by mean absolute differences (also expressed as a percentage of the mean volume at 3T). To further evaluate these differences we determined coefficients of repeatability as well as Bland Altman plots. The coefficient of repeatability is calculated by multiplying the standard deviation of the absolute differences (i.e., square root of the mean squared difference) between measurements at 3T and 1.5T by 1.96.[26] It thus represents the upper limit of the

mean difference between two measurements in 95% of cases. Bland Altman plots give a graphical representation of presence/absence of systematic bias and the amount of variation between measurements. In these plots, a mean difference close to zero indicates absence of systematic bias. A narrow width of the limits of agreement reflects a small amount of variation between measurements at 3T and 1.5T. In secondary analyses we repeated the entire analysis for the high versus low resolution comparison.

Accuracy analysis

Study population and MRI data. To determine accuracy, scans from healthy control subjects were selected from a cohort study of functionally independent elderly subjects (65–80 years of age) without a history of stroke or other brain diseases.[27] Subjects were scanned on 3T MRI with an identical scanning protocol as the subjects of the robustness analysis. Written informed consent was provided by all participants and the study was approved by the local medical ethics committee.

Reference data. Manual segmentations were used as reference data. The procedure for manual segmentations was described previously (for details see[28]). First, the 3D T1 and 2D T1-IR scans were registered to the 2D FLAIR scan by means of Elastix.[29] The 3D T1 scan was downsampled so that all scans had a resulting voxel size of 0.96 × 0.96 × 3.00 mm. Subsequently, bias correction was performed using SPM8.[30] Manual segmentations were performed on the axial T1, T1-IR and FLAIR slices by trained research assistants, using an inhouse developed tool based on MeVisLab (MeVis Medical Solutions AG, Bremen, Germany). This tool allowed a closed freehand spline drawing technique, which was used to delineate the outline of each tissue compartment (GM, WM and CSF). The closed contours were then converted into hard segmentations. The resulting images were checked and corrected by three experts (WB, AM, JdB).

Because manual segmentations that separate the cerebellum in GM and WM cannot be performed with high reliability, we chose not to differentiate between GM and WM in the manual segmentations of the cerebellum and other infratentorial structures. A mask of the manually segmented infratentorial structures was used to obtain supratentorial GM and WM volumes for each of the three automated segmentation methods for the analysis of accuracy in MeVisLab (MeVis Medical Solutions AG, Bremen, Germany, version 2.5). In the accuracy analysis, the infratentorial structures were not excluded from the TBV, CSF volume and ICV for all methods.

Statistical analysis. Non-parametric statistical tests were used because of the limited number of subjects. We performed similar analyses as for the robustness part, but now

volume measurements of the methods were compared with the reference standard. Furthermore, we also calculated a Dice's similarity coefficient (DSC) to evaluate spatial overlap between the segmentations of the methods and the reference data. As required for these analyses, the probabilistic segmentations of SPM and FSL were thresholded on a probability of 0.5. For Freesurfer the spatial overlap analyses required the output to be brought to native space by nearest neighbor interpolation (using the following command: 'mri_vol2vol—mov aseg.mgz—targ rawavg.mgz—regheader—o asegCorrect.mgz—nearest—no-save-reg') and divided in the three tissue compartments (GM, WM, CSF).

RESULTS

Quality assessment

Examples of the performed measurements of one subject using SPM, Freesurfer and FSL are shown in Figure 2.1 for the robustness analysis and in Figure 2.2 for the accuracy analysis. Output of all subjects was visually checked and was considered to be of good quality. No manual editing was performed. None of the patients proved to have (major) structural abnormalities on their scans that could influence automated segmentation results. Minor segmentation differences between methods can visually be appreciated in the figure. For example FSL generally segments less GM in the basal ganglia and thalamus, while this was less pronounced in SPM (Figures 2.1 and 2.2).

Robustness across field strength

Ten patients (four male, six female) were included for the robustness analyses. They had a mean age of 64 ± 7 years. For the evaluation of robustness across 3T and 1.5T, mean and individual brain volume measurements are presented in Table 2.1 and Supplementary Figure S2.1.

TBV. Measurements of TBV at 3T and 1.5T were robust for Freesurfer and FSL (i.e., non-significant mean differences between field strengths as shown in Table 2.2; see also the Bland Altman plots in Figure 2.3). Mean absolute differences were also small. Freesurfer gave a mean absolute difference ± SD of 8.4 ± 5.6 cc, which is < 1% of mean TBV as measured by this method at 3T. Corresponding figures for FSL were 14 ± 12 cc; 1%. The coefficients of repeatability were in line with these findings (see Figure 2.3). By comparison, SPM was less robust across field strength for TBV (mean difference ± SD: -42 ± 33 cc; $p = 0.007$; see also the Bland Altman plots in Figure 2.3). The mean absolute difference (43 ± 33 cc; 4%) was also larger than that of the other methods.

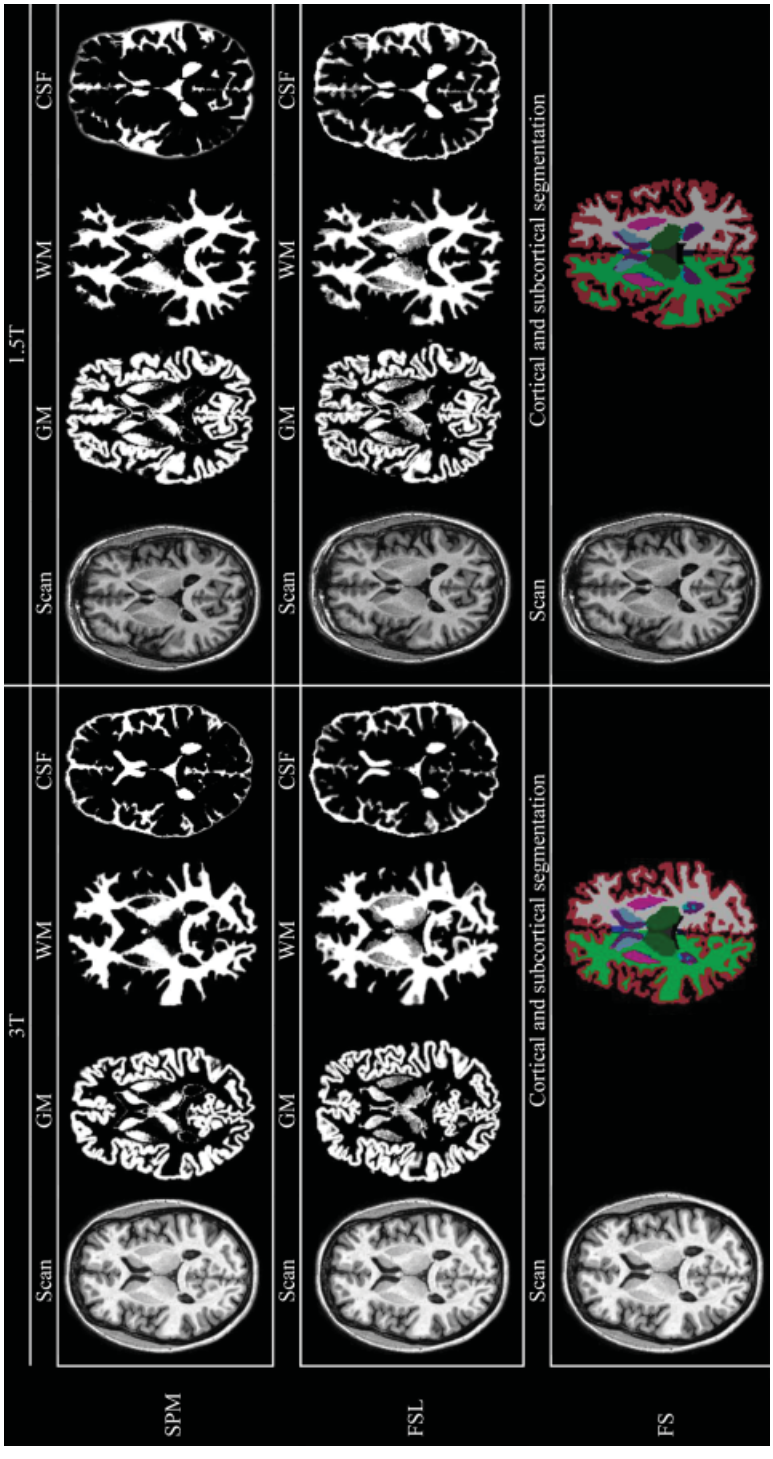

Figure 2.1 | Automated brain volume measurements at 3T and 1.5T. Examples of the performed measurements for the robustness analysis for one subject on 3T and 1.5T MRI. Individual measurements are shown using a probabilistic (SPM and FSL) or a binary approach (Freesurfer). GM, gray matter; WM, white matter; CSF, cerebrospinal fluid.

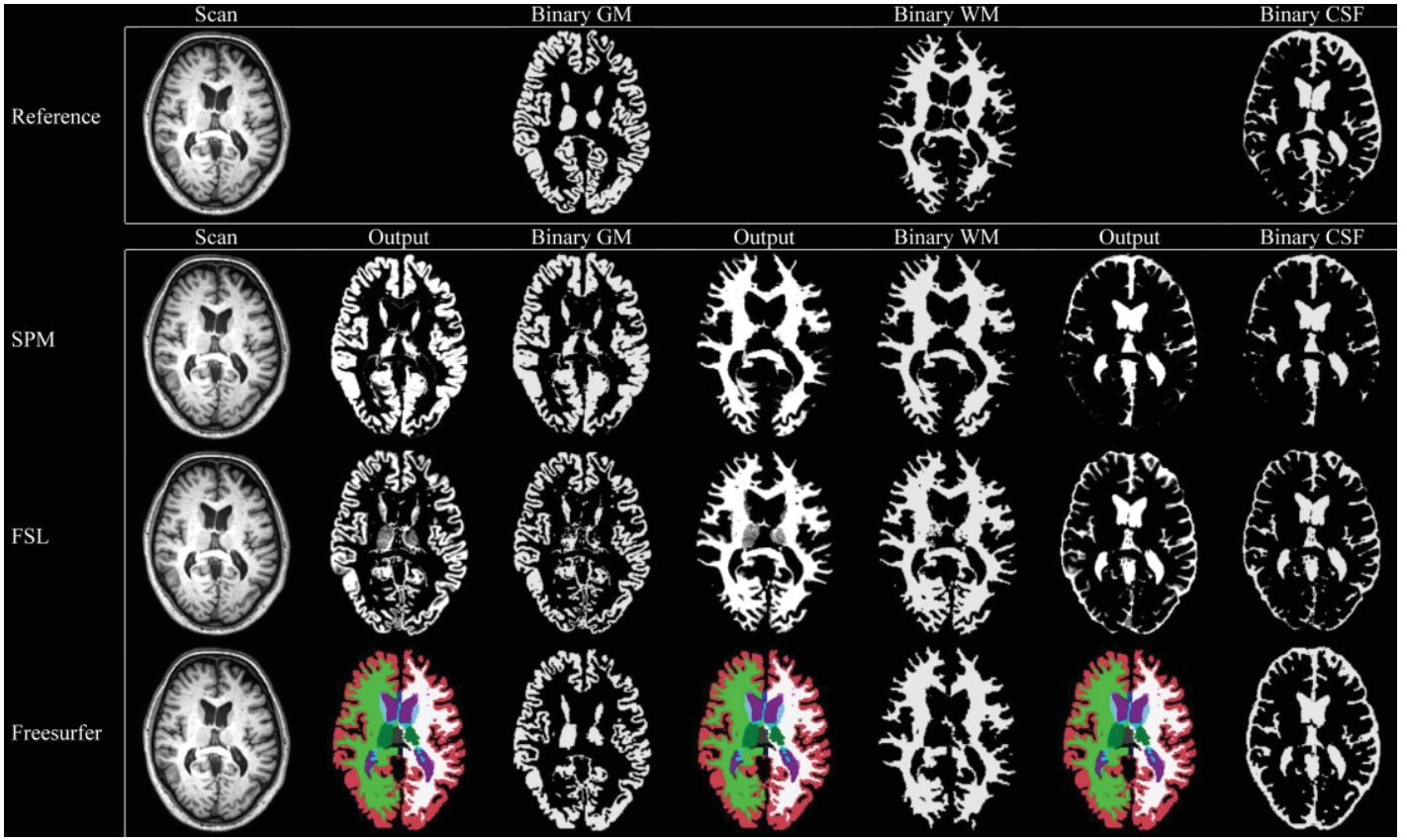

Figure 2.2 | Reference measurements and automated brain volume measurements at 3T. Examples of the performed measurements for the accuracy analysis for one subject on 3T MRI. Individual measurements are shown in native space (probabilistic for SPM and FSL, and binary for Freesurfer). Also, binary measurements for each tissue compartment are shown for all methods (using a threshold of 0.5 in case of probabilistic segmentation). GM, gray matter; WM, white matter; CSF, cerebrospinal fluid.

Table 2.1 | Automated volume measurements at 3T and 1.5T (n = 10)

			SPM	Freesurfer	FSL
TBV	1.5T	3D	1062 ± 80	1016 ± 72	1042 ± 74
	3T	3D	1020 ± 57	1013 ± 67	1049 ± 82
GM	1.5T	3D	610 ± 46	548 ± 38	552 ± 41
	3T	3D	590 ± 29	545 ± 37	554 ± 43
WM	1.5T	3D	452 ± 38	468 ± 38	491 ± 39
	3T	3D	430 ± 33	468 ± 36	495 ± 42
CSF	1.5T	3D	294 ± 56	440 ± 72	333 ± 36
	3T	3D	323 ± 90	342 ± 118	364 ± 43
ICV	1.5T	3D	1356 ± 121	1456 ± 102	1376 ± 99
	3T	3D	1343 ± 128	1355 ± 168	1413 ± 111

All volumes are expressed as means (in cc) ± SD. TBV, total brain volume; GM, gray matter volume; WM, white matter volume; CSF, cerebrospinal fluid volume; ICV, intracranial volume.

GM volume. Freesurfer and FSL were robust for GM volume measurements across field strength (Table 2.2 and the Bland Altman plots in Figure 2.3) and the mean absolute differences were small: Freesurfer (8 ± 6 cc; 1%); FSL (10 ± 8 cc; 2%). SPM was less robust for GM volume across field strength (-20 ± 32 cc; $p = 0.047$; see also the Bland Altman plots in Figure 2.3). In line with this, the mean absolute difference (26 ± 26 cc; 5%) was larger compared with Freesurfer and FSL (Table 2.2; see also the coefficient of repeatability in Table 2.2).

WM volume. WM volume measurements were robust across field strengths for Freesurfer and FSL (Table 2.2 and the Bland Altman plots in Figure 2.3) and the mean absolute differences were small: Freesurfer (8 ± 5 cc; 2%); FSL (13 ± 9 cc; 3%). For SPM, WM volume was less robust across field strength (-22 ± 6 cc; $p = 0.005$). The mean absolute difference (22 ± 6 cc; 4%) was also larger than for the other methods (Table 2.2).

CSF volume. None of the methods were robust for CSF. Substantial relative and absolute differences in measured CSF volume across field strength were observed for all methods (Table 2.2, Figure 2.3), which was also reflected in a large coefficient of repeatability (Table 2.2).

ICV. ICV measurements were robust across field strengths for SPM (Table 2.2 and the Bland Altman plots in Figure 2.3) with also a small mean absolute difference (23 ± 21 cc; 2%). ICV measurements were less robust across field strength for Freesurfer (-100 ± 113 cc; $p = 0.037$) and FSL (38 ± 48 cc; $p = 0.028$; see also the Bland Altman plots in Figure 2.3). The mean absolute difference was smaller for FSL (47 ± 39 cc; 3%) than for Freesurfer (115 ± 95 cc; 9%); which was reflected in the coefficient of repeatability (Table 2.2).

Table 2.2 | Robustness analysis across different field strengths (n = 10)

			SPM	Freesurfer	FSL
TBV	3T vs 1.5T (3D)	Mean difference	-42 ± 35*	-2 ± 10	7 ± 17
		Mean absolute difference	43 ± 33	8 ± 6	14 ± 12
		as % of mean TBV at 3T	4	< 1	1
		Coefficient of repeatability	107	20	35
		as % of mean TBV at 3T	11	2	3
GM	3T vs 1.5T (3D)	Mean difference	-20 ± 32*	-2 ± 10	2 ± 13
		Mean absolute difference	26 ± 26	8 ± 6	10 ± 8
		as % of mean GM at 3T	5	1	2
		Coefficient of repeatability	72	20	25
		as % of mean GM at 3T	13	4	5
WM	3T vs 1.5T (3D)	Mean difference	-22 ± 6*	< 1 ± 10	4 ± 16
		Mean absolute difference	22 ± 6	8 ± 5	13 ± 9
		as % of mean WM at 3T	4	2	3
		Coefficient of repeatability	46	18	32
		as % of mean WM at 3T	11	4	6
CSF	3T vs 1.5T (3D)	Mean difference	29 ± 56	-98 ± 113	31 ± 35*
		Mean absolute difference	45 ± 43	115 ± 93	36 ± 29
		as % of mean CSF at 3T	14	34	10
		Coefficient of repeatability	122	291	90
		as % of mean CSF at 3T	36	85	25
ICV	3T vs 1.5T (3D)	Mean difference	-13 ± 30	-100 ± 113*	38 ± 48*
		Mean absolute difference	23 ± 21	115 ± 95	46 ± 39
		as % of mean ICV at 3T	2	9	3
		Coefficient of repeatability	62	293	118
		as % of mean ICV at 3T	5	22	8

All volumes (in cc) are expressed as means ± SD. Coefficients of repeatability are expressed as a volume (in cc). TBV, total brain volume; GM, gray matter volume; WM, white matter volume; CSF, cerebrospinal fluid volume; ICV, intracranial volume. Mean differences between 3T and 1.5T were tested for each method separately using Wilcoxon signed rank test (* $p < 0.05$).

Robustness across different spatial resolutions

In secondary analyses we assessed robustness across different spatial resolutions (high versus low, i.e., 3T 3D T1 versus downsampled T1). Mean brain volume measurements at 3D and downsampled resolutions are shown in Supplementary Table S2.1 and measurements per subject are shown in Supplementary Figure S2.2. For SPM and FSL, results were comparable with the across field strength analysis (see Supplementary Table S2.2). The performance of Freesurfer was less robust for TBV (18 ± 9 cc; $p = 0.005$), GM (25 ± 9 cc; $p = 0.005$) and WM (-6 ± 5 cc; $p = 0.013$; see also Bland Altman plots in Supplementary Figure S2.3) when using low resolution T1-weighted MR-images for segmentation. The mean absolute differences for Freesurfer (as % of mean volume at 3D for TBV, GM and

WM: 2%; 5%; 1%) were also larger compared with the 3T versus 1.5T comparison of Freesurfer (1%; 1%; 1%). The other results for Freesurfer were in line with the results of the 3T versus 1.5T comparison.

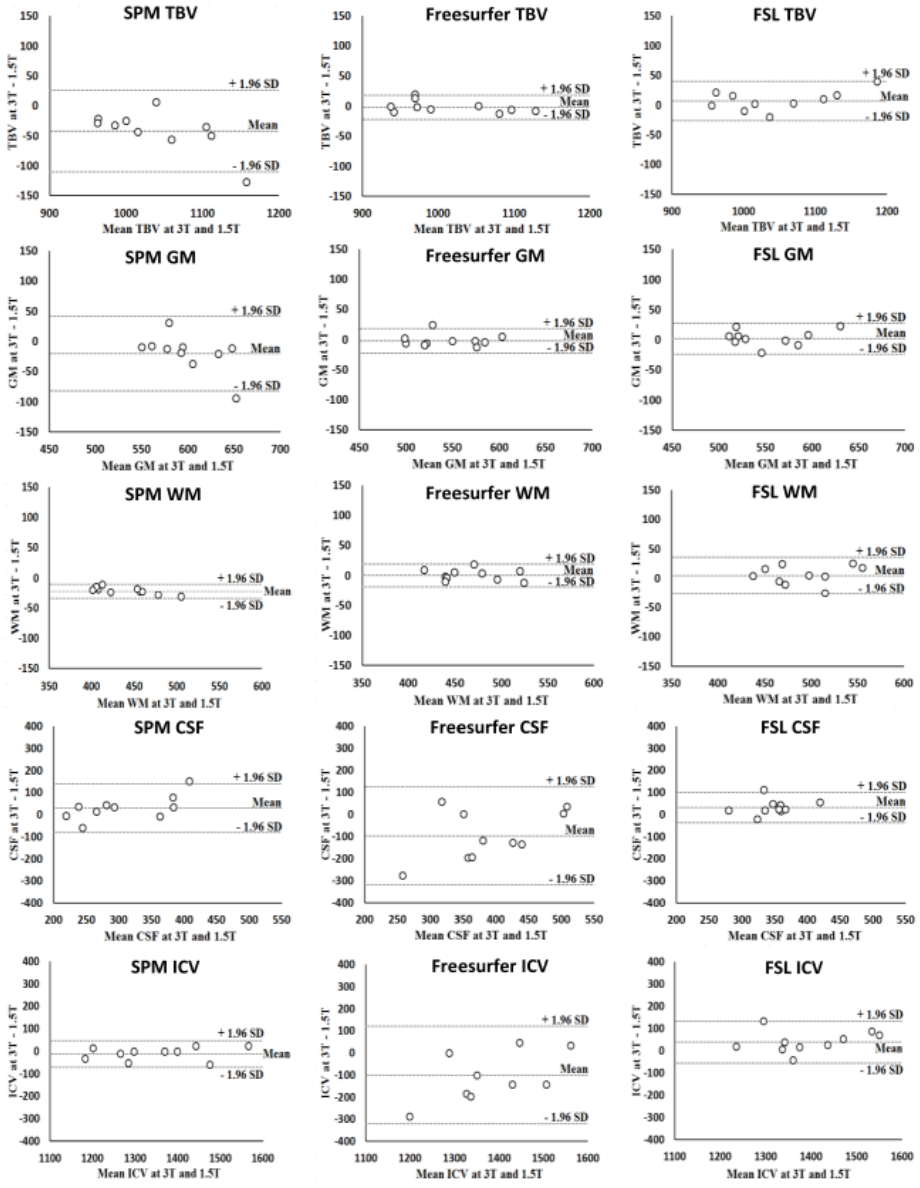

Figure 2.3 | Bland-Altman plots at 3T and 1.5T. X-axis: mean brain volume measurements at 3T and 1.5T. Y-axis: difference (in cc) in brain volume measurements between 3T and 1.5T. The mean, lower (-1.96 SD) and upper (+1.96 SD) limits of agreement are shown. A negative difference on the y-axis is seen when brain volume measurements at 1.5T were larger than at 3T. TBV, total brain volume; GM, gray matter volume; WM, white matter volume; CSF, cerebrospinal fluid volume; ICV, intracranial volume.

Accuracy assessments

Twenty subjects (ten male, ten female) were included for the accuracy analysis. They had a mean age of 71 ± 4 years. For the comparison between the automated methods and manual segmentation, individual brain volume measurements are presented in Supplementary Figures S2.4 and S2.5.

TBV. Measurements of TBV were accurate compared to manual segmentation for FSL and SPM (non-significant mean differences as shown in Table 2.3; see also the Bland Altman plots in Figure 2.4) with small mean absolute differences: FSL, when compared to mean TBV as measured by manual segmentation (29 ± 15 cc; 3%); SPM (36 ± 34 cc; 3%). Freesurfer was less accurate in measuring TBV (mean difference: -50 ± 36 cc; $p < 0.001$; also see the Bland Altman Plots in Figure 2.4). The mean absolute difference (52 ± 32 cc; 5%) was also larger for Freesurfer than for to the other methods.

GM volume. SPM was accurate for supratentorial GM volume, but FSL (-47 ± 43 cc; $p < 0.001$) and Freesurfer (-69 ± 38 cc; $p < 0.001$) were less accurate (Table 2.3 and the Bland Altman plots in Figure 2.4). The mean absolute difference was also smaller for SPM (35 ± 31 cc; 7%) than for FSL (49 ± 40 cc; 9%) and Freesurfer (69 ± 38 cc; 13%).

WM volume. Supratentorial WM volume measurements for Freesurfer were accurate (Table 2.3 and the Bland Altman plots in Figure 2.4). The mean absolute difference (26 ± 15 cc; 7%) was also smaller for Freesurfer than for the other methods. SPM (17 ± 37 cc; $p = 0.037$) and FSL (75 ± 31 cc; $p < 0.001$) were both less accurate, but the mean absolute differences were smaller for SPM (31 ± 26 cc; 8%) than for FSL (75 ± 31 cc; 20%).

CSF volume. FSL showed accurate CSF measurements (Table 2.3 and the Bland Altman plots in Figure 2.4). The mean absolute difference was also smaller for FSL (42 ± 23 cc; 10%) than for the other methods. Both SPM (-80 ± 77 cc; $p = 0.001$) and Freesurfer (120 ± 68 cc; $p < 0.001$) were less accurate for CSF volume (see also the Bland Altman plots in Figure 2.4) and had large mean absolute differences: SPM (95 ± 56 cc; 24%); Freesurfer (120 ± 68 cc; 30%).

ICV. FSL was accurate for ICV (Table 2.3 and the Bland Altman plots in Figure 2.4). The mean absolute difference was also smaller for FSL (39 ± 21 cc; 3%) than for the other methods. Both SPM (-78 ± 63 cc; $p < 0.001$) and Freesurfer (70 ± 55 cc; $p < 0.001$) were less accurate for ICV (also see the Bland Altman plots in Figure 2.4) and had large mean absolute differences: Freesurfer (74 ± 50 cc; 5%); SPM (84 ± 55 cc; 6%).

Table 2.3 | Accuracy of automated volume measurements (n = 20)

		SPM	Freesurfer	FSL
TBV	Volume (method)	1045 ± 82	994 ± 85	1044 ± 85
	Volume (manual segmentation)	1044 ± 97	1044 ± 97	1044 ± 97
	Mean difference	1 ± 50	-50 ± 36*	< 1 ± 33
	Mean absolute difference	36 ± 34	52 ± 32	29 ± 15
	as % of mean TBV with manual segmentation	3	5	3
	Dice's similarity coefficient	0.94 ± 0.008	0.92 ± 0.007	0.94 ± 0.006
SGM	Volume (method)	526 ± 44	459 ± 33	481 ± 38
	Volume (manual segmentation)	528 ± 59	528 ± 59	528 ± 59
	Mean difference	-2 ± 47	-69 ± 38*	-47 ± 43*
	Mean absolute difference	35 ± 31	69 ± 38	49 ± 40
	as % of mean SGM with manual segmentation	7	13	9
	Dice's similarity coefficient	0.79 ± 0.03	0.77 ± 0.02	0.77 ± 0.03
SWM	Volume (method)	390 ± 50	384 ± 56	448 ± 46
	Volume (manual segmentation)	373 ± 56	373 ± 56	373 ± 56
	Mean difference	17 ± 37*	11 ± 28	75 ± 31*
	Mean absolute difference	31 ± 26	26 ± 15	75 ± 31
	as % of mean SWM with manual segmentation	8	7	20
	Dice's similarity coefficient	0.85 ± 0.03	0.85 ± 0.02	0.84 ± 0.03
CSF	Volume (method)	324 ± 83	523 ± 77	413 ± 45
	Volume (manual segmentation)	403 ± 68	403 ± 68	403 ± 68
	Mean difference	-80 ± 77*	120 ± 68*	10 ± 48
	Mean absolute difference	95 ± 56	120 ± 68	42 ± 23
	as % of mean CSF with manual segmentation	24	30	10
	Dice's similarity coefficient	0.69 ± 0.05	0.65 ± 0.03	0.70 ± 0.03
ICV	Volume (method)	1368 ± 119	1517 ± 144	1458 ± 121
	Volume (manual segmentation)	1447 ± 118	1447 ± 118	1447 ± 118
	Mean difference	-78 ± 63*	70 ± 55*	11 ± 43
	Mean absolute difference	84 ± 55	74 ± 50	39 ± 21
	as % of mean ICV with manual segmentation	6	5	3
	Dice's similarity coefficient	0.95 ± 0.01	0.93 ± 0.007	0.95 ± 0.007

All volumes are expressed as means (in cc) ± SD. The DSC is shown as mean ± SD. TBV, total brain volume (sum of supratentorial GM and WM, cerebellar and brainstem volume); SGM, supratentorial GM volume; SWM, supratentorial WM volume; CSF, total cerebrospinal fluid volume; ICV, intracranial volume. Differences between automated and manual measurements were tested for each method separately using Wilcoxon signed rank test (* $p < 0.05$).

Summary

A summary of the results of the robustness across field strengths as well as the accuracy analysis can be found in Table 2.4.

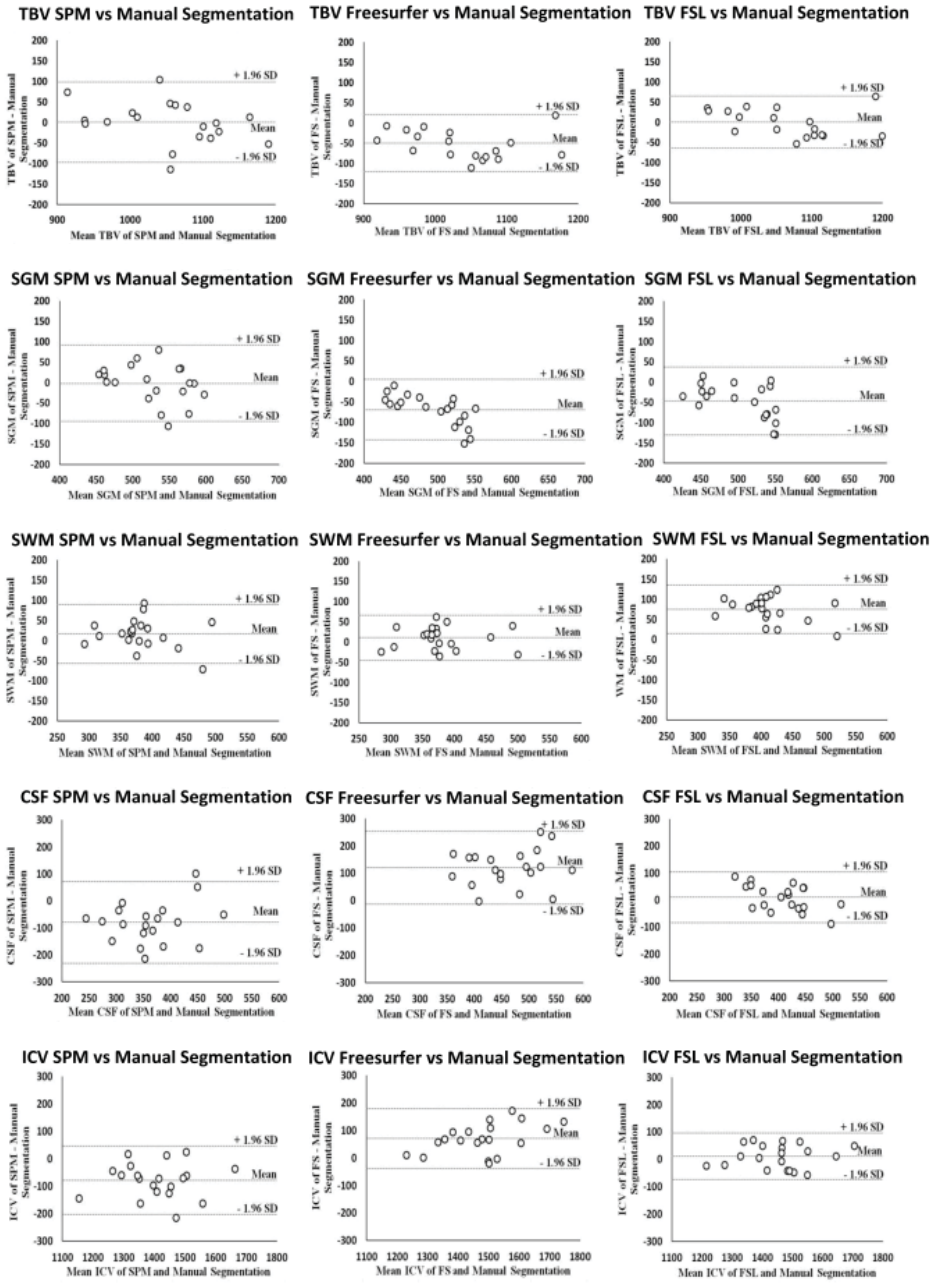

Figure 2.4 | Bland-Altman plots automated versus manual volume measurements. X-axis: mean brain volume measurement of automated and manual volume measurements. Y-axis: difference (in cc) in brain volume measurement between automated and manual volume measurements. The mean, lower (-1.96 SD) and upper (+ 1.96 SD) limits of agreement are shown. A negative difference on the y-axis is seen when brain volume measurements were larger with manual volume measurements than with automated volume measurements. TBV, total brain volume; GM, gray matter volume; WM, white matter volume; CSF, cerebrospinal fluid volume; ICV, intracranial volume.

Table 2.4 | Summary of robustness across field strength and accuracy results

	TBV		GM		WM		CSF		ICV	
	R	A	R	A	R	A	R	A	R	A
SPM	4%	3%	5%	7%	4%	8%	14%	24%	2%	6%
Freesurfer	< 1%	5%	1%	13%	2%	7%	34%	30%	9%	5%
FSL	1%	3%	2%	9%	3%	20%	10%	10%	3%	3%

R, robustness, shown as the mean absolute difference between 3T and 1.5T measurements as a percentage of the mean measurement at 3T; A, accuracy, shown as the mean absolute difference between automated and manual measurements as a percentage of the mean manual measurement.

DISCUSSION

Brain volumes and ICV could be measured quite robustly in scans acquired using different MRI acquisition techniques. However, performance of SPM, Freesurfer and FSL varied depending on the assessed compartment.

Comparison with previous studies

Few studies have evaluated the robustness across different field strengths of brain volume and ICV measurements. Previous work has focused on ICV measurements with older software versions of SPM, Freesurfer and/or FSL.[4,5] One study assessed robustness of ICV measurements across field strengths using SPM5 and the Brain Extraction Tool (BET) of FSL and compared it with their own method.[5] This study showed that especially SPM5 and to a lesser extent BET showed large differences between ICV measurements at 3T and 1.5T. Another study focused on ICV measurements across field strengths obtained with Freesurfer.[4] This study showed that, using Freesurfer, systematic bias occurred in ICV measurements between 3T and 1.5T. The findings of both studies are in line with our study, showing that bias can occur in ICV measurements between 3T and 1.5T MRI data, especially when using Freesurfer. This might be caused by Freesurfer's registration procedure, which is susceptible to (slight) differences in MRI acquisition techniques. Contrary to a previous study, SPM did show robust ICV measurements in our study.[5] This could be due to recent improvements in the segmentation algorithm (tissue classification, bias correction and image registration in the same generative model). The suboptimal performance of Freesurfer for ICV assessment is clearly an important issue. Correction for inter-subject variation in head size by using ICV is common practice in studies of brain volume and brain atrophy.[31] Hence, bias in ICV thus also affects brain volume analyses.[32] To avoid this, a segmentation method should be chosen that has a robust ICV segmentation. Since none of the methods in our current study was robust as well as accurate for all

volumes, it may be feasible to combine measurements obtained with different methods to get both robust and accurate brain volume and ICV measurements. As for robustness across spatial resolutions, we found similar results than two previous studies.[4,33] These studies, that only investigated the performance of (older versions of) Freesurfer, showed differences in spatial resolution could lead to variations in brain volume measurements. For a detailed overview of previous studies on robustness of brain volumes and other brain MRI abnormalities, specifically in the context of ageing related cerebrovascular disease, we refer to recently published work.[34]

Strengths and limitations

The strength of our study is the set of high quality scan-rescan data, the selection of subjects (comparable with subjects in brain ageing studies, but without a primary cerebral disease) and the large number of manually segmented scans that allowed us to make a reliable comparison of the performance of the brain segmentation methods. In addition, our study is the first that assessed the robustness across different MRI acquisition techniques as well as accuracy of the most recent versions of three widely used automated methods for brain volume measurements in a common framework.

A limitation could be that manual segmentations were performed on MRI slices with a thickness of 3 mm. Although manual segmentations of higher resolution data might be preferable (i.e. with a slice thickness of 1 mm), creating these manual segmentations is very labor intensive. By selecting a lower resolution we chose to invest in a higher quantity of datasets to better include variations in brain anatomy. Importantly, our results were similar for non-down sampled 3D T1 images. Another limitation could be the relatively small sample size. However, we chose to invest in a high quality dataset that could assess both robustness and accuracy.

As is common in brain segmentation studies, we have compared binary manual segmentations with probabilistic (partial volume estimated) automated segmentations. Another approach could be the creation of probabilistic manual segmentations (e.g. by combining binary manual segmentations of the same subject but performed by different raters into a single probabilistic segmentation.[35] However, this is very labor intensive and has limited added value compared with manually segmenting more subjects.

Another limitation could be that variations in scanner related parameters might give differences in the measures of robustness of the different methods. Therefore, MRI data acquired with scanner parameters that are different from the ones we have used could possibly lead to a different ranking in performance of the methods for one or more of the

tissue compartments considered. Moreover, presence of severe brain abnormalities (for example as seen in patients with dementia or multiple sclerosis) could potentially also lead to a different ranking in performance of the methods, as some methods might be more robust for brain abnormalities. Generalizability of our results should therefore be performed with caution.

Conclusions

We showed that robust brain volume measurements can be obtained with state-of-the-art generic brain MRI analysis packages in datasets with different MRI acquisitions (such as different field strengths). However, all methods showed variations in robustness and accuracy over various tissue compartments. This needs to be taken into account when selecting an appropriate method in multicenter brain imaging studies.

Acknowledgments

The authors thank Hugo Kuijf for his contribution to this study in obtaining brain volume measurements with MeVisLab for FSL segmentation results. The authors also thank Nora Visser and Nicolette Notermans for their help with recruiting patients that were used in the robustness analysis.

REFERENCES

1. Carrillo MC, Bain LJ, Frisoni GB, Weiner MW. Worldwide Alzheimer's disease neuroimaging initiative. Alzheimers Dement. 2012;8:337–42.
2. Williamson JD, Miller ME, Bryan RN, Lazar RM, Coker LH, Johnson J, et al. The Action to Control Cardiovascular Risk in Diabetes Memory in Diabetes Study (ACCORD-MIND): Rationale, Design, and Methods. Am J Cardiol. 2007;99:112–22.
3. Mueller SG, Weiner MW, Thal LJ, Petersen RC, Jack CR, Jagust W, et al. Ways toward an early diagnosis in Alzheimer's disease: The Alzheimer's Disease Neuroimaging Initiative (ADNI). Alzheimer's Dement. 2005;1:55–66.
4. Jovicich J, Czanner S, Han X, Salat D, van der Kouwe A, Quinn B, et al. MRI-derived measurements of human subcortical, ventricular and intracranial brain volumes: Reliability effects of scan sessions, acquisition sequences, data analyses, scanner upgrade, scanner vendors and field strengths. Neuroimage. 2009;46:177–92.
5. Keihaninejad S, Heckemann RA, Fagiolo G, Symms MR, Hajnal J V., Hammers A A robust method to estimate the intracranial volume across MRI field strengths (1.5T and 3T). Neuroimage. 2010;50:1427–37.
6. Jovicich J, Marizzoni M, Sala-Llonch R, Bosch B, Bartre's-Faz D, Arnold J, et al. Brain morphometry reproducibility in multi-center 3T MRI studies: A comparison of cross-sectional and longitudinal segmentations. Neuroimage. 2013;83:472–84.
7. De Bresser J, Tiehuis AM, Van Den Berg E, Reijmer YD, Jongen C, Kappelle LJ, et al. Progression of cerebral atrophy and white matter hyperintensities in patients with type 2 diabetes. Diabetes Care. 2010;33:1309–14.
8. de Bresser J, Portegies MP, Leemans A, Biessels GJ, Kappelle LJ, Viergever MA. A comparison of MR based segmentation methods for measuring brain atrophy progression. Neuroimage. 2011;54:760–8.
9. Ashburner J, Friston KJ. Unified segmentation. Neuroimage. 2005;26:839–51.
10. Fischl B, Salat DH, Busa E, Albert M, Dieterich M, Haselgrove C, et al. Whole brain segmentation: Automated labeling of neuroanatomical structures in the human brain. Neuron. 2002;33:341–55.
11. Smith SM, Zhang Y, Jenkinson M, Chen J, Matthews PM, Federico A, et al. Accurate, robust, and automated longitudinal and cross-sectional brain change analysis. Neuroimage. 2002;17:479–89.
12. Weiskopf N, Suckling J, Williams G, Correia M. MM, Inkster B, Tait R, et al. Quantitative multi-parameter mapping of R1, PD*, MT, and R2* at 3T: A multi-center validation. Front Neurosci. 2013;7:1–11.
13. Dale AM, Fischl B, Sereno MI. Cortical Surface-Based Analysis. Neuroimage. 1999;9:179–94.
14. Fischl B, Salat DH, Van Der Kouwe AJW, Makris N, Ségonne F, Quinn BT, et al. Sequence-independent segmentation of magnetic resonance images. Neuroimage. 2004;23:69–84.
15. Sled JG, Zijdenbos AP, Evans AC. A nonparametric method for automatic correction of intensity nonuniformity in MRI data. IEEE Trans Med Imaging. 1998;17:87–97.
16. Ségonne F, Dale AM, Busa E, Glessner M, Salat D, Hahn HK, et al. A hybrid approach to the skull stripping problem in MRI. Neuroimage. 2004;22:1060–75.
17. Fischl B. FreeSurfer. NeuroImage. 2012;62:774–81.
18. Smith SM, De Stefano N, Jenkinson M, Matthews PM. Normalized accurate measurement of longitudinal brain change. J Comput Assist Tomogr. 2001;25:466–75.
19. Smith SM, Jenkinson M, Woolrich MW, Beckmann CF, Behrens TEJ, Johansen-Berg H, et al. Advances in functional and structural MR image analysis and implementation as FSL. Neuroimage. 2004;23:208-19.

20. Smith SM. Fast robust automated brain extraction. Hum Brain Mapp. 2002;17:143–55.
21. Jenkinson M, Smith S. A global optimisation method for robust affine registration of brain images. Med Image Anal. 2001;5:143–56.
22. Jenkinson M, Bannister P, Brady M, Smith S. Improved optimization for the robust and accurate linear registration and motion correction of brain images. Neuroimage. 2002;17: 825–41.
23. Zhang Y, Brady M, Smith S. Segmentation of brain MR images through a hidden Markov random field model and the expectation-maximization algorithm. IEEE Trans Med Imaging. 2001;20:45–57.
24. Popescu V, Battaglini M, Hoogstrate WS, Verfaillie SCJ, Sluimer IC, van Schijndel RA, et al. Optimizing parameter choice for FSL-Brain Extraction Tool (BET) on 3D T1 images in multiple sclerosis. Neuroimage. 2012;61:1484–94.
25. Visser NA, Vrancken AFJE, Van Der Schouw YT, Van Den Berg LH, Notermans NC. Chronic idiopathic axonal polyneuropathy is associated with the metabolic syndrome. Diabetes Care. 2013;36:817–22.
26. Martin Bland J, Altman D. Statistical Methods for Assessing Agreement Between Two Methods of Clinical Measurement. Lancet. 1986;327:307–10.
27. Reijmer YD, Leemans A, Brundel M, Kappelle LJ, Biessels GJ. Disruption of the cerebral white matter network is related to slowing of information processing speed in patients with type 2 diabetes. Diabetes. 2013;62:2112–5.
28. Mendrik AM, Vincken KL, Kuijf HJ, Breeuwer M, Bouvy WH, De Bresser J, et al. MRBrainS Challenge: Online Evaluation Framework for Brain Image Segmentation in 3T MRI Scans. Comput Intell Neurosci. 2015;2015:813696.
29. Klein S, Staring M, Murphy K, Viergever MA, Pluim JPW. Elastix: A toolbox for intensity-based medical image registration. IEEE Trans Med Imaging. 2010;29:196–205.
30. Friston K. Dynamic causal models for fMRI. Statistical Parametric Mapping: The Analysis of Functional Brain Images. London: Academic Press; 2007.
31. Barnes J, Ridgway GR, Bartlett J, Henley SMD, Lehmann M, Hobbs N, et al. Head size, age and gender adjustment in MRI studies: A necessary nuisance? Neuroimage. 2010;53:1244–55.
32. Nordenskjöld R, Malmberg F, Larsson EM, Simmons A, Brooks SJ, Lind L, et al. Intracranial volume estimated with commonly used methods could introduce bias in studies including brain volume measurements. Neuroimage. 2013;83:355–60.
33. Wonderlick JS, Ziegler DA, Hosseini-Varnamkhasti P, Locascio JJ, Bakkour A, van der Kouwe A, et al. Reliability of MRI-derived cortical and subcortical morphometric measures: Effects of pulse sequence, voxel geometry, and parallel imaging. Neuroimage. 2009;44:1324–33.
34. De Guio F, Jouvent E, Biessels GJ, Black SE, Brayne C, Chen C, et al. Reproducibility and variability of quantitative magnetic resonance imaging markers in cerebral small vessel disease. J Cereb Blood Flow Metab. 2016;36:1319–37.
35. De Bresser J, Vincken KL, Kaspers AJ, Rinkel GJE, Viergever MA, Biessels GJ. Quantification of cerebral volumes on MRI 6 months after aneurysmal subarachnoid hemorrhage. Stroke. 2012;43:2782–4.

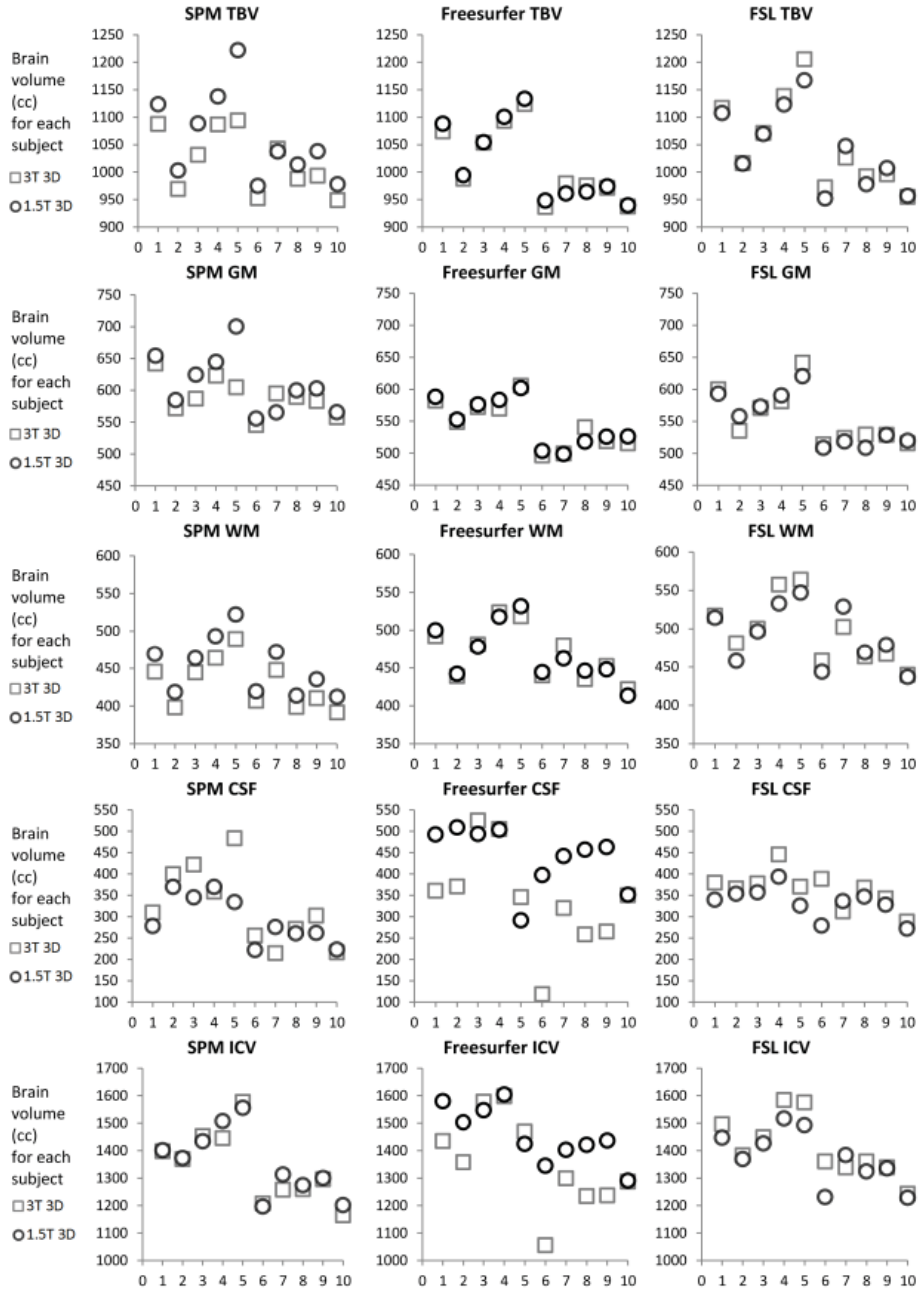

Supplementary Figure S2.1 | Individual automated volume measurements 3T and 1.5T. X-axis: subject number. Y-axis: individual brain volume measurements (in cc). TBV, total brain volume; GM, gray matter volume; WM, white matter volume; CSF, cerebrospinal fluid volume; ICV, intracranial volume.

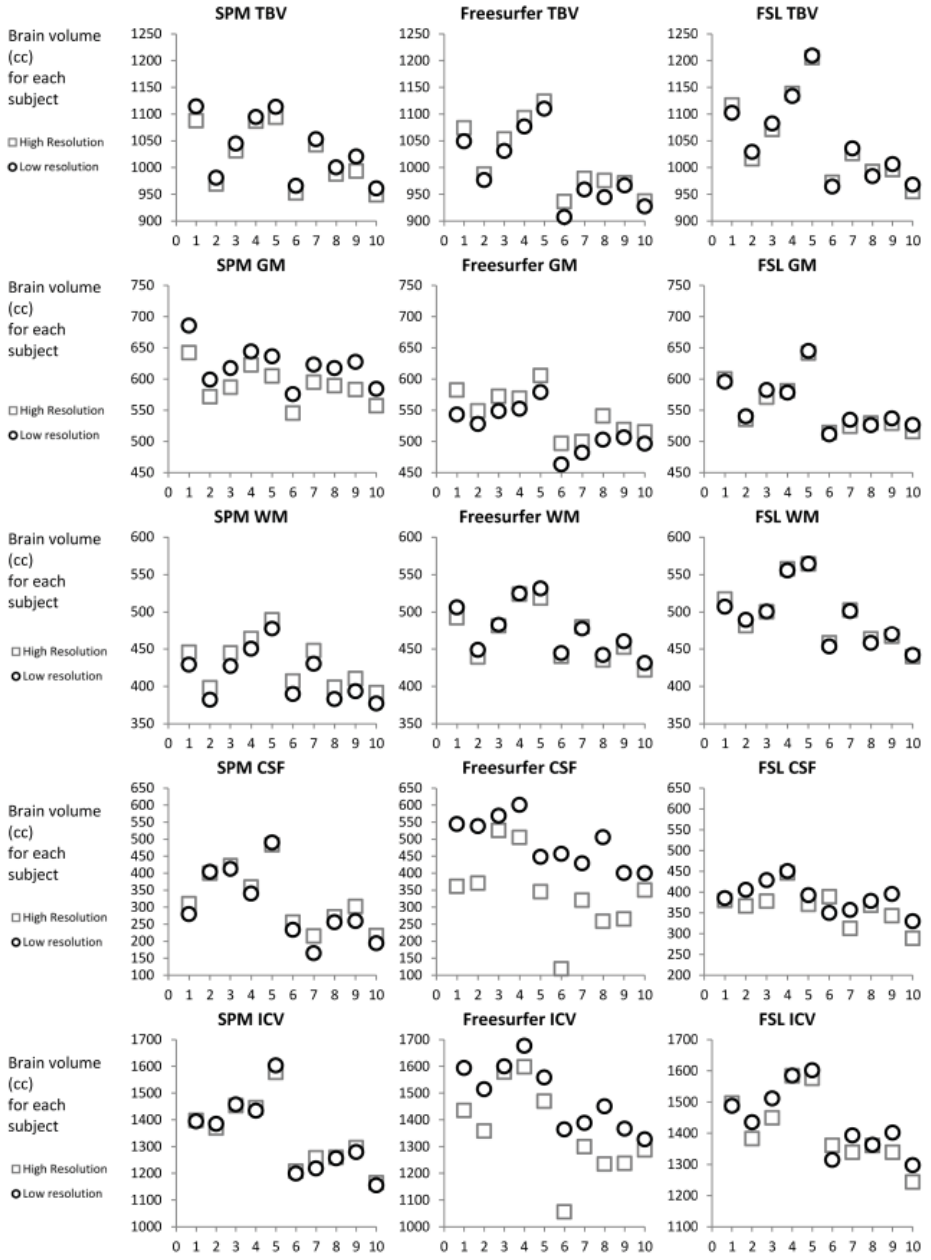

Supplementary Figure S2.2 | Individual automated volume measurements high and low spatial resolution. X-axis: subject number. Y-axis: individual brain volume measurements (in cc). TBV, total brain volume; GM, gray matter volume; WM, white matter volume; CSF, cerebrospinal fluid volume; ICV, intracranial volume.

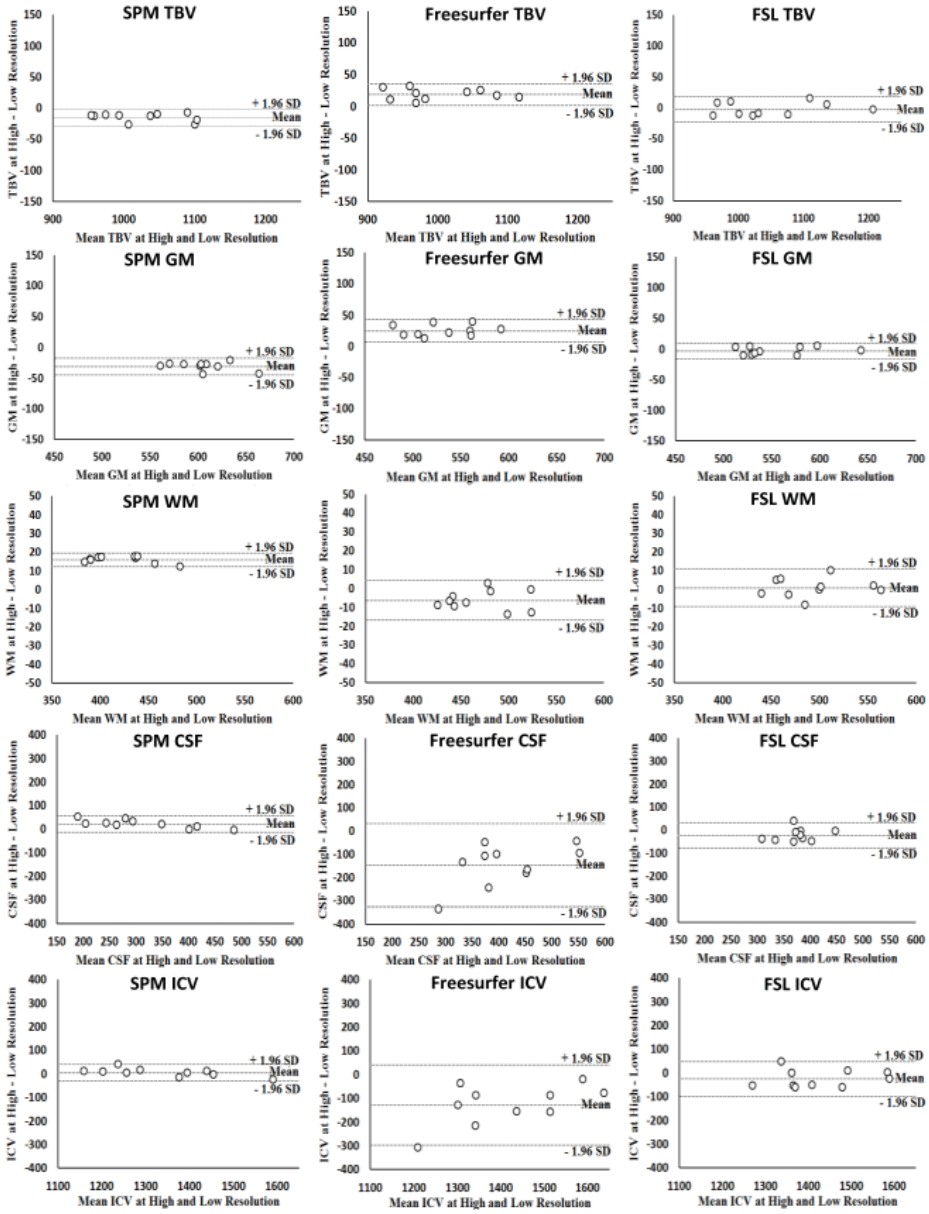

Supplementary Figure S2.3 | Bland-Altman plots high and low spatial resolution. X-axis: mean brain volume measurement at high and low spatial resolution. Y-axis: difference (in cc) in brain volume measurement between high and low spatial resolution. The mean, lower (-1.96 SD) and upper (+1.96 SD) limits of agreement are shown. A negative difference on the y-axis is seen when brain volume measurement at a lower resolution was larger than at a higher resolution. TBV, total brain volume; GM, gray matter volume; WM, white matter volume; CSF, cerebrospinal fluid volume; ICV, intracranial volume.

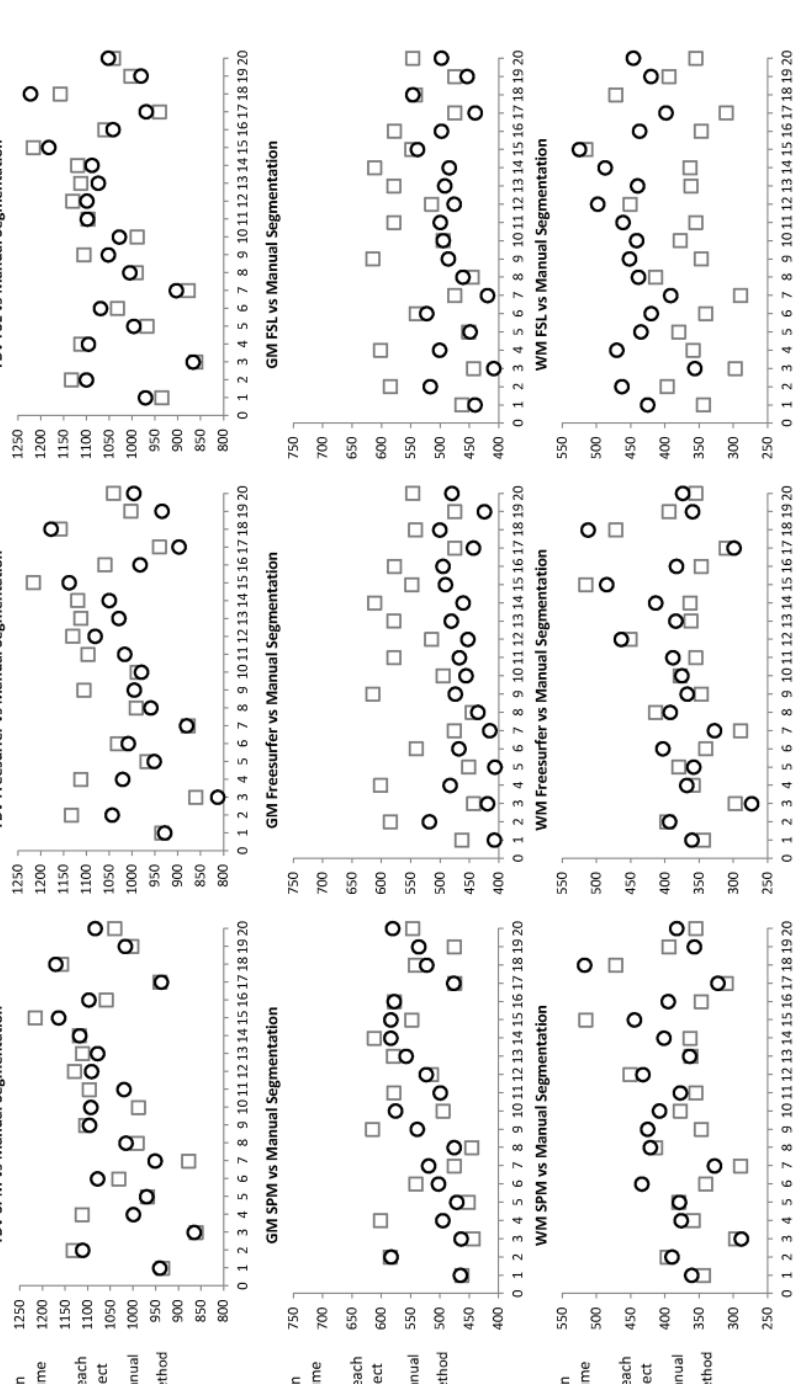

Supplementary Figure S2.4 | Individual automated and manual TBV, GM and WM measurements. TBV, total brain volume; GM, supratentorial gray matter volume; WM, supratentorial white matter volume.

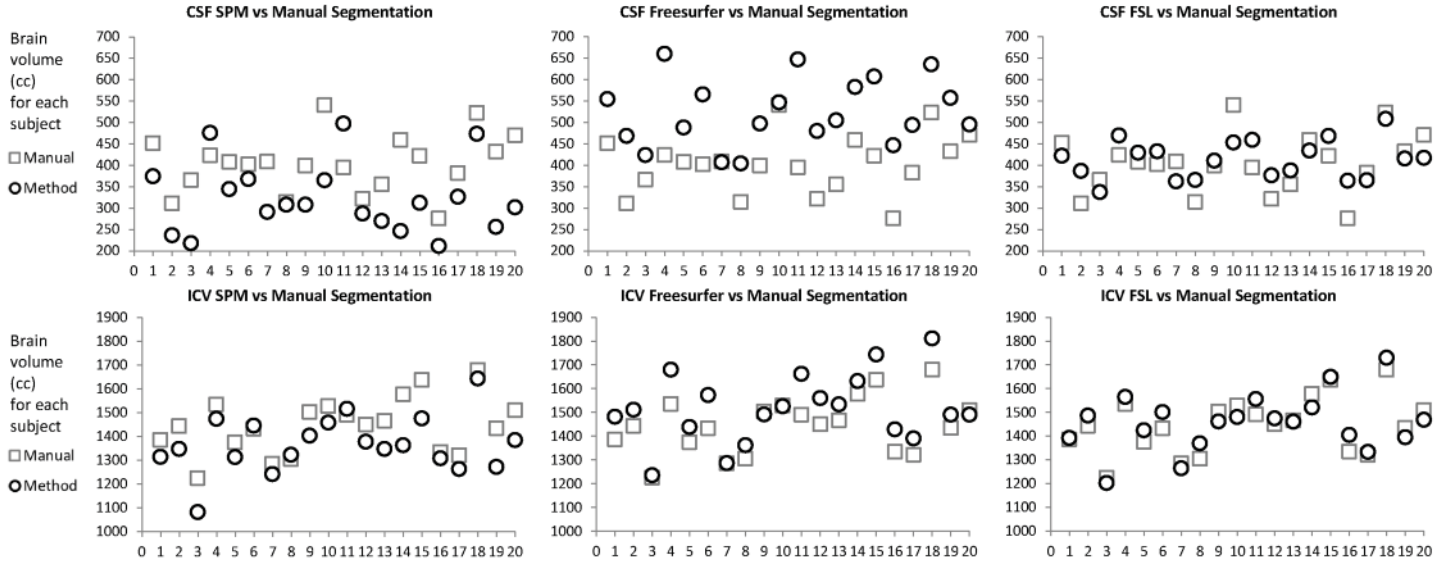

Supplementary Figure S2.5 | Individual automated and manual CSF and ICV measurements. CSF, total cerebrospinal fluid volume; ICV, intracranial volume.

Supplementary Table S2.1 | Automated volume measurements across different spatial resolutions (n = 10)

		Resolution	SPM	Freesurfer	FSL
TBV	3T	Low	1035 ± 59	995 ± 68	1052 ± 80
		High	1020 ± 57	1013 ± 67	1049 ± 82
GM	3T	Low	621 ± 32	520 ± 36	558 ± 42
		High	590 ± 29	545 ± 37	554 ± 43
WM	3T	Low	414 ± 34	475 ± 36	494 ± 41
		High	430 ± 33	468 ± 36	495 ± 42
CSF	3T	Low	303 ± 105	489 ± 72	387 ± 36
		High	323 ± 90	342 ± 118	364 ± 43
ICV	3T	Low	1338 ± 140	1484 ± 121	1439 ± 106
		High	1343 ± 128	1355 ± 168	1413 ± 111

All volumes are expressed as means (in cc) ± SD. TBV, total brain volume; GM, gray matter volume; WM, white matter volume; CSF, cerebrospinal fluid volume; ICV, intracranial volume; T, Tesla.

Supplementary Table S2.2 | Robustness analysis across different spatial resolutions (n = 10)

			SPM	Freesurfer	FSL
TBV	High vs low (3T)	Mean difference	-15 ± 7*	18 ± 9*	-3 ± 11
		Mean absolute difference	15 ± 7	18 ± 9	10 ± 4
		as % of mean TBV at 3D	2	2	1
		Coefficient of repeatability	33	40	21
		as % of mean TBV at 3D	3	4	2
GM	High vs low (3T)	Mean difference	-31 ± 7*	25 ± 9*	-3 ± 7
		Mean absolute difference	31 ± 7	25 ± 9	6 ± 4
		as % of mean GM at 3D	5	5	1
		Coefficient of repeatability	64	53	14
		as % of mean GM at 3D	11	10	3
WM	High vs low (3T)	Mean difference	16 ± 2*	-6 ± 5*	< 1 ± 5
		Mean absolute difference	16 ± 2	7 ± 5	4 ± 3
		as % of mean WM at 3D	4	1	1
		Coefficient of repeatability	32	16	10
		as % of mean WM at 3D	7	4	2
CSF	High vs low (3T)	Mean difference	20 ± 18	-147 ± 91*	-23 ± 29*
		Mean absolute difference	22 ± 15	147 ± 91	31 ± 19
		as % of mean CSF at 3D	7	43	9
		Coefficient of repeatability	53	341	71
		as % of mean CSF at 3D	16	99.8	20
ICV	High vs low (3T)	Mean difference	5 ± 18	-129 ± 86*	-26 ± 38*
		Mean absolute difference	14 ± 12	129 ± 86	37 ± 25
		as % of mean ICV at 3D	1	9	3
		Coefficient of repeatability	35	305	88
		as % of mean ICV at 3D	3	23	6

All volumes (in cc) are expressed as means ± SD. Coefficients of repeatability are expressed as a volume (in cc). TBV, total brain volume; GM, gray matter volume; WM, white matter volume; CSF, cerebrospinal fluid volume; ICV, intracranial volume; T, Tesla. Mean differences between high and low resolutions were tested for each method separately using Wilcoxon signed rank test (* $p < 0.05$).

Chapter 3

Performance of five automated white matter hyperintensity segmentation methods in a multicenter dataset

Rutger Heinen
Martijn D. Steenwijk
Frederik Barkhof
J. Matthijs Biesbroek
Wiesje M. van der Flier
Hugo J. Kuijf
Niels D. Prins
Hugo Vrenken
Geert Jan Biessels
Jeroen de Bresser
on behalf of the TRACE-VCI study group*

* Members of TRACE-VCI study group are mentioned in the acknowledgements

In revision

ABSTRACT

White matter hyperintensities (WMHs) are a common manifestation of cerebral small vessel disease, that is increasingly studied with large, pooled multicenter datasets. This data pooling increases statistical power, but poses challenges for automated WMH segmentation. Although there is extensive literature on the evaluation of automated WMH segmentation methods, such evaluations in a multicenter setting are lacking. We performed WMH segmentations in sixty patients scanned on six different magnetic resonance imaging (MRI) scanners (10 patients per scanner) using five freely available and fully-automated WMH segmentation methods (Cascade, kNN-TTP, Lesion-TOADS, LST-LGA and LST-LPA). Different MRI scanner vendors and field strengths were included. We compared these automated WMH segmentations with manual WMH segmentations as a reference. Performance of each method both within and across scanners was assessed using spatial and volumetric correspondence with the reference segmentations by Dice's similarity coefficient (DSC) and intra-class correlation coefficient (ICC) respectively. We found the best performance, both within and across scanners, for kNN-TTP, followed by LST-LPA and LST-LGA, with worse performance for Lesion-TOADS and Cascade. Our findings can serve as a guide for choosing a method and also highlight the importance to further improve and evaluate consistency of methods in a multicenter setting.

INTRODUCTION

Pooling of multicenter brain magnetic resonance imaging (MRI) data is a trend in various research fields, including studies on ageing related brain diseases.[1–3] Pooling of multicenter data increases sample size (and thus statistical power) and can support a faster patient inclusion. Moreover, findings of multicenter studies may have a larger external validity and are more readily translatable to a clinical setting. However, pooling of brain MRI data poses challenges in automated segmentation due to variations in image acquisition.

White matter hyperintensities of presumed vascular origin (WMHs) are frequently encountered in studies on ageing related brain diseases. Achieving accurate and precise WMH segmentations can be challenging across MRI scanners of different vendors, field strengths and scan protocols. Variability in MRI acquisition can lead to differences in the contrast and borders of WMHs and thereby quantification bias.[4–6]

Several automated and semi-automated methods to segment WMHs currently exist, using various algorithms that rely on intensity, spatial information, or both.[5] These methods can be broadly classified as supervised (i.e. trained using manual segmentations as a reference),[7,8] unsupervised (without training)[9–11] and semi-supervised (with only a small portion of the available data used for training.[12] A recent study provided an extensive overview of existing supervised, unsupervised and semi-supervised methods.[13] Challenges for these methods include false positive (e.g. artefacts, infarcts) and false negative (often for punctate lesions) results. Other challenges include dealing with varying WMH lesion loads (usually lower in MS than in patients with WMHs of presumed vascular origin) and with co-occurring pathologies (e.g. extensive atrophy). There is extensive literature on the evaluation of WMH segmentation methods in different settings, also addressing these challenges.[4] However, the performance of such methods is typically evaluated on single center, single scanner datasets. For WMHs of presumed vascular origin, there is a lack of studies comparing performance of these methods in multicenter, multiscanner datasets and this is an important knowledge gap.[4,14]

Therefore, the present study aimed to assess performance, in terms of spatial and volumetric correspondence with reference segmentations, of five automated WMH segmentation methods in a multicenter, multiscanner dataset of patients with WMHs of presumed vascular origin. In particular, we also addressed which methods showed variation in performance across scanners. In addition, we assessed if performance was dependent on WMH lesion load. To this end, we selected five methods that were fully automatic and freely available for academic research: Cascade,[15,16] k-nearest neighbor classification with tissue type priors (kNN-TTP),[17] Lesion-TOpology-preserving Anatomical Segmentation

(Lesion-TOADS),[11] the Lesion Segmentation Tool Lesion Prediction Algorithm (LST-LPA) and the Lesion Segmentation Tool Lesion Growth Algorithm (LST-LGA).[10]

RESULTS

Reference segmentations

The reference segmentations showed a very good inter-rater agreement regarding spatial (Dice's similarity coefficient (DSC) ± standard deviation (SD): 0.80 ± 0.09) and volumetric agreement (Intra-class correlation coefficient (ICC): 0.97). The intra-rater agreement (DSC ± SD: 0.80 ± 0.08; ICC: 0.99) was also very good. In the test set, seventeen subjects had a Fazekas rating of 1, eighteen subjects had a 2 and seven subjects had a 3. The mean WMH volume (± SD) was 21 ± 10 mL with a median of 10 mL and volumes per patient ranging from 0.9 to 199 mL (see Table 3.1).

Table 3.1 | Mean WMH volume of the reference segmentations and the segmentations of the methods for each scanner (n = 42; n = 7 per scanner)

WMH volume	GE Signa HDx 1.5T	GE Signa HDxt 3T	GE Discovery MR750 3T	Philips Ingenuity 3T	Philips Ingenia 3T	Philips Achieva 3T	Overall mean ± SD
Reference	22 ± 31	16 ± 18	9 ± 10	14 ± 17	41 ± 71	24 ± 26	21 ± 10
Cascade	26 ± 20	19 ± 11	13 ± 5	19 ± 10	12 ± 4	11 ± 5	17 ± 5
kNN-TTP	16 ± 19	14 ± 13	9 ± 10	14 ± 17	32 ± 49	20 ± 22	18 ± 7
Lesion-TOADS	19 ± 20	16 ± 12	11 ± 9	36 ± 24	30 ± 45	31 ± 16	24 ± 9
LST-LGA	20 ± 19	19 ± 23	12 ± 15	15 ± 20	22 ± 28	14 ± 17	17 ± 4
LST-LPA	18 ± 22	15 ± 18	11 ± 13	14 ± 18	33 ± 51	18 ± 22	18 ± 7

Values represent mean WMH volumes ± SD in mL. Reference: reference segmentations.

Quality assessment

Examples of the automated WMH segmentation results are shown in Figure 3.1. Several differences between methods can be visually appreciated. For example, methods seemed to differ on how they segment (over or under) different types of WMHs (i.e. periventricular, confluent and punctuate WMHs). Also, the nature of segmentation errors varied between methods (i.e. false-positive (FP) versus false-negative (FN) WMH voxels: see Figure 3.1). In a quantitative analysis, kNN-TTP showed the lowest mean FP and FN volumes (mean FP volume ± SD / mean FN volume ± SD: 2 ± 2 / 5 ± 11 mL), followed by LST-LPA (4 ± 4 / 6

± 10 mL), LST-LGA (5 ± 5 / 8 ± 19 mL). Cascade showed a lower mean FP volume (8 ± 7 mL) but higher mean FN volume (12 ± 29 mL) than Lesion-TOADS (10 ± 16 / 7 ± 12 mL).

Figure 3.1 | WMH segmentations of the methods regarding periventricular, confluent and punctuate WMHs. Example of WMH segmentations for a subject (subject A) with predominantly periventricular WMHs (panel A), a subject (subject B) with large confluent WMHs (panel B) and a subject (subject C) with predominantly punctuate WMHs (panel C). Top row panels A-C: original FLAIR scan and WMH reference segmentation (green) and WMH segmentations of all methods (red) are shown. Bottom row panels A-C: false negative voxels are shown in blue; false positive voxels are shown in yellow.

Performance of WMH segmentation methods

Performance of each method, both within and averaged across all scanners, is shown in Table 3.2. The highest mean performance across scanners was seen for kNN-TTP, both in terms of spatial correspondence with the reference segmentations (mean DSC ± SD: 0.73 ± 0.03) as in terms of volumetric correspondence with the reference segmentations (mean ICC ± SD: 0.97 ± 0.02) (see Table 3.2). LST-LPA showed a slightly lower performance in terms of volumetric correspondence (mean ICC ± SD: 0.92 ± 0.03) and performed less than

Table 3.2 | Performance of the WMH segmentation methods compared to the reference segmentations (n = 42; n = 7 per scanner)

Method	Measure	GE Signa HDxt 1.5T	GE Signa HDxt 3T	GE Discovery MR750 3T	Philips Ingenuity 3T	Philips Ingenia 3T	Philips Achieva 3T	Overall mean ± SD
Ref	WMH	22 ± 31	16 ± 18	9 ± 10	14 ± 17	41 ± 71	24 ± 26	21 ± 10
Cascade	ΔWMH	4 ± 15	4 ± 19	4 ± 11	6 ± 12	-29 ± 68	-13 ± 22	-4 ± 13
	|ΔWMH|	12 ± 9	14 ± 12	10 ± 5	11 ± 6	32 ± 66	15 ± 21	16 ± 7
	DSC	0.48 ± 0.29	0.35 ± 0.20	0.34 ± 0.25	0.43 ± 0.22	0.40 ± 0.21	0.41 ± 0.14	0.40 ± 0.05
	ICC	0.45 (-0.19;0.87)	0.45 (-0.18;0.87)	*	0.44 (-0.16;0.86)	0.43 (-0.40;0.87)	0.46 (-0.32;0.88)	0.44 ± 0.01
kNN-TTP	ΔWMH	-5 ± 13	-2 ± 7	0.8 ± 3	0.9 ± 2	-9 ± 22	-4 ± 4	-3 ± 4
	|ΔWMH|	6 ± 13	5 ± 6	2 ± 2	1 ± 2	10 ± 21	4 ± 4	5 ± 3
	DSC	0.74 ± 0.11	0.68 ± 0.11	0.71 ± 0.12	0.74 ± 0.10	0.75 ± 0.14	0.76 ± 0.07	0.73 ± 0.03
	ICC	0.99 (0.94;1.00)	0.95 (0.73;0.99)	0.97 (0.76;0.99)	0.96 (0.80;0.99)	0.99 (0.95;1.00)	0.98 (0.88;1.00)	0.97 ± 0.02
Lesion-TOADS	ΔWMH	-3 ± 10	0.5 ± 9	2 ± 3	23 ± 31	-11 ± 26	7 ± 24	3 ± 10
	|ΔWMH|	5 ± 9	6 ± 6	3 ± 2	25 ± 29	14 ± 24	16 ± 18	12 ± 8
	DSC	0.63 ± 0.21	0.56 ± 0.20	0.49 ± 0.22	0.43 ± 0.34	0.61 ± 0.15	0.46 ± 0.32	0.53 ± 0.08
	ICC	0.80 (0.28;0.96)	0.77 (0.22;0.96)	0.69 (-0.01;0.94)	*	0.93 (0.65;0.99)	0.08 (-0.54;0.73)	0.65 ± 0.29
LST-LGA	ΔWMH	-2 ± 13	4 ± 7	4 ± 6	2 ± 4	-19 ± 44	-10 ± 10	-4 ± 8
	|ΔWMH|	7 ± 11	6 ± 6	4 ± 5	3 ± 2	19 ± 44	10 ± 10	8 ± 5
	DSC	0.58 ± 0.16	0.53 ± 0.18	0.54 ± 0.12	0.53 ± 0.17	0.63 ± 0.18	0.59 ± 0.11	0.57 ± 0.03
	ICC	0.95 (0.70;0.99)	0.92 (0.62;0.99)	0.97 (0.78;1.00)	0.92 (0.61;0.99)	0.90 (0.32;0.98)	0.89 (-0.03;0.99)	0.92 ± 0.03
LST-LPA	ΔWMH	-3 ± 10	-0.2 ± 7	2 ± 5	0.6 ± 4	-8 ± 21	-6 ± 6	-2 ± 4
	|ΔWMH|	5 ± 8	4 ± 5	3 ± 5	3 ± 2	10 ± 20	7 ± 5	5 ± 2
	DSC	0.65 ± 0.13	0.52 ± 0.20	0.53 ± 0.17	0.59 ± 0.17	0.69 ± 0.15	0.63 ± 0.11	0.60 ± 0.06
	ICC	0.97 (0.85;1.00)	0.87 (0.47;0.98)	0.94 (0.71;0.99)	0.88 (0.43;0.98)	0.96 (0.80;0.99)	0.93 (0.54;0.99)	0.92 ± 0.04

WMH, ΔWMH, |ΔWMH| and DSC are shown as means ± SD. ICC is shown with 95% confidence interval. Ref, Reference; WMH, WMH volume (mL); ΔWMH, difference in WMH volume (mL) between the reference segmentations and segmentations of the methods; |ΔWMH|, absolute difference in WMH volume (mL) between the reference segmentations and segmentations of the methods; DSC, dice similarity coefficient; ICC, intra-class correlation coefficient. *, negative ICC (not used for calculating the overall mean ICC).

kNN-TTP in terms of spatial correspondence (mean DSC ± SD: 0.60 ± 0.06). The mean absolute WMH volume differences between the methods and the reference segmentations were also lowest for kNN-TTP (5 ± 3 mL; percentage of the mean WMH volume of the reference segmentations: 24%) and LST-LPA (5 ± 2 mL; 24%) (see Table 3.2). Both methods did show a tendency for slight underestimation of the WMH volume compared to the reference segmentations. LST-LGA showed a performance comparable to LST-LPA (mean DSC ± SD: 0.57 ± 0.03; mean ICC ± SD: 0.65 ± 0.29) but with a larger mean absolute WMH volume difference (8 ± 5 mL; 38%). Performance was lower for Lesion-TOADS (0.53 ± 0.08 / 0.65 ± 0.29) and Cascade (0.40 ± 0.05 / 0.44 ± 0.01) with also markedly higher mean absolute WMH volume differences for both methods (Lesion-TOADS: 12 ± 8 mL; 57%; Cascade: 16 ± 7 mL; 76%) (see Table 3.2).

Because some methods (Cascade, Lesion-TOADS, LST-LGA, and LST-LPA) do not necessarily have to be trained, analyses were repeated on all subjects (n = 60) without training of the methods. This did not change the ranking of methods (data not shown). The average run time was shortest for Cascade (2 minutes), followed by kNN-TTP (10 minutes), LST-LPA (12 minutes), LST-LGA (25 minutes) and Lesion-TOADS (30 minutes).

Variations in performance across scanners

For each method, we determined if the DSC (i.e. spatial correspondence with the reference standard) for each scanner differed relative to the other five scanners (Table 3.3). In this analysis, consistency of a method across scanners is reflected in small effect sizes. kNN-TTP showed the smallest variation in performance with the smallest effect sizes (range unstandardized beta coefficient: -0.06 to 0.01), followed by LST-LGA (-0.04 to 0.07), Cascade (-0.08 to 0.09), LST-LPA (-0.10 to 0.11) and Lesion-TOADS (-0.12 to 0.12). None of the effect sizes were significant after family wise error rate correction for multiple testing. Along the same lines, consistency of volumetric correspondence across scanners was assessed, by determining for each method the interaction between scanner and the relation between the assessed volume and the reference volume. Here we found a significant interaction for Lesion-TOADS on the Philips Ingenuity 3T scanner (family wise error rate corrected $p < 0.05$), indicating that performance was biased by scanner type. All other interactions were not significant (data not shown).

Performance of WMH segmentation methods for different WMH lesion loads

For all methods the DSC increased when Fazekas scores increased (see Table 3.4), as the DSC is particularly dependent on the absolute lesion load and the size of the individual lesions.18 kNN-TTP and LST-LPA showed a good volumetric correspondence compared to

Table 3.3 | Variation in performance across scanners by means of multiple linear regression analyses (n = 42; n = 7 per scanner)

Method	GE Signa HDxt 1.5T	GE Signa HDxt 3T	GE Discovery MR750 3T	Philips Ingenuity 3T	Philips Ingenia 3T	Philips Achieva 3T
Cascade	0.09 [-0.09;0.27]	-0.06 [-0.24;0.12]	-0.08 [-0.26;0.10]	0.03 [-0.15;0.21]	0.003 [-0.18;0.18]	0.01[-0.17;0.19]
kNN-TTP	0.01 [-0.08;0.10]	-0.06 [-0.15;0.03]	-0.03 [-0.12;0.07]	0.02 [-0.08;0.11]	0.03 [-0.06;0.12]	0.03 [-0.06;0.12]
Lesion-TOADS	0.12 [-0.08;0.33]	0.04 [-0.17;0.24]	-0.05 [-0.26;0.16]	-0.12 [-0.33;0.08]	0.10 [-0.11;0.30]	-0.08 [-0.29;0.12]
LST-LGA	0.02 [-0.11;0.14]	-0.04 [-0.17;0.09]	-0.03 [-0.16;0.10]	-0.04 [-0.17;0.09]	0.07 [-0.05;0.20]	0.02 [-0.10;0.15]
LST-LPA	0.06 [-0.07;0.20]	-0.10 [-0.24;0.03]	-0.09 [-0.23;0.05]	-0.01 [-0.15;0.13]	0.11 [-0.03;0.24]	0.03 [-0.10;0.17]

Data are represented as unstandardized beta coefficients with 95% confidence intervals. We assessed whether the DSC (as an outcome) depended on scanner (as a categorical variable with each scanner being compared to all other scanners as the reference) using linear regression analysis. A significant relation between a certain scanner and the DSC (family wise error rate corrected p-value of < 0.05 using a Bonferroni correction) indicates that the performance (in terms of spatial correspondence with the reference segmentation) was biased for that segmentation method by the use of that scanner (compared to the other scanners). As can be seen in the table, no significant relations were seen for any of the methods.

the reference segmentations across all WMH lesion loads (see Table 3.4 and Supplementary Figure S3.1). Also, variation in WMH volume measurements of these methods was small (i.e. narrow limits of agreement in the Bland Altman plots; see Figure 3.2). Cascade, Lesion-TOADS and LST-LGA showed greater variation for different WMH lesion loads (i.e. wider limits of agreement in the Bland Altman plots, see Figure 3.2). LST-LGA underestimated WMH volume at higher WMH lesion loads (see Figure 3.2 and Supplementary Figure S3.1). Cascade and Lesion-TOADS overestimated WMH volumes at lower WMH lesion loads, while Cascade underestimated WMH volumes at higher WMH lesion loads (see Figure 3.2 and Supplementary Figure S3.1).

Table 3.4 | Performance of WMH segmentation methods for different WMH lesion loads

Method	Fazekas scale	WMH volume reference	WMH volume method	ΔWMH	|ΔWMH|	DSC	ICC
Cascade	1	4 ± 4	12 ± 6	8 ± 6	8 ± 6	0.24 ± 0.16	0.02 (-0.12;0.27)
	2	16 ± 10	18 ± 11	2 ± 12	10 ± 6	0.50 ± 0.15	0.31 (-0.16;0.67)
	3	73 ± 61	26 ± 18	-47 ± 62	49 ± 60	0.54 ± 0.22	0.13 (-0.23;0.67)
kNN-TTP	1	4 ± 4	5 ± 4	0.4 ± 1	0.9 ± 0.6	0.64 ± 0.10	0.91 (0.67;0.97)
	2	16 ± 10	15 ± 9	-1 ± 3	3 ± 2	0.78 ± 0.06	0.96 (0.90;0.99)
	3	73 ± 61	56 ± 41	-17 ± 22	18 ± 21	0.82 ± 0.06	0.92 (0.62;0.99)
Lesion TOADS	1	4 ± 4	18 ± 20	13 ± 21	13 ± 21	0.35 ± 0.21	0.11 (-0.13;0.43)
	2	16 ± 10	19 ± 11	3 ± 13	6 ± 12	0.61 ± 0.20	0.50 (0.08;0.78)
	3	73 ± 61	53 ± 37	-20 ± 24	22 ± 22	0.77 ± 0.06	0.90 (0.49;0.98)
LST-LGA	1	4 ± 4	4 ± 5	-0.3 ± 2	2 ± 2	0.47 ± 0.12	0.76 (0.46;0.91)
	2	16 ± 10	15 ± 10	-0.4 ± 7	5 ± 5	0.61 ± 0.14	0.84 (0.63;0.94)
	3	73 ± 61	53 ± 17	-20 ± 48	31 ± 40	0.70 ± 0.08	0.68 (-0.11;0.94)
LST-LPA	1	4 ± 4	5 ± 5	0.3 ± 3	2 ± 2	0.49 ± 0.13	0.76 (0.45;0.91)
	2	16 ± 10	14 ± 10	-2 ± 6	4 ± 4	0.64 ± 0.14	0.85 (0.60;0.94)
	3	73 ± 61	62 ± 39	-11 ± 23	16 ± 18	0.78 ± 0.07	0.90 (0.53;0.98)

WMH, ΔWMH, |ΔWMH| and DSC are shown as means ± SD. ICC is shown as means (95% confidence interval). ΔWMH, mean difference in WMH volume (mL) between the reference segmentations and segmentations of the methods; |ΔWMH|, mean absolute difference in WMH volume (mL) between the reference segmentations and segmentations of the methods; DSC, dice similarity coefficient; ICC, intra-class correlation coefficient. Seventeen subjects had a Fazekas scale of 1, eighteen subjects had a Fazekas scale of 2 and seven subjects had a Fazekas scale of 3.

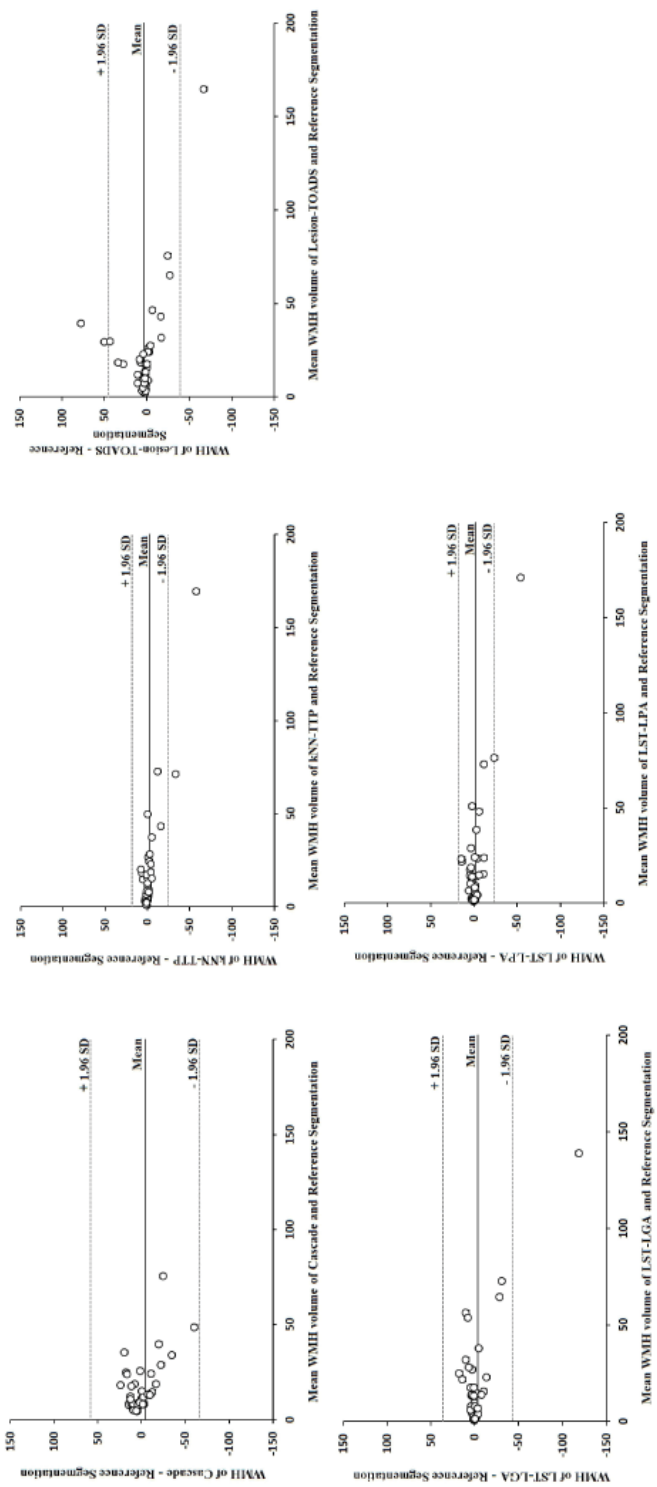

Figure 3.2 | Bland Altman plots comparing WMH volume of each method versus the WMH volume of the reference segmentations. X-axis: mean WMH volume (in mL) of the automated and reference segmentations. Y-axis: difference (in mL) in WMH volume between the automated and reference segmentations. The lower (-1.96 SD) and upper (+1.96 SD) limits of agreement (dashed lines) and mean (straight line) are shown. A narrow width of the limits of agreement reflects a small amount of variation between the measurements of the reference and automated WMH segmentations. A positive difference on the y-axis is seen when WMH volume as measured by the automated method was larger than the reference WMH volume (i.e. overestimation). A negative difference on the y-axis is seen when WMH volume as measured by the automated method was smaller than the reference WMH volume (i.e. underestimation).

DISCUSSION

The current study is the first to investigate the performance of five freely available and fully automated segmentation methods in a multicenter dataset of patients with WMHs of presumed vascular origin. Overall, performance of methods in terms of spatial and volumetric correspondence varied markedly both within and across scanners, with kNN-TTP and LST-LPA being the most consistent and best performing methods.

Many different automated methods currently exist to segment WMHs. Evaluation of these methods has mainly been performed in a single-center, single scanner setting, with variable performance across methods.[6–8,10,11,17,19–40] Some of these methods have also been assessed for scan-rescan reproducibility,[6,8,18] which is of particular importance when performing longitudinal research. However, since pooling of data across multiple centers is an important trend in small vessel disease research,[41] there also is a need for automated WMH segmentation methods that perform well across different scanners. Clearly, a multicenter setting with different scan vendors poses challenges, as the method cannot be tuned to one single scan protocol. The question is thus which methods perform robustly enough in such a setting, but this has been explored by few studies. A recent study, coordinated by our group, compared the performance of twenty methods, but in contrast to the present study, many of the tested methods are not freely available yet.[42] Two previous studies compared different linear and nonlinear classification techniques to segment WMHs of presumed vascular origin.[43,44] The important difference between these and the current is that they primarily focused on the optimal choice of classifiers for WMH segmentation, using a general preprocessing pipeline. By contrast, we evaluated some of the same classifiers as an integral part of a fully automated WMH segmentation method, where the classifier only partially determines the performance of the entire method.

We observed that for segmentation of WMHs of presumed vascular origin, performance of the five tested methods varied markedly, both within and across scanners. kNN-TTP and LST-LPA were the most consistent methods across scanners. kNN-TTP was also the best performing method within scanners with a DSC comparable to a manual segmentation as performed by a trained rater and an excellent ICC, whereas LST-LPA performed less with regard to spatial correspondence with the reference segmentations. This could be relevant when choosing a method to segment WMHs for further analysis where spatial information of WMHs is of particular importance (e.g. lesion symptom mapping).[45] By contrast, when analyzing WMH volumes as a primary outcome, both methods could be suitable.

All methods tended to slightly underestimate WMH volumes at higher lesion loads, but this was most prominent for LST-LGA and Lesion-TOADS. Lesion-TOADS and Cascade

showed the lowest spatial and volumetric correspondence compared to the reference segmentation and especially performance of Lesion-TOADS also varied across scanners. A possible explanation for the differences in performance between methods, both within and across scanners, could be that some methods are more robust to sources of variation in MRI acquisition than others. In our study it is impossible to determine which MRI related factors contribute most to this variation. Future studies are therefore encouraged to determine these sources of variation and the relation to various methods. Another explanation within our study might be the variation in WMH volumes between scanners, which might have introduced variation caused by selection bias. Above all, our study highlights the need to further improve WMH segmentation methods. An important initiative was recently taken in the form of a WMH segmentation challenge.[42] In this challenge, new WMH segmentation methods were developed and evaluated on a multicenter dataset. The best performing method showed a similar DSC compared to kNN-TTP in the present study.

White matter lesions can also have a non-vascular etiology, like in multiple sclerosis (MS). White matter lesions in MS show a different load, morphology and distribution compared to WMHs of presumed vascular origin.[5] Nevertheless, evaluation of methods for segmentation of MS lesions can still be informative for WMH of vascular origin. In the field of MS, a previous study assessed the performance across scanners of Cascade, kNN-TTP, Lesion-TOADS, LST-LGA and LST-LPA47. This study showed the highest performance across scanners for kNN-TTP (DSC mean ± SD: 0.44 ± 0.14), followed by LST-LPA (0.37 ± 0.23), Lesion-TOADS (0.35 ± 0.18), LST-LGA (0.31 ± 0.23) and Cascade (0.26 ± 0.17). Although the etiology of MS lesions is different, the overall ranking of methods is comparable to the ranking in our study, with Cascade being the method with the worst performance. The overall performance for MS lesion segmentation of each method is however lower than in our study. This discrepancy can possibly be explained by the difference in white matter lesion load between the previous study in MS (WMH volume mean ± SD: 5 ± 7 mL) and our study (20 ± 9 mL). Particularly for the segmentation of multiple small lesions, the DSC can become relatively low.

The main strength of our study is that it allows a direct comparison in performance of these methods for multicenter use. To achieve this goal, we have constructed a high quality MRI dataset consisting of reference segmentations. A possible limitation could be the downsampling of the 3D FLAIR images, since performance of automated methods tends to be better at higher resolution. However, downsampling was necessary for a fair comparison across all scanners. Furthermore, manual segmentation of 3D FLAIR scans is more time consuming than 2D FLAIR scans. Another limitation could be the comparison of binary reference segmentations with binary automated segmentations (i.e. thresholding the initial

probabilistic output of the automated methods). However, the alternative approach of creating probabilistic manual segmentations (e.g. by combining binary manual segmentations of the same subject performed by multiple raters into a single probabilistic segmentation) is very labor intensive. Moreover, it has limited added value over manual segmentation of a larger number of subjects. We have therefore invested in manual segmentations of more subjects in combination with determining optimal thresholds of the automated segmentations by using the training set. Another possible limitation of our study could be that we did not scan the same subject(s) on all six scanners. However, the aim of our study was not to assess (and quantify) the source of variation that could be introduced by using different MRI-scanners, but to determine the performance across scanners of widely used automated WMH segmentation methods in a dataset with different MRI-scanners that reflects general practice. A final limitation could be the selection of subjects for the present study. We chose to exclude subjects with severe motion artifacts and/or presence of large (sub)cortical brain infarcts. However, these brain abnormalities can often be observed in patients with WMH of presumed vascular origin and this could potentially lead to a different ranking in performance of the methods, as some methods might be more robust for these brain abnormalities.

In conclusion, performance of different methods for WMH segmentation varied markedly both within and across scanners. Our findings can serve as a guide for choosing a method and also highlight the importance to further improve and evaluate consistency of methods in a multicenter setting. Studies planning to segment WMHs from multicenter datasets should assess performance of their method of choice using a pilot sample of their data with manual segmentations.

MATERIALS AND METHODS

Study population

Subjects with WMHs of presumed vascular origin (as defined by the STRIVE criteria)[47] were selected from the TRACE-VCI study. This is a multicenter study on subjects with vascular cognitive impairment (VCI; n = 860) in the Netherlands and was described earlier.[48] In short, all patients that presented with cognitive complaints and vascular brain injury on MRI (i.e. possible VCI) were eligible to participate. Subjects scanned on six different MRI scanners were included. Four scanners were located at the Amsterdam University Medical Center (Amsterdam UMC), Amsterdam, the Netherlands (General Electric (GE) Signa HDxt 1.5T; GE Signa HDxt 3T; GE Discovery MR750 3T [General Electric Healthcare, Milwaukee, Wisconsin, USA] and Philips Ingenuity 3T [Philips Medical Systems, Best, the Netherlands]). Two scanners were located at the University Medical Center Utrecht

(UMCU), Utrecht, the Netherlands (Philips Achieva 3T and Philips Ingenia 3T [Philips Medical Systems, Best, the Netherlands]). For the present study, ten subjects with varying WMH lesion load (Fazekas scale 1 to 3)[49] were randomly selected per MRI scanner to represent the variation in WMH lesion load across the entire cohort. This led to inclusion of a total of 60 subjects (38 females, 22 males; age 68 ± 8 years). Compared to the entire cohort, there was no significant difference in age in the current study population (Student's t-test; $p > 0.05$). There was a significant difference in gender (chi-square test; $p < 0.05$) with a relatively higher percentage of females in the current study population compared to the entire cohort.[48] Subjects with severe motion artifacts and/or presence of large (sub) cortical brain infarcts (less than 10% of the total cohort) were not considered for the present study. From the 60 subjects, we selected a training set of 18 subjects (i.e. three subjects per scanner; one randomly selected subject per Fazekas scale for each scanner) and a test set of 42 subjects (i.e. seven subjects per scanner). The training set and test set showed no significant difference in age (Student's t test; $p > 0.05$), gender (chi-square test; $p > 0.05$) or WMH volume (Mann-Whitney U test; $p > 0.05$). The study was approved by the institutional review boards of the Amsterdam UMC and the UMCU (approval number 14-083/C). All procedures were in accordance with the ethical standards of the responsible committee on human experimentation (institutional and national) and with the Helsinki Declaration of 1975, as revised in 2013. All participating subjects provided written informed consent.

MR imaging

All subjects were scanned using an MRI protocol that included a 3D T1-weighted and fluid-attenuated inversion recovery (FLAIR) sequence.[48] The MRI sequence parameters are shown in Table 3.5. To make a fair comparison across all MRI scanners, all 3D FLAIR scans from subjects who were scanned at the Amsterdam UMC, were resampled in the axial plane to better match the 2D FLAIR acquisitions from the UMCU. This was done using a linear interpolation tool in MeVisLab (MeVis Medical Solutions AG, Bremen, Germany), resulting in 3 mm slices with an in-plane resolution of 0.95–1.21 mm.[50]

Reference segmentations

WMH reference segmentations were constructed as reference data for training and testing the automated WMH segmentation methods and were obtained for all subjects using the following procedure. An in-house developed MeVisLab (MeVis Medical Solutions AG, Bremen, Germany) tool was used to semi-automatically delineate the contour of WMHs on all axial slices.[46,51] In short, WMHs were segmented using an iso-contouring technique.

Table 3.5 | Overview of MRI sequence parameters for each scanner

Center	Scanner vendor, type	Tesla	Sequence	Slices	TR (ms)	TE (ms)	TI (ms)	Voxel size (mm)
A	GE, Signa HDxt	1.5	3D T1	172	12.3	5.2	-	0.98 × 0.98 × 1.50
			3D FLAIR	128	6500	117	1987	1.21 × 1.21 × 1.30
A	GE, Signa HDxt	3	3D T1	176	7.8	3.0	-	0.94 × 0.94 × 1.00
			3D FLAIR	132	8000	126	2340	0.98 × 0.98 × 1.20
A	GE, Discovery MR750	3	3D T1	176	8.2	3.2	-	0.94 × 0.94 × 1.00
			3D FLAIR	160	8000	130	2340	0.98 × 0.98 × 1.20
A	Philips, Ingenuity	3	3D T1	180	9.9	4.6	-	0.87 × 0.87 × 1.00
			3D FLAIR	321	4800	279	1650	1.04 × 1.04 × 0.56
B	Philips, Achieva	3	3D T1	192	7.9	4.5	-	1.00 × 1.00 × 1.00
			2D FLAIR	48	11000	125	2800	0.96 × 0.95 × 3.00
B	Philips, Ingenia	3	3D T1	192	7.9	4.5	-	1.00 × 1.00 × 1.00
			2D FLAIR	48	11000	125	2800	0.96 × 0.95 × 3.00

A, Amsterdam University Medical Center; B, Utrecht University Medical Center; TR, repetition time; TE, echo time; TI, inversion time.

Contours were converted into binary segmentation masks by including all voxels having a (sub)voxel volume of at least 20% within the contour. This threshold value was chosen by visual comparison of images thresholded with values between 0 and 100% (intervals of 5%). All reference segmentations were constructed by a single rater (RH). To assess inter-rater reliability of the reference segmentations, JMB constructed reference segmentations on a subset of twenty subjects by using the same semi-automatic procedure. To assess intra-rater reliability of the reference segmentations, RH constructed a second segmentation on a subset of twenty subjects.

Automated WMH segmentation methods

For the present study, we included methods that were fully-automated and freely available for academic research: Cascade, kNN-TTP, Lesion-TOADS, LST-LGA, and LST-LPA. All methods were run on FLAIR and 3D T1-weighted MR-images of all subjects to obtain WMH segmentations. Default settings were used as much as possible. The training set of subjects (n = 18) was used to train and tune each of the methods (i.e. to determine optimal thresholds). We did not exclude specific brain regions (such as the brain stem or basal ganglia where often higher false positive rates can be observed) from the analyses, since the aim of our study was to evaluate methods using their own processing. For a detailed overview of the workflow used for each method, see the Supplementary Information.

Statistical analysis

All automated WMH segmentation methods were evaluated on the test set (n = 42; i.e. 7 subjects per scanner). Several evaluation metrics currently exist to evaluate performance of WMH segmentation methods, each with their own advantages and disadvantages (for an overview see[51]). For the present study, we chose frequently used evaluation metrics that have been used in recent comparative studies on WMH segmentation.[8,46]

Quality assessment. We evaluated all methods qualitatively by visually comparing the output of each method with the reference segmentations. Next, we evaluated all methods quantitatively by calculating false positive (FP) volumes (in mL) and false negative (FN) volumes (in mL) of the WMH segmentations of each method using the reference segmentations.

Performance within scanners. The performance of each method was assessed per scanner by measuring: a) the spatial (i.e. voxel-wise) correspondence with the reference segmentations by using the DSC; b) the volumetric correspondence with the reference WMH volumes by using the ICC (two-way mixed model with absolute agreement after log-transforming

WMH volumes because of non-normal distribution); c) the mean differences and mean absolute differences between WMH volumes of each method and the reference WMH volumes. Because specific methods (Cascade, Lesion-TOADS, LST-LGA, and LST-LPA) do not necessarily have to be trained, performance was also determined in secondary analyses on all subjects (n = 60) without training of the methods.

Mean performance across scanners. The mean performance of each method across scanners was determined by averaging the mean DSC, ICC and absolute volume differences of each scanner.

Variations in performance across scanners. To investigate the variation in performance across scanners of each method, we performed the following two analyses:

a) For each method, we assessed whether the DSC (as an outcome) depended on scanner (as a categorical variable with each scanner being compared to all other scanners as the reference) using linear regression analysis. This resulted in an unstandardized beta coefficient with 95% confidence intervals for each scanner. A significant relation between a certain scanner and the DSC (family wise error rate corrected p-value of < 0.05 using a Bonferroni correction) indicates that the performance (in terms of spatial correspondence with the reference segmentation) was biased by the use of that scanner (compared to the other scanners).
b) For each method, we assessed whether the relation between the reference WMH volumes (as an outcome) and WMH volumes of the automated WMH segmentation method (as a determinant) depended on scanner (as a categorical variable with each scanner being compared to all other scanners as the reference) by using linear regression analyses. Because of non-normal distribution, WMH volumes of each method and the reference WMH volumes were log-transformed. A significant interaction between the log transformed WMH volume of a method and a certain scanner (family wise error rate corrected p-value of < 0.05), indicates that performance of that method (in terms of volumetric correspondence with the reference segmentation) was biased by the use of that scanner (compared to the other scanners).

Performance for different WMH lesion loads. In addition, the MRI scans of all subjects were stratified based on the Fazekas scale (Fazekas scale 1 / 2 / 3: n = 17 / n = 18 / n = 7). We then assessed whether the performance of each method was dependent on the WMH lesion load (i.e. Fazekas scale) using DSC, ICC and mean (absolute) volume differences. In addition, Bland-Altman plots were made to compare WMH volume of each method with the reference WMH volumes.[52] Bland Altman plots provide a graphical representation of the amount of variation from the mean when comparing WMH volumes of the WMH

segmentation methods and the reference segmentations. In these plots, a narrow width of the limits of agreement reflects a small amount of variation between WMH volumes of the WMH segmentation methods and the reference segmentations. The difference between WMH volumes of the WMH segmentation methods and the reference segmentation reflects over- or underestimation of the WMH segmentation methods. Both a change in the direction of WMH volume differences (i.e. positive or negative differences) as well as the distribution of WMH volume differences (narrow or wide) for different WMH lesion loads, can reflect performance of a WMH segmentation method to be dependent on the WMH lesion load.

Data availability

The data that support the findings of this study are available from the final author, upon reasonable request.

Acknowledgements

Members of the TRACE-VCI study group (in alphabetical order, per department): University Medical Center Utrecht, Utrecht University, Utrecht, The Netherlands, Department of Neurology: E. van den Berg, G.J. Biessels, J.M.F. Boomsma, L.G. Exalto, D.A. Ferro, C.J.M. Frijns, O.N. Groeneveld, R. Heinen, N.M. van Kalsbeek, J.H. Verwer; Department of Radiology: J. de Bresser; Image Sciences Institute: H.J. Kuijf; Department of Geriatrics: M.E. Emmelot-Vonk, H.L. Koek. Amsterdam UMC, Vrije Universiteit Amsterdam, Amsterdam, The Netherlands: Alzheimer Center and Department of Neurology: M.R. Benedictus, J. Bremer, W.M. van der Flier, A.E. Leeuwis, J. Leijenaar, N.D. Prins, P. Scheltens, B.M. Tijms; Department of Radiology and Nuclear Medicine: F. Barkhof, M.P. Wattjes; Department of Clinical Chemistry: C.E. Teunissen; Department of Medical Psychology: T. Koene; Onze Lieve Vrouwe Gasthuis West, Amsterdam, The Netherlands: Department of Neurology: J.M.F. Boomsma, H.C. Weinstein; Hospital Diakonessenhuis, Zeist, The Netherlands: M. Hamaker, R. Faaij, M. Pleizier, M. Prins, E. Vriens. N.P.A. Zuithoff, assistant professor in Biostatistic Research for his help in the statistical analyses.

REFERENCES

1. Carrillo MC, Bain LJ, Frisoni GB, Weiner MW. Worldwide Alzheimer's disease neuroimaging initiative. Alzheimer's Dement. 2012;8:337–42.
2. Williamson JD, Miller ME, Bryan RN, Lazar RM, Coker LH, Johnson J, et al. The Action to Control Cardiovascular Risk in Diabetes Memory in Diabetes Study (ACCORD-MIND): Rationale, Design, and Methods. Am J Cardiol. 2007;99:112–22.
3. Mueller SG, Weiner MW, Thal LJ, Petersen RC, Jack CR, Jagust W, et al. Ways toward an early diagnosis in Alzheimer's disease: The Alzheimer's Disease Neuroimaging Initiative (ADNI). Alzheimer's Dement. 2005;1:55–66.
4. De Guio F, Jouvent E, Biessels GJ, Black SE, Brayne C, Chen C, et al. Reproducibility and variability of quantitative magnetic resonance imaging markers in cerebral small vessel disease. J Cereb Blood Flow Metab. 2016;36:1319–37.
5. Caligiuri ME, Perrotta P, Augimeri A, Rocca F, Quattrone A, Cherubini A. Automatic Detection of White Matter Hyperintensities in Healthy Aging and Pathology Using Magnetic Resonance Imaging: A Review. Neuroinformatics. 2015;13:261–76.
6. Jain S, Sima DM, Ribbens A, Cambron M, Maertens A, van Hecke W, et al. Automatic segmentation and volumetry of multiple sclerosis brain lesions from MR images. NeuroImage Clin. 2015;8:367–75.
7. Ghafoorian M, Karssemeijer N, van Uden IW, de Leeuw FE, Heskes T, Marchiori E, et al. Automated detection of white matter hyperintensities of all sizes in cerebral small vessel disease. Med Phys. 2016;43:6246–58.
8. Griffanti L, Zamboni G, Khan A, Li L, Bonifacio G, Sundaresan V, et al. BIANCA (Brain Intensity AbNormality Classification Algorithm): A new tool for automated segmentation of white matter hyperintensities. Neuroimage. 2016;141:191–205.
9. Bowles C, Qin C, Ledig C, Guerrero R, Gunn R, Hammers A, et al. Pseudo-healthy image synthesis for white matter lesion segmentation. Lecture Notes in Computer Science. 2016;9968:87–96.
10. Schmidt P, Gaser C, Arsic M, Buck D, Förschler A, Berthele A, et al. An automated tool for detection of FLAIR-hyperintense white-matter lesions in Multiple Sclerosis. Neuroimage. 2012;59:3774–83.
11. Shiee N, Bazin PL, Ozturk A, Reich DS, Calabresi PA, Pham DL. A topology-preserving approach to the segmentation of brain images with multiple sclerosis lesions. Neuroimage. 2010;49:1524–35.
12. Qin C, Guerrero R, Bowles C, Chen L, Dickie DA, Valdés-Hernández MC, et al. A large margin algorithm for automated segmentation of white matter hyperintensity. Pattern Recognit. 2018;77:150–9.
13. Guerrero R, Qin C, Oktay O, Bowles C, Chen L, Joules R, et al. White matter hyperintensity and stroke lesion segmentation and differentiation using convolutional neural networks. NeuroImage Clin. 2018;17:918–34.
14. Ling Y, Jouvent E, Cousyn L, Chabriat H, De Guio F. Validation and Optimization of BIANCA for the Segmentation of Extensive White Matter Hyperintensities. Neuroinformatics. 2018;16:269–81.
15. Damangir S, Manzouri A, Oppedal K, Carlsson S, Firbank MJ, Sonnesyn H, et al. Multispectral MRI segmentation of age related white matter changes using a cascade of support vector machines. J Neurol Sci. 2012;322:211–6.
16. Damangir S, Westman E, Simmons A, Vrenken H, Wahlund LO, Spulber G. Reproducible segmentation of white matter hyperintensities using a new statistical definition. Magn Reson Mater Physics Biol Med. 2017;30:227–37.

17. Steenwijk MD, Pouwels PJ, Daams M, van Dalen JW, Caan MW, Richard E, et al. Accurate white matter lesion segmentation by k nearest neighbor classification with tissue type priors (kNN-TTPs). NeuroImage Clin. 2013;3:462–9.
18. Admiraal-Behloul F, van den Heuvel DM, Olofson H, van Osch MJ, van der Grond J, van Buchem MA, et al. Fully automatic segmentation of white matter hyperintensities in MR images of the elderly. Neuroimage. 2005;28:607–17.
19. Anbeek P, Vincken KL, Van Osch MJ, Bisschops RHC, van der Grond J. Probabilistic segmentation of white matter lesions in MR imaging. Neuroimage. 2004;21:1037–44.
20. Beare R, Srikanth V, Chen J, Phan TG, Stapleton J, Lipshut R, et al. Development and validation of morphological segmentation of age-related cerebral white matter hyperintensities. Neuroimage. 2009;47:199–203.
21. Brickman AM, Sneed JR, Provenzano FA, Garcon E, Johnert L, Muraskin J, et al. Quantitative approaches for assessment of white matter hyperintensities in elderly populations. Psychiatry Res. 2011;193:101–6.
22. de Boer R, Vrooman HA, van der Lijn F, Vernooij MW, Ikram MA, van der Lugt A, et al. White matter lesion extension to automatic brain tissue segmentation on MRI. Neuroimage. 2009;45:1151–61.
23. Erus G, Zacharaki EI, Davatzikos C. Individualized statistical learning from medical image databases: Application to identification of brain lesions. Med Image Anal. 2014;18:542–54.
24. Gibson E, Gao F, Black SE, Lobaugh NJ. Automatic segmentation of white matter hyperintensities in the elderly using FLAIR images at 3T. J Magn Reson Imaging. 2010; 31:1311–22.
25. Herskovits EH, Bryan RN, Yang F. Automated Bayesian segmentation of microvascular white-matter lesions in the ACCORD-MIND study. Adv Med Sci. 2008;53:182–90.
26. Iorio M, Spalletta G, Chiapponi C, Luccichenti G, Cacciari C, Orfei MD, et al. White matter hyperintensities segmentation: A new semi-automated method. Front Aging Neurosci. 2013;5:76.
27. Ithapu V, Singh V, Lindner C, Austin BP, Hinrichs C, Carlsson CM, et al. Extracting and summarizing white matter hyperintensities using supervised segmentation methods in Alzheimer's disease risk and aging studies. Hum Brain Mapp. 2014;35:4219–35.
28. Khayati R, Vafadust M, Towhidkhah F, Nabavi M. Fully automatic segmentation of multiple sclerosis lesions in brain MR FLAIR images using adaptive mixtures method and markov random field model. Comput Biol Med. 2008;38:379–90.
29. Lao Z, Shen D, Liu D, Jawad AF, Melhem ER, Launer LJ, et al. Computer-Assisted Segmentation of White Matter Lesions in 3D MR Images Using Support Vector Machine. Acad Radiol. 2008;15:300–13.
30. Moeskops P, de Bresser J, Kuijf HJ, Mendrik AM, Biessels GJ, Pluim JPW, et al. Evaluation of a deep learning approach for the segmentation of brain tissues and white matter hyperintensities of presumed vascular origin in MRI. NeuroImage Clin. 2017;17:251–62.
31. Ramirez J, Gibson E, Quddus A, Lobaugh NJ, Feinstein A, Levine B, et al. Lesion Explorer: A comprehensive segmentation and parcellation package to obtain regional volumetrics for subcortical hyperintensities and intracranial tissue. Neuroimage. 2011;54:963–73.
32. Rincón M, Díaz-López E, Selnes P, Vegge K, Altmann M, Fladby T, et al. Improved Automatic Segmentation of White Matter Hyperintensities in MRI Based on Multilevel Lesion Features. Neuroinformatics. 2017;15:231–45.
33. Sajja BR, Datta S, He R, Mehta M, Gupta RK, Wolinsky JS, et al. Unified approach for multiple sclerosis lesion segmentation on brain MRI. Ann Biomed Eng. 2006;34:142–51.
34. Simões R, Mönninghoff C, Dlugaj M, Weimar C, Wanke I, van Cappellen van Walsum AM, et al. Automatic segmentation of cerebral white matter hyperintensities using only 3D FLAIR images. Magn Reson Imaging. 2013;31:1182–9.

35. Smart SD, Firbank MJ, O'Brien JT. Validation of automated white matter hyperintensity segmentation. J Aging Res. 2011;2011:391783.
36. Tsai JZ, Peng SJ, Chen YW, Wang KW, Li CH, Wang JY, et al. Automated segmentation and quantification of white matter hyperintensities in acute ischemic stroke patients with cerebral infarction. PLoS One. 2014;9:e104011.
37. Wang R, Li C, Wang J, Wei X, Li Y, Zhu Y, et al. Automatic segmentation and volumetric quantification of white matter hyperintensities on fluid-attenuated inversion recovery images using the extreme value distribution. Neuroradiology. 2015;57:307–20.
38. Wang R, Li C, Wang J, Wei X, Li Y, Hui C, et al. Automatic segmentation and quantitative analysis of white matter hyperintensities on FLAIR images using trimmed-likelihood estimator. Acad Radiol. 2014;21:1512–23.
39. Wu Y, Warfield SK, Tan IL, Wells WM 3rd, Meier DS, van Schijndel RA, et al. Automated segmentation of multiple sclerosis lesion subtypes with multichannel MRI. Neuroimage. 2006;32:1205–15.
40. Zhong Y, Utriainen D, Wang Y, Kang Y, Haacke EM. Automated White Matter Hyperintensity Detection in Multiple Sclerosis Using 3D T2 FLAIR. Int J Biomed Imaging. 2014;2014:239123.
41. Dichgans M, Wardlaw J, Smith E, Zietemann V, Seshadri S, Sachdev P, et al. METACOHORTS for the study of vascular disease and its contribution to cognitive decline and neurodegeneration: An initiative of the Joint Programme for Neurodegenerative Disease Research. Alzheimer's Dement. 2016;12:1235–49.
42. Kuijf HJ, Biesbroek JM, de Bresser J, Heinen R, Andermatt S, Bento M, et al. Standardized Assessment of Automatic Segmentation of White Matter Hyperintensities; Results of the WMH Segmentation Challenge. IEEE Trans Med Imaging. 2019:1–36.
43. Dadar M, Maranzano J, Misquitta K, Anor CJ, Fonov VS, Tartaglia MC, et al. Performance comparison of 10 different classification techniques in segmenting white matter hyperintensities in aging. Neuroimage. 2017;157:233–49.
44. Samaille T, Fillon L, Cuingnet R, Jouvent E, Chabriat H, Dormont D, et al. Contrast-Based Fully Automatic Segmentation of White Matter Hyperintensities: Method and Validation. PLoS One. 2012;7:e48953.
45. Biesbroek JM, Weaver NA, Hilal S, Kuijf HJ, Ikram MK, Xu X, et al. Impact of Strategically Located White Matter Hyperintensities on Cognition in Memory Clinic Patients with Small Vessel Disease. PLoS One. 2016;11:e0166261.
46. de Sitter A, Steenwijk MD, Ruet A, Versteeg A, Liu Y, van Schijndel RA, et al. Performance of five research-domain automated WM lesion segmentation methods in a multi-center MS study. Neuroimage. 2017;163:106–14.
47. Wardlaw JM, Smith EE, Biessels GJ, Cordonnier C, Fazekas F, Frayne R, et al. Neuroimaging standards for research into small vessel disease and its contribution to ageing and neurodegeneration. The Lancet Neurology. 2013;12:822–38.
48. Boomsma JMF, Exalto LG, Barkhof F, van den Berg E, de Bresser J, Heinen R, et al. Vascular Cognitive Impairment in a Memory Clinic Population: Rationale and Design of the 'Utrecht-Amsterdam Clinical Features and Prognosis in Vascular Cognitive Impairment' (TRACE-VCI) Study. JMIR Res Protoc. 2017;6:e60.
49. Fazekas F, Chawluk JB, Alavi A, Hurtig HI, Zimmerman RA. MR signal abnormalities at 1.5 T in Alzheimer's dementia and normal aging. American Journal of Neuroradiology. 1987;8:421–6.
50. Ritter F, Boskamp T, Homeyer A, Laue H, Schwier M, Link F, et al. Medical image analysis. IEEE Pulse. 2011;2:60–70.
51. Taha AA, Hanbury A. Metrics for evaluating 3D medical image segmentation: Analysis, selection, and tool. BMC Med Imaging. 2015;15:29.
52. Martin Bland J, Altman D. Statistical Methods for Assessing Agreement Between Two Methods of Clinical Measurement. Lancet. 1986;327:307–10.

SUPPLEMENTARY INFORMATION

MATERIALS AND METHODS

Cascade

Cascade (version 1.1; available via https://github.com/Damangir/Cascade[1,2] is an unsupervised method based on a proposed statistical definition of WMH. It uses a single node support vector machine (SVM) to preselect tissues that show differences in white matter (WM) intensity compared to normal gray and white matter. These changes in WM are then tested against a statistical definition of WMH. By applying a threshold (α), a selection of WMH is made. A probability map is then generated by applying a morphological filter and removing small lesions. Finally, a binary WMH segmentation is generated by applying another threshold (based on the lesion p-value). A recent paper on Cascade suggest any form of preprocessing can be done as long as all input images for Cascade have been registered and corrected for inhomogeneity and initial brain segmentation in WM, gray matter (GM) and cerebrospinal fluid (CSF) has been performed.[2] To minimize differences in preprocessing between other methods (i.e. Lesion-TOADS), we chose to use the following preprocessing. Bias correction of both the T1 and FLAIR images was performed using SPM12 (default settings). Brain segmentation was performed using CAT12 (version r864; http://dbm.neuro.uni-jena.de/cat/). CAT12 is a SPM tool that uses voxel-based morphometry to classify GM, WM and CSF. Internal Cascade tools were then used to refined the initial brain segmentation of CAT12 using the bias-corrected FLAIR image. During refining, intensities of the FLAIR image were used to correct for misclassified WMH (e.g. as GM instead of WMH). Next, the refined brain tissue segmentation and bias-corrected T1 were registered to the original, bias-corrected FLAIR image using Elastix.[3] These three images were then used for WMH segmentation by Cascade. To determine the optimal settings, we chose the settings that generated the highest DSC in the training set (in the current study: lower threshold = 0.95; upper threshold = 0.975; rest of the settings were kept at default).

kNN-TTP

kNN-TTP is a supervised method based on a k-nearest neighbor algorithm, combined with tissue type priors derived from healthy controls to segment WMHs.[4] WMHs are segmented by comparing each voxel of the labelled training set with new data of the test set. The lesion-probability map is then converted to a binary WMH segmentation by applying a lesion probability threshold. For our study, we used the original T1 and FLAIR images as well as

the brain masks (that were acquired as described earlier). kNN-TTP uses its own standard preprocessing pipeline (for details see [4]). After preprocessing, kNN-TTP extracts eight features for kNN classification: FLAIR and T1 signal intensity, MNI-normalized spatial coordinates x, y and z, and tissue type probabilities pCSF, pGM and pWM. These features are normalized using variance scaling to account for different ranges for different features. Next, classification of each voxel was performed by determining the fraction of *k*-nearest neighbors that were labeled as being a lesion in the training set. For our study, *k* was set to 40.[5] The output of kNN-TTP is a probabilistic lesion map. Finally, a threshold of 0.45 was used to obtain a binary WMH segmentation. This threshold was chosen by determining the best DSC in the training set using thresholds between 0 and 1 (intervals of 0.05).

Lesion-TOADS

Lesion Topology-preserving Anatomical Segmentation (Lesion-TOADS; version 1.9) is an unsupervised method that is available as a plug-in for the MIPAV software (http://mipav.cit.nih.gov/).[6] Lesion-TOADS uses an algorithm for fuzzy classification of image intensities, using a combination of topological and statistical atlases. An additional WMH lesion class is added to the brain segmentation model, using the same spatial prior as WM. Next, WMH and WM are separated by selecting, inside the grouped region, whichever has the higher membership value. The distances to certain areas (e.g. distance to ventricles) are used to correct for possible false positives. For Lesion-TOADS the following preprocessing was performed. First, FLAIR images were registered to T1 using Elastix. Next, bias correction was performed using SPM12 (default settings) on both T1 and coregistered FLAIR images. Subsequently, a brain mask was obtained using CAT12 (and manually corrected if needed). The resulting brain mask was used to skull strip both T1 and coregistered FLAIR images. The coregistered, bias corrected and skull-stripped T1 and FLAIR images were then used by Lesion-TOADS. For our current study, default settings were used. To compare the WMH segmentation of Lesion-TOADS (in 3D T1 space) with the manual segmentations (in FLAIR space), the following procedure was performed. First, Elastix was used to perform a rigid registration of the 3D T1 to the FLAIR image.[3] Next, the resulting translation parameters were used to transform the WMH map to FLAIR space. A final threshold of 0.35 was applied to obtain a binary WMH map. This threshold was chosen by determining the best DSC in the training set using thresholds between 0 and 1 (intervals of 0.05).

LST (LGA and LPA)

LST-LGA is part of the Lesion Segmentation Tool (version 2.0.14), a toolbox that can be downloaded and subsequently implemented in SPM12 (www.statisticalmoddeling.de/

lst/html).[7] It segments the T1 image into three main tissue classes (GM, WM and CSF). These segmentations are then combined with the coregistered FLAIR intensities in order to calculate WMH ('lesion belief' maps). By thresholding these maps with a pre-chosen initial threshold (kappa), an initial binary WMH map is obtained, which is subsequently grown along voxels that are hyperintense on the FLAIR image. The result is a lesion probability map.

LST-LPA is part of the LST toolbox (version 2.0.14) and consists of a binary classifier in the form of a logistic regression model trained on the data of 53 subjects with multiple sclerosis with severe lesion patterns (http://www.applied-statistics.de/lst.html). Data were obtained at the Department of Neurology, Technische Universität München, Munich, Germany. As covariates for this model a similar WMH ('lesion belief') map as for the LST-LGA was used as well as a spatial covariate that takes into account voxel specific changes in WMH probability. Parameters of this model fit are used to segment WMH in new images by providing an estimate for the WMH probability for each voxel. This results in a WMH probability map.

No preprocessing was performed, as LST uses internal SPM preprocessing tools. To compare the probabilistic WMH segmentation of LST (in 3D T1 space) with the binary manual segmentations (in FLAIR space), Elastix was used to perform a rigid registration of the 3D T1 to the FLAIR image.[3] Next, the WMH probability map was transformed to FLAIR space. A final threshold of 0.2 was applied for LST-LGA and 0.3 for LST-LPA to obtain a binary WMH map. These thresholds were chosen by determining the best DSC in the training set using thresholds between 0 and 1 (intervals of 0.05). For LST-LGA we tested different thresholds for kappa that were between 0 and 1 (intervals of 0.05) and determined the optimal threshold (0.25) with the highest observed DSC in the training set.

SUPPLEMENTARY REFERENCES

1. Damangir S, Manzouri A, Oppedal K, Carlsson S, Firbank MJ, Sonnesyn H, et al. Multispectral MRI segmentation of age related white matter changes using a cascade of support vector machines. J Neurol Sci. 2012;322:211–6.
2. Damangir S, Westman E, Simmons A, Vrenken H, Wahlund LO, Spulber G. Reproducible segmentation of white matter hyperintensities using a new statistical definition. Magn Reson Mater Physics Biol Med. 2017;30:227–37.
3. Klein S, Staring M, Murphy K, Viergever MA, Pluim JPW. Elastix: A toolbox for intensity-based medical image registration. IEEE Trans Med Imaging. 2010;29:196–205.
4. Steenwijk MD, Pouwels PJW, Daams M, van Dalen JW, Caan MWA, et al. Accurate white matter lesion segmentation by k nearest neighbor classification with tissue type priors (kNN-TTPs). NeuroImage Clin. 2013;3:462–9.
5. Anbeek P, Vincken K, Viergever M. Automated MS-lesion segmentation by k-nearest neighbor classification. Midas J. 2008;1–8.
6. Shiee N, Bazin P-L, Ozturk A, Reich DS, Calabresi PA, Pham DL. A topology-preserving approach to the segmentation of brain images with multiple sclerosis lesions. Neuroimage. 2010;49:1524–35.
7. Schmidt P, Gaser C, Arsic M, Buck D, Förschler A, Berthele A, et al. An automated tool for detection of FLAIR-hyperintense white-matter lesions in Multiple Sclerosis. Neuroimage. 2012;59:3774–83.

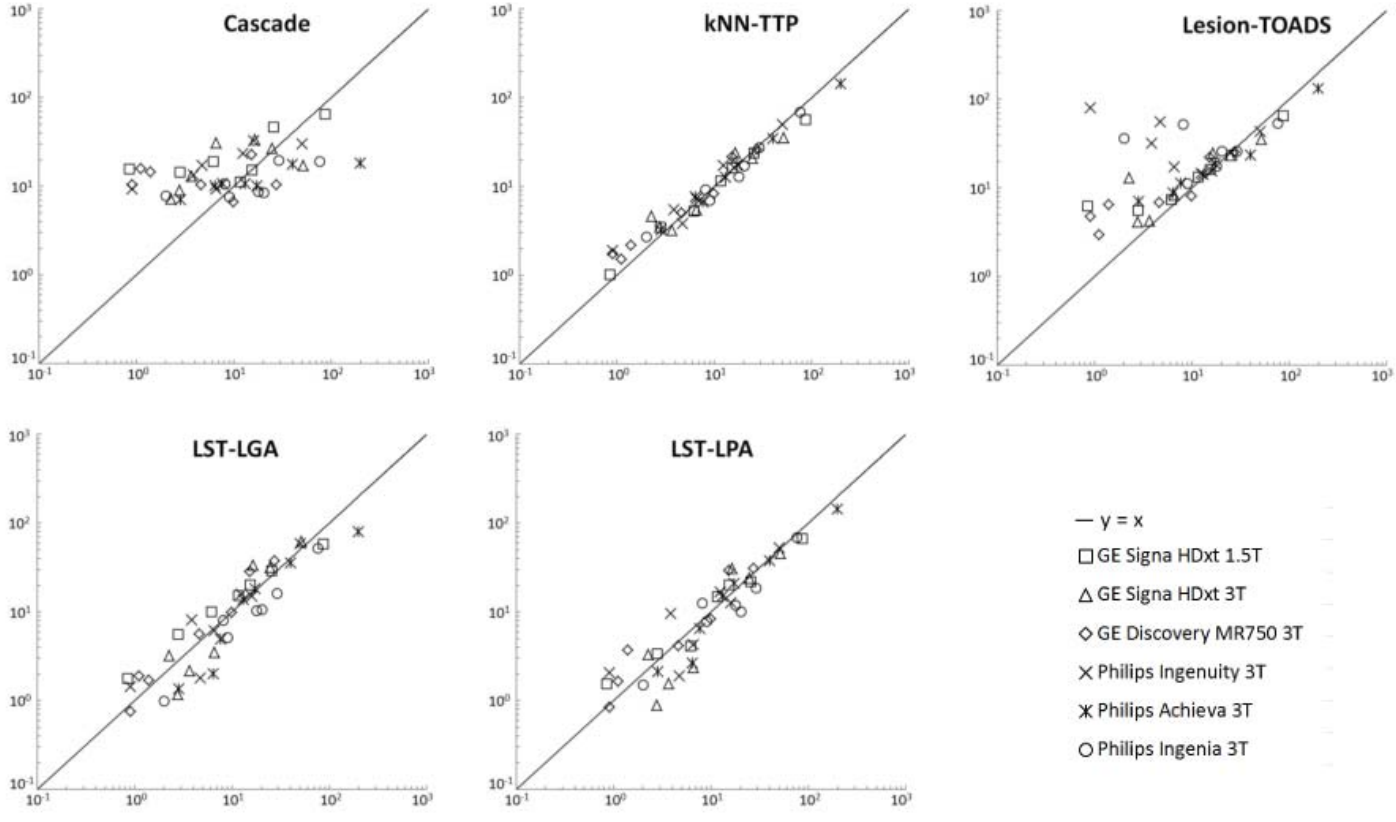

Supplementary Figure S3.1 | WMH volume measurements of each method compared to reference WMH segmentation. WMH volume measurements (in mL) of WMH segmentation methods (left to right, up to down: Cascade, kNN-TTP, Lesion-TOADS, LST-LGA and LST-LPA) shown on x-axis against the mean WMH volume measurements (in mL) of the reference segmentations on y-axis. Note: log scale is used for both axes.

PART TWO

Effects of cerebral small vessel disease beyond the visible lesions and the interplay with Alzheimer's disease

Chapter 4

Cortical microinfarcts and white matter connectivity in memory clinic patients

Doeschka Ferro*
Rutger Heinen*
Bruno de Brito Robalo
Hugo J. Kuijf
Geert Jan Biessels
Yael Reijmer
on behalf of the Utrecht VCI study group

* These authors have contributed equally to this work

Front Neurol. 2019;10:571

ABSTRACT

Cerebral microinfarcts (CMIs) are associated with cognitive impairment and dementia. CMIs might affect cognitive performance through disruption of cerebral networks. We investigated in memory clinic patients whether cortical CMIs are clustered in specific brain regions and if presence of cortical CMIs is associated with reduced white matter (WM) connectivity in tracts projecting to these regions.

164 memory clinic patients with vascular brain injury with a mean age of 72 ± 11 years (54% male) were included. All underwent 3 tesla MRI, including a diffusion MRI and cognitive testing. Cortical CMIs were rated according to established criteria and their spatial location was marked. Diffusion imaging-based tractography was used to reconstruct WM connections and voxel based analysis (VBA) to assess integrity of WM directly below the cortex. WM connectivity and integrity were compared between patients with and without cortical CMIs for the whole brain and regions with a high CMI burden.

30 patients (18%) had at least 1 cortical CMI [range 1–46]. More than 70% of the cortical CMIs were located in the superior frontal, middle frontal, and pre- and postcentral brain regions (covering 16% of the cortical surface). In these high CMI burden regions, presence of cortical CMIs was not associated with WM connectivity after correction for conventional neuroimaging markers of vascular injury. WM connectivity in the whole brain and WM voxels directly underneath the cortical surface did not differ between patients with and without cortical CMIs.

Cortical CMIs displayed a strong local clustering in highly interconnected frontal, pre- and postcentral brain regions. Nevertheless, WM connections projecting to these regions were not disproportionally impaired in patients with compared to patients without cortical CMIs. Alternative mechanisms, such as focal disturbances in cortical structure and functioning, may better explain CMI associated cognitive impairment.

INTRODUCTION

Cerebral microinfarcts (CMIs) are small (< 5 mm) ischemic lesions that are increasingly recognized as a clinically relevant marker in stroke and dementia.[1] Besides post-mortem detection at autopsy, CMIs can now also be detected in vivo on MRI as chronic cortical CMIs on T1-weighted MRI and acute CMIs on diffusion-weighted MRI.[2]

Both pathology and MRI studies have found a consistent association between CMI presence and cognitive impairment, also after adjustments for the presence of co-occurring Alzheimer's disease[3] and conventional neuroimaging markers of vascular injury.[4–7] Although these findings suggest that CMIs play a causative role in the process of cognitive decline, the exact mechanism by which CMIs and cognitive impairment are linked is not yet clear.

Several manifestations of cerebral small vessel disease (SVD), such as white matter hyperintensities (WMHs), lacunes, and cerebral microbleeds have been suggested to affect cognitive functioning by disruption of the WM network.[8–12] It appears that the severity and location of these SVD lesions determine their impact on the brain network and consequently cognition.[12,13] Disruption of WM connectivity may also play a role in the relation between cortical CMIs and cognitive impairment. We hypothesized that cortical CMIs exert their effect on the brain network by secondary degeneration of connecting WM pathways. A small study with cerebral amyloid angiopathy (CAA) patients showed that acute subcortical CMIs were indeed associated with changes in the surrounding local WM microstructural integrity.[14] Whether similar effects on WM connectivity occur in relation to chronic cortical CMIs is unknown.

We have previously reported that presence of CMIs in memory clinic patients with vascular brain injury is associated with other neuroimaging markers of vascular injury, a diagnosis of vascular dementia and reduced performance in multiple cognitive domains.[4] In the present study we investigated whether cortical CMIs in this cohort predominantly occur in specific brain regions and if presence of cortical CMIs is associated with impaired WM connectivity in tracts projecting to these regions.

METHODS

Study population

This study involved patients from the TRACE-VCI cohort of the University Medical Center (UMC) Utrecht, an observational prospective cohort study of memory clinic patients with vascular brain injury (i.e., possible VCI) recruited between September 2009 and December

2013 [details described previously[4,15]]. Patients were included in the cohort if they presented with cognitive complaints at the memory clinic, and had evidence of vascular brain injury on MRI, operationalized as: (1) WMHs with a Fazekas scale grade ≥ 2;[16] (2) ≥ 1 lacunar or non-lacunar infarcts; (3) ≥ 1 cerebral microbleeds; (4) ≥ 1 intracerebral hemorrhage(s) or (5) Fazekas scale grade 1 combined with ≥ 2 vascular risk factors.[15] In line with proposed VCI criteria, patients with possible co-existing neurodegenerative disorders (such as Alzheimer's disease) were included in this study cohort, but patients with primary non-vascular or nonneurodegenerative causes of cognitive dysfunction (e.g., brain tumors, depression) were excluded.[15] All patients (n = 196) underwent a standardized clinical assessment and 3 tesla brain MRI. Patients were included for the present study if they had complete MRI data, including a diffusion weighted scan (n = 177), another 13 patients were excluded due to poor quality of the MRI (n = 3) or DTI (n = 9, including 2 network outliers) and 1 failure to co-register the AAL-template, resulting in a study population of 164.

Ethical approval was provided by the institutional review board of the UMC Utrecht. All procedures were in accordance with the ethical standards of the responsible committee on human experimentation (institutional and national) and with the Helsinki Declaration of 1975, as revised in 2013. Written informed consent was obtained from all participants prior to any research related procedures.

Clinical diagnosis of cognitive impairment

Educational level was rated according to the 7-point Verhage scale.[17] The Clinical Dementia Rating scale (CDR; range: 0–3) was used to assess the severity of cognitive symptoms and functional deficits.[18] The mini-mental state examination (MMSE) in Dutch was used as a global measure of cognitive performance.[19]

Severity of cognitive impairment was classified at a multidisciplinary consensus meeting. No objective cognitive impairment (NOCI) was defined as cognitive complaints, but without objective cognitive impairment on neuropsychological testing. Mild cognitive impairment (MCI) was defined as complaints or deterioration from prior functioning and objective impairment in at least one cognitive domain, but with no or mild impairment of activities in daily living. Dementia was defined as deficits in two or more cognitive domains at neuropsychological testing and who experienced interference of these deficits in daily living. Further etiological diagnoses of dementia were made based on internationally established diagnostic criteria (without knowledge of CSF biomarkers) into vascular dementia (VaD),[20] Alzheimer's disease (AD),[21] or other (i.e., dementia such as Lewy body, primary progressive aphasia, cortical basal syndrome, unknown etc.[15]

MRI

All patients were scanned on a 3 tesla MRI scanner (Philips Achieva or Philips Ingenia [Philips Medical Systems, Best, the Netherlands]). The standardized MRI protocol included a 3D T1-weighted sequence (192 slices, voxel size: 1.00 × 1.00 × 1.00 mm, repetition time (TR)/echo time (TE): 7.9/4.5 ms); the following transversal 2D sequences (48 slices, voxel size: 0.96 × 0.96 × 3.00 mm): T2-weighted turbo spin echo (TSE; TR/TE: 3198/140 ms), T2*-weighted (TR/TE: 1653/20 ms), and fluid attenuated inversion recovery (FLAIR; TR/TE/inversion time: 11000/125/2800 ms); and diffusion-weighted imaging [DWI; 48 slices, voxel size: 1.72 × 1.72 × 2.50 mm, TR/TE: 6600/73 ms, 45 gradient directions with a b-value of 1,200 s/mm^2 and one with a b-value of 0 s/mm^2 (3 averages)].

Neuroimaging markers

The following neuroimaging markers were rated according to the STRIVE criteria[22] by or under supervision of a neuroradiologist, who was blinded to the clinical condition of the participants: (1) WMHs on the Fazekas scale;[16] (2) Lacunes (presence and number); (3) Cerebral microbleeds (presence and number); (4) Medial temporal lobe atrophy (MTA) using the Scheltens scale averaged for both hemispheres.[23]

Brain volume measurements

The following semi-automated workflow was used to obtain brain volumes: (1) automated WMH segmentation of 2D FLAIR images using kNN-TTP;[24] (2) lesion-filling of 3D T1 images using SLF toolbox (http://atc.udg.edu/nic/slfToolbox/index.html) for Statistical Parametric Mapping 12 (SPM Wellcome Department of Cognitive Neurology, Institute of Neurology, Queen Square London) with default settings;[25,26] (3) default settings were used to obtain probabilistic segmentations for gray matter, WM, and CSF. Total brain volume was defined as the sum of the gray and WM volume. Brain volumes were expressed as a percentage of the total intracranial volume.

Rating of cortical CMIs

Cortical CMIs were rated by visual inspection according to previously proposed criteria.[2,27] Cortical CMIs were rated on 3 tesla MRI and were hypointense on T1-weighted imaging, hyper- or isointense on FLAIR or T2-weighted imaging and isointense on T2*-weighted imaging. Lesions had to be strictly intracortical and ≤ 4 mm in the greatest dimension on T1. If the lesions measured substantially larger than 4 mm on T2-weighted imaging or within 1 cm proximity of a larger stroke, it was disregarded as the lesion was considered part of a larger stroke. The lesion had to be visible in two viewing planes of the brain (e.g.,

sagittal, transversal, or coronal plane) and distinct from other structures and lesions such as arteries, veins, enlarged perivascular spaces and cerebral microbleeds. Rating were carried out using MeVisLab (MeVis medical solutions, Bremen, Germany),[28] while the rater was blinded to the clinical condition of the subjects. There was a good intra-rater and interrater (both intra-class correlation coefficient > 0.95) agreement, details regarding the intra- and interrater reliability were published previously.[4]

Cortical CMI spatial mapping

Cortical CMI locations from all patients were registered to Montreal Neurological Institute (MNI) space. The automated anatomic labeling (AAL) template[29] was used as overlay on this sample-averaged CMI map. The number of CMIs within each AAL region was determined to assess whether CMIs predominantly occurred in specific brain regions. The AAL regions with a relatively high number of CMI were defined as high CMI burden regions, other AAL regions were defined as low CMI burden regions. The threshold for high vs. low CMI burden regions was arbitrarily set at > 5 CMIs (for a histogram of the CMI numbers per AAL region, see Supplementary Figure S4.1). For 3D rendering of the spatial distribution of cortical CMIs see Figure 4.1. The volume per AAL region was calculated using automated segmentation using CAT12 after registering the AAL template to the T1 image in patient space.

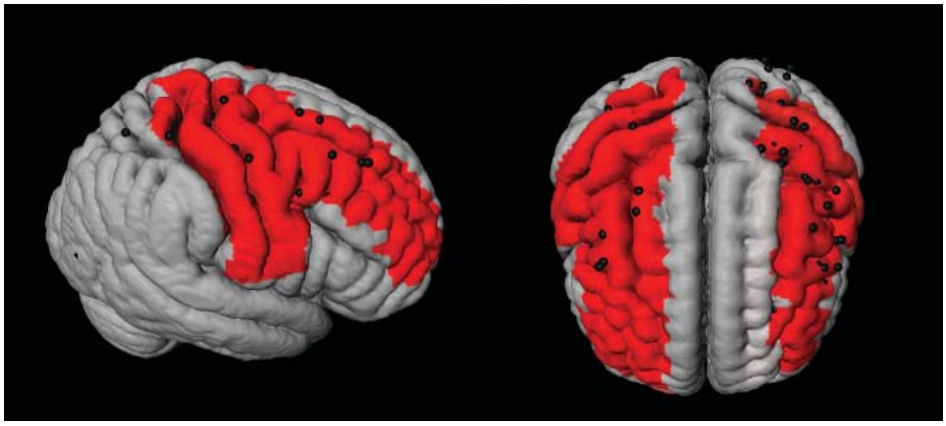

Figure 4.1 | 3D representation of the spatial distribution of cortical microinfarcts (CMIs; represented as black dots) across the brain in the cohort. The red areas represent the Automated Anatomical Labeling (AAL)-atlas regions with a high CMI burden (i.e., the 7 brain regions which contained 75% of all the cortical CMIs).

Diffusion MRI processing and network reconstruction

Diffusion tensor imaging (DTI) scans were preprocessed as previously described[12,30] using ExploreDTI version 4.8.6 (www.exploredti.com) and included subject motion correction, unwarping of eddy current and EPI induced distortions and a robust tensor estimation (including adjustment of the B-matrix).[31–33] Next, whole brain deterministic WM tractography was performed using constrained spherical deconvolution (CSD)-based tractography, which is different from standard tensorbased tractography, as it allows reconstruction of crossing fiber pathways.[34–36] Reconstruction of fiber tracts was performed by using uniformly distributed starting seed samples throughout the brain's WM at every voxel with a fiber orientation distribution (FOD) > 0.1 (indicating WM) at a 2 × 2 × 2 mm resolution. Fiber reconstruction was terminated if either a deflection in an angle of more than 45 degrees occurred or if a fiber entered a voxel with a FOD of < 0.1 (indicating no WM). An additional terminating mask was not applied. Brain network nodes were defined using the same AAL template as used for the cortical CMI mapping described above, consisting of 90 cortical and subcortical gray matter regions. The AAL template is a commonly used atlas to define nodes in clinical network studies.[8,9,11] The atlas has the advantage that the gray matter regions also contain a small portion of WM, which allows streamlines that terminate just before the gray-white matter border to be included in the network, thereby reducing the chance of false negative connections. Nodes were considered to be connected if two end points of a reconstructed fiber bundle lay within those nodes, resulting in a 90 × 90 binary connectivity matrix. This matrix was then weighted by multiplying each connection by the mean fractional anisotropy (FA) or mean diffusivity (MD) of that connection, resulting in two weighted-connectivity matrices for each patient. To reduce partial volume effects in WM connections a threshold of FA > 0.2 was applied to all the connectivity matrices. See Figure 4.2 (upper part A-D) for a graphical representation of this workflow.

Measures of whole brain and regional WM connectivity

The Brain Connectivity Toolbox (http://www.brainconnectivity-toolbox.net) was used to calculate network properties, including nodal degree (i.e., number of WM connections per node) and nodal strength (here defined as the mean FA or MD of all WM connections to that node).[37] For this study we used the following constructs: whole brain WM connectivity was assessed by the average FA and MD-weighted nodal strength of all network nodes. WM connectivity in high and low CMI burden regions was assessed by the average FA- and MD-weighted nodal strength of the high and low CMI burden regions, respectively (see Cortical CMI spatial mapping section, for an overview of regions see Figure 4.1).

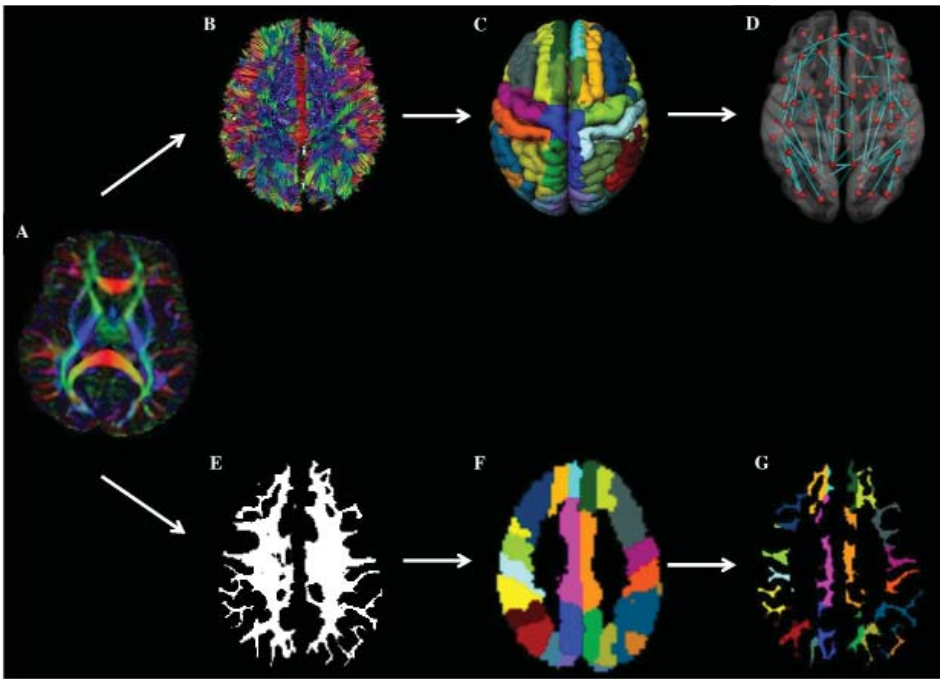

Figure 4.2 | Overview of workflow. In the top panel (network-based approach): from a patients' DTI images (A), WM connections are reconstructed using fiber tractography (B). Next, brain network nodes were defined using the cortical parcellation using the AAL template (C). Subsequently, the structural brain network was reconstructed (D). Weighting of the network was done by multiplying each connection by the mean fractional anisotropy (FA) or mean diffusivity (MD). Finally, the mean FA and MD of connections towards high and low cortical microinfarcts (CMI) burden regions were compared between patients with and without CMIs. In the bottom panel (voxel-based approach), the patient's DTI image A) is combined with the patient's WM segmentation results (E) and AAL template (F) to assess diffusion properties of the WM voxels in the AAL region (i.e. directly underneath the cortex) (G).

Voxel-based WM diffusion analysis

In addition to the network-based connectivity analyses we also performed a WM voxel-based analysis to assess differences in mean FA and MD. Although we assume that secondary degeneration affects the whole axon running from the cortex to the deep WM, one may speculate that the WM directly underneath the CMI containing cortical (i.e., juxtacortical) surface is primarily affected. As can be seen in Figure 4.2 (lower part) AAL regions mainly consist of GM, but also contain a small WM section in close proximity to the cortical surface. Therefore, we also calculated the mean FA and MD of the WM voxels within each AAL region (using a WM mask with a WM probability threshold of 75). The FA and MD was averaged across all AAL regions for the high and low CMI burden regions respectively, see Figure 4.2 (lower part E-G) for a graphical representation).

Statistical analysis

Differences in baseline characteristics between patients with and without cortical CMIs were analyzed using independent sample t-tests (for continuous normally distributed data), χ-square test (for proportions), and Mann-Whitney U-test (for continuous, non-normally distributed data). Differences in volume and connectivity strength between brain regions that were identified as high and low CMI burden regions were compared using a paired sample t-test (regardless of CMI presence).

The association between the presence of cortical CMIs (predictor) and FA- and MD-weighted WM connectivity (outcome) was analyzed using linear regression and included sex and age (Model 1) and sex, age and conventional neuroimaging markers (WMH Fazekas scale grade 3, presence of lacunar and non-lacunar infarcts) (Model 2) as covariates. Beta values are reported with 95% confidence interval (CI) and corresponding t-values and degrees of freedom (df). These analyses were carried out separately for whole brain, high and low CMI burden regions. Within the group of patients with cortical CMIs, patients with 1 vs. patients with multiple cortical CMIs (predictor) were compared on WM connectivity (outcome) using an independent t-tests and corresponding df. Using a voxel based approach, the association between cortical CMI presence (predictor) and the mean FA and MD of WM voxels in close proximity to the cortex (outcome) was analyzed using linear regression, adjusted for age and sex. A possible interaction effect between cortical CMI presence and clinical diagnosis on WM connectivity was explored in a regression analysis with post hoc Helmert contrasts, where each clinical diagnosis (except the first) was compared to the main effect of all previous diagnoses. Post-hoc power analysis was carried out using G*Power (Heinrich-Heine University, Dusseldorf, Germany).[38] All analyses were carried out using IBM SPSS statistics (version 22). A p-value of < 0.05 was considered significant, p-values were not adjusted for multiple comparisons, as all analyses were planned (not post-hoc).

Data availability statement

Any data on the VCI cohort used in these analyses that is not published within this article is available by request from any qualified investigator.

RESULTS

Baseline characteristics of patients with and without cortical CMIs

The 164 patients had a mean age of 72 (± 11) years and 88 (54%) were male. A total of 134 cortical CMIs were detected in 30 (18%) of the 164 patients. The number of cortical CMIs

per patient ranged between 1 and 46, 14 patients had 1 cortical CMI and 16 patients had 2 or more cortical CMIs. Baseline characteristics of patients with and without cortical CMIs are presented in Table 4.1. We have previously published the detailed cognitive profile of patients with cortical CMIs in this specific cohort.[4] In short patients with cortical CMIs were more often male, had more non-lacunar infarcts and were more often diagnosed with vascular dementia (all $p < 0.05$).

Characteristics of high and low CMI burden regions

The spatial location of the cortical CMIs was highly clustered, as more than 70% (n = 99) of all cortical CMIs were located within 7 AAL regions (High CMI burden regions: middle frontal and pre- and postcentral regions of both hemispheres and the right superior frontal region; Figure 4.1). The other 83 supratentorial brain regions (i.e., low CMI burden region)

Table 4.1 | Characteristics of patients with and without CMIs

	Cortical CMI absent (N = 134)	Cortical CMI present (N = 30)
Demographics		
Age (years)	72 ± 11	71 ± 11
Sex (males)	**67 (50)**	**21 (70)***
Level of education (7 categories)	5 [4–6]	5 [4–6]
Cognitive performance		
MMSE (n = 161)	26 ± 3	25 ± 3
CDR	0.5 [0.5–1]	0.5 [0.5–1]
Clinical diagnosis (n = 154)		
NOCI	24 (19)	3 (11)
MCI	49 (39)	7 (25)
Alzheimer's dementia	48 (38)	13 (46)
Vascular dementia	**5 (4)**	**5 (18)***
Other[a]	8 (6)	2 (7)
Neuroimaging markers		
Total brain volume (% of TIV)	68 ± 4	67 ± 3
Gray matter volume (% of TIV)	36 ± 2	35 ± 2
WMH (Fazekas scale)	2 [1–2]	2 [1–2]
Presence of non-lacunar infarcts	**26 (19)**	**19 (63)¥**
Presence of lacunar infarcts	43 (32)	12 (40)
Presence of cerebral microbleeds	46 (35)	10 (35)

CMI, Cortical microinfarct; MMSE, mini-mental state examination; CDR, Clinical dementia rating scale; NOCI, No objective cognitive impairment; MCI, Mild cognitive impairment; TIV, total intracranial volume; WMH, White matter hyperintensities.

[a] Other: includes dementia such as Lewy body, primary progressive aphasia, cortical basal syndrome, unknown etc. Data presented as mean ± SD, n (percentages) or median [interquartile range].

* $p < 0.05$; ¥ $p < 0.0001$.

contained the remaining 37 cortical CMIs. The mean volume of the high CMI burden regions was 68 ± 8.5 ml (16% of total cortical GM volume) compared to 349 ± 41 ml of the low CMI burden regions. Network analyses showed that the high CMI burden regions were more highly connected to the rest of the network than the low CMI burden regions. This was reflected in a higher nodal degree (high burden: 27.2 ± 4.1 vs. low burden: 24.0 ± 2.8), higher FA-weighted nodal strength (high burden: 0.300 ± 0.020 vs. low burden: 0.293 ± 0.016) and higher MD-weighted nodal strength (high burden: 0.940×10^{-3} mm^2/s ± 0.059 vs. low burden: 0.985×10^{-3} mm^2/s ± 0.059 all comparisons $p < 0.0001$).

Association between cortical CMI presence and WM connectivity

The presence of cortical CMIs was not associated with whole brain FA- and MD-weighted WM connectivity (Table 4.2). Within the group of patients with cortical CMIs, the number of cortical CMIs (cortical CMI = 1 vs. cortical CMI ≥ 2) also was not related to whole brain FA- ($t_{(df=28)} = 0.71$, $p = 0.485$) or MD-weighted WM connectivity ($t_{(df=28)} = 0.05$, $p = 0.964$). Regional analyses showed that in the high CMI burden regions, patients with cortical CMIs had marginally higher MD-weighted WM connectivity (reflecting greater WM disruption), although not statistically significant ($p = 0.071$) while a similar FA-weighted

Table 4.2 | Association between cortical CMI presence and whole brain and regional FA- and MD-weighted WM connectivity in high and low CMI burden regions

	Cortical CMI absent (N = 134)	Cortical CMI present (N = 30)	Model 1		Model 2	
			Beta [95% CI]	p	Beta [95% CI]	p
Global WM connectivity						
FA	.294 ± .017	.290 ± .017	-.093 [-.256;.070]	.234	-.052 [-.234;.104]	.490
MD[a]	.979 ± .057	.993 ± .061	.087 [-.047;.228]	.208	.018 [-.108;.138]	.795
High cortical CMI burden regions						
FA	.301 ± .020	.296 ± .021	-.109 [-.254;.036]	.165	-.059 [-.216;.098]	.440
MD[a]	.936 ± .057	.958 ± .066	.136 [-.013;.285]	***.071***	.030 [-.102;.162]	.683
Low cortical CMI burden regions						
FA	.294 ± .016	.290 ± .016	-.091 [-.228;.068]	.247	-.051 [-.204;.102]	.501
MD[a]	.983 ± .058	1.000 ± .063	.082 [-.050;.208]	.231	.017 [-.102;.130]	.808

CMI, Cerebral microinfarct; FA, Fractional anisotropy-weighted WM connectivity; MD, Mean diffusivity-weighted WM connectivity. Lower FA and higher MD indicated impaired WM connectivity. [a] MD values × 10^{-3} mm^2/s .

Model 1: Covariates age and sex (degrees of freedom = 160).

Model 2: Covariates sex, age, WMH Fazekas grade 3, presence of lacunar and non-lacunar infarct (degrees of freedom = 157).

connectivity was observed (Table 4.2). These associations remained non-significant when conventional neuroimaging markers of vascular injury were entered as covariates in the model (Model 2; Table 4.2). Within the low CMI burden regions, cortical CMI presence was not associated with FA or MD-weighted WM connectivity (Table 4.2).

Since not all cortical CMIs were located in the high burden regions, a sensitivity analysis was performed between patients who had CMIs exclusively in the high burden regions (n = 20) and patients without CMIs, which yielded similar results.

A post-hoc power analysis for CMI presence in high CMI burden regions indicated a power of 0.24 for FA- and 0.44 for MD-weighted connectivity.

Voxel-based WM analysis

Limiting our analysis to WM voxels in close proximity to the cortex showed similar results, i.e., the presence of cortical CMIs was not associated with abnormal mean FA and MD in high CMI burden regions [FA: $t_{(df=158)} = -1.01$, $p = 0.314$; MD: $t_{(df=158)} = 0.753$, $p = 0.452$] or in low CMI burden regions [FA: $t_{(df=158)} = -0.97$, $p = 0.336$, MD: $t_{(df=158)} = 1.28$, $p = 0.204$].

Association between clinical diagnosis, WM connectivity and cortical CMI presence

Clinical diagnosis (NOCI, MCI, AD, or VaD) was a significant predictor of whole brain FA- [$F_{(df=4,152)} = 13.9$, $p = 0.005$) and MD-weighted WM connectivity [$F_{(df=4,152)} = 10.2$, $p = 0.008$]. Post-hoc analyses revealed that this effect was driven by the patients with the most severe clinical diagnosis, i.e., patients with AD and VaD had abnormal WM connectivity compared to the other groups (Figure 4.3). No significant interaction was observed between cortical CMI presence and clinical diagnosis on FA- or MD-weighted WM connectivity [$F_{(df=4,152)} = 0.42$, $p = 0.783$] or MD [$F_{(dfc=4,152)} = 0.67$, $p = 0.700$], indicating that the association between cortical CMI presence and WM connectivity did not differ across the various clinical diagnoses. In a sensitivity analysis of patients without dementia (n = 83) presence of cortical CMIs was also not associated with whole brain FA [$t_{(df=79)} = 0.43$, $p = 0.667$] or MD [$t_{(df=79)} = -0.92$, $p = 0.359$).

DISCUSSION

This study shows that cortical CMIs in memory clinic patients vascular brain injury display a strong spatial clustering, as more than 70% of the cortical CMIs were located in frontal, precentral, and postcentral brain regions covering only 16% of the cortical surface. These high

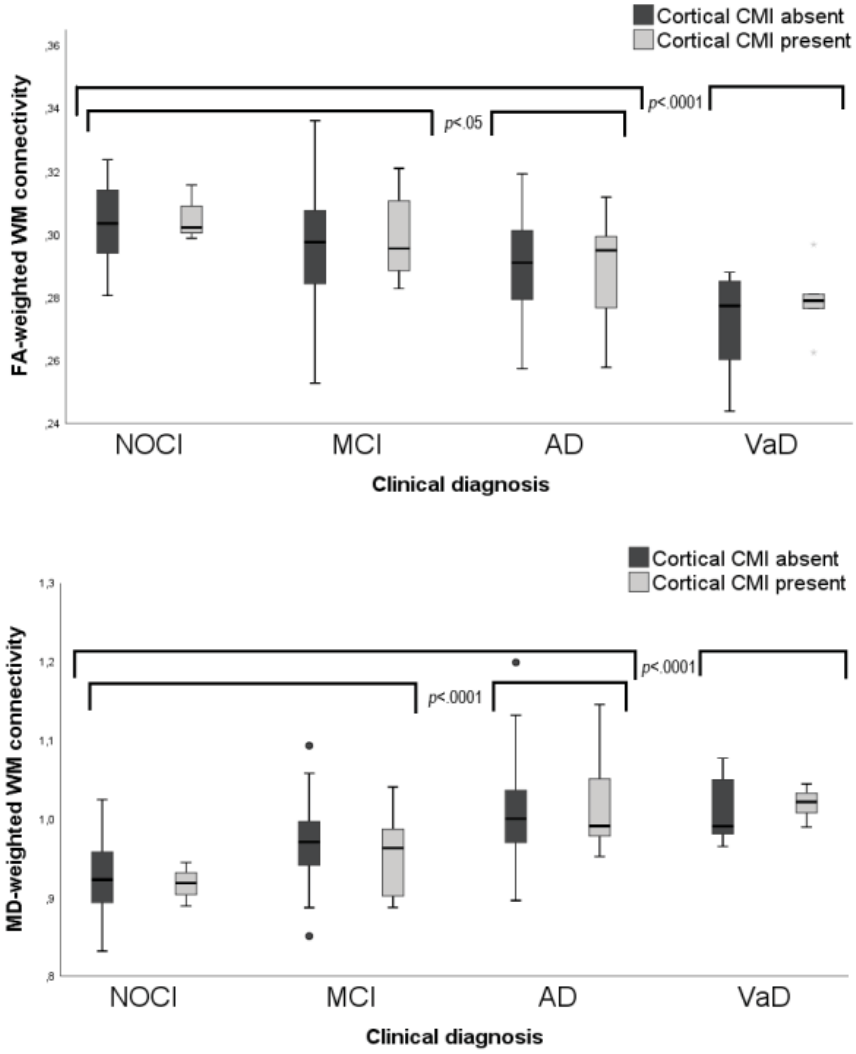

Figure 4.3 | Box plots of FA-(upper) and MD-(lower) weighted WM connectivity between patients with and without cortical CMIs (labels) clinical diagnosis (X-axis). MD values × 10^{-3} mm^2/s. CMI, Cortical microinfarct; NOCI, No objective cognitive impairment; MCI, Mild cognitive impairment; AD, Alzheimer's disease; VaD, Vascular dementia.

CMI burden regions proved to be strongly connected with the rest of the network. However, we found no evidence that the actual presence of cortical CMIs was related to disruption of WM connections to either the high CMI burden regions or within the whole brain.

Cortical CMIs showed a strong predilection for the frontal, precentral, and postcentral brain regions. A similar pattern of CMIs has been found in memory clinic patients,[6] but also

in patients with ischemic stroke,[7,39] Alzheimer's disease[40] and even in patients with CAA, where vessels are typically affected in the posterior brain regions.[41] This preferential lesion location is likely to be of etiological significance. A similar predilection for frontal, pre- and postcentral brain regions was observed in patients with poststroke cognitive impairment, where a thromboembolic origin has been suggested.[42] Future research is encouraged to further explore the relation between lesion location and the pathophysiological origin of cortical CMIs using larger study samples.

We hypothesized that cortical CMIs might affect cognitive performance by disruption of cerebral networks. We have previously reported a relationship between cortical CMIs and reduced cognitive performance on multiple domains in this same cohort.[4] In the current study we investigated impaired WM connectivity as possible underlying mechanism. As lesion location could be crucial for its effect on the cerebral network,[13] regions with high and low CMI burden were compared. We established no convincing relationship between cortical CMIs and WM connectivity, as the association between cortical CMIs and impaired WM connectivity in high CMI burden regions disappeared after correcting for conventional neuroimaging markers of vascular injury. These findings were in line with our voxel based analysis, showing no local disturbances in the WM directly below the cortical surface of high CMI burden regions. Independent of CMI presence, we did find that patients with dementia, especially VaD, presented with impaired WM connectivity, which corresponds to the known association between network disruption and cognitive deficits.[43]

Previous studies in patients with SVD found a disruptive effect of SVD MRI- manifestations, such as WMHs and lacunes, on WM connectivity.[8–10,12,14,44–46] Our study is the first to assess the effect of cortical CMIs and did not observe an effect on WM connectivity. This contrasting finding could be explained by the fact that these subcortical manifestations of SVD have a more direct impact on WM integrity, while cortical CMIs are thought to exert their effect indirectly through secondary degeneration. The limited size of the cortical CMIs could also account for the lack of association, as for macroscopic cortical infarcts the size of the lesion is directly correlated to the extent of the axonal injury.[47] Considering the average lesion volume of cortical CMIs on 3 tesla MRI is max 0.1 ml, their effect on WM connectivity could indeed be modest and not of major clinical relevance.

Since cortical CMIs were not related to WM connectivity, other underlying mechanisms should be considered to explain how cortical CMIs affect cognitive impairment. Our earlier work showed that the cortical CMIs were mainly associated with deficits in "cortical" cognitive domains, including visuoconstruction and language[4,6] suggesting that cortical CMIs potentially affect cognition by disruption of local cortical processes. This notion is supported by a mouse study, that found diminished neural activity and neurovascular coupling in the

cortical tissue surrounding the CMI.[48] An alternative explanation is that cortical CMIs are a marker of more widespread vascular brain damage that affects cognitive performance.[1,2] As cortical CMIs smaller than 1 mm escape detection on 3 tesla MRI, larger visible cortical CMIs probably only represent the tips of the iceberg. Moreover, it is important to clarify the etiological underpinning of both the detectable as well as these smaller cortical CMIs in order to develop therapeutic strategies that counter cognitive decline.

The strength of our study includes the use of high quality imaging and clinical data of this memory clinic cohort and the systematic approach in cortical CMI rating. Moreover, this study utilized two different DTI approaches to assess the relation with cortical CMIs; a network-based analysis and a voxel-based analysis. However, this study also has some limitations. Firstly, the sample size of cortical CMI cases in our cohort was small, since MRI detectable cortical CMIs occur only in approximately a quarter of memory clinic patients.[6] Based on our post-hoc power analysis for the observed effect sizes in our study, it would be recommended to replicate results in a larger cohort. Another possible limitation concerns the heterogeneity of the cohort, which includes memory clinic patients with different etiologies, severity of cognitive dysfunction and with large variation in cortical CMI burden. Although this reflects daily clinical practice, it may have reduced our sensitivity to detect abnormalities in WM connectivity due to cortical CMIs.

CONCLUSION

We showed that cortical CMIs in memory clinic patients displayed a strong local clustering in frontal and central brain regions, which warrants further investigations into their etiology. Nevertheless, the WM connections projecting to these regions were not impaired in patients with cortical CMIs. This does not support the hypothesis that cortical CMIs affect the brain's integrity through disturbance of WM connections, although further studies, also in larger cohorts with high burden of cortical CMIs, are recommended to confirm our observations.

ETHICS STATEMENT

Ethical approval was provided by the institutional review board of the UMC Utrecht. All procedures were in accordance with the ethical standards of the responsible committee on human experimentation (institutional and national) and with the Helsinki Declaration of 1975, as revised in 2013. Informed consent was obtained from all participants prior to any research related procedures.

ACKNOWLEDGMENTS

We would like to thank Hamed Yousefi Mesri MSc for technical support in the voxel-based analysis.

Members of the Utrecht VCI study group

Study group involved in the present study (in alphabetical order by department): University Medical Center Utrecht, the Netherlands, Department of Neurology: E. van den Berg, J.M. Biesbroek, G.J. Biessels, M. Brundel, W.H. Bouvy, L.G. Exalto, C.J.M. Frijns, O. Groeneveld, S.M. Heringa, N. Kalsbeek, L.J. Kappelle, Y.D. Reijmer, J. Verwer; Department of Radiology/Image Sciences Institute: J. de Bresser, H.J. Kuijf, A. Leemans, P.R. Luijten, M.A. Viergever, K.L. Vincken, J.J.M. Zwanenburg; Department of Geriatrics: H.L. Koek; Hospital Diakonessenhuis Zeist, the Netherlands: M. Hamaker, R. Faaij, M. Pleizier, E. Vriens.

REFERENCES

1. Smith EE, Schneider JA, Wardlaw JM, Greenberg SM. Cerebral microinfarcts: the invisible lesions. Lancet Neurol. 2012;11:272–82.
2. Van Veluw SJ, Shih AY, Smith EE, Chen C, Schneider JA, Wardlaw JM, et al. Detection, risk factors, and functional consequences of cerebral microinfarcts. Lancet Neurol. 2017;16:730–40.
3. Arvanitakis Z, Leurgans SE, Barnes LL, Bennett DA, Schneider JA. Microinfarct pathology, dementia, and cognitive systems. Stroke. 2011;42:722–7.
4. Ferro DA, van Veluw SJ, Koek HL, Exalto LG, Biessels GJ. Cortical cerebral microinfarcts on 3 tesla MRI in patients with vascular cognitive Impairment. J Alzheimer's Dis. 2017;60:1443–50.
5. Hilal S, Sikking E, Shaik MA, Chan QL, van Veluw SJ, Vrooman H, et al. Cortical cerebral microinfarcts on 3T MRI. Neurology. 2016;87:1583–90.
6. Van Veluw SJ, Hilal S, Kuijf HJ, Ikram MK, Xin X, Yeow TB, et al. Cortical microinfarcts on 3T MRI: Clinical correlates in memory-clinic patients. Alzheimer's Dement. 2015;11:1500–9.
7. Wang Z, van Veluw SJ, Wong A, Liu W, Shi L, Yang J, et al. Risk factors and cognitive relevance of cortical cerebral microinfarcts in patients with ischemic stroke or transient ischemic attack. Stroke. 2016;47:2450–55.
8. Lawrence AJ, Chung AW, Morris RG, Markus HS, Barrick TR. Structural network efficiency is associated with cognitive impairment in smallvessel disease. Neurology. 2014;83:304–11.
9. Tuladhar AM, van Dijk E, Zwiers MP, van Norden AGW, de Laat KF, Shumskaya E, et al. Structural network connectivity and cognition in cerebral small vessel disease. Hum Brain Mapp. 2016;37:300–10.
10. D'Souza MM, Gorthi S, Vadwala K, Trivedi R, Vijayakumar C, Kaur P, et al. Diffusion tensor tractography in cerebral small vessel disease: correlation with cognitive function. Neuroradiol J. 2018;31:83–9.
11. Reijmer YD, Fotiadis P, Martinez-Ramirez S, Salat DH, Schultz A, Shoamanesh A, et al. Structural network alterations and neurological dysfunction in cerebral amyloid angiopathy. Brain. 2015;138:179–88.
12. Heinen R, Vlegels N, de Bresser J, Leemans A, Biessels GJ, Reijmer YD. The cumulative effect of small vessel disease lesions is reflected in structural brain networks of memory clinic patients. NeuroImage Clin. 2018;19:963–9.
13. Reijmer YD, Fotiadis P, Piantoni G, Boulouis G, Kelly KE, Gurol ME, et al. Small vessel disease and cognitive impairment: The relevance of central network connections. Hum Brain Mapp. 2016;37:2446–54.
14. Auriel E, Edlow BL, Reijmer YD, Fotiadis P, Ramirez-Martinez S, Ni J, et al. Microinfarct disruption of white matter structure: a longitudinal diffusion tensor analysis. Neurology. 2014;83:182–8.
15. Boomsma JMF, Exalto LG, Barkhof F, van den Berg E, de Bresser J, Heinen R, et al. Vascular cognitive impairment in a memory clinic population: rationale and design of the "Utrecht-Amsterdam clinical features and prognosis in vascular cognitive impairment" (TRACE-VCI) study. JMIR Res Protoc. 2017;6:e60.
16. Fazekas F, Chawluk J, Alavi A, Hurtig H, Zimmerman R. MR signal abnormalities at 1.5 T in Alzheimer's dementia and normal aging. Am J Roentgenol. 1987;149:351–6.
17. Verhage F. Intelligentie en Leeftijd: Onderzoek bij Nederlanders Van Twaalf tot Zevenenzeventig Jaar. Van Gorcum. 1964.
18. Hughes CP, Berg L, Danziger WL, Coben LA, Martin RL. A new clinical scale for the staging of dementia. Br J Psychiatry. 1982;140:566–72.

19. Folstein MF, Folstein SE, McHugh PR. "Mini-mental state." A practical method for grading the cognitive state of patients for the clinician. J Psychiatr Res. 1975;12:189–98.
20. Román GC, Tatemichi TK, Erkinjuntti T, Cummings JL, Masdeu JC, Garcia JH, et al. Vascular dementia: diagnostic criteria for research studies. Report of the NINDS-AIREN international workshop. Neurology. 1993;43:250–60.
21. McKhann G, Drachman D, Folstein M, Katzman R, Price D, Stadlan EM. Clinical diagnosis of Alzheimer's disease: report of the NINCDS-ADRDA Work Group under the auspices of Department of Health and Human Services Task Force on Alzheimer's Disease. Neurology. 1984;34:939–44.
22. Wardlaw JM, Smith EE, Biessels GJ, Cordonnier C, Fazekas F, Frayne R, et al. Neuroimaging standards for research into small vessel disease and its contribution to ageing and neurodegeneration. Lancet Neurol. 2013;12:822–38.
23. Scheltens P, Launer LJ, Barkhof F, Weinstein HC, van Gool WA. Visual assessment of medial temporal lobe atrophy on magnetic resonance imaging: interobserver reliability. J Neurol. 1995;242:557–60.
24. Steenwijk MD, Pouwels PJW, Daams M, van Dalen JW, Caan MWA, Richard E, et al. Accurate white matter lesion segmentation by k nearest neighbor classification with tissue type priors (kNN-TTPs). NeuroImage Clin. 2013;3:462–9.
25. Valverde S, Oliver A, Roura E, Pareto D, Vilanova JC, Ramió-Torrentà L, et al. Quantifying brain tissue volume in multiple sclerosis with automated lesion segmentation and filling. NeuroImage Clin. 2015;9:640–7.
26. Valverde S, Oliver A, Lladó X. A white matter lesion-filling approach to improve brain tissue volume measurements. NeuroImage Clin. 2014;6:86–92.
27. Van Veluw SJ, Zwanenburg JJM, Engelen-Lee J, Spliet WGM, Hendrikse J, Luijten PR, et al. In vivo detection of cerebral cortical microinfarcts with high-resolution 7T MRI. J Cereb Blood Flow Metab. 2013;33:322–9.
28. Ritter F, Boskamp T, Homeyer A, Laue H, Schwier M, Link F, et al. Medical image analysis. IEEE Pulse. 2011;2:60–70.
29. Tzourio-Mazoyer N, Landeau B, Papathanassiou D, Crivello F, Etard O, Delcroix N, et al. Automated anatomical labeling of activations in SPM using a macroscopic anatomical parcellation of the MNI MRI single-subject brain. Neuroimage. 2002;15:273–89.
30. Reijmer YD, Leemans A, Caeyenberghs K, Heringa SM, Koek HL, Biessels GJ. Disruption of cerebral networks and cognitive impairment in Alzheimer disease. Neurology. 2013;80: 1370–7.
31. Leemans A, Jones DK. The B-matrix must be rotated when correcting for subject motion in DTI data. Magn Reson Med. 2009;61:1336–49.
32. Veraart J, Sijbers J, Sunaert S, Leemans A, Jeurissen B. Weighted linear least squares estimation of diffusion MRI parameters: strengths, limitations, and pitfalls. Neuroimage. 2013;81:335–46.
33. Tax CMW, Otte WM, Viergever MA, Dijkhuizen RM, Leemans A. REKINDLE: robust extraction of kurtosis INDices with linear estimation. Magn Reson Med. 2015;73:794–808.
34. Jeurissen B, Leemans A, Jones DK, Tournier JD, Sijbers J. Probabilistic fiber tracking using the residual bootstrap with constrained spherical deconvolution. Hum Brain Mapp. 2011;32: 461–79.
35. Tax CMW, Jeurissen B, Vos SB, Viergever MA, Leemans A. Recursive calibration of the fiber response function for spherical deconvolution of diffusion MRI data. Neuroimage. 2014;86:67–80.
36. Tournier JD, Calamante F, Connelly A. Robust determination of the fibre orientation distribution in diffusion MRI: non-negativity constrained super-resolved spherical deconvolution. Neuroimage. 2007;35:1459–72.

37. Rubinov M, Sporns O. Complex network measures of brain connectivity: uses and interpretations. Neuroimage. 2010;52:1059–69.
38. Faul F, Erdfelder E, Lang A-G, Buchner A. G*Power: A flexible statistical power analysis program for the social, behavioral, and biomedical sciences. Behav Res Methods. 2007;39: 175–91.
39. Fu R, Wang Y, Wang Y, Liu L, Zhao X, Wang DZ, et al. The development of cortical microinfarcts is associated with intracranial atherosclerosis: data from the Chinese intracranial atherosclerosis study. J Stroke Cerebrovasc Dis. 2015;24:2447–54.
40. Suter OC, Sunthorn T, Kraftsik R, Straubel J, Darekar P, Khalili K, et al. Cerebral hypoperfusion generates cortical watershed microinfarcts in Alzheimer disease. Stroke. 2002;33:1986–92.
41. van den Brink H, Zwiers A, Switzer AR, Charlton A, McCreary CR, Goodyear BG, et al. Cortical Microinfarcts on 3T magnetic resonance imaging in cerebral amyloid angiopathy. Stroke. 2018;49:1899–905.
42. Zhao L, Biesbroek JM, Shi L, Liu W, Kuijf HJ, Chu WWC, et al. Strategic infarct location for post-stroke cognitive impairment: a multivariate lesionsymptom mapping study. J Cereb Blood Flow Metab. 2017;38:1299–311.
43. Palesi F, De Rinaldis A, Vitali P, Castellazzi G, Casiraghi L, Germani G, et al. Specific patterns of white matter alterations help distinguishing Alzheimer's and vascular dementia. Front Neurosci. 2018;12:274.
44. Heringa SM, Reijmer YD, Leemans A, Koek HL, Kappelle LJ, Biessels GJ. Multiple microbleeds are related to cerebral network disruptions in patients with early Alzheimer's disease. J Alzheimer's Dis. 2014;38:211–21.
45. Papma JM, de Groot M, de Koning I, Mattace-Raso FU, van der Lugt A, Vernooij MW, et al. Cerebral small vessel disease affects white matter microstructure in mild cognitive impairment. Hum Brain Mapp. 2014;35:2836–51.
46. Kim HJ, Im K, Kwon H, Lee JM, Kim C, Kim YJ, et al. Clinical effect of white matter network disruption related to amyloid and small vessel disease. Neurology. 2015;85:63–70.
47. Mark VW, Taub E, Perkins C, Gauthier LV, Uswatte G, Ogorek J. Poststroke cerebral peduncular atrophy correlates with a measure of corticospinal tract injury in the cerebral hemisphere. Am J Neuroradiol. 2008;29:354–8.
48. Summers PM, Hartmann DA, Hui ES, Nie X, Deardorff RL, McKinnon ET, et al. Functional deficits induced by cortical microinfarcts. J Cereb Blood Flow Metab. 2017;37:3599–614.

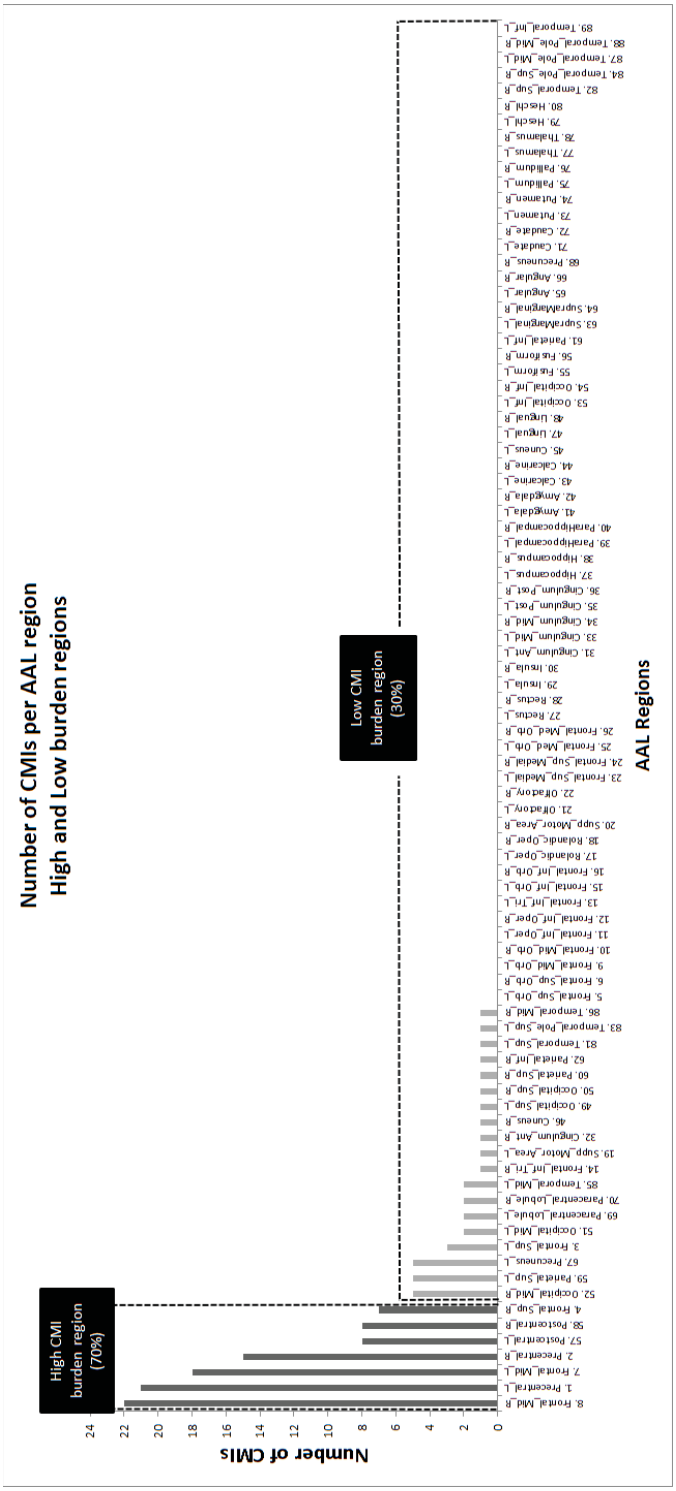

Supplementary Figure S4.1 | Histogram of the number of cortical CMIs per AAL region and allocation of high and low CMI burden regions.

Chapter 5

The cumulative effect of small vessel disease lesions is reflected in structural brain networks of memory clinic patients

Rutger Heinen*
Naomi Vlegels*
Jeroen de Bresser
Alexander Leemans
Geert Jan Biessels
Yael Reijmer
on behalf of the Utrecht VCI study group

* These authors have contributed equally to this work

Neuroimage Clin. 2018;19:963–9

ABSTRACT

Mechanisms underlying cognitive impairment in patients with small vessel disease (SVD) are still unknown. We hypothesized that cognition is affected by the cumulative effect of multiple SVD-related lesions on brain connectivity. We therefore assessed the relationship between the total SVD burden on MRI, global brain network efficiency, and cognition in memory clinic patients with vascular brain injury.

173 patients from the memory clinic of the University Medical Center Utrecht underwent a 3T brain MRI scan (including diffusion MRI sequences) and neuropsychological testing. MRI markers for SVD were rated and compiled in a previously developed total SVD score. Structural brain networks were reconstructed using fiber tractography followed by graph theoretical analysis. The relationship between total SVD burden score, global network efficiency and cognition was assessed using multiple linear regression analyses.

Each point increase on the SVD burden score was associated with 0.260 [-0.404 – -0.117] SD units decrease of global brain network efficiency ($p < 0.001$). Global network efficiency was associated with in-formation processing speed (standardized $B = -0.210$, $p = 0.004$) and attention and executive functioning ($B = 0.164$, $p = 0.042$), and mediated the relationship between SVD burden and information processing speed ($p = 0.027$) but not with executive functioning ($p = 0.12$).

Global network efficiency is sensitive to the cumulative effect of multiple manifestations of SVD on brain connectivity. Global network efficiency may therefore serve as a useful marker for functionally relevant SVD-related brain injury in clinical trials.

INTRODUCTION

Small vessel disease (SVD) is a common cause of cognitive decline and dementia.[1] However, the mechanisms underlying cognitive impairment in SVD remain largely unknown. A proposed mechanism is that SVD-related lesions (such as white matter hyperintensities (WMH), lacunes, cerebral microbleeds (CMB), and perivascular spaces (PVS)) affect structural brain connectivity and thereby the efficiency of the brain network to process information. Due to recently developed techniques, we can now estimate the efficiency of the brain network using diffusion MRI and graph theory analyses. Several studies have shown that global network efficiency is related to reduced processing speed and executive functioning in patients with SVD.[2–5] In these studies, associations between network efficiency and cognition were found to be stronger than between individual MRI markers of SVD and cognition.[6] One reason for the strong associations between network efficiency and cognition, could be a sensitivity of network efficiency to the cumulative effect of multiple types of SVD-related injury on brain connectivity.[7] In previous studies a total SVD burden score was used to capture these multiple types of SVD-related injury.[8–10] To date, the association between increasing SVD burden and brain network efficiency has not yet been assessed in memory clinic patients. In the current study, we used a previously developed total SVD score that combines various well-established MRI markers of SVD[8–10] to test the relationship between SVD, global network efficiency, and cognition. We expected that with increasing SVD burden (i.e. a higher SVD burden score), global network efficiency would decrease. Secondly, we hypothesized that global network efficiency mediates the association between total SVD score and cognition (i.e. processing speed and executive functioning).

METHODS

Study population

Patients in the current study were recruited from the memory clinic at the University Medical Center Utrecht (UMC Utrecht) between September 2009 and December 2013. This study sample has been described in detail earlier.[11] In short, all patients that presented with cognitive complaints and vascular brain injury on MRI (i.e. possible VCI) were eligible to participate. In order to capture the whole spectrum of possible VCI, we defined no threshold for cognitive impairment or specific patterns of vascular brain injury. Vascular brain injury was operationalized as:[11] either (1) WMH with a Fazekas scale grade ≥ 2, (2) Fazekas scale grade 1 combined with two or more vascular risk factors (hypertension, hypercholesterolemia, diabetes mellitus, obesity or current

smoking) (3) presence of ≥ 1 lacunar infarcts, (4) presence of ≥ 1 non-lacunar infarct (5) presence of ≥ 1 cerebral microbleeds or (6) presence of ≥ 1 intracerebral haemorrhage. All markers were rated according to the STRIVE criteria.[12] Absence or presence of possible co-existing neurodegenerative disorders did not play a role in the selection of patients.[11] Patients with a primary etiology other than vascular brain injury or an etiology other than neurodegeneration were excluded. All patients underwent a one-day evaluation consisting of an interview, a physical and a neurological examination, neuropsychological assessment and a brain MRI scan. During the interview and physical examination, information on education, smoking, medical history, use of medication, BMI and blood pressure was collected. In total, 173 patients were included in the analyses. The study was approved by the institutional review board of the UMC Utrecht. All patients provided informed consent prior to any research procedures.

MRI data acquisition

All patients underwent a brain MRI scan using a Philips 3T scanner (Achieva, Philips, Best, the Netherlands). The standardized MRI protocol included the following transversal 2D sequences (48 slices, voxel size: 0.96 × 0.96 × 3.00 mm): T2-weighted (repetition time (TR)/ echo time (TE): 3198/140 ms), T2*-weighted (TR/TE: 1653/20 ms), and fluid-attenuated inversion recovery sequence (FLAIR; TR/TE/Inversion time: 11000/125/2800 ms). The MRI protocol also included a 3D T1-weighted sequence (192 slices, voxel size: 1.00 × 1.00 × 1.00 mm, TR/TE: 7.9/4.5 ms), and a diffusion-weighted sequence 48 slices, voxel size: 1.72 × 1.72 × 2.50 mm, TR/TE: 6600/73 ms, 45 gradient directions with a b-value of 1200 s/mm^2 and one with a b value of 0 s/mm^2 (number of signal averages = 3).

Small vessel disease burden on MRI

MRI images were rated for the presence of WMH of presumed vascular origin, lacunes of presumed vascular origin, CMB, and basal ganglia PVS by trained and experienced raters (RH under supervision of JdB) according to the STRIVE criteria.[12] Perivascular and deep WMH were rated using the Fazekas scale on the FLAIR sequence.[13] Lacunes were defined as hypointense areas between 2 and 15 mm on both FLAIR and T1-weighted images with a hyperintense rim on FLAIR images. CMB were defined as small, homogenous, round, focal areas of hypointense areas on T2*-weighted images. Basal ganglia PVS were defined as small linear hyperintensities on T2-weighted images. PVS were rated according to a semi-quantitative scale ranging from 0 to 4.[14] Subsequently, a total SVD score was constructed for each patient according to a previously developed scale, see Figure 5.1.[8–10] This score summarizes the presence or severity of each of four SVD MRI markers: beginning confluent to confluent deep WMH (deep WMH Fazekas grade ≥ 2) and/or irregular periventricular

WMH extending into the deep white matter (periventricular WMH Fazekas grade 3) (one point); presence of lacunes (one point); presence of CMB (one point); and moderate to severe PVS in the basal ganglia (grade 2–4 on semi-quantitative scale)[14] (one point). Due to motion artifacts, CMB and basal ganglia PVS could not be scored for 2 patients. For these 2 patients, CMB and basal ganglia PVS were not included in the calculation of the total SVD score.

Total brain volume

For all patients, segmentations of grey matter, white matter and cerebrospinal fluid were obtained for an earlier study with FreeSurfer version 5.3.0 (http://surfer.nmr.mgh.harvard.edu/)[15] using the 3D T1-weighted sequence. All brain volume segmentations underwent a visual quality check and were manually edited if needed. Manual edits consisted of correcting for large ventricles, correcting the brain mask and correcting for WMH. Total brain volume was defined as the sum of the grey and white matter volumes. To normalize total brain volume for variations in head size, total brain volume was adjusted for intracranial volume. Normalized total brain volumes were generated from linear regression of the residuals.[16]

Diffusion MRI processing and tractography

Brain networks were reconstructed as described previously,[2,3] using ExploreDTI version 4.8.6 (http://www.exploredti.com)[17] Preprocessing of the data included correction for subject motion and eddy current induced geometric distortions followed by robust tensor estimation (including adjustment of the B-matrix).[18–20] During the motion-distortion correction, all scans were rigidly registered to Montreal Neurological Institute space. For each patient, whole-brain white matter tractography was performed using constrained spherical deconvolution (CSD)-based tractography, which allows for the reconstruction of pathways that go through crossing fiber regions.[21–24] Fiber tracts were reconstructed by starting seed samples uniformly distributed throughout the white matter of the brain at a 2 mm isotropic resolution. Fiber tracts were terminated when they deflected in an angle of > 45° or if they entered a voxel with a fiber orientation distribution threshold of < 0.1. Brain network nodes were defined using the automated anatomic labeling (AAL) template,[25] resulting in 90 cortical and subcortical brain regions. Two brain regions were considered to be connected if two end points of a reconstructed fiber bundle lay within both regions. This resulted in a 90 × 90 binary connectivity matrix. For all patients, each connection was multiplied by the mean fractional anisotropy (FA) of that connection which resulted in a 90 × 90 weighted connectivity matrix. For a graphical representation, see Figure 5.1.

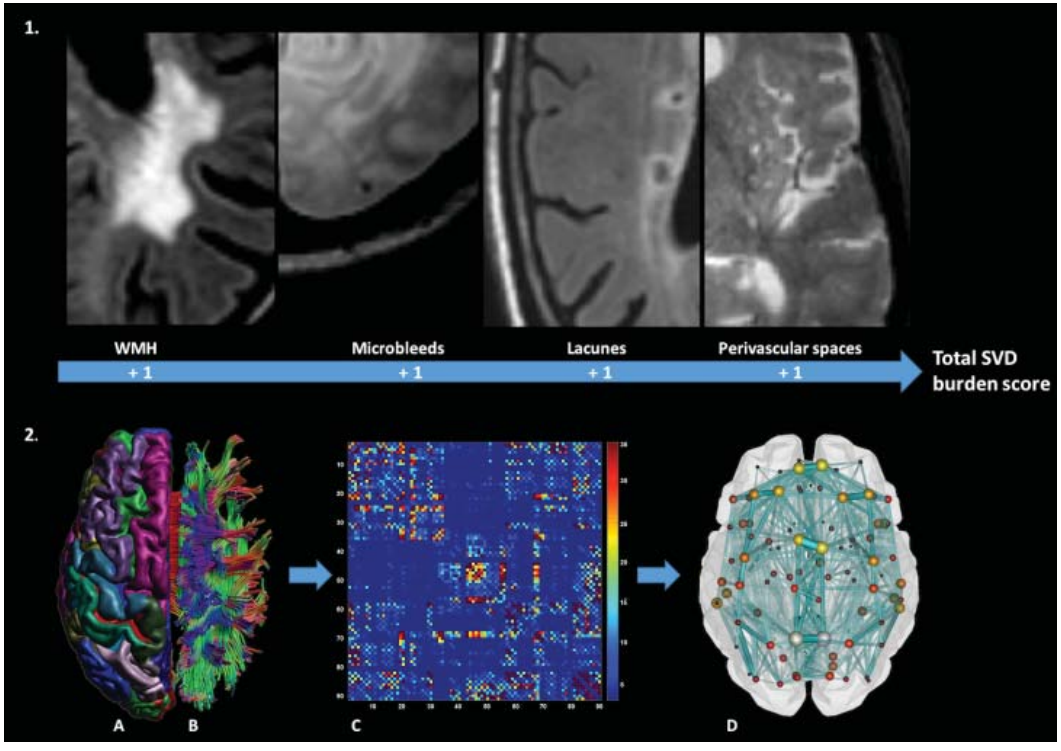

Figure 5.1 | Flowchart of construction of SVD burden score and structural network reconstruction. Panel 1 depicts the calculation of the total small vessel disease burden score. One point is added to the score for the presence for (1) Deep WMH (Fazekas grade ≥ 2) or perivascular WMH (Fazekas grade 3), (2) Presence of microbleeds, (3) Presence of lacunes, and (4) > 10 perivascular spaces. Panel 2 depicts (A) The coregistration of an Automated Anatomical Labeling atlas (AAL) template, consisting of 90 cortical and subcortical brain regions to (B) the whole-brain Constrained Spherical Deconvolution (CSD)-based tractography, (C) For any two regions of the AAL template, it was established if a connection was present. Each connection was multiplied by the mean fractional anisotropy (FA) of that connection, resulting in a 90 × 90 weighted connectivity matrix. (D) The weighted connectivity matrix can be viewed as a graph composed of nodes (brain regions) and edges (white matter connections). Network measures such as global network efficiency were calculated on individual structural brain networks.

Brain network characteristics

Characteristics of the organization of the reconstructed structural brain networks were computed using the Brain Connectivity Toolbox.[26] First, the degree of the structural brain network was calculated on the binary connectivity matrices. Degree is defined as the number of connections per node.[26] Next global efficiency was computed on the FA-weighted connectivity matrices. Global efficiency reflects the ability to rapidly exchange information between distributed brain regions.[26] Global efficiency was calculated as the inverse of the characteristic path length. The characteristic path length quantifies the average number of connections between regions along the shortest path. The shorter the path length, the higher the efficiency of the network.[26] Global network efficiency was transformed into standardized z-scores to ease interpretation of the results.

Cognitive testing

All patients underwent standardized neuropsychological testing. The present study focused on the domains "information processing speed" and "attention and executive functioning" as these are among the most frequently impaired cognitive domains in patients with VCI.[27] Information processing speed was assessed by completion time of the Trail Making Test (TMT) A[28] and completion time of the Stroop Color Word test I and II,[29] and the Digit symbol-coding test.[30] Attention and executive functioning was assessed by the ratio of completion time of the TMT-A and TMT-B,[28] and completion time of the Stroop Color Word test part III (adjusted for part I and II),[29] and two verbal fluency tasks: category naming and lexical fluency.[31] Z-scores were calculated for each test using the means and standard deviations of the present sample and averaged for tests comprising one cognitive domain.

Statistical analysis

The relationship between the total SVD score and global brain network efficiency was evaluated with multiple linear regression analysis (resulting in unstandardized betas with a 95% confidence interval and p-values ($\alpha = 0.05$)). Next, correction for possible confounding effects of age, sex, vascular risk factors (hypertension, hypercholesterolemia, diabetes mellitus, and current smoking) and normalized total brain volume was performed by adding those variables as covariates in the model. Correction was also performed for the degree of the network. In a sensitivity analysis, the regression was repeated in patients without a clinical diagnosis of Alzheimer's disease (AD). To verify whether the associations with the total SVD burden score were not driven by WMH, the most common SVD marker in our cohort, we recalculated SVD-scores without WMH. To check whether the tractography

was affected by WMH, we assessed the association between WMH severity and number of network connections.

To assess the association between the total SVD score/global network efficiency and cognition, multiple linear regression analyses were performed. Correction was performed for possible confounding effects of age, sex and education and subsequently for vascular risk factors and normalized total brain volume. Correction was performed for normalized total brain volume and degree of the structural brain network.

Finally, a mediation analysis was performed using the PROCESS (v2.16.3) macro[32] in SPSS to test whether the relationship between SVD burden and cognition was mediated by global network efficiency. The indirect effect of the mediation was tested with 5000 bootstrapping samples and 95% confidence interval.

RESULTS

Patient characteristics

Patient characteristics are shown in Table 5.1. 98% of the patients had some degree of WMH (Fazekas grade 1 or more), with 58% having moderate to severe WMH (Fazekas grade 2–3). Almost all patients (96%) had moderate to severe PVS (PVS score grade 2–4). Mean ± SD total brain volume of the patients was 962 ± 108 (normalized for intracranial volume 959 ± 96 cm^3). As a reference, non-normalized brain volumes in non-demented elderly controls have been estimated at 1013 ± 96 cm^3, using the same method.[33]

Relationship between total SVD score and global network efficiency

The analysis between total SVD score and structural brain network measures showed that with each point increase in total SVD burden on MRI, there was a decrease in global network efficiency (regression coefficient: B [95% CI] = -0.260 [-0.406 – -0.114], p = 0.001, see Figure 5.2). In other words, there was a dose-response relationship between the cumulative effect of SVD markers and global network efficiency. After controlling for age, sex, vascular risk factors (hypertension, hypercholesterolemia, diabetes mellitus and current smoking) and normalized total brain volume this association remained significant (B = -0.239 [-0.390 – -0.089], p = 0.002). The association between total SVD burden and global network efficiency was not changed by controlling for degree of the network (B = -0.285 [-0.366 – -0.204], p < 0.001), indicating that the association with network efficiency was not driven by variations in the network density. A sensitivity analysis in patients without a diagnosis of AD showed similar results (B = -0.361 [-0.523 – -0.199], p < 0.001). Exclusion

Table 5.1 | Patient characteristics

	Total SVD score				
	0 N = 6	1 N = 47	2 N = 65	3 N = 37	4 N = 18
Age in years	64 ± 10	69 ± 10	73 ± 10	76 ± 11	71 ± 12
Female sex, %	33	47	43	49	39
Level of education[a]	5 (3–7)	5 (1–7)	5 (2–7)	5 (2–7)	6 (2–7)
MMSE	27.5 (25–28)	26 (7–30)	27 (17–30)[†]	26 (21–30)	27 (21–30)[‡]
Vascular risk factors					
Hypertension, %	100	96	89	95	100
Hypercholesterolemia, %	100	89	63	62	78
Diabetes mellitus, %	33	47	25	40.5	44
Current smokers, %	50	32[†]	9[†]	8	22
Neuroimaging markers					
Basal ganglia PVS score	1 (1)	2 (2–3)	2 (1–3)	3 (2–4)	3 (2–3)
WMH Fazekas scale grade					
Periventricular	1 (1)	1 (0–3)	2 (0–3)	2 (1–3)	2.5 (1–3)
Deep	1 (0–1)	1 (0–3)	1 (0–3)	2 (1–3)	2.5 (1–3)
Total SVD score					
Presence of lacunes, %	-	-	32	59.5	100
Presence of microbleeds, %	-	-	32	57	100
Basal ganglia PVS (grade 2–4)	-	98	98.5	100	100
Moderate to severe WMH (Fazekas: PV = 3 or Deep ≥ 2)	-	2	37	84	100

Data are given as mean ± SD, percentages or median (range). MMSE, Mini Mental State Exam; PVS, Perivascular Spaces; WMH, White Matter Hyperintensities; PV, periventricular. [a] Verhage scale: (1) less than six years of primary education, (2) finished six years of primary education, (3) six years primary education and less than two years of low level secondary education, (4) four years of low level secondary education, (5) four years of average level secondary education, (6) five years of high level secondary education, (7) university degree.[34] [b] 2 missing. [c] 1 missing.

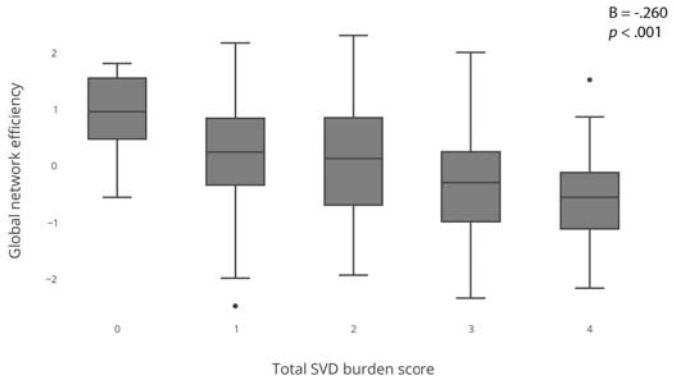

Figure 5.2 | Relationship between total SVD score and global network efficiency. Boxplots showing the relationship between total small vessel disease burden score and global network efficiency (z-scores) in patients with vascular cognitive impairment.

of WMH from the total SVD score showed that the association with global efficiency was not primarily driven by WMH (B = -0.247 [-0.445 – -0.050], p = 0.014). Because 96% of the sample obtained a point for the presence of basal ganglia PVS, we re-calculated the total SVD score using a stricter cut-off value (i.e. > 20 PVS, 45% of the sample). The adapted total SVD score, however, did not change the association with global network efficiency (B = -0.208 [-0.328 – -0.088], p = 0.001).

There was no relationship between number of network connections and WMH severity (B = 0.048 [-0.176–0.273], p = 0.671), indicating that WMH severity did not significantly affect the tractography results.

Relationship between total SVD score, global network efficiency and cognition

The analysis between total SVD score and cognition showed that the total SVD score tended to be associated with performance on both information processing speed (B = -0.123 [-0.273–0.026], trend p = 0.105) and attention and executive functioning (B = -0.140 [-0.289–0.008], trend p = 0.064), albeit not significantly (see Figure 5.3). After correction for age, sex, education and vascular risk factors the effect remained non-significant (information processing speed B = -0.115 [-0.254–0.025], p = 0.106; attention and executive functioning: B = -0.119 [-0.273–0.035], p = 0.129).

As can be seen in Figure 5.4, global efficiency was associated with both information processing speed (B = 0.265 [0.115–0.414], p = 0.001) and attention and executive functioning (B = 0.171 [0.019–0.324], p = 0.028). After correction for age, sex, education, vascular risk factors and normalized total brain volume, this effect remained significant for information processing speed (B = 0.223 [0.087–0.359], p = 0.001) and attention and executive functioning (B = 0.175 [0.021–0.330], p = 0.027). Lastly, correcting for the degree of the structural networks did not change the results (information processing speed: B = 0.320 [0.082–0.588], p = 0.009; attention and executive functioning: B = 0.298 [0.056–0.539], p = 0.016).

Mediation analysis

The association between SVD burden and cognition was similar as reported in a previous study.[10] Albeit, not significant in our study. This could be due to a lower number of subjects. Nevertheless, a valid indirect mediation effect can still be established in the absence of a significant total effect as was shown in previous studies.[35–37] In the current study, mediation analysis showed that global network efficiency mediated the relationship between SVD burden and information processing speed (indirect effect B = -0.059 [-0.126 – -0.017],

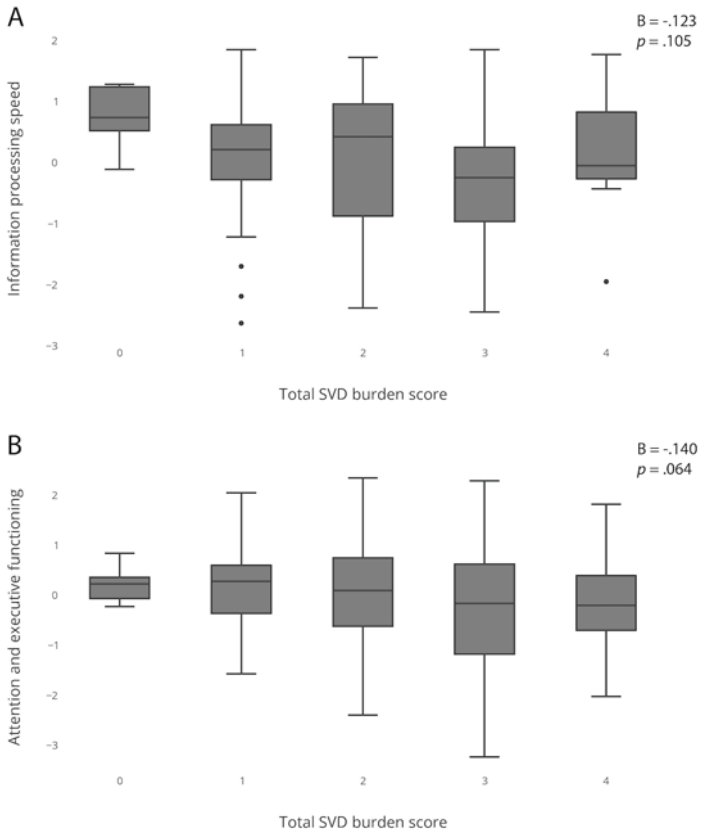

Figure 5.3 | Relationship between total SVD score and cognition. Boxplots showing the relationship between total small vessel disease burden score and information processing speed (A) and attention and executive functioning (B). Information processing speed and attention and executive functioning are shown as z-scores.

p = 0.027), but not the relationship between SVD burden and attention and executive functioning (indirect effect B = -0.035 [-0.089 – -0.005], p = 0.12).

DISCUSSION

The present study showed a dose-response relationship between the total SVD burden on MRI and decreased global network efficiency in memory clinic patients with vascular brain injury. Furthermore, global network efficiency mediated the association between SVD burden and information processing speed. These findings indicate that the cumulative effect of different manifestations of SVD partly affect cognition by disrupting structural brain connectivity.

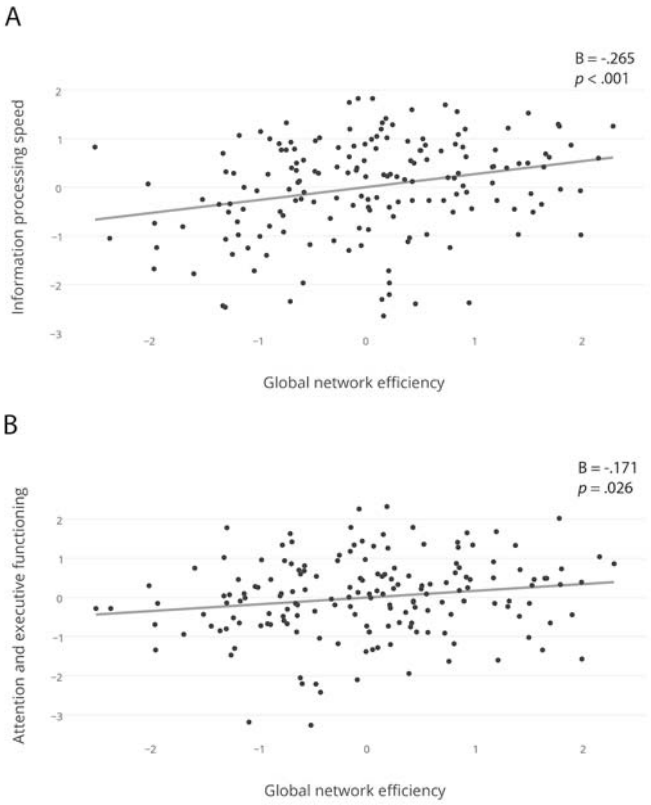

Figure 5.4 | Relationship between global network efficiency and cognition. Scatterplot showing the relationship between global network efficiency and information processing speed (A) and attention and executive functioning (B). Both global network efficiency and cognitive performance are shown as z-scores.

Our results complement earlier studies that assessed the relationship between SVD, structural network measures and cognition.[4,5,10] Two previous studies found a mediating role for global network measures in the relationship between individual SVD markers and cognition.[4,5] Our results indicate that this mechanistic pathway might be better studied by considering the total burden of SVD than by individual markers. The greater the SVD burden, the lower the efficiency of the brain network to integrate information between remotely connected brain regions. The functional consequences of these network impairments seem to primarily involve information processing speed and executive functioning.[4,5] However, the mediation effect in our study was only significant for processing speed. While it is common to only perform mediation analysis in case of a significant total effect (as described earlier),[38] which in our case would be a significant association between total SVD burden and cognition, recent studies have demonstrated

that a valid indirect mediation effect can be established in the absence of a significant total effect.[35–37]

SVD is a heterogeneous disease that manifests itself in different ways. We expected that a total SVD burden score could be better capable of capturing this heterogeneity than individual SVD markers. In the present study, we indeed found that the relationship between total SVD burden and structural brain connectivity was not driven by one of the common individual SVD markers, such as WMH, supporting the cumulative effect of SVD markers on the structural brain network. A previous study has shown that SVD markers also have a cumulative effect on cognition.[10] However, the strength of the association between total SVD burden score and cognition in our sample and in the previous study[10] were modest, and in our case not significant, which can be explained by the smaller sample size.

Measures of global network connectivity quantify more than what is visible on conventional MRI. For example, diffusion MRI can also detect subtle changes in the so-called normal appearing white matter (NAWM). Diffusion abnormalities in the NAWM, such as decreased FA, are very common in patients with SVD and have been associated with SVD-related cognitive impairment.[39–42] However, whether the diffusion abnormalities in the NAWM indeed reflect SVD-related pathology is not known. Alternatively, it may reflect white matter damage caused by non-vascular pathologies, such as neurodegeneration and age.[7] In our view, diffusion measures and structural network measures should thus not be seen as a specific marker for SVD, but as a sensitive marker that integrates impairments in brain connectivity caused by multiple factors that together explain part of the cognitive performance in patients with SVD.

This study is the first to assess the association between total SVD burden, global network efficiency and cognitive performance in a relatively large sample of patients with different degrees of vascular brain injury. High quality, standardized structural MRI data were used in combination with detailed cognitive testing. One limitation of the DTI data is that only one b-zero image was acquired, which might have confounded the DTI estimates. Also regions in which WMH is present, have relatively low FA values.[43,44] This may have affected the tractography results. However we found no association between WMH severity and number of network connections. A possible limitation to this study could be the selection of our patients. Since all patients were recruited from the memory clinic and no selection was made based on absence or presence of co-existing neurodegenerative disorders, patients with mixed diagnoses and mixed pathologies were included in this study sample. As vascular brain injury commonly co-occurs with other pathologies, this does reflect clinical practice. Moreover, a sensitivity analysis in which all patients with AD were excluded, showed that the cumulative effect of SVD markers on global network efficiency was even stronger in

this subset of patients. Our sample was selected based on the presence of SVD, which explains why almost all patients had some degree of basal ganglia PVS (96%). However, recalculating the total SVD score for all patients with a higher cut-off for PVS did not change the results. The construction of the total SVD score might be another limitation of this study. The score takes neither location nor number of individual SVD marker into account. Also, the same weight is assigned to each marker. Future studies should evaluate whether the total SVD score can be improved by including such information.

CONCLUSION

Our findings support the hypothesis that global network efficiency is sensitive to the cumulative effect of multiple manifestations of SVD on brain connectivity and may therefore serve as a useful marker for functionally relevant disease progression in clinical trials.

ACKNOWLEDGMENTS

Members of the Utrecht Vascular Cognitive Impairment (VCI) study group involved in the present study (in alphabetical order by department): University Medical Center Utrecht, the Netherlands, Department of Neurology: E. van den Berg, G.J. Biessels, L.G. Exalto, C.J.M. Frijns, O. Groeneveld, R. Heinen, S.M. Heringa, L.J. Kappelle, Y.D. Reijmer, J. Verwer, N. Vlegels; Department of Radiology/Image Sciences Institute: J. de Bresser, H.J. Kuijf, A. Leemans; Department of Geriatrics: H.L. Koek; Hospital Diakonessenhuis Zeist, the Netherlands: M. Hamaker, R. Faaij, M. Pleizier, E. Vriens.

REFERENCES

1. Gorelick PB, Scuteri A, Black SE, DeCarli C, Greenberg SM, Iadecola C, et al. Vascular contributions to cognitive impairment and dementia: a statement for healthcare professionals from the American heart association/American stroke association. Stroke. 2011;42:2672–713.
2. Reijmer YD, Leemans A, Caeyenberghs K, Heringa SM, Koek HL, Biessels GJ, Utrecht Vascular cognitive impairment study group. Disruption of cerebral networks and cognitive impairment in Alzheimer disease. Neurology. 2013;80:1370–7.
3. Reijmer YD, Fotiadis P, Martinez-Ramirez S, Salat DH, Schultz A, Shoamanesh A, et al. Structural network alterations and neurological dysfunction in cerebral amyloid angiopathy. Brain. 2015;138:179–88.
4. Lawrence AJ, Chung AW, Morris RG, Markus HS, Barrick TR. Structural network efficiency is associated with cognitive impairment in small-vessel disease. Neurology. 2014;83:304–11.
5. Tuladhar AM, van Dijk E, Zwiers MP, van Norden AGW, de Laat K, Shumskaya E, et al. Structural network connectivity and cognition in cerebral small vessel disease. Hum Brain Mapp. 2016;37:300–10.
6. Patel B, Markus HS. Magnetic resonance imaging in cerebral small vessel disease and its use as a surrogate disease marker. Int J Stroke. 2011;6:47–59.
7. Sun X, Salat D, Upchurch K, Deason R, Kowall N, Budson A, et al. Destruction of white matter integrity in patients with mild cognitive impairment and Alzheimer disease. J Investig Med. 2014;62:927–33.
8. Huijts M, Duits A, Van Oostenbrugge RJ, Kroon AA, de Leeuw PW, Staals J. Accumulation of MRI markers of cerebral small vessel disease is associated with decreased cognitive function. A study in first-ever lacunar stroke and hypertensive patients. Front Aging Neursci. 2013;5:72.
9. Staals J, Makin S, Doubal F, Dennis M, Wardlaw JM. Stroke subtype, vascular risk factors and total MRI brain small-vessel disease burden. Neurology. 2014;83:1228–34.
10. Staals J, Booth T, Morris Z, Bastin ME, Gow AJ, Corley J, et al. Total MRI load of cerebral small vessel disease and cognitive ability in older people. Neurobiol Aging. 2015;36:2806–11.
11. Boomsma JMF, Exalto LG, Barkhof F, van den Berg E, de Bresser J, Heinen R, et al. Vascular cognitive impairment in a memory clinic population: rationale and design of the "Utrecht-Amsterdam clinical features and prognosis in vascular cognitive impairment" (TRACE-VCI) study. JMIR Res Protoc. 2017;6:e60.
12. Wardlaw JM, Smith EE, Biessels GJ, Cordonnier C, Fazekas F, Frayne R, et al. Neuroimaging standards for research into small vessel disease and its contribution to ageing and neurodegeneration. Lancet Neurol. 2013;12:822–38.
13. Fazekas F, Chawluk JB, Alavi A, Hurtig HI, Zimmerman RA. MR signal abnormalities at 1.5 T in Alzheimer's dementia and normal aging. AJR Am J Roentgenol. 1987;149:351–6.
14. Doubal FN, Maclullich AM, Ferguson KJ, Dennis MS, Wardlaw JM. Enlarged perivascular spaces on MRI are a feature of cerebral small vessel disease. Stroke. 2010;41:450–4.
15. Fischl B, Salat DH, Busa E, Albert M, Dieterich M, Haselgrove C, et al. Whole brain segmentation: automated labeling of neuroanatomical structures in the human brain. Neuron. 2002;33:341–55.
16. Voevodskaya O, Simmons A, Nordenskjöld R, Kullberg J, Ahlström H, Lind L, et al. The effects of intracranial volume adjustment approaches on multiple regional MRI volumes in healthy aging and Alzheimer's disease. Front Aging Neurosci. 2014;6:264.
17. Leemans A, Jeurissen B, Sijbers J, Jones DK. ExploreDTI: a graphical toolbox for processing, analyzing and visualizing diffusion MR data. In: 17th annual meeting of Intl Soc Mag Reson Med. 2009:3537.

18. Leemans A, Jones DK. The B-matrix must be rotated when correcting for subject motion in DTI data. Magn Reson Med. 2009;61:1336–49.
19. Veraart J, Sijbers J, Sunaert S, Leemans A, Jeurissen B. Weighted linear least squares estimation of diffusion MRI parameters: strengths, limitations, and pitfalls. NeuroImage. 2013;81:335–46.
20. Tax CM, Otte WM, Viergever MA, Dijkhuizen RM, Leemans A. REKINDLE: robust extraction of kurtosis INDices with linear estimation. Magn Reson Med. 2015;73:794–808.
21. Jeurissen B, Leemans A, Jones DK, Tournier JD, Sijbers J. Probabilistic fiber tracking using the residual bootstrap with constrained spherical deconvolution. Hum Brain Mapp. 2011; 32:461–79.
22. Tax CM, Jeurissen B, Vox SB, Viergever MA, Leemans A. Recursive calibration of the fiber response function for spherical deconvolution of diffusion MRI data. NeuroImage. 2014;86: 67–80.
23. Tournier JD, Calamante F, Connelly A. Robust determination of the fibre orientation distribution in diffusion MRI: non-negativity constrained super-resolved spherical deconvolution. NeuroImage. 2007;35:1459–72.
24. Jeurissen B, Leemans A, Tournier JD, Jones DK, Sijbers J. Investigating the prevalence of complex fiber configurations in white matter tissue with diffusion magnetic resonance imaging. Hum Brain Mapp. 2013;34:2747–66.
25. Tzourio-Mazoyer N, Landeau B, Papathanassiou D, Crivello F, Etard O, Delcroix N, et al. Automated anatomic labelling of activations in SPM using a macroscopic anatomical parcellation of the MNI MRI single-subject brain. NeuroImage. 2002;15:273–89.
26. Rubinov M, Sporns O. Complex network measures of brain connectivity: uses and interpretations. NeuroImage. 2010;52:1059–69.
27. Prins ND, van Dijk EJ, den Heijer T, Vermeer, SE, Jolles J, Koudstaal PJ, et al. Cerebral small-vessel disease and decline in information processing speed, executive function and memory. Brain. 2005;128:2034–41.
28. Corrigan JD, Hinkeldy NS. Relationships between parts A and B of the trail making test. J Clin Psychol. 1987;43:402–9.
29. Stroop JR. Studies of interference in serial verbal reactions. J Exp Psychol. 1935;18:643–62.
30. Moses Jr JA, Pritchard DA, Adams RL. Neuropsychological information in the Wechsler adult intelligence scale-revised. Arch Clin Neuropsychol. 1997;12:97–109.
31. Deelman BG, Liebrand WB, Koning-Haanstra M, van den Berg W. Measurements of aphasic disorders: a brief description of the SAN-battery. Gerontologie. 1980;11:17–21.
32. Hayes AF. Introduction to Mediation, Moderation, and Conditional Process Analysis: A Regression Based Approach. The Guilford Press, New York, NY. 2013.
33. Heinen R, Bouvy WH, Mendrik AM, Viergever MA, Biessels GJ, de Bresser J. Robustness of automated methods for brain volume measurements across different MRI field strengths. PLoS One. 2016;10:e0165719.
34. Verhage F. Intelligentie en leeftijd: onderzoek bij Nederlanders van twaalf tot zevenenzeventig jaar. 1964.
35. Shrout PE, Bolger N. Mediation in experimental and nonexperimental studies: new procedures and recommendations. Psychol Methods. 2002;7:422–45.
36. Hayes AF. Beyond Baron and Kenny: statistical mediation analysis in the new millennium. Commun Monogr. 2009;76:408–20.
37. Zhao X, Lynch Jr JG, Chen Q. Reconsidering Baron and Kenny: myths and truths about mediation analysis. J Consum Res. 2010;37:197–206.
38. Baron RM, Kenny DA. Moderator-mediator variables distinction in social psychological research: conceptual, strategic, and statistical considerations. J Pers Soc Psychol. 1986;51: 1173–82.

39. O'Sullivan M, Summers PE, Jones DK, Jarosz JM, Williams SCR, Markus HS. Normal-appearing white matter in ischaemic leukoaraiosis: a diffusion tensor MRI study. Neurology. 2001;57:2307–10.
40. O'Sullivan M, Morris RG, Huckstep B, Jones DK, Williams SCR, Markus HS. Diffusion tensor MRI correlates with executive functioning in patients with ischaemic leukoaroaiosis. J Neurol Neurosurg Psychiatry. 2004;75:441–7.
41. VanNorden AGW, de Laat KF, van Dijk EJ, Van Uden IWM, Van Oudheusden LJB, Gons RAR, et al. Diffusion tensor imaging and cognition in cerebral small vessel disease: The RUN DMC study. Biochim Biophys Acta. 2012;1822:401–7.
42. Tuladhar AM, van Norden AGW, de Laat KF, Zwiers MP, van Dijk EJ, Norris DG, et al. White matter integrity in small vessel disease is related to cognition. NeuroImage Clinical. 2015;7:518–24.
43. Bastin ME, Clayden JD, Pattie A, Gerrish IF, Wardlaw JM, Deary IJ. Diffusion tensor and magnetization transfer MRI measurements of periventricular white matter hyperintensities in old age. Neurobiol Aging. 2009;30:125–36.
44. Maniega SM, Valdes Hernandez MC, Clayden JD, Royle NA, Murray C, Morris Z, et al. White matter hyperintensities and normal-appearing white matter integrity in the aging brain. Neurobiol Aging. 2015;36:909–18.

Chapter 6

Amyloid status modifies the relation between small vessel disease lesion type and brain atrophy

Rutger Heinen
Onno N. Groeneveld
Frederik Barkhof
Jeroen de Bresser
Lieza G. Exalto
Hugo Kuijf
Niels D. Prins
Philip Scheltens
Wiesje M. van der Flier
Geert Jan Biessels
On behalf of the TRACE-VCI study group*

* Members of TRACE-VCI study group are mentioned in the acknowledgements

Submitted

ABSTRACT

Brain atrophy in memory clinic patients may be due to Alzheimer's disease, but can also develop as a consequence of cerebral small vessel disease. Cerebral small vessel disease is an etiologically heterogeneous construct manifesting itself by different types of vascular brain lesions on MRI, such as white matter hyperintensities, lacunes and cerebral microbleeds. Whether different types of cerebral small vessel disease, possibly in interplay with co-occurring Alzheimer's disease, differentially affect brain atrophy is unknown. In 725 memory clinic patients (mean age 67 years, 48% female) with cerebral small vessel disease, but without large infarcts or hemorrhages, we assessed the relation between lesion type and severity and pattern of brain atrophy. We also determined whether CSF amyloid biomarker status modified this relationship. Total brain, gray matter and white matter volumes were obtained using a semi-automated segmentation pipeline. Brain volumes were compared between patients with each lesion type (moderate/severe white matter hyperintensities (Fazekas score 2–3; n = 326), lacunes (n = 132), and cerebral microbleeds (n = 321)) and a reference group with Fazekas score 1, but no lacunes or microbleeds (n = 197). Stratified analyses were performed in CSF amyloid-positive (n = 261) or negative (n = 227) patients and we assessed if atrophy in relation to cerebral small vessel disease occurred in specific brain regions. Compared to the reference group, patients with moderate/severe white matter hyperintensities had a smaller gray matter volume (standardized β [95% confidence interval] = -0.07 [-0.14; -0.002]), but total brain and white matter volumes did not differ. Patients with cerebral microbleeds or lacunes had no significant brain volume differences compared to the reference group. In stratified analyses according to CSF amyloid status, significant associations between lesion type and brain volumes were only seen in amyloid-negative patients: moderate/severe white matter hyperintensities were associated with smaller gray matter volume (β = -0.14 [-0.27; -0.01]), and presence of lacunes with smaller total brain (β = -0.22 [-0.37; -0.07]) and gray matter volumes (β = -0.22 [-0.37; -0.08]). The relation between white matter hyperintensities and brain atrophy was most evident in the frontal (cortical) gray matter, again predominantly in amyloid-negative patients. In conclusion, different manifestations of cerebral small vessel disease related differentially to brain atrophy in memory clinic patients, but mainly in the absence of markers of amyloid pathology. The relations of subcortical lesions (white matter hyperintensities and lacunes) with "distant atrophy", in predominantly frontal cortical areas, may reflect secondary neurodegeneration mediated through disconnection.

INTRODUCTION

Brain atrophy is common in memory clinic patients and is related to cognitive decline.[1,2] In light of its functional impact, better understanding of the etiology of brain atrophy in these patients is important. An important cause of brain atrophy, and often the first to be considered, is (primary) neurodegeneration, due to Alzheimer's disease or other neurodegenerative disorders such as Lewy body or frontotemporal dementia.[3,4] Vascular brain injury is increasingly recognized as another potential cause of brain atrophy, in particular cerebral small vessel disease.[5]

Cerebral small vessel disease is an etiological heterogeneous construct. The most common forms are arteriolosclerosis (or age-related and hypertension-related cerebral small vessel diseases) and cerebral amyloid angiopathy.[6] Different forms of cerebral small vessel disease manifest themselves in different types of vascular brain lesions, which can be seen on MRI: white matter hyperintensities of presumed vascular origin (WMHs), lacunes and cerebral microbleeds.[5]

Although the relation between cerebral small vessel disease and brain atrophy has been established,[7] it remains unclear whether different MRI manifestations of cerebral small vessel disease differentially relate to brain atrophy. Previous studies have mostly focused on a single lesion type, in particular WMHs, without directly comparing different lesion types. Yet different lesion types can reflect different disease processes affecting different vessels, in different parts of the brain, potentially with different relationships with gray matter degeneration.[8] Directly comparing different lesion types in investigating brain atrophy in memory clinic patients could therefore give more insight in these underlying disease processes.

A substantial proportion of memory clinic patients with cerebral small vessel disease will also have Alzheimer's disease.[9,10] However, the possible interplay between vascular brain injury and Alzheimer's pathological processes is not well understood. It has been hypothesized that their relation could be additive or synergistic.[11] The need for a large study that incorporates both processes to explore the etiology of brain atrophy was recently stressed.[12] We therefore investigated the relation between different cerebral small vessel disease lesion types on MRI and brain atrophy (in terms of severity and pattern) in a large population of memory clinic patients and determined whether this relation was modified by CSF amyloid biomarker status.

MATERIALS AND METHODS

Study population

Patients were included from the TRACE-VCI study cohort. The TRACE-VCI study is an observational multicenter cohort study on memory clinic patients with vascular brain injury on MRI (i.e. possible vascular cognitive impairment; n = 860) in the Netherlands. The study design was described earlier.[13] In short, the cohort consists of consecutive patients attending the memory clinics of the Amsterdam University Medical Center and from the two outpatient memory clinics of the University Medical Center Utrecht between September 2009 and December 2013 who met the inclusion criteria and had a full work-up including MRI. Patients were included regardless of severity of their cognitive deficit, including patients with no objective cognitive impairment, mild cognitive impairment and dementia. There had to be evidence of vascular brain injury on MRI (i.e. possible vascular cognitive impairment) which was operationalized as the presence of at least one of the following: (1) mild WMHs (Fazekas scale grade 1)[14] and the presence of ≥ 2 vascular risk factors (hypertension, hypercholesterolemia, diabetes mellitus, obesity, current smoking or a reported history of a vascular event other than stroke); (2) moderate/severe WMHs (Fazekas scale grade ≥ 2); (3) ≥ 1 lacune(s); (4) ≥ 1 (sub)cortical infarct(s); (5) ≥ 1 cerebral microbleed(s) (6) ≥ 1 intracerebral hemorrhage(s). Patients with a primary non-vascular and non-neurodegenerative etiology (e.g., brain tumor, hydrocephalus, or excessive alcohol consumption) were not included in the cohort. For the current study on cerebral small vessel disease, we excluded patients with (sub)cortical infarcts (n = 96) and intracerebral hemorrhages (n = 11), since presence of these lesions can substantially affect brain volumes. Of the remaining 753 patients, brain volume measurements were available in 725 patients, which comprise the current study population (see Supplementary Figure S6.1).

The study was approved by the institutional review boards of the Amsterdam Medical Center Amsterdam (approval number 2016.061) and the University Medical Center Utrecht (approval number 14-083/C). All procedures were in accordance with the ethical standards of the responsible committee on human experimentation (institutional and national) and with the Helsinki Declaration of 1975, as revised in 2013. All subjects provided written informed consent prior to any research related procedures.

Image acquistion

Patients were scanned on one of six different MRI scanners. Four at the Amsterdam University Medical Center, Amsterdam, the Netherlands (General Electric Signa HDxt 1.5 tesla; General Electric Signa HDxt 3 tesla; General Electric Discovery MR750 3 tesla

[General Electric Healthcare, Milwaukee, Wisconsin, USA] and Philips Ingenuity 3 tesla [Philips Medical Systems, Best, the Netherlands]) and two at the University Medical Center Utrecht, Utrecht, the Netherlands (Philips Achieva 3 tesla and Philips Ingenia 3 tesla [Philips Medical Systems, Best, the Netherlands]). All patients were scanned using an MRI protocol that included a 3D T1-weighted, fluid-attenuated inversion recovery (FLAIR) and T2*-weighted/susceptibility-weighted imaging sequence[13] (for details regarding the MRI sequence parameters see Supplementary Material). For the present study, we used segmentation tools that were relatively insensitive to interscanner differences (these tools are described in the section regarding WMH and brain volume measurements).

3D FLAIR scans from subjects scanned at the Amsterdam Medical Center, were resampled in the axial plane to better match 2D FLAIR scans from the University Medical Center Utrecht, using linear interpolation in MeVisLab (MeVis Medical Solutions AG, Bremen, Germany) resulting in 3 mm slices with an in-plane resolution of 0.95–1.21 mm.[15]

Cerebral small vessel disease lesion types on MRI

Presence of WMHs (using the Fazekas scale[14]), lacunes and cerebral microbleeds was rated on FLAIR and T2*/susceptibility weighted images by or under supervision of a neuroradiologist (in training) using the STRIVE criteria.[5]

WMH and brain volume measurements

The following semi-automated processing pipeline was used to obtain WMH and brain volumes. First, WMHs were automatically segmented using k-nearest neighbor classification with tissue type priors.[16] All WMH segmentations were checked visually. Minimal corrections were performed in < 1% of patients. Presence of WMHs can lead to misclassification of various tissue compartments in automated brain segmentation.[17,18] Lesion filling methods have been shown to reduce this misclassification and improve brain volume measurements.[19,20] Therefore, we performed lesion filling on 3D T1 images using the SLF-toolbox (http://atc.udg.edu/nic/slfToolbox/index.html) for Statistical Parametric Mapping 12 (SPM Wellcome Department of Cognitive Neurology, Institute of Neurology, Queen Square London) with default settings.[20,21] Since WMH segmentation was performed on 2D FLAIR scans, binary WMH segmentations were transformed using Elastix before using it in the SLF toolbox.[22] Next, lesion-filled 3D T1 images were automatically segmented using the Computational Anatomical Toolbox (CAT12, version r864, http://www.neuro.uni-jena.de/cat/) for SPM12. This method has been shown to perform well in a previous study in the elderly.[23] Default settings were used to obtain probabilistic volume segmentations for GM, WM and CSF. Quality assessment was performed visually on all segmentations

and no manual editing was performed. Next, lacunes, non-lacunar infarcts, intracerebral hemorrhages and incidental findings were segmented manually using an in-house developed MeVisLab (MeVis Medical Solutions AG, Bremen, Germany)[15] tool.[24,25] These manual segmentations were subsequently used as a mask to correct WMH segmentations, GM, WM and CSF volumes.

Total brain volume (TBV) was defined as the sum of GM and WM volumes (including the volume of pathology). Total intracranial volume was determined by summing up TBV and CSF volumes. Regional GM, WM and CSF volumes were obtained using the Hammers atlas in CAT12, dividing the brain into 68 regions of interest: 32 per hemisphere and 4 infratentorial regions (http://brain-development.org).[26–29] To compensate for variability in head size, all brain volumes were normalized using the 'residual normalization method'.[30] This method uses residuals of a least-square derived linear regression between brain volumes and total intracranial volume to calculate normalized brain volumes. Since the relation between brain volumes and total intracranial volume is not necessarily sustained in the case of pathology, we chose to use the residuals from a subset of patients with no objective cognitive impairment to normalize brain volumes. This was also advised in an earlier study.[30]

Cerebrospinal fluid testing

CSF concentrations of amyloid-β_{42} (or $A\beta_{42}$), tau and/or total tau phosphorylated at threonine 181 (or p-tau) were measured at a central laboratory for clinics at the Department of Clinical Chemistry of the Amsterdam Medical Center.[31] $A\beta_{42}$, total tau, and p-tau were measured with commercially available ELISAs (Innotest β-amyloid($_{1-42}$), Innotest hTAU-Ag and Innotest Phosphotau($_{181Q}$), respectively; Innogenetics, Ghent, Belgium) on a routine basis.[31] Patients were considered CSF amyloid-positive when the level of $A\beta_{42}$ in CSF was less than 640 ng/L.[32] For the present study, CSF data was available for 488 patients (67%).

Statistical analysis

All analyses were performed using IBM SPSS version 25 unless specified. Tests were two-tailed with α set at $p < 0.05$ and corrected for multiple comparisons using Bonferroni correction if needed. In case of missing data, analyses were restricted to patients with complete data on all variables required for a particular analysis. All demographic, clinical and MRI variables were checked for normality using the Kolmogorov-Smirnov test and histogram inspection; WMH volumes were log-transformed. Differences in baseline characteristics and occurrence of vascular lesion types between amyloid-positive and amyloid-negative patients were analyzed using independent sample t-tests (for continuous

normally distributed data), χ-square tests (for proportions) and Mann-Whitney U tests (for continuous, non-normally distributed data).

Relationship between lesion type and brain atrophy

The relation between lesion type and brain atrophy was explored with linear regression analyses as well as with Bayesian network analyses. TBV, GM and WM volumes (normalized for head size) were compared between each lesion type and a reference group with only Fazekas score 1 and ≥ 2 vascular risk factors (but no other lesions) using linear regression analysis, adjusting for age, gender and scanner effect and additionally for clinical diagnosis (no objective cognitive impairment, mild cognitive impairment or dementia) and the number of vascular risk factors. We also used log-transformed WMH volume as a continuous variable.

Bayesian network analyses (bnlearn R package[33]; settings described earlier[34]) were used to assess the conditional dependencies between each lesion type, age and gender (potential determinants) and brain volumes (outcome). Variables with a deterministic influence on the outcome are identified and separated from others with, although showing a correlation with the outcome, only an indirect influence when taking the direct determinants into account (conditionally independent variables). Networks are produced in which direct determinants are connected directly to the outcome, while conditionally independent variables are connected only indirectly, via other variables. Normalized brain volumes were standardized into z-scores using the mean and standard deviation of the whole study sample and corrected for scanner effect. The strength of the connections between direct determinants and outcome was assessed by 100 bootstrap replications.[24]

We also assessed if atrophy in relation to cerebral small vessel disease occurred in specific brain regions. Normalized regional brain volumes were standardized into z-scores using the mean and standard deviation of the whole study sample and corrected for age, gender and scanner effect. Two-sample t-tests were used to compare for each lesion type that was significantly associated with brain volumes in the previous analyses, the difference in regional brain volumes (Δz-score) in 68 brain regions (correcting for multiple testing using Bonferroni correction).

Modification by co-occurring amyloid pathology

To investigate whether the relation between lesion type and brain atrophy was modified by co-occurring amyloid pathology, we assessed possible interactions between each lesion type and CSF amyloid status in relation to brain atrophy. We also performed post-hoc

analyses stratified for CSF amyloid status. Normalized brain volumes were standardized in the same manner as described before, but using the mean and standard deviation of the CSF subgroup, amyloid-negative or amyloid-positive subgroup depending on the specific analysis.

Data availability

The data that support the findings of this study are available from the corresponding author, upon reasonable request.

RESULTS

Baseline characteristics

The 725 patients had a mean (± SD) age of 67 (± 8) years and 348 (48%) were female. Baseline characteristics are shown in Table 6.1. 176 patients (24%) had no objective cognitive impairment, 175 (24%) had mild cognitive impairment and 374 (52%) had dementia. Baseline characteristics of the subgroup of patients with available CSF (n = 488, 67) are shown in Supplementary Table S6.1. Patients with available CSF were younger ($t = 2.8$, $p < 0.05$), less often hypertensive ($\chi^2 = 8.6$, $p < 0.05$), had less often hypercholesterolemia ($\chi^2 = 8.7$, $p < 0.05$) and less often obese ($\chi^2 = 4.2$, $p < 0.05$) compared to those without available CSF. In the CSF subgroup, amyloid-negative patients were younger ($t = -4.6$, $p < 0.001$) and more often obese ($\chi^2 = 10.2$, $p < 0.05$) than amyloid-positive patients. Clinical diagnoses also differed as amyloid-negative patients more often had no objective cognitive impairment ($\chi^2 = 72.3$, $p < 0.001$) and were less often demented ($\chi^2 = 52.9$, $p < 0.001$) than amyloid-positive patients.

The occurrence of each lesion type (and the overlap between lesion types) is shown in Figure 6.1. 321 patients (44%) had multiple lesion types. Moderate/severe WMHs (Fazekas score 2 or 3) were present in 326 patients (45%), lacunes in 132 patients (18%) and cerebral microbleeds in 321 patients (44%). The reference group of only Fazekas score 1 and ≥ 2 vascular risk factors (but no other lesions) consisted of 197 patients (27%). In the CSF subgroup, amyloid-positive patients more often had moderate/severe WMHs compared to amyloid-negative patients ($\chi^2 = 4.5$, $p = 0.04$). Occurrence of lacunes and cerebral microbleeds did not differ between amyloid-negative and amyloid-positive patients (see Figure 6.1).

In the entire study population, the mean TBV (normalized for head size, in mL) was 1042 ± 60 mL, mean GM volume 565 ± 44 mL and mean WM volume 477 ± 33 mL. Median

Table 6.1 | Baseline characteristics of the total study population

	Number of patients, n total = 725
Demographics	
Age, years	67 ± 8
Gender, female	346 (48)
Level of education, Verhage scale[35]	5 [4–6]
Vascular risk factors	
Hypertension	610 (84)
Hypercholesterolemia	304 (42)
Diabetes Mellitus	132 (18)
Current smoker	140 (19)
Obesity, Body Mass Index ≥ 30	149 (21)
History of reported vascular events other than stroke	66 (9)
Number of vascular risk factors	2 [1–3]
Clinical diagnosis	
No objective cognitive impairment	176 (24)
Mild cognitive impairment	175 (24)
Dementia	374 (52)
Vascular	21 (3)
Neurodegenerative	329 (45)
Alzheimer's disease	254 (35)
Frontotemporal disease	23 (3)
Lewy body dementia	17 (2)
Others*	35 (5)
Unknown etiology§	24 (3)

Data are presented as mean ± standard deviation, number of patients (percentage of total study population) or median [interquartile range]. For level of education data was present in 720 patients. For vascular risk factors current smoker and obesity data was present in 718 and 713 patients respectively. * Such as Primary Progressive Aphasia, Cortical Basal Syndrome and Progressive Supranuclear Palsy. § Dementia of unknown origin, further examination needed to state diagnosis.

WMH volume was 6 mL (range 0.05–166 mL). In the CSF subgroup, amyloid-positive patients had a smaller TBV (amyloid-positive: 1035 ± 24 mL; amyloid-negative: 1064 ± 30 mL; standardized β coefficient [95% CI], adjusted for age, gender and scanner effect: -0.19 [-0.27; -0.11], $p < 0.001$) and GM volume (amyloid-positive: 558 ± 20 mL; amyloid-negative: 585 ± 23 mL; β: -0.26 [-0.33; -0.18], $p < 0.001$), but similar WM volume (amyloid-positive: 476 ± 14 mL; amyloid-negative: 479 ± 15 mL; β: -0.01 [-0.09; 0.08], $p = 0.86$) compared to the amyloid-negative patients.

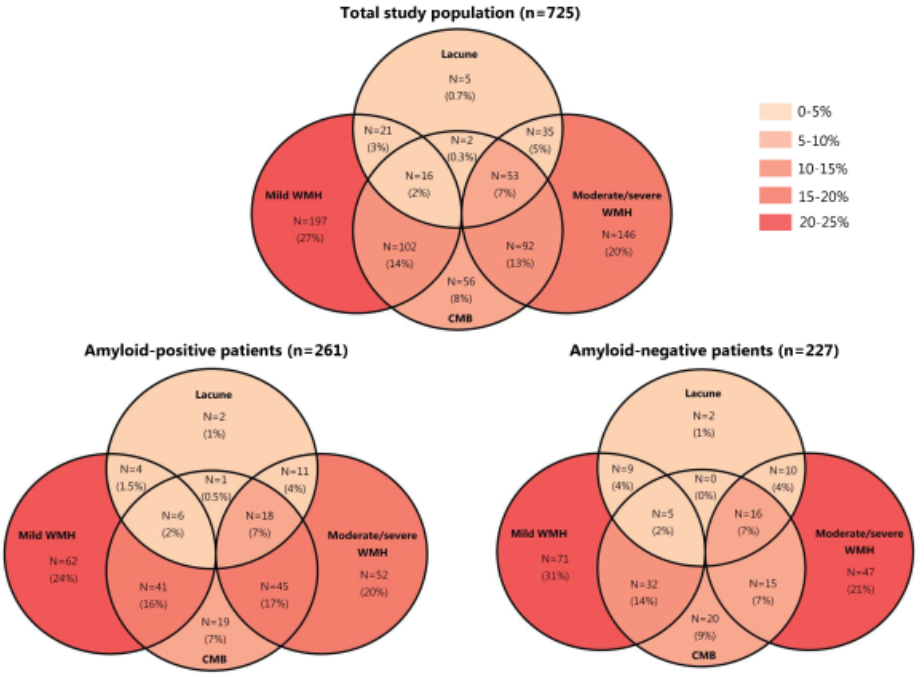

Figure 6.1 | Occurrence of lesion types. Venn diagram showing the occurrence of lesion types in the entire study population (n = 725) as well as in the CSF amyloid-positive (n = 261) and amyloid-negative (n = 227) patients in the CSF subgroup. The number of patients with a certain lesion type (alone or in combination with another lesion type) is shown, as well as the (color-coded) percentage of the respective patient group. The majority of patients only had mild WMHs (Fazekas score of 1) or moderate/severe WMHs (Fazekas score 2 or 3) but no other lesions. Multiple lesion types occurred in 321 patients (44%) of the entire study population. 71 patients (10%) had multiple lacunes (max: 30). In 719 patients (99%), information regarding presence/absence of cerebral microbleeds (CMBs) was present. 171 patients (24%) had multiple cerebral microbleeds (CMBs; max: 500). Of the patients with CMBs, 37 patients (12%) had only deep CMBs, 212 patients (66%) had only lobar CMBs and 70 patients (22%) both had deep and lobar CMBs. In 2 patients, no information regarding CMB location was available.

WMHs relate to GM atrophy

WMHs in particular, were related to brain atrophy: compared to the reference group (Fazekas score 1), patients with moderate/severe WMHs (Fazekas score 2–3) had smaller GM volume (standardized β coefficient [95% CI]: -0.07 [-0.14; -0.002], $p < 0.05$; additionally adjusted for clinical diagnosis: -0.05 [-0.12; 0.01], $p = 0.08$), but TBV and WM volumes were not significantly affected (Table 6.2). When WMH volume was entered as a continuous variable, it was also significantly associated with TBV (-0.16 [-0.22; -0.09], $p < 0.001$; additionally adjusted for clinical diagnosis: -0.09 [-0.15; -0.03, $p = 0.003$) as well as GM volume (-0.24 [-0.30; -0.17], $p < 0.001$; additionally adjusted for clinical diagnosis: -0.17 [-0.22; -0.11, $p < 0.001$), but WM volume was not significantly affected. Patients

with lacunes had no significant differences in brain volumes compared to the reference group, although a trend with smaller GM volume was observed (-0.08 [-0.17; 0.004], p = 0.06; additionally adjusted for clinical diagnosis: -0.08 [-0.15; -0.004, p < 0.05). Patients with cerebral microbleeds had no significant differences in brain volumes compared to the reference group. This was also the case for patients with multiple (≥ 5), lobar (pure or any) or deep microbleeds. Adjusting for the number of vascular risk factors did not change any of the previous results. There was no significant interaction between clinical diagnosis and moderate/severe WMHs, lacunes or microbleeds in relation to TBV, GM or WM volume (interaction terms p > 0.05).

The Bayesian network analyses integrating all lesion types confirmed the relation between WMHs and GM volume (see Figure 6.2). These analyses showed WMHs directly determined GM volume, independent of lacunes and cerebral microbleeds.

Pattern of brain atrophy related to cerebral small vessel disease

Brain atrophy in relation to WMHs occurred in specific brain regions (see Figure 6.3). Differences were most evident in frontotemporal cortical regions, but also the postcentral gyrus, thalamus and anterior and posterior cingulate gyrus (see Supplementary Table S6.3). In the superior parietal gyrus, patients with low WMH burden had smaller GM volumes compared to patients with high WMH burden, albeit not significant (see Figure 6.3).

Relation between WMHs and GM atrophy is modified by amyloid status

Analyses in patients with available CSF (n = 488) showed that the relation between lesion type and brain atrophy was influenced by co-occurring amyloid pathology (see Table 6.2). There was a significant inverse interaction between CSF amyloid status and lesion type in relation to brain atrophy (interaction term WMH burden x CSF amyloid status for TBV: p = 0.012; GM volume: p = 0.006), lacunes (TBV: p = 0.012; GM volume: p = 0.006) and cerebral microbleeds (TBV: p = 0.01; GM volume: p = 0.02)). In amyloid-negative patients, moderate/severe WMHs were associated with smaller GM volume (-0.14 [-0.27; -0.01], p < 0.05) and lacunes with smaller TBV (-0.22 [-0.37; -0.07], p < 0.05) and GM volume (-0.22 [-0.37; -0.08], p < 0.05) compared to the reference group. By contrast, in amyloid-positive patients, none of the small vessel lesion types was associated with brain atrophy (see Table 6.2). Vice versa, the effect size of the reduction in TBV and GM volume associated with a positive compared to negative CSF amyloid status was almost twice as large in patients with a low WMH burden relative to patients with a high WMH burden (see Supplementary Table S6.2). The same was observed for the relation between the CSF amyloid status and TBV and GM volume in the absence versus the presence of lacunes.

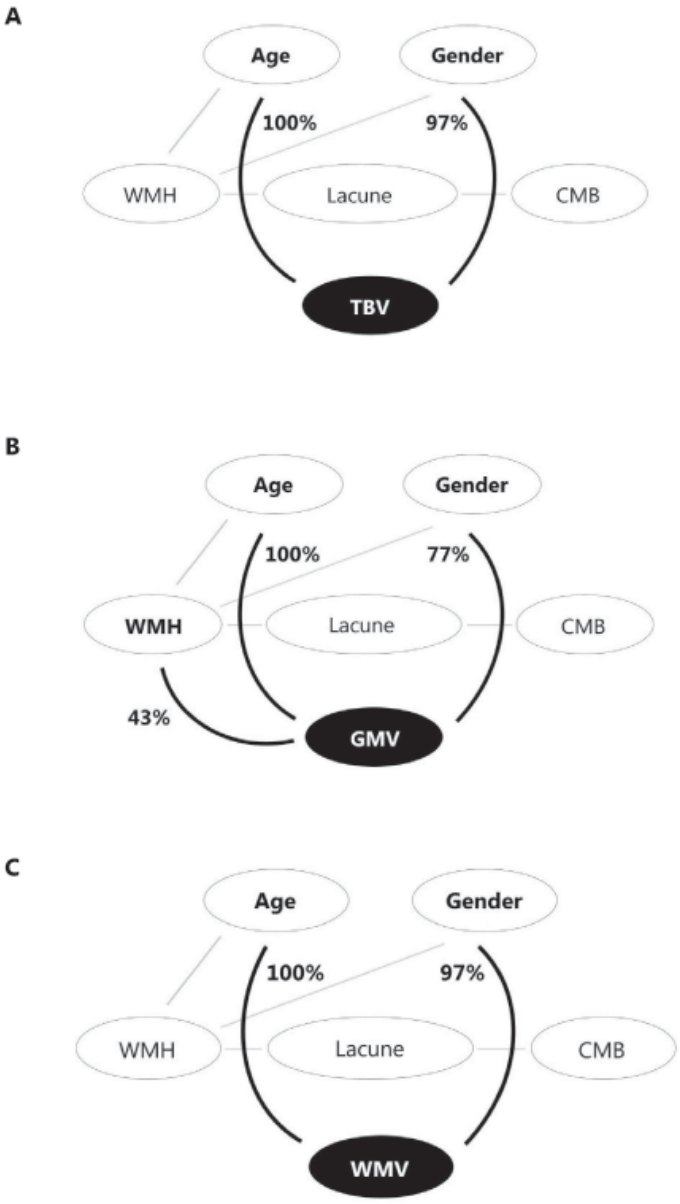

Figure 6.2 | Bayesian networks. Bayesian networks for total brain volume (TBV, panel A), gray matter volume (GMV, panel B) and white matter volume (WMV, panel C). Variables that are directly connected to one of the cognitive domains are identified as direct determinants. Variables that are connected indirectly to the cognitive domains (via other variables) are conditionally independent. As such, this method separates determinants with a direct deterministic influence on the outcome variable from other determinants that, although showing a univariate correlation with the outcome variable, have only an indirect influence when taking the direct determinants into account. Percentages indicate the confidence level of the arcs towards brain volumes determined by 100 bootstrap replications. These analyses showed WMHs directly determined gray matter volume, independent of lacunes and cerebral microbleeds. CMB, presence of cerebral microbleed(s); WMH, moderate/severe WMHs (Fazekas score 2 or 3).

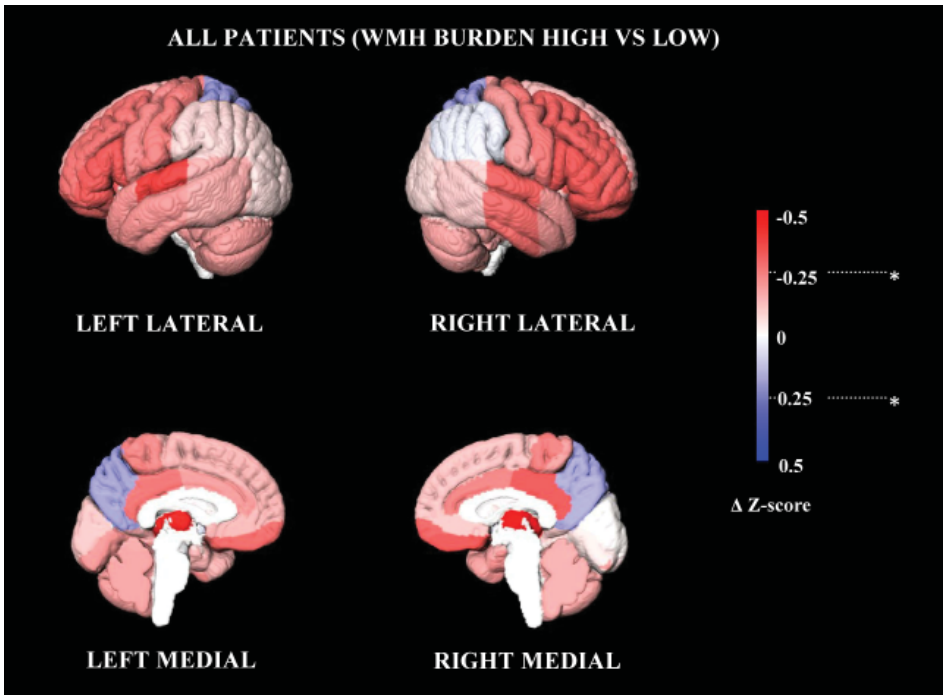

Figure 6.3 | Regional brain volume analysis. Effect size map showing regional gray matter volume differences between patients with high versus low white matter hyperintensity (WMH) burden (median split on WMH volume) in all patients (n = 725). Differences in z-scores (ΔZ) are shown (red: gray matter volume smaller in patients with high versus low WMH burden; blue: gray matter volume smaller in patients with low versus high WMH burden). Panel A shows that across all patients higher WMH burden was associated with smaller gray matter volume. * Bonferroni-corrected $p < 0.05$.

The Bayesian network analyses confirmed the relation between lesion type and brain atrophy in amyloid-negative patients (see Supplementary Figure S6.2), with lacunes directly determining GM volume. Additionally, WMHs had an indirect effect (via lacunes) on GM volume (see Supplementary Figure S6.2).

CSF amyloid status also affected the pattern of brain atrophy related to cerebral small vessel disease (see Figure 6.4). In amyloid-negative patients, right mid frontal gyrus, left and right thalamus and right precentral gyrus, GM volumes were significantly smaller in patients with high WMH burden compared to patients with low WMH burden (Bonferroni-corrected $p < 0.05$, see Supplementary Table S6.4). In amyloid-positive patients, only left superior temporal gyrus GM volumes were significantly smaller in patients with high WMH burden compared to patients with low WMH burden (Bonferroni-corrected $p < 0.05$, see Supplementary Table S6.4). No significant interaction between WMH burden and CSF amyloid status was found after correcting for multiple testing (Bonferroni-corrected p >

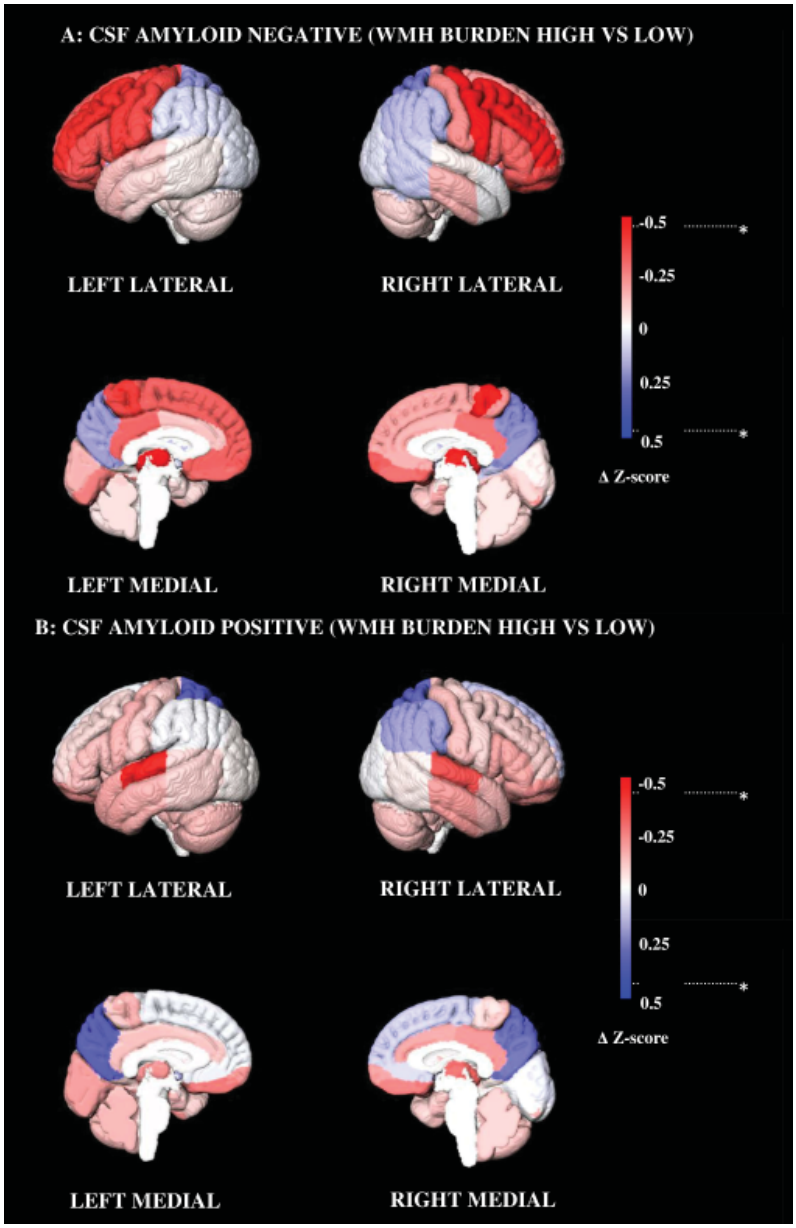

Figure 6.4 | Regional brain volume analysis in CSF subgroup. Effect size map showing regional gray matter volume differences between patients with high versus low white matter hyperintensity (WMH) burden (median split on WMH volume). A) CSF amyloid-negative patients (n = 273); B) CSF amyloid-positive patients (n = 215). Differences in z-scores (ΔZ) are shown (red: gray matter volume smaller in patients with high versus low WMH burden; blue: gray matter volume smaller in patients with low versus high WMH burden). The stratified analyses show that the effect is highly dependent on CSF amyloid status. While amyloid-positive patients have a lower gray matter volume than amyloid-negative patients, the association between high WMH burden and more gray matter atrophy was more pronounced in several brain regions for amyloid-negative patients only. * Bonferroni-corrected $p < 0.05$.

Table 6.2 | Relationship between lesion type and brain volumes for total study population and stratified for CSF amyloid biomarker status

	Total brain volume	Gray matter volume	White matter volume
Total study population (n = 725)			
Mild WMHs and ≥ 2 VRF (reference; n = 197)	-	-	-
Moderate/severe WMHs (n = 326)	-0.02 [-0.10;0.05]	**-0.07 [-0.14;-0.002]***	0.05 [-0.03;0.13]
Lacunes (n = 132)	-0.06 [-0.15;0.03]	-0.08 [-0.17;0.004]	0.0001 [-0.10;0.10]
Cerebral microbleeds (n = 321)	-0.02 [-0.09;0.06]	-0.05 [-0.12;0.03]	0.03 [-0.05;0.11]
CSF amyloid-negative (n = 227)			
Mild WMHs and ≥ 2 VRF (reference, n = 71)	-	-	-
Moderate/severe WMHs (n = 88)	-0.10 [-0.24;0.04]	**-0.14 [-0.27;-0.01]***	-0.002 [-0.15;0.14]
Lacunes (n = 42)	**-0.22 [-0.37;-0.07]***	**-0.22 [-0.37;-0.08]***	-0.10 [-0.27;0.07]
Cerebral microbleeds (n = 88)	-0.09 [-0.23;0.05]	-0.07 [-0.21;0.06]	-0.06 [-0.21;0.08]
CSF amyloid-positive (n = 261)			
Mild WMHs and ≥ 2 VRF (reference; n = 62)	-	-	-
Moderate/severe WMHs (n = 126)	0.08 [-0.05;0.22]	0.05 [-0.08;0.18]	0.08 [-0.06;0.22]
Lacunes (n = 42)	0.08 [-0.10;0.26]	0.07 [-0.10;0.25]	0.04 [-0.14;0.23]
Cerebral microbleeds (n = 130)	0.12 [-0.02;0.25]	0.10 [-0.03;0.23]	0.08 [-0.06;0.21]

Data are presented as standardized beta coefficients with 95% confidence intervals after correction for age, gender and scanner effect. All brain volumes were corrected for variations in head size using the total intracranial volume. VRF, vascular risk factors.
* $p < 0.05$.

0.05). Regional brain volume analyses were not performed for patients with and without lacunes, due to a lack of power.

DISCUSSION

This study demonstrates that different manifestations of cerebral small vessel disease differentially affect brain atrophy in memory clinic patients, especially in the absence of concurrent amyloid pathology. In particular WMHs and lacunes were related to brain atrophy. WMH associated brain atrophy was most pronounced in frontal cortical GM regions.

Cerebral small vessel disease related brain atrophy

Cerebral small vessel disease burden has previously been shown to be related to brain atrophy in memory clinic patients.[7] While it is a trend in cerebral small vessel disease

research to use a cerebral small vessel disease burden score to capture multiple types of cerebral small vessel disease related brain injury in a single measure,[36] the effects of different lesion types are of interest since different lesion types can reflect different underlying pathological processes.[8,37–40] Previous studies investigating the relation between cerebral small vessel disease and brain atrophy have often focused on a single lesion type, without directly comparing different lesion types. Most of the research has been done on WMHs,[41–46] and has shown that WMHs were related to brain atrophy. For lacunes, results have been conflicting, with most studies finding a relation with brain atrophy,[41,47–49] while some studies do not.[42] We are aware of only one study that investigated the relation between cerebral microbleeds and brain atrophy and found no association.[46] We now directly compared different lesion types in relation to brain atrophy in a large cohort of memory clinic patients and indeed observed WMHs and lacunes, but not cerebral microbleeds were related to brain atrophy.

Pattern of cerebral small vessel disease related brain atrophy

Previous studies that investigated the pattern of cerebral small vessel disease related brain atrophy found a relation between WMHs and predominantly cortical GM atrophy.[41,42,45,47–49] Regarding lacunes, most studies also found a relation with cortical GM atrophy,[41,47–49] while one study also found an association with subcortical GM atrophy.[47]

Only three of the previous studies[41,45,49] have specifically investigated the regional pattern of cortical GM atrophy. Two of those studies[45,49] were done in patients with symptomatic lacunes with moderate/severe WMHs, while the other[41] used memory clinic patients with a history of stroke due to small vessel disease or a lacune on MRI. All three studies found a rather global pattern of cortical GM atrophy (frontal, limbic (cingulate), (superior)temporal and parietal-occipital regions) in relation to WMHs, with relative sparing of hippocampal and medial temporal regions. In the present study, investigating memory clinic patients with cerebral small vessel disease, GM atrophy in relation to WMHs was predominantly seen in frontotemporal, but not parietal-occipital regions.

Modification by amyloid pathology

The interplay between cerebral small vessel disease and Alzheimer's pathological processes (whether their relation is additive or interactive) has gained increasing attention in the past decade.[11] While many studies have investigated the interaction between amyloid and WMHs in relation to cognition and prognosis, with variable results (for an overview see[50]), brain atrophy as an outcome has hardly been studied.[51,52] We now show that there is indeed an interaction between WMHs and CSF amyloid status in relation to brain atrophy.

WMHs and lacunes were related to atrophy, but primarily in amyloid-negative patients. Vice versa, the relation between CSF amyloid status and brain atrophy was much stronger in patients with a low burden of WMH or lacunes.

A previous study that assessed the relation of both WMHs and CSF amyloid level to brain atrophy in controls and patients with either mild cognitive impairment or a clinical diagnosis of early Alzheimer's disease, observed that these relations differed according to disease stage.[51] In controls WMH volume and lower amyloid level were independently associated with brain atrophy, while in subjects with mild cognitive impairment amyloid but not WMH volume was associated with brain atrophy. In patients with early Alzheimer's disease, neither amyloid nor WMH volume was associated with brain atrophy. No interaction analysis was performed.

Another previous cross-sectional study that investigated the relation of both WMH volume and CSF amyloid level to hippocampal volume in memory clinic patients, found no independent effect of WMHs on hippocampal volume, but did find a significant interaction between WMHs and abnormal CSF amyloid levels in non-demented individuals.[52] The interaction was not present when patients with a clinical diagnosis of Alzheimer's disease were included.

Converging evidence thus that both cerebral small vessel disease and Alzheimer's pathological processes contribute to brain atrophy in memory clinic patients, but for each this is most evident in the absence of the other. This could perhaps be explained by a ceiling effect, possibly linked to disease stage. Longitudinal studies could give more insight into the combined effects of WMHs and amyloid beta on brain atrophy over time and reveal the temporality of both disease processes.

'Distant' effects of cerebral small vessel disease

The exact mechanism by which cerebral small vessel disease contributes to brain atrophy is not yet clear. It has been suggested cerebral small vessel disease can lead to secondary degeneration: a process in which cortical gray matter atrophy occurs as a result of disconnection of white matter tracts.[42,44,47,53–55] This 'disconnection phenomenon' has been demonstrated in patients with cerebral autosomal dominant arteriopathy with subcortical infarcts and leukoencephalopathy[54] and ischemic stroke.[56] The underlying cellular mechanisms behind this process are not clear yet: retrograde or anterograde degeneration, neuronal apoptosis or a combination of these mechanisms have been hypothesized.[57] Our results showed primarily subcortical lesions (white matter hyperintensities and lacunes) were related with predominantly frontal cortical gray matter atrophy. This 'distant' cortical

atrophy in relation to these subcortical vascular lesions may indeed reflect secondary neurodegeneration through disconnection.

Strengths and limitations

Strengths of our study include the large sample size, and detailed information on brain volumes and all cerebral small vessel disease lesion types. Furthermore, CSF was available in a substantial subset of patients, allowing us to assess the impact of cerebral small vessel disease both in the absence and presence of biomarker evidence of concomitant amyloid pathology.

A few limitations need to be addressed. First, selection bias could play a role since patients were included at a tertiary memory clinic and not all patients underwent a lumbar puncture. Second, all patients in the present study had some degree of vascular brain injury (since this was part of the inclusion criteria for the TRACE-VCI study), which could have led to an underestimation of the observed effects. However, there was a great variability in the burden of vascular brain injury, which should have allowed us to detect relevant effects. Fourth, information bias could play a role in the measured brain volumes since we used heterogeneous multicenter MRI data. However, we used a high quality, semi-automatic segmentation pipeline (including lesion filling) and corrected for scanner effect in our analyses. Both amyloid-positive and -negative patients were scanned using the same variety of MRI scanners instead of a single (different) scanner for each subgroup and therefore the differences found in these patients cannot be explained by a scanner effect. Finally, the cross-sectional design of the present study does not allow us to infer causality regarding small vessel disease and brain atrophy.

CONCLUSION

In this study, we demonstrate that different manifestations of cerebral small vessel disease related differentially to brain atrophy in memory clinic patients. In particular WMHs and lacunes were related to brain atrophy, but mainly in the absence of concurrent amyloid pathology. WMH associated brain atrophy was most pronounced in frontal cortical GM regions. This distant cortical atrophy may reflect neurodegeneration through disconnection. Cerebral small vessel disease and Alzheimer's pathological processes both have effects on brain atrophy. For each the effect is most evident in the absence of the other. Our findings provide further insight into the contribution of both cerebral small vessel disease and Alzheimer's disease to brain atrophy, which is relevant since their treatment differs.

ACKNOWLEDGEMENTS

Members of the TRACE-VCI study group (in alphabetical order, per department): University Medical Center Utrecht, Utrecht University, Utrecht, The Netherlands: Department of Neurology: E. van den Berg, G.J. Biessels, J.M.F. Boomsma, L.G. Exalto, D.A. Ferro, C.J.M. Frijns, O.N. Groeneveld, R. Heinen, N.M. van Kalsbeek, J.H. Verwer; Department of Radiology: J. de Bresser; Image Sciences Institute: H.J. Kuijf; Department of Geriatrics: M.E. Emmelot-Vonk, H.L. Koek; Amsterdam UMC, Vrije Universiteit Amsterdam, Amsterdam, The Netherlands: Alzheimer Center and Department of Neurology: M.R. Benedictus, J. Bremer, W.M. van der Flier, A.E. Leeuwis, J. Leijenaar, N.D. Prins, P. Scheltens, B.M. Tijms; Department of Radiology and Nuclear Medicine: F. Barkhof, M.P. Wattjes; Department of Clinical Chemistry: C.E. Teunissen; Department of Medical Psychology: T. Koene; Onze Lieve Vrouwe Gasthuis West, Amsterdam, The Netherlands: Department of Neurology: J.M.F. Boomsma, H.C. Weinstein; Hospital Diakonessenhuis, Zeist, The Netherlands: M. Hamaker, R. Faaij, M. Pleizier, M. Prins, E. Vriens.

REFERENCES

1. Jack CR, Shiung MM, Weigand SD, O'Brien PC, Gunter JL, Boeve BF, et al. Brain atrophy rates predict subsequent clinical conversion in normal elderly and amnestic MCI. Neurology. 2005;65:1227–31.
2. Jokinen H, Lipsanen J, Schmidt R, Fazekas F, Gouw AA, Van Der Flier WM, et al. Brain atrophy accelerates cognitive decline in cerebral small vessel disease The LADIS study. Neurology. 2012;78:1785–92.
3. Whitwell JL, Jack CR, Parisi JE, Knopman DS, Boeve BF, Petersen RC, et al. Rates of cerebral atrophy differ in different degenerative pathologies. Brain. 2007;130:1148–58.
4. Mak E, Gabel S, Mirette H, Su L, Williams GB, Waldman A, et al. Structural neuroimaging in preclinical dementia: From microstructural deficits and grey matter atrophy to macroscale connectomic changes. Ageing Res Rev. 2017;35:250–64.
5. Wardlaw JM, Smith EE, Biessels GJ, Cordonnier C, Fazekas F, Frayne R, et al. Neuroimaging standards for research into small vessel disease and its contribution to ageing and neurodegeneration. Lancet Neurol. 2013;12:822–38.
6. Pantoni L. Cerebral small vessel disease: from pathogenesis and clinical characteristics to therapeutic challenges. Lancet Neurol. 2010;9:689–701.
7. Banerjee G, Jang H, Kim HJ, Kim ST, Kim JS, Lee JH, et al. Total MRI Small Vessel Disease Burden Correlates with Cognitive Performance, Cortical Atrophy, and Network Measures in a Memory Clinic Population. J Alzheimer's Dis. 2018;63:1485–97.
8. Gouw AA, Seewann A, Van Der Flier WM, Barkhof F, Rozemuller AM, Scheltens P, et al. Heterogeneity of small vessel disease: A systematic review of MRI and histopathology correlations. J Neurol Neurosurg Psychiatry. 2011;82:126–35.
9. Toledo JB, Arnold SE, Raible K, Brettschneider J, Xie SX, Grossman M, et al. Contribution of cerebrovascular disease in autopsy confirmed neurodegenerative disease cases in the National Alzheimer's Coordinating Centre. Brain. 2013;136:2697–706.
10. Jack CR, Bennett DA, Blennow K, Carrillo MC, Dunn B, Haeberlein SB, et al. NIA-AA Research Framework: Toward a biological definition of Alzheimer's disease. Alzheimer's Dement. 2018;14:535–62.
11. Koncz R, Sachdev PS. Are the brain's vascular and Alzheimer pathologies additive or interactive? Curr Opin Psychiatry. 2018;31:147–52.
12. Peres R, De Guio F, Chabriat H, Jouvent E. Alterations of the cerebral cortex in sporadic small vessel disease: A systematic review of in vivo MRI data. J Cereb Blood Flow Metab. 2015;36:681–95.
13. Boomsma JMF, Exalto LG, Barkhof F, van den Berg E, de Bresser J, Heinen R, et al. Vascular Cognitive Impairment in a Memory Clinic Population: Rationale and Design of the 'Utrecht-Amsterdam Clinical Features and Prognosis in Vascular Cognitive Impairment' (TRACE-VCI) Study. JMIR Res Protoc. 2017;6:e60.
14. Fazekas F, Chawluk JB, Alavi A. MR signal abnormalities at 1.5 T in Alzheimer's dementia and normal aging. Am J Neuroradiol. 1987;8:421–6.
15. Ritter F, Boskamp T, Homeyer A, Laue H, Schwier M, Link F, et al. Medical image analysis. IEEE Pulse. 2011;2:60–70.
16. Steenwijk MD, Pouwels PJW, Daams M, van Dalen JW, Caan MWA, Richard E, et al. Accurate white matter lesion segmentation by k nearest neighbor classification with tissue type priors (kNN-TTPs). NeuroImage Clin. 2013;3:462–9.
17. Battaglini M, Jenkinson M, De Stefano N. Evaluating and reducing the impact of white matter lesions on brain volume measurements. Hum Brain Mapp. 2012;33:2062–71.

18. Valverde S, Oliver A, Díez Y, Cabezas M, Vilanova JC, Ramió-Torrentà L, et al. Evaluating the effects of white matter multiple sclerosis lesions on the volume estimation of 6 brain tissue segmentation methods. Am J Neuroradiol. 2015;36:1109–15.
19. Popescu V, Ran NCG, Barkhof F, Chard DT, Wheeler-Kingshott CA, Vrenken H. Accurate GM atrophy quantification in MS using lesion-filling with co-registered 2D lesion masks. NeuroImage Clin. 2014;4:366–73.
20. Valverde S, Oliver A, Roura E, Pareto D, Vilanova JC, Ramió-Torrentà L, et al. Quantifying brain tissue volume in multiple sclerosis with automated lesion segmentation and filling. NeuroImage Clin. 2015;9:640–7.
21. Valverde S, Oliver A, Lladó X. A white matter lesion-filling approach to improve brain tissue volume measurements. NeuroImage Clin. 2014;6:86–92.
22. Klein S, Staring M, Murphy K, Viergever MA, Pluim JPW. Elastix: A toolbox for intensity-based medical image registration. IEEE Trans Med Imaging. 2010;29:196–205.
23. Mendrik AM, Vincken KL, Kuijf HJ, Breeuwer M, Bouvy WH, De Bresser J, et al. MRBrainS Challenge: Online Evaluation Framework for Brain Image Segmentation in 3T MRI Scans. Comput Intell Neurosci. 2015;2015:813696.
24. Biesbroek JM, Leemans A, Den Bakker H, Duering M, Gesierich B, Koek HL, et al. Microstructure of Strategic White Matter Tracts and Cognition in Memory Clinic Patients with Vascular Brain Injury. Dement Geriatr Cogn Disord. 2018;44:268–82.
25. Biesbroek JM, Weaver NA, Hilal S, Kuijf HJ, Ikram MK, Xu X, et al. Impact of Strategically Located White Matter Hyperintensities on Cognition in Memory Clinic Patients with Small Vessel Disease. PLoS One. 2016;11:e0166261.
26. Hammers A, Allom R, Koepp MJ, Free SL, Myers R, Lemieux L, et al. Three-dimensional maximum probability atlas of the human brain, with particular reference to the temporal lobe. Hum Brain Mapp. 2003;19:224–47.
27. Heckemann RA, Hajnal JV, Aljabar P, Rueckert D, Hammers A. Automatic anatomical brain MRI segmentation combining label propagation and decision fusion. Neuroimage. 2006;33:115–26.
28. Heckemann RA, Keihaninejad S, Aljabar P, Rueckert D, Hajnal J V., Hammers A. Improving intersubject image registration using tissue-class information benefits robustness and accuracy of multi-atlas based anatomical segmentation. Neuroimage. 2010;51:221–7.
29. Gousias IS, Rueckert D, Heckemann RA, Dyet LE, Boardman JP, Edwards AD, et al. Automatic segmentation of brain MRIs of 2-year-olds into 83 regions of interest. Neuroimage. 2008;40:672–84.
30. Voevodskaya O. The effects of intracranial volume adjustment approaches on multiple regional MRI volumes in healthy aging and Alzheimer's disease. Front Aging Neurosci. 2014; 6:264.
31. Mulder C, Verwey NA, van der Flier WM, Bouwman FH, Kok A, van Elk EJ, et al. Amyloid-beta(1-42), total tau, and phosphorylated tau as cerebrospinal fluid biomarkers for the diagnosis of Alzheimer disease. Clin Chem. 2010;56:248–53.
32. Zwan M, van Harten A, Ossenkoppele R, Bouwman F, Teunissen C, Adriaanse S, et al. Concordance between cerebrospinal fluid biomarkers and [11C]PIB PET in a memory clinic cohort. J Alzheimers Dis. 2014;41:801–7.
33. Scutari M. Learning Bayesian Networks with the bnlearn R Package. J Stat Softw. 2010;35:1–22.
34. Duering M, Gesierich B, Seiler S, Pirpamer L, Gonik M, Hofer E, et al. Strategic white matter tracts for processing speed deficits in age-related small vessel disease. Neurology. 2014; 82:1946–50.
35. Verhage F. Intelligentie en leeftijd: onderzoek bij Nederlanders van twaalf tot zevenzeventig jaar [Intelligence and Age: study with Dutch people aged 12 to 77]. Assen Van Gorcum. 1964.

36. Staals J, Booth T, Morris Z, Bastin ME, Gow AJ, Corley J, et al. Total MRI load of cerebral small vessel disease and cognitive ability in older people. Neurobiol Aging. 2015;36:2806–11.
37. Lammie GA, Brannan F, Wardlaw JM. Incomplete lacunar infarction (Type Ib lacunes). Acta Neuropathol. 1998;96:163–71.
38. Shoamanesh A, Kwok CS, Benavente O. Cerebral microbleeds: Histopathological correlation of neuroimaging. Cerebrovasc Dis. 2011;32:528–34.
39. Van Veluw SJ, Biessels GJ, Klijn CJM, Rozemuller AJM. Heterogeneous histopathology of cortical microbleeds in cerebral amyloid angiopathy. Neurology. 2016;86:867–71.
40. Ghaznawi R, Geerlings MI, Jaarsma-Coes MG, Zwartbol MH, Kuijf HJ, van der Graaf Y, et al. The association between lacunes and white matter hyperintensity features on MRI: The SMART-MR study. J Cereb Blood Flow Metab. 2018:0271678X1880046.
41. Fein G, Di Sclafani V, Tanabe J, Cardenas V, Weiner MW, Jagust WJ, et al. Hippocampal and cortical atrophy predict dementia in subcortical ischemic vascular disease. Neurology. 2000;55:1626–35.
42. Du A-T, Schuff N, Chao LL, Kornak J, Ezekiel F, Jagust WJ, et al. White matter lesions are associated with cortical atrophy more than entorhinal and hippocampal atrophy. Neurobiol Aging. 2005;26:553–9.
43. Reid AT, Van Norden AGW, De Laat KF, Van Oudheusden LJB, Zwiers MP, Evans AC, et al. Patterns of cortical degeneration in an elderly cohort with cerebral small vessel disease. Hum Brain Mapp. 2010;31:1983–92.
44. Tuladhar AM, Reid AT, Shumskaya E, De Laat KF, Van Norden AGW, Van Dijk EJ, et al. Relationship between white matter hyperintensities, cortical thickness, and cognition. Stroke. 2014;46:425–32.
45. Lambert C, Sam Narean J, Benjamin P, Zeestraten E, Barrick TR, Markus HS. Characterising the grey matter correlates of leukoaraiosis in cerebral small vessel disease. NeuroImage Clin. 2015;9:194–205.
46. Smith EE, O'Donnell M, Dagenais G, Lear SA, Wielgosz A, Sharma M, et al. Early cerebral small vessel disease and brain volume, cognition, and gait. Ann Neurol. 2015;77:251–61.
47. Appelman APA, Vincken KL, Van Der Graaf Y, Vlek ALM, Witkamp TD, Mali WPTM, et al. White matter lesions and lacunar infarcts are independently and differently associated with brain atrophy: The SMART-MR study. Cerebrovasc Dis. 2009;29:28–35.
48. Kloppenborg RP, Nederkoorn PJ, Grool AM, Vincken KL, Mali WPTM, Vermeulen M, et al. Cerebral small-vessel disease and progression of brain atrophy: The SMART-MR study. Neurology. 201;79:2029–36.
49. Lambert C, Benjamin P, Zeestraten E, Lawrence AJ, Barrick TR, Markus HS. Longitudinal patterns of leukoaraiosis and brain atrophy in symptomatic small vessel disease. Brain. 2016;139:1136–51.
50. Roseborough A, Ramirez J, Black SE, Edwards JD. Associations between amyloid β and white matter hyperintensities: A systematic review. Alzheimer's Dement. 2017;13:1154–67.
51. Barnes J, Carmichael OT, Leung KK, Schwarz C, Ridgway GR, Bartlett JW, et al. Vascular and Alzheimer's disease markers independently predict brain atrophy rate in Alzheimer's Disease Neuroimaging Initiative controls. Neurobiol Aging. 2013;34:1996–2002.
52. Freeze WM, Jacobs HIL, Gronenschild EH, Jansen JFA, Burgmans S, Aalten P, et al. White matter hyperintensities potentiate hippocampal volume reduction in non-demented older individuals with abnormal amyloid-β. J Alzheimer's Dis. 2016;55:333–42.
53. Seo SW, Ahn J, Yoon U, Im K, Lee J-M, Tae Kim S, et al. Cortical thinning in vascular mild cognitive impairment and vascular dementia of subcortical type. J Neuroimaging. 2010; 20:37–45.
54. Duering M, Righart R, Csanadi E, Jouvent E, Herve D, Chabriat H, et al. Incident subcortical infarcts induce focal thinning in connected cortical regions. Neurology. 2012;79:2025–8.

55. Kim HJ, Im K, Kwon H, Lee JM, Kim C, Kim YJ, et al. Clinical effect of white matter network disruption related to amyloid and small vessel disease. Neurology. 2015;85:63–70.
56. Duering M, Righart R, Wollenweber FA, Zietemann V, Gesierich B, Dichgans M. Acute infarcts cause focal thinning in remote cortex via degeneration of connecting fiber tracts. Neurology. 2015;84:1685–92.
57. Siffrin V, Vogt J, Radbruch H, Nitsch R, Zipp F. Multiple sclerosis - candidate mechanisms underlying CNS atrophy. Trends Neurosci. 2010;33:202–10.

SUPPLEMENTARY INFORMATION

METHODS

The MRI sequence parameters were as follows:

- 1.5 tesla GE Signa HDxt: 3D T1-weighted sequence (sagittal, 172 slices, voxel size: 0.98 × 0.98 × 1.50 mm, repetition time/echo time = 12.3/5.2 ms), 3D FLAIR sequence (sagittal, 128 slices, voxel size: 1.21 × 1.21 × 1.30 mm, repetition time/echo time/inversion time = 6500/117/1987 ms) and 2D T2*-weighted sequence (axial, 48 slices, voxel size: 0.98 × 0.98 × 3.00 mm, repetition time/echo time = 1000/24 ms).
- 3 tesla GE Signa HDxt: 3D T1-weighted sequence (sagittal, 176 slices, voxel size: 0.94 × 0.94 × 1.00 mm, repetition time/echo time = 7.8/3.0 ms), 3D FLAIR sequence (sagittal, 132 slices, voxel size: 0.98 × 0.98 × 1.2 mm, repetition time/echo time/inversion time = 8000/126/2340 ms) and 2D susceptibility weighted imaging sequence (axial, 48 slices, voxel size: 0.49 × 0.49 × 3.00 mm, repetition time/echo time = 31/25 ms).
- 3 tesla GE Discovery MR750: 3D T1-weighted sequence (sagittal, 176 slices, voxel size: 0.94 × 0.94 × 1.00 mm, repetition time/echo time = 8.2/3.2 ms), 3D FLAIR sequence (sagittal, 160 slices, voxel size: 0.98 × 0.98 × 1.2 mm, repetition time/echo time/inversion time = 8000/130/2340 ms) and 2D susceptibility weighted imaging sequence (axial, 44 slices, voxel size: 0.49 × 0.49 × 3.00 mm, repetition time/echo time = 31/25 ms).
- 3 tesla Philips Ingenuity: 3D T1-weighted sequence (sagittal, 180 slices, voxel size: 0.87 × 0.87 × 1.00 mm, repetition time/echo time = 9.9/4.6 ms), 3D FLAIR sequence (sagittal, 321 slices, voxel size: 1.04 × 1.04 × 0.56 mm, repetition time/echo time/inversion time = 4800/279/1650 ms) and 2D susceptibility weighted imaging sequence (axial, 247 slices, voxel size: 0.43 × 0.43 × 0.60 mm, repetition time/echo time = 29 × 20 ms).
- 3 tesla Philips Achieva and Philips Ingenia: 3D T1-weighted sequence (sagittal, 192 slices, voxel size: 1.00 × 1.00 × 1.00 mm, repetition time/echo time = 7.9/4.5 ms), 2D FLAIR sequence (axial, 48 slices, voxel size: 0.96 × 0.95 × 3.00 mm, repetition time/echo time/inversion time = 11000/125/2800 ms) and 2D T2*-weighted sequence (axial, 48 slices, voxel size: 0.96 × 0.96 × 3.00 mm, repetition time/echo time = 1653/20 ms).

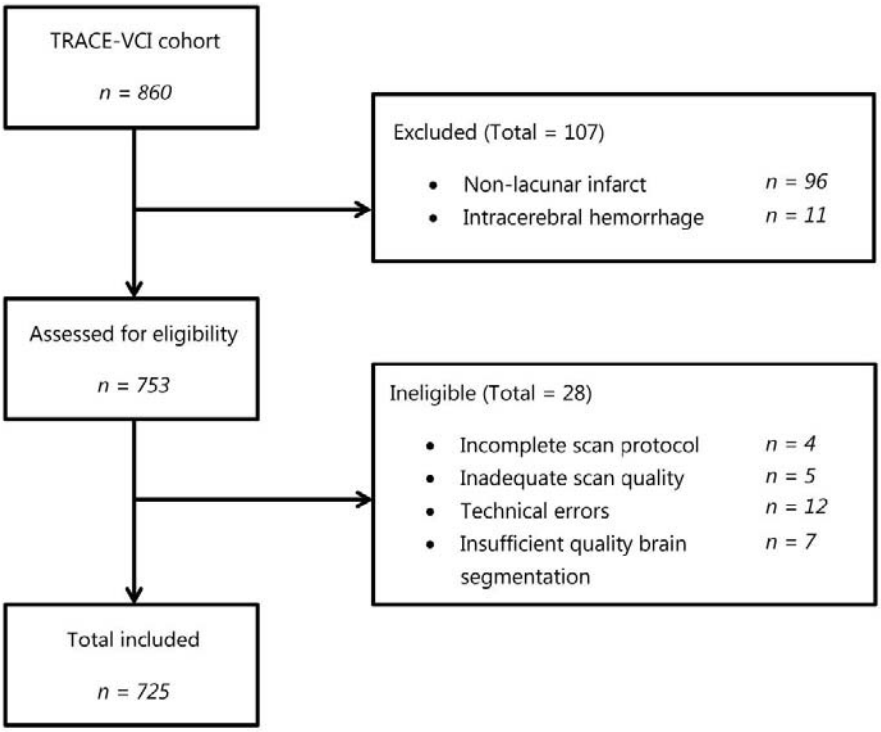

Supplementary Figure S6.1 | Flowchart. Flowchart demonstrating reasons for exclusion (presence of non-lacunar infarct or intracerebral hemorrhage) and ineligibility (incomplete scan protocol, inadequate scan quality, technical errors when running the semi-automated segmentation pipeline, insufficient quality of the brain segmentation).

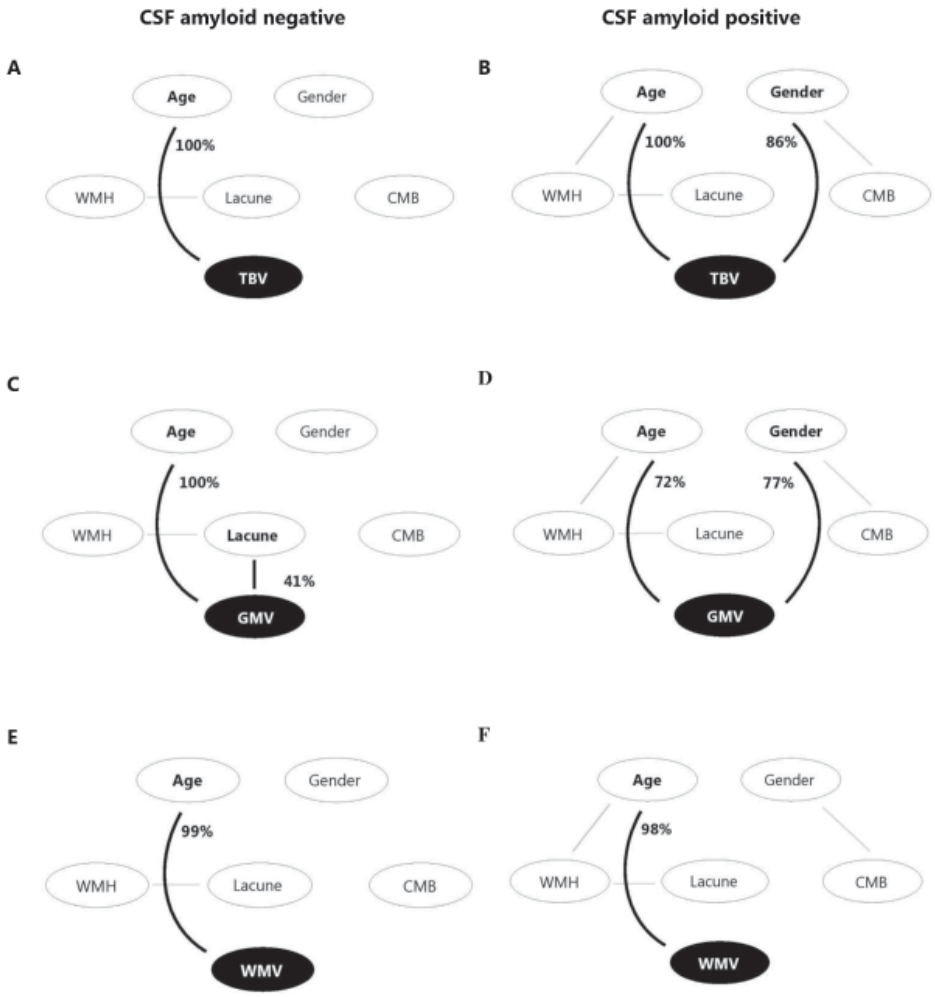

Supplementary Figure S6.2 | Bayesian networks in CSF subgroup. Bayesian networks for total brain volume (TBV, panel A and B), gray matter volume (GMV, panel C and D) and white matter volume (WMV, panel E and F) after stratifying the CSF subgroup in amyloid-negative and amyloid-positive patients. Variables that are directly connected to one of the cognitive domains are identified as direct determinants. Percentages indicate the confidence level of the arcs towards brain volumes determined by 100 bootstrap replications. CMB, presence of cerebral microbleeds; WMH, moderate/severe WMHs (Fazekas score 2 or 3).

Supplementary Table S6.1 | Baseline characteristics of the total study population

	Total CSF N = 488	Amyloid-negative N = 227	Amyloid-positive N = 261
Demographics			
Age, years	67 ± 8	**65 ± 8**	**68 ± 7**†
Gender, female	226 (46)	96 (42)	130 (50)
Level of education, Verhage scale[35]	5 [4–6]	5 [4–6]	5 [4–6]
Vascular risk factors			
Hypertension	397 (81)	182 (80)	215 (82)
Hypercholesterolemia	190 (39)	90 (40)	100 (38)
Diabetes Mellitus	74 (15)	40 (18)	34 (13)
Current smoker	95 (20)	51 (23)	44 (17)
Obesity, Body Mass Index ≥ 30	90 (19)	**56 (25)**	**34 (13)***
History of reported vascular events other than stroke	39 (8)	22 (10)	17 (7)
Number of vascular risk factors	2 [1–3]	2 [1–3]	2 [1–2]
Clinical diagnosis			
No objective cognitive impairment	118 (24)	**95 (42)**	**23 (9)**†
Mild cognitive impairment	112 (23)	52 (23)	60 (23)
Dementia	258 (53)	**80 (35)**	**178 (68)**†
Vascular	13 (3)	6 (3)	7 (3)
Neurodegenerative			
Alzheimer's disease	173 (36)	24 (11)	149 (57)
Frontotemporal disease	19 (4)	17 (8)	2 (1)
Lewy body dementia	13 (3)	6 (3)	7 (3)
Others#	23 (5)	17 (8)	6 (2)
Unknown etiology¥	17 (4)	10 (4)	7 (3)

Data are presented as mean ± standard deviation, number of patients (percentage of total study population) or median [interquartile range]. # Such as Primary Progressive Aphasia, Cortical Basal Syndrome and Progressive Supranuclear Palsy. ¥ Dementia of unknown origin, further examination needed to state diagnosis. * $p < 0.05$; † $p < 0.0001$.

Supplementary Table S6.2 | Relationship between CSF amyloid biomarker status and brain volumes stratified for WMH burden (high or low) and stratified for presence/absence lacunes

	Total brain volume	Gray matter volume	White matter volume
CSF subgroup (n = 488)			
Amyloid + vs Amyloid -	**-0.19 [-0.27;-0.11]**†	**-0.26 [-0.33;-0.18]**†	-0.01 [-0.09;0.08]
High WMH burden (n = 235)			
Amyloid + vs Amyloid -	**-0.14 [-0.26;-0.03]***	**-0.18 [-0.29;-0.07]***	-0.03 [-0.14;0.09]
Low WMH burden (n = 253)			
Amyloid + vs Amyloid -	**-0.23 [-0.35;-0.12]**†	**-0.31 [-0.42;-0.21]**†	0.01 [-0.11;0.13]
Presence of lacunes (n = 84)			
Amyloid + vs Amyloid -	-0.07 [-0.26;0.12]	-0.12 [-0.30;0.05]	0.02 [-0.19;0.22]
Absence of lacunes (n = 404)			
Amyloid + vs Amyloid -	**-0.22 [-0.31;-0.13]**†	**-0.28 [-0.36;-0.20]**†	-0.02 [-0.11;0.07]

This table shows the relation between CSF amyloid biomarker status (amyloid-positive or amyloid-negative) and brain volumes. In the first row, the relation in the CSF subgroup is shown, presented as standardized beta coefficients with 95% confidence intervals after correction for age, gender and scanner effect. Next, analyses are stratified for WMH burden (high or low). Finally, analyses are stratified for presence or absence of lacunes. All brain volumes were corrected for variations in head size using the total intracranial volume.
* $p < 0.05$; † $p < 0.001$.

Supplementary Table S6.3 | Regional gray matter volume analysis in entire study population (n = 725)

	Left	Right
Frontal		
Middle frontal gyrus	**-0.28***	**-0.31***
Precentral gyrus	-0.23	**-0.27***
Rectal gyrus	**-0.31***	**-0.36***
Orbitofrontal gyrus	**-0.30***	**-0.33***
Inferior frontal gyrus	**-0.33***	**-0.33***
Superior frontal gyrus	-0.15	-0.13
Parietal		
Inferior lateral parietal lobe	-0.08	0.03
Postcentral gyrus	**-0.26***	-0.20
Superior parietal gyrus	0.19	0.18
Temporal		
Hippocampus	-0.19	-0.23
Amygdala	-0.09	-0.15
Anterior medial temporal lobe	-0.15	-0.19
Anterior lateral temporal lobe	-0.21	-0.20
Ambient and parahippocampus gyri	-0.16	-0.22
Superior temporal gyrus	**-0.39***	**-0.32***
Inferior middle temporal gyrus	-0.21	**-0.29***
Fusiform gyrus	-0.24	-0.21
Posterior temporal lobe	-0.17	-0.10
Insula and cingulate gyri		
Insula	-0.05	-0.12
Anterior cingulate gyrus	-0.21	**-0.27***
Posterior cingulate gyrus	**-0.29***	**-0.36***
Occipital		
Lateral occipital lobe	-0.07	-0.07
Lingual gyrus	-0.21	-0.06
Precuneus	-0.12	-0.01
Central structures		
Caudate nucleus	-0.06	-0.07
Accumbent nucleus	-0.09	-0.11
Putamen	0.03	0.04
Thalamus	**-0.46***	**-0.50***
Pallidum	0.06	0.06
Infratentorial		
Cerebellum	-0.19	-0.18

Data are presented as standardized z-scores (Δz-score) between patients with high WMH burden and low WMH burden, after correction for age, gender and scanner effect. * Bonferroni-corrected p-value < 0.05. Note: ventricular, corpus callosum and brainstem ROIs were not compared since this analysis focused on gray matter regions.

Supplementary Table S6.4 | Regional gray matter volume analysis, stratified for CSF biomarker amyloid status

	Amyloid-negative		Amyloid-positive	
	Left	Right	Left	Right
Frontal				
Middle frontal gyrus	-0.43	**-0.47***	-0.07	-0.10
Precentral gyrus	-0.41	**-0.49***	-0.16	-0.09
Rectal gyrus	-0.31	-0.33	-0.27	-0.28
Orbitofrontal gyrus	-0.34	-0.36	-0.21	-0.21
Inferior frontal gyrus	-0.35	-0.31	-0.13	-0.18
Superior frontal gyrus	-0.32	-0.20	0.02	0.11
Parietal				
Inferior lateral parietal lobe	0.07	0.13	0.01	0.19
Postcentral gyrus	-0.37	-0.24	-0.11	-0.13
Superior parietal gyrus	0.19	0.25	0.33	0.30
Temporal				
Hippocampus	-0.14	-0.11	-0.23	-0.25
Amygdala	-0.01	-0.04	-0.06	-0.10
Anterior medial temporal lobe	-0.07	-0.12	-0.09	-0.10
Anterior lateral temporal lobe	-0.13	0.01	-0.18	-0.14
Ambient and parahippocampus gyri	-0.08	-0.17	-0.13	-0.13
Superior temporal gyrus	-0.13	-0.03	**-0.46***	-0.35
Inferior middle temporal gyrus	-0.08	-0.16	-0.16	-0.20
Fusiform gyrus	-0.14	-0.13	-0.22	-0.12
Posterior temporal lobe	-0.03	0.10	-0.09	-0.04
Insula and cingulate gyri				
Insula	0.17	0.09	-0.09	-0.15
Anterior cingulate gyrus	-0.12	-0.19	-0.11	-0.21
Posterior cingulate gyrus	-0.32	-0.32	-0.12	-0.25
Occipital				
Lateral occipital lobe	0.04	0.04	-0.02	0.01
Lingual gyrus	-0.26	-0.12	-0.19	0.01
Precuneus	-0.15	-0.06	-0.19	0.05
Central structures				
Caudate nucleus	0.15	0.14	-0.06	-0.13
Accumbent nucleus	-0.09	-0.14	0.003	-0.04
Putamen	0.22	0.24	0.06	0.04
Thalamus	**-0.50***	**-0.49***	-0.22	-0.31
Pallidum	0.11	0.14	0.18	0.11
Infratentorial				
Cerebellum	-0.06	-0.09	-0.14	-0.12

Data are presented as standardized z-scores (Δz-score) between patients with high WMH burden and low WMH burden, after correction for age, gender and scanner effect. * Bonferroni-corrected p-value < 0.05. Note: ventricular, corpus callosum and brainstem ROIs were not compared since this analysis focused on gray matter regions.

Chapter 7

Pattern of impaired white matter connectivity in Alzheimer's disease versus small vessel disease

Rutger Heinen
Bruno M. de Brito Robalo
Huiberdina L. Koek
Naomi Vlegels
Arno de Wilde
Geert Jan Biessels
Yael D. Reijmer
on behalf of the Utrecht VCI study group*

* Members of TRACE-VCI study group are mentioned in the acknowledgements

Submitted

ABSTRACT

To determine whether the pattern of impaired white matter (WM) connectivity differs between patients with primarily Alzheimer's disease (AD) pathology and patients with primarily cerebral small vessel disease (SVD) pathology.

We included 38 cognitively healthy controls and 39 memory clinic patients who were either amyloid beta (Aβ)+/SVD- (n = 20) or Aβ-/SVD+ (n = 19), based on CSF or PET biomarker status and the presence of SVD on MRI. WM networks were reconstructed from diffusion MRI data and consisted of 90 (sub)cortical nodes. The fractional anisotropy (FA)- and mean diffusivity (MD)-weighted connectivity strength of each network node was compared between groups, as well as the FA and MD of long versus short WM connections and connections between hub nodes versus other WM connections.

Aβ-/SVD+ but not Aβ+/SVD- patients had impaired FA-weighted WM connectivity compared to controls (false-discovery rate corrected $p < 0.05$). MD-weighted WM connectivity was globally impaired in both patient groups, with Aβ+/SVD- patients showing the largest effect sizes ($\beta \geq 0.40$) in medial and parietal-occipital nodes and Aβ-/SVD+ patients in frontal nodes. In both patient groups, long WM connections were more severely affected than short WM connections and WM connections between hub nodes more severely affected than all other connections (group x tract interaction terms all $p < 0.07$).

The manifestation and spatial pattern of impairments in WM connectivity differ between patients with primarily AD pathology and SVD pathology. This suggests that these pathologies affect the WM network through partly different mechanisms.

INTRODUCTION

Impaired white matter (WM) connectivity is a frequent observation in patients with Alzheimer's disease (AD)[1–4] and cerebral small vessel disease (SVD).[5–8] Impairments in WM connectivity can be detected with diffusion tensor imaging (DTI) and quantified by using network theory analysis.[9] Studies in patient cohorts have shown that diffusion abnormalities in the WM network relate to cognitive impairment and can predict conversion to dementia.[10–12]

The pathological processes leading to impaired WM connectivity in AD and SVD have not been fully elucidated. Several mechanisms have been suggested in AD, such as Wallerian degeneration,[13] damage to oligodendrocytes[14] and cerebral hypoperfusion.[15] In SVD, vascular brain lesions can be seen on MRI, such as white matter hyperintensities (WMHs), lacunes and cerebral microbleeds.[16] These lesions are pathologically heterogeneous[17] and occur within the WM, where they have (peri)lesional as well as remote effects on WM connectivity.[18]

Because AD and SVD pathology often co-occur in the same patient,[19] it is difficult to determine whether both processes independently affect the WM, or via common pathways. Previous studies on WM connectivity in patients with AD/SVD have often included patients using clinical diagnoses[20,21] rather than biomarker evidence of specific pathologies,[22] or heterogeneous samples without excluding the presence of AD or SVD pathology. In this study, we increased the homogeneity of the study sample by investigating selected patient groups with either AD or SVD pathology. Hereby we aimed to identify WM network regions that are specifically vulnerable to AD or SVD.

MATERIALS AND METHODS

Study population

Patients were included from the memory clinic at the University Medical Center Utrecht, the Netherlands, between November 2009 and April 2017 as part of the Parelsnoer Institute (PSI) Neurodegenerative diseases cohort study.[23] All patients underwent a standardized one-day evaluation including an interview, physical and neurological examination, laboratory testing, neuropsychological assessment and a brain MRI scan. Information regarding educational level and vascular risk factors (hypertension, hypercholesterolemia, diabetes mellitus, current smoking, obesity and clinically manifest non-cerebral atherosclerotic disease) was collected. Lumbar puncture was optional for participants in this study. Amyloid positron emission tomography (PET) scans were obtained from patients recruited from December 2015 as part of a sub-study.[24]

For the current study, patients were eligible to be included if amyloid beta (Aβ) CSF and/or PET data and an adequate diffusion-weighted imaging (DWI) sequence were available. This was the case for 65 of 229 (28%) patients, in which CSF data was available in 41 of 65 (63%) patients and PET data in 27 (42%) patients. All 65 patients were rated for Aβ positivity/negativity using CSF or PET as well as SVD positivity/negativity using brain MRI. Patients were considered as having either: 1) positive CSF and/or PET Aβ status and minimal or absent cerebral SVD on MRI (Aβ+/SVD-) or 2) negative CSF and/or PET Aβ status and evidence of cerebral SVD on MRI (Aβ-/SVD+). Cut-off values for CSF Aβ are detailed in section 2.2. Criteria for SVD presence and severity are detailed in section 2.4. Twenty-one patients met the criteria for Aβ+/SVD- and twenty patients met the criteria for Aβ-/SVD+. Two patients were excluded due to inadequate 3D T1 images (n = 1) or registration issues (n = 1), leaving 39 patients for the current study (Aβ+/SVD-: n = 20; Aβ-/SVD+: n = 19).

In addition, non-demented elderly participants were selected from the Utrecht Diabetic Encephalopathy Study 2 (UDES2) to serve as a control group.[25] To this end, all participants from the control sample of the UDES2 study were eligible, combined with a random sample of participants with type 2 diabetes to obtain a non-demented reference group with a proportion of diabetes (13%) compatible with the diabetes prevalence in the Dutch population for this age group.[26] Participants for the UDES2 study were recruited through their general practitioners in Utrecht and surrounding areas and underwent a comparable one-day evaluation as the patients, including a brain MRI scan with the same scan protocol on the same MR scanner as the patient sample. All participants were cognitively healthy, i.e. no history of cognitive impairment and a Mini-Mental State Examination (MMSE) score ≥ 27. No CSF and/or PET data was available for any of the controls. Fifty-two participants met the inclusion criteria. DWI- or T1-weighted MR images of two individuals contained movement artefacts and could not be used. Participants with moderate/severe WMHs (Fazekas scale ≥ 1) and/or multiple lacunes were excluded (n = 10). The two youngest controls were also excluded in order to obtain a comparable age distribution as the patient groups, leaving 38 participants for the current analyses.

The study was approved by the institutional review boards of the University Medical Center Utrecht (approval number 09-211/C). All procedures were in accordance with the ethical standards of the responsible committee on human experimentation (institutional and national) and with the Helsinki Declaration of 1975, as revised in 2013. All participants provided written informed consent prior to any research related procedures.

Amyloid biomarkers

CSF concentrations of $A\beta_{42}$ were measured at a central laboratory for clinics at the Department of Clinical Chemistry of the Amsterdam University Medical Center in a subset of patients using commercially available ELISAs (Innotest β-amyloid($_{1-42}$); Innogenetics, Ghent, Belgium).[23] For the present study, a cut-off value for $A\beta_{42}$ < 640 ng/L was used to define Aβ positivity, based on a previous study.[27]

Amyloid PET/CT scans were acquired using a Siemens Biograph™ 40 mCT scanner (Siemens Healthcare, Erlangen, Germany). Patients were injected with a tracer dose of approximately 300 MBq ± 20% ^{18}F-florbetaben (Neuraceq™). The image acquisition window extends from 90 to 110 minutes (4 × 5-minute frames) after dose injection. PET scans were visually assessed by an experienced nuclear physician for Aβ positivity (yes/no).[24]

Image acquisition

MRI data were acquired on a Philips 3.0 tesla Achieva scanner (Philips, Best, the Netherlands) with a standardized protocol that consisted of a 3D T1-weighted sequence (192 slices, voxel size: 1.00 × 1.00 × 1.00 mm, repetition time (TR)/echo time (TE): 7.9/4.5 ms); a 2D T2-weighted sequence (48 slices, voxel size: 0.96 × 0.96 × 3.00 mm, TR/TE: 3198/140 ms), a 2D T2*-weighted scan (48 slices, voxel size: 0.99 × 0.99 × 3.00 mm, TR/TE: 1653/20 ms); a 2D fluid-attenuated inversion recovery (FLAIR) scan (48 slices, voxel size 0.96 × 0.95 × 3.00 mm, TR/TE/inversion time: 11000/125/2800 ms) and a diffusion-weighted sequence (48 slices, voxel size: 2.50 × 2.50 × 2.50 mm, TR/TE: 6600/73 ms, 45 gradient directions with a b-value of 1200 s/mm^2 and one with a b value of 0 s/mm^2 (number of signal averages = 3)). Of note, one patient was scanned on a Philips 3.0 tesla Ingenia scanner (Philips, Best, the Netherlands) using the same scan protocol as described above.

SVD MRI markers and brain volumes

Presence of WMHs (using the Fazekas scale),[28] lacunes and cerebral microbleeds was rated on FLAIR and T2* weighted images by or under supervision of a neuroradiologist using the STRIVE criteria.[16] Cerebral SVD on MRI was defined as presence of WMHs (Fazekas scale of ≥1) or lacune(s)/cerebral microbleed(s). Since there were very few cases with no cerebral SVD on MRI, we also included patients with minimal cerebral SVD on MRI in the SVD- group. Minimal SVD on MRI was defined as mild WMHs (Fazekas scale of 1) and no or a single lacune/cerebral microbleed. A previously described semi-automated workflow (including lesion filling) was performed with Statistical Parametric Mapping 12 software (SPM Wellcome Department of Cognitive Neurology, Institute of Neurology, Queen Square London) to obtain total brain volume and total intracranial volume.[29]

Diffusion MRI processing and tractography

Diffusion tensor imaging (DTI) scans were analyzed and processed using ExploreDTI version 4.8.6 (www.exploredti.com). Preprocessing included subject motion, eddy current and echo-planar imaging distortion correction and a robust tensor estimation using the REKINDLE approach (including adjustment of the B-matrix).[30] For each patient, whole-brain WM tractography was performed using constrained spherical deconvolution (CSD)-based deterministic fiber tractography.[31] This method allows fiber tracking to proceed through crossing fiber regions. Reconstruction of fiber tracts was performed by using uniformly distributed seed samples throughout the brain's WM at a 2 mm isotropic resolution. Fiber tracts were terminated when they deflected in an angle of $> 45^{o}$ or if they entered a voxel with a fiber orientation distribution threshold of < 0.1. Tract length thresholds were set between 50 and 500 mm.

Network reconstruction

3D T1 weighted images were segmented using the Computational Anatomy Toolbox (CAT12, version r864, http://www.neuro.uni-jena.de/cat/) for Statistical Parametric Mapping 12 (SPM Wellcome Department of Cognitive Neurology, Institute of Neurology, Queen Square London)). The brain was automatically parcellated in 90 cortical and subcortical grey matter regions defined using the automated anatomic labeling (AAL) template.[32] Each region represented a node in the brain network. Two regions were considered to be connected if the end points of the reconstructed fiber bundle lay within both regions, resulting in a 90×90 binary connectivity matrix. A weighted connectivity matrix was then obtained for patients and controls by multiplying each edge by the mean fractional anisotropy (FA) or mean diffusivity (MD) of that edge, resulting in two weighted connectivity matrices for each patient. A FA threshold of > 0.2 was used on all connectivity matrices to minimize errors due to partial volume effects.

WM connectivity

The Brain Connectivity Toolbox (www.brain-connectivity-toolbox.net) was used to calculate all network characteristics. To ensure that the number of connections within the network was equal between groups, we calculated the density of the network (defined as the ratio between the number of edges present and the total number of possible edges in a network).

The primary analyses were performed on measures of regional WM connectivity. This included the *FA- and MD-weighted connectivity strength* per node (here defined as the mean FA or MD of all WM fibers connected to that node). In addition, we examined the mean

FA and MD of two types of WM connections that have been suggested to be particularly vulnerable to AD and/or SVD pathology due to a relatively high metabolic demand:[4,33,34] 1) '*relatively long WM connections*' and 2) '*WM connections between hub nodes*'. Relatively long WM connections were defined as the 50% connections with the longest tract length of all network connections within the study sample (range tract length: 50–250 mm; median: 107.5 mm). Short WM connections were defined as the 50% connections with the shortest tract length. Network hubs were identified by selecting the top 10 nodes with the highest betweenness centrality of all networks from the control sample.[35] The betweenness centrality is the fraction of shortest paths passing through a given node.[36] Thus, nodes with a high betweenness centrality are crucial for network integration and are therefore often considered to be network 'hubs'.

Statistical analysis

Statistical analysis was performed in IBM SPSS statistics (version 25). A p-value of < 0.05 was considered significant. Normality of continuous variables was checked.

First we determined the pattern of impaired regional WM connectivity in each patient group compared to the control group. FA- and MD-weighted mean connectivity strength per node was compared between each patient group and controls using linear regression analysis, adjusted for age and gender. P-values of nodal comparisons were adjusted for multiple testing using false discovery rate (FDR) correction.[37] We also determined whether certain types of WM connections were more severely affected by comparing the mean FA and MD of relatively long versus short connections and connections between hub nodes versus other connections between each patient group and controls. We used repeated measures ANOVA with group as between-subject factor and type of WM connection (relatively long or short; hub or other) as within-subject factor, adjusted for age and gender). Possible interactions between group x tract length (short or long) and group x connections between hubs (yes or no) were also tested to evaluate whether these type of WM connections are particularly affected in AD and/or SVD.

Finally, we repeated the above-mentioned analyses, but now comparing both patient groups with each other.

Data availability statement

The data that support the findings of this study are available from the final author, upon reasonable request.

RESULTS

Study sample characteristics

The characteristics for patient groups and controls are shown in Table 7.1. For both Aβ+/SVD- and Aβ-/SVD+ patients MMSE scores were significantly lower than controls ($p < 0.05$, adjusted for age, gender and level of education), but MMSE scores did not differ between the two patient groups ($p = 0.47$, adjusted for age, gender and level of education). Both patient groups also showed significantly smaller total brain volume compared to controls ($p < 0.05$, adjusted for age and gender) but brain volumes did not differ between Aβ+/SVD- and Aβ-/SVD+ patients ($p = 0.56$, adjusted for age and gender).

Table 7.1 | Baseline characteristics of the study population

	Aβ+/SVD- (n = 20)	Aβ-/SVD+ (n = 19)	Controls (n = 38)
Demographics			
Age, years	70 ± 7	74 ± 8	72 ± 5
Gender, female	10 (50)	6 (32)	16 (42)
Education Level, Verhage scale[50]	5 [4–6]	5 [4–6]	4 [3–5]
MMSE score	27 [24–28]	27 [24–29]	29 [27–30]
Clinical diagnosis			
Subjective cognitive complaints	3 (15)	1 (5)	[a]
Mild cognitive impairment	13 (65)	11 (58)	[a]
Dementia	4 (20)	7 (37)	[a]
MRI markers			
WMH, Fazekas score			
0	3 (15)	0	19 (50)
1	17 (85)	14 (74)	19 (50)
2	[b]	4 (21)	[b]
3	[b]	1 (5)	[b]
Lacunes	1 (5)	6 (32)	7 (18)
Cerebral microbleeds	2 (11)	3 (16)	2 (5)
Brain volumes			
Total brain volume, fraction of TIV	0.68 ± 0.03	0.68 ± 0.03	0.71 ± 0.03

Aβ, amyloid-beta; SVD, cerebral small vessel disease; WMH, white matter hyperintensities; TIV, total intracranial volume. Presented are baseline characteristics for patients with primarily Alzheimer's Disease pathology (Aβ+/SVD-), patients with primarily cerebral small vessel disease pathology (Aβ-/SVD+), and controls. Data are presented as mean ± SD, numbers (percentages) or median [interquartile range].

[a] Controls were cognitively healthy (i.e. no history of cognitive impairment, and a Mini-Mental State Examination (MMSE) score ≥ 27).

[b] Aβ+/SVD- patients and controls with a Fazekas score > 1 were excluded.

Brain network characteristics

Network density did not differ between any of the groups (mean (SD) controls: 0.28 (0.03); Aβ+/SVD-: 0.29 (0.04); Aβ-/SVD+: 0.28 (0.04), all $p > 0.05$). The top ten nodes with the highest betweenness centrality in the control group classified as hub nodes were: the left and right precuneus, left and right superior parietal gyrus, left and right middle temporal pole, left superior temporal gyrus, right superior frontal gyrus, left and right middle superior frontal gyrus.

Pattern of impaired WM connectivity in patients versus controls

In Aβ+/SVD- patients, no significant differences in FA-weighted WM connectivity were found compared to controls (FDR-corrected $p > 0.05$; Figure 7.1). By contrast, in Aβ-/SVD+ patients, FA-weighted WM connectivity of frontal, parietal and occipital nodes was lower than in controls (FDR-corrected $p < 0.05$; Figure 7.1). In both Aβ+/SVD- and Aβ-/SVD+ patients, MD-weighted WM connectivity of widely distributed nodes was increased compared to controls (FDR-corrected $p < 0.05$; Figure 7.2), indicating global impairments in WM connectivity. The severity of impairments, however, showed a slightly different pattern in both patient groups: for Aβ+/SVD- patients, largest effect sizes (standardized

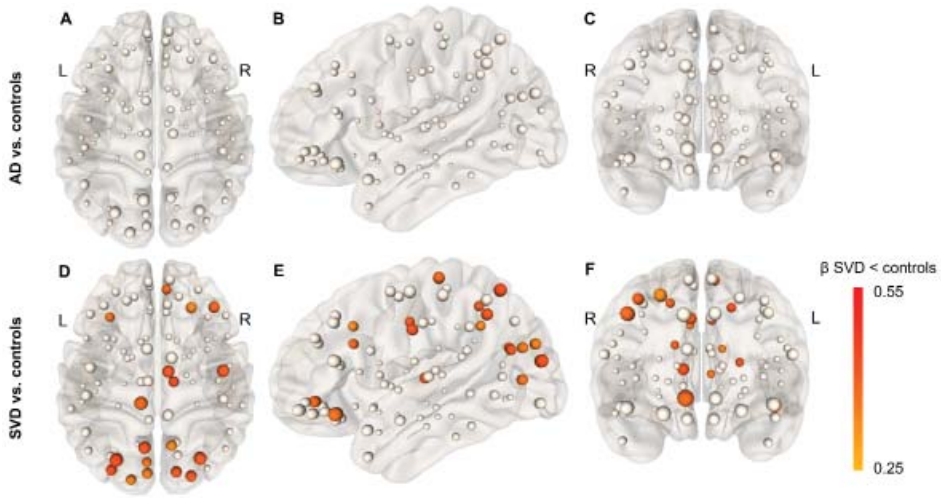

Figure 7.1 | Pattern of impaired regional FA-weighted white matter connectivity. AD, Alzheimer's disease; SVD, cerebral small vessel disease; FA, fractional anisotropy. Presented are reductions in FA-weighted nodal strength between patients with primarily AD (Aβ+/SVD-) vs. controls (A-C) and patients with primarily SVD (Aβ-/SVD+) vs. controls (D-F). The size and color of the nodes are scaled according to the standardized beta-coefficients (β, adjusted for age and gender). Only nodes with a false discovery rate (FDR)-corrected p-value < 0.05 are color coded. For AD vs. Controls, none of the effect sizes remained significant after FDR correction.

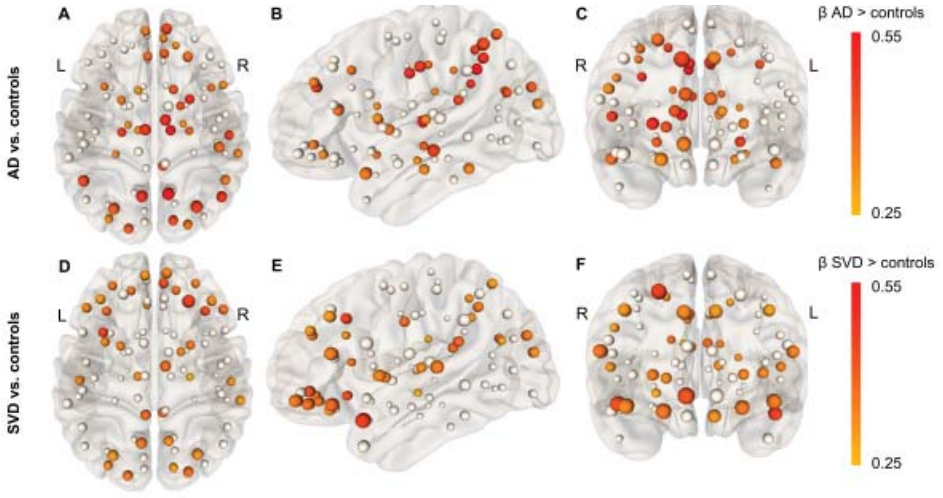

Figure 7.2 | Pattern of impaired regional MD-weighted white matter connectivity. AD, Alzheimer's disease; SVD, cerebral small vessel disease; FA, fractional anisotropy. Presented are increases in MD-weighted nodal strength between patients with primarily AD (Aβ+/SVD-) vs. controls (A-C) and patients with primarily SVD (Aβ-/SVD+) vs. controls (D-F). The size and color of the nodes are scaled according to the standardized beta-coefficients (β, adjusted for age and gender). Only nodes with a false discovery rate (FDR)-corrected p-value < 0.05 are color coded.

beta coefficient [β] ≥ 0.40, adjusted for age and gender) were seen in nodes with WM connections projecting towards medial and parietal-occipital regions, whereas in Aβ-/SVD+ patients, largest effect sizes were seen in WM connections projecting towards frontal regions.

Relatively long WM connections were more severely affected than short connections. This was reflected by a greater decrease in FA of long versus short connections in Aβ-/SVD+ patients compared to controls (tract length x group interaction term: $p < 0.05$) and a trend towards a greater decrease in FA in Aβ+/SVD- patients (interaction term: $p = 0.07$; Table 7.2, Figure 7.3). When the MD of long and short WM connections was examined, no interaction effect was found: in both patient groups, the MD of both long and short WM connections was affected relative to controls (all $p < 0.05$; Table 7.2). In both Aβ+/SVD- and Aβ-/SVD+ patients, WM connections between hub nodes were more severely affected than other connections, reflected by a greater decrease in FA compared to controls (interaction term: $p < 0.05$; Table 7.2, Figure 7.3). Also, the MD of connections between hub nodes showed a greater increase compared to controls than the MD of other WM connections (interaction term Aβ-/SVD+: $p < 0.05$; for Aβ+/SVD-: $p = 0.09$; Table 7.2, Figure 7.3).

Table 7.2 | White matter connectivity of different types of network connections in patients with primarily AD (Aβ+/SVD-) or SVD (Aβ-/SVD+) pathology and controls

	AD	SVD	Controls
FA			
Long connections	0.337 (0.013)	0.323 (0.017)[a,c]	0.341 (0.015)
Short connections	0.284 (0.008)	0.275 (0.011)[a,b,c]	0.284 (0.010)
MD[d]			
Long connections	0.949 (0.044)[a]	0.964 (0.058)[a]	0.915 (0.034)
Short connections	0.935 (0.035)[a]	0.952 (0.056)[a]	0.908 (0.031)
FA			
Connections between hub nodes	0.320 (0.018)[a,c]	0.308 (0.024)[a,c]	0.333 (0.023)
Other connections	0.311 (0.010)[c]	0.300 (0.012)[a,b,c]	0.312 (0.012)
MD[d]			
Connections between hub nodes	0.937 (0.049)[a]	0.963 (0.074)[a,c]	0.891 (0.044)
Other connections	0.972 (0.046)[a]	0.988 (0.065)[a,c]	0.935 (0.037)

AD, Alzheimer's disease; SVD, cerebral small vessel disease; Aβ, amyloid-beta; FA, fractional anisotropy; MD, mean diffusivity. Presented are mean (SD) FA or MD of relatively long and short connections and connections between hub nodes and other connections are shown. [a] $p < 0.05$ vs. controls (corrected for age and gender). [b] $p < 0.05$ vs patients with primarily AD (corrected for age and gender). [c] $p < 0.05$ for interaction term (group x type of WM connection). [d] MD values $\times 10^{-3}$ mm^2/s.

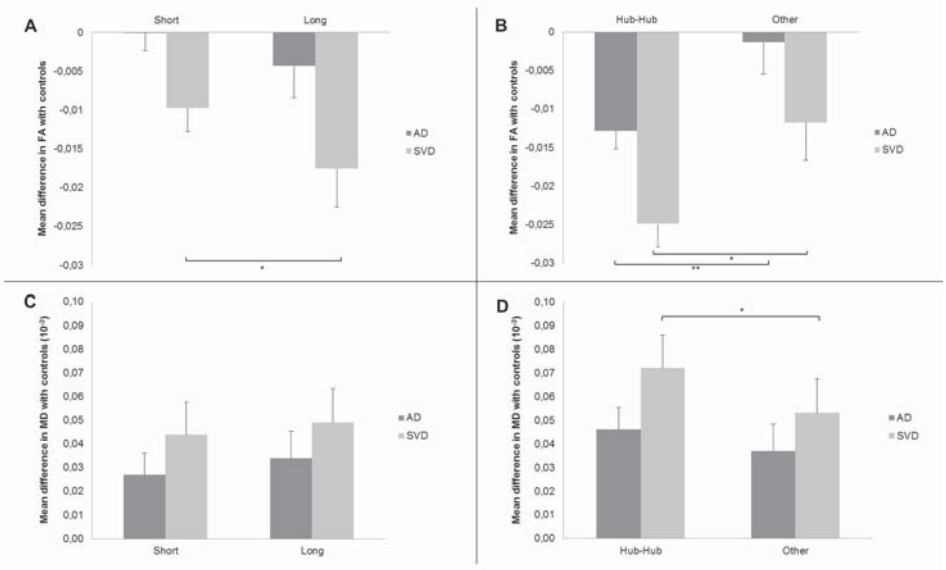

Figure 7.3 | Impairments in long-range and connections between hub nodes. AD, Alzheimer's disease; SVD, cerebral small vessel disease; FA, fractional anisotropy; MD, mean diffusivity. Presented are mean differences ± SEM in FA (A, B) and MD (C, D) of relatively short and long connections (A, C) and of connections between hub nodes and other connections (B, D) for patients with primarily AD (Aβ+/SVD-) vs. controls and patients with primarily SVD (Aβ-/SVD+) vs. controls. Group x tract interaction: * $p < 0.05$; ** $p < 0.001$ (adjusted for age and gender).

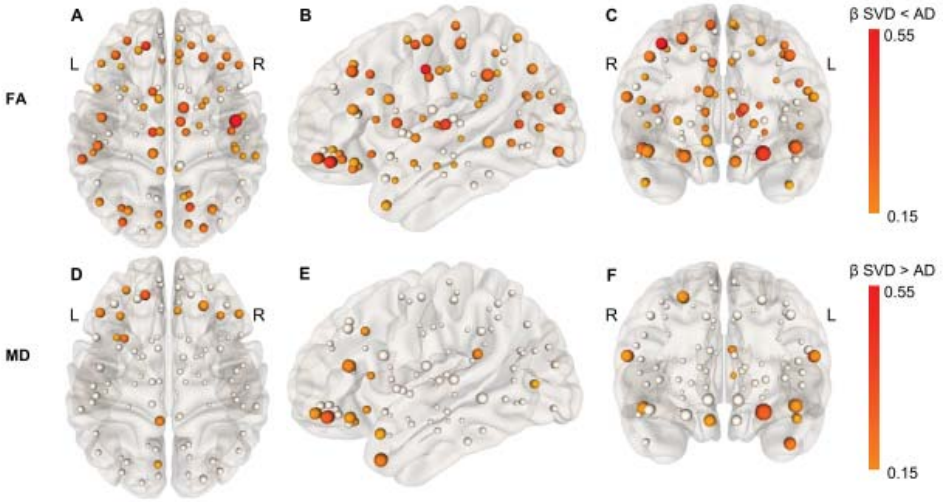

Figure 7.4 | Impaired regional white matter connectivity in patients with primarily SVD versus patients with primarily AD. AD, Alzheimer's disease; SVD, cerebral small vessel disease; FA, fractional anisotropy; MD, mean diffusivity. Presented are reductions in FA-weighted (A-C) and increases in MD-weighted (D-F) nodal strength in patients with primarily SVD (Aβ-/SVD+) vs. patients with primarily AD (Aβ+/SVD-). The size and the color of the nodes are scaled according to the standardized beta-coefficient [β] after correction for age and gender. Only nodes with β > 0.15 are shown in color. None of the effect sizes remained significant after FDR correction.

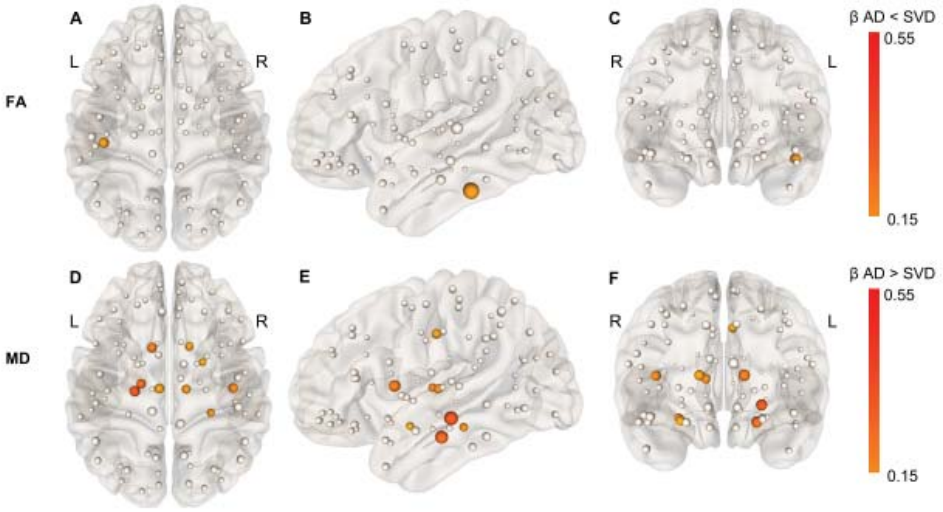

Figure 7.5 | Impaired regional white matter connectivity in patients with primarily AD versus patients with primarily SVD. AD, Alzheimer's disease; SVD, cerebral small vessel disease; FA, fractional anisotropy; MD, mean diffusivity. Presented are reductions in FA (A-C) and increases in MD (D-F)-weighted nodal strength between patients with primarily AD (Aβ+/SVD-) vs. patients with primarily SVD (Aβ-/SVD+). The size and the color of the nodes are scaled according to the standardized beta-coefficient [β] after correction for age and gender. Only nodes with β > 0.15 are shown in color. None of the effect sizes remained significant after FDR correction.

Direct comparison of WM connectivity between AD and SVD-related pathology

Compared to Aβ+/SVD- patients, Aβ-/SVD+ patients showed greater impairments in FA-weighted WM connectivity across the whole brain, and greater frontal impairments in MD-weighted WM connectivity (Figure 7.4; although none of the differences in connectivity between patient groups survived FDR correction). On the other hand, Aβ+/SVD- patients showed greater impairments in limbic and striatal MD-weighted WM connectivity compared to Aβ-/SVD+ patients (Figure 7.5; although none of the differences in connectivity between patient groups survived FDR correction). Regarding different types of WM connections, there were no significant interaction effects between patient group and type of WM connection (Table 7.2).

DISCUSSION

The present study demonstrates that both AD and SVD are associated with widespread impairments in WM connectivity, but differences exist in the manifestation and spatial distribution of the diffusion abnormalities across the WM network. Patients with primarily SVD pathology (Aβ-/SVD+) but not patients with primarily AD pathology (Aβ+/SVD-) had impaired FA-weighted WM connectivity compared to controls. Both patient groups had impaired MD-weighted WM connectivity, with largest impairments seen for Aβ+/SVD- patients in parietal-occipital regions and for Aβ-/SVD+ patients in frontal regions. In both patient groups, relatively long WM connections were more severely affected than short WM connections, and WM connections between hub nodes were more severely affected than all other WM connections.

This study extends current knowledge from previous studies regarding impairments in WM connectivity in patients with AD and SVD in a memory clinic setting by investigating highly selected patient samples. Where previous studies often included patients using clinical diagnoses (rather than biomarker evidence of specific pathologies[22]) or investigated heterogeneous samples without excluding the presence of AD or SVD pathology, our approach was to strive for homogeneity of the study sample by investigating patients with either biomarker-confirmed AD or SVD pathology. While it can be argued that this selection procedure might lead to less generalizable results, we should emphasize that our specific intention was to give more insight in the underlying pathophysiological mechanisms of each pathology. We found widespread impairments in WM connectivity in both patient groups, which is in line with previous studies.[1,3,5–7] However, we also found a difference in the spatial pattern of impaired WM connectivity between both patient groups. Aβ-/SVD+ patients showed greater impairments in FA-weighted WM connectivity across

the whole brain, and greater frontal impairments in MD-weighted WM connectivity than Aβ+/SVD- patients. Although none of the differences survived correction for multiple testing, the effect sizes showed the same magnitude and direction as those seen in the comparison to cognitive healthy controls. This could suggest a lack of power to detect significant differences when comparing both patient groups with each other. All in all, our results suggest that both pathologies affect the WM network through partly different mechanisms (e.g. ischemia, hypoperfusion, inflammation, amyloid-induced toxicity), possibly with a different initial target (e.g. Aβ deposition in association cortices in AD[38] compared to chronic ischemia of the deep WM in SVD[39]) and/or a different propagation throughout the brain. Another explanation could be overlapping mechanisms (e.g. blood brain-barrier dysfunction[18,40]) but with a different regional distribution. For instance, regional differences in blood brain-barrier dysfunction have been shown for various neurodegenerative pathologies.[40] Since the present study could not infer causality, future longitudinal studies are needed to further identify the underlying mechanisms of WM impairments in patients with AD and SVD.

We also found that relatively long WM connections were more severely affected than short WM connections and WM connections between hub nodes were more severely affected than all other WM connections in both patient groups. This is in line with previous studies.[1,4,10,33,34,41] Why these types of connections are predominantly affected is not clear and various theories have been suggested. For instance, the vulnerability of connections between hub nodes could be due a relatively higher metabolic demand resulting from a longer fiber length and/or a high level of activity, making hub nodes more vulnerable to changes in metabolic processes and/or cerebral perfusion. For SVD the vulnerability of connections between hub regions might also be explained in part by the location of SVD lesions in the brain, which often overlaps with the location of hub nodes.[10] In turn, the occurrence of SVD lesions might depend on vulnerability of certain brain regions to specific pathological processes such as ischemia or cerebral hypoperfusion.[42] In AD an overlap exists between hub nodes and regions with higher Aβ deposition.[43] Several hypotheses have been postulated to explain this overlap: firstly, high metabolism in hub nodes could lead to deposition of Aβ and subsequent disconnection of hub nodes ('Aβ-cascade hypothesis').[44] Secondly, Aβ deposition could result from an exhausted compensatory activity of hub nodes in response to an initially local network failure ('cascading network failure theory').[45] Alternatively, other factors could drive both Aβ deposition and impairments in WM connectivity. Future longitudinal studies might help resolve this issue by clarifying the temporal evolution of impairments in WM connectivity by investigating whether WM connections between hub nodes are preferentially affected or occur secondary to impairments in other (peripheral) WM connections.[46]

We also found differences in the manifestation of the diffusion abnormalities. Reductions in anisotropy (i.e. FA) in WM connections were primarily seen in patients with Aβ-/SVD+ but not Aβ+/SVD- patients, while increased WM diffusion (i.e. MD) was found in both patient groups. Interpreting differences in diffusion tensor profiles remains a topic of debate.[47] Despite the wide use of DTI to investigate impaired WM connectivity, little is known about the mechanisms underlying diffusion changes in AD and SVD. A decrease in FA and an increase in MD are often thought to result from microstructural WM damage, for instance axonal degeneration, a loss of myelin, disruption of the blood-brain barrier or other processes. Recent studies have suggested new models and measures that could be more sensitive to certain microstructural processes, such as free water imaging[48] and diffusion kurtosis imaging.[49] Integrating these new models in network based analyses could further improve our understanding of the mechanisms leading to impaired WM connectivity.

A strength of the present study is the high quality multi-modal MRI that was collected in a well-described population of memory clinic patients, in which we aimed to increase the homogeneity of the study sample by investigating selected patient groups with predominant AD or SVD-related pathology. Limitations concern the cross-sectional design, which does not allow us to infer causality. Also, the sample sizes are rather small, which could have led to an underestimation of the effects found. Another issue is the lack of CSF/PET data in the control group, therefore the presence of AD pathology could not be ruled out. In patients with primarily AD pathology, no definite diagnosis of AD[22] could be made due to missing data on tau-pathology in 45% of Aβ+/SVD- patients. Finally, the presence of SVD could not completely be ruled out in Aβ+/SVD- patients and controls, since absence of any marker of SVD on MRI was rare in the study cohort from which we sampled.

CONCLUSION

This study shows that memory clinic patients with primarily SVD pathology have a different pattern of impaired WM connectivity than patients with primarily AD pathology. Our findings suggest that these pathologies affect the WM network through partly different mechanisms. Future longitudinal studies should further identify these mechanisms, which is highly relevant since it may ultimately support development of treatment.

REFERENCES

1. Lo C-Y, Wang P-N, Chou K-H, Wang J, He Y, Lin C-P. Diffusion Tensor Tractography Reveals Abnormal Topological Organization in Structural Cortical Networks in Alzheimer's Disease. J Neurosci. 2010;30:16876–85.
2. Reijmer YD, Leemans A, Caeyenberghs K, Heringa SM, Koek HL, Biessels GJ. Disruption of cerebral networks and cognitive impairment in Alzheimer disease. Neurology. 2013;80:1370–7.
3. Prescott JW, Guidon A, Doraiswamy PM, Choudhury KR, Liu C, Petrella JR. The Alzheimer Structural Connectome: Changes in Cortical Network Topology with Increased Amyloid Plaque Burden. Radiology. 2014;279:328.
4. Fang R, Yan X-X, Wu Z-Y, et al. Disrupted Structural Brain Network in AD and aMCI: A Finding of Long Fiber Degeneration. Curr Alzheimer Res. 2015;12:572–84.
5. Lawrence AJ, Chung AW, Morris RG, Markus HS, Barrick TR. Structural network efficiency is associated with cognitive impairment in small-vessel disease. Neurology. 2014;83:304–11.
6. Kim HJ, Im K, Kwon H, et al. Clinical effect of white matter network disruption related to amyloid and small vessel disease. Neurology. 2015;85:63–70.
7. Tang J, Zhong S, Chen Y, et al. Aberrant white matter networks mediate cognitive impairment in patients with silent lacunar infarcts in basal ganglia territory. J Cereb Blood Flow Metab. 2015;35:1426–34.
8. Banerjee G, Jang H, Kim HJ, et al. Total MRI Small Vessel Disease Burden Correlates with Cognitive Performance, Cortical Atrophy, and Network Measures in a Memory Clinic Population. J Alzheimer's Dis. 2018;63:1485–97.
9. Bullmore E and OS. Complex brain networks: graph theoretical analysis of structural and functional systems. Nat Rev Neurosci. 2009;10:186–98.
10. Tuladhar AM, Lawrence A, Norris DG, Barrick TR, Markus HS, de Leeuw FE. Disruption of rich club organisation in cerebral small vessel disease. Hum Brain Mapp. 2017;38:1751–66.
11. Beheshti I, Maikusa N, Daneshmand M, Matsuda H, Demirel H, Anbarjafari G. Classification of Alzheimer's disease and prediction of mild cognitive impairment conversion using histogram-based analysis of patient-specific anatomical brain connectivity networks. J Alzheimer's Dis. 2017;60:295–304.
12. Lawrence AJ, Zeestraten EA, Benjamin P, et al. Longitudinal decline in structural networks predicts dementia in cerebral small vessel disease. Neurology. 2018;90:e1898–e1910.
13. McAleese KE, Walker L, Graham S, et al. Parietal white matter lesions in Alzheimer's disease are associated with cortical neurodegenerative pathology, but not with small vessel disease. Acta Neuropathol. 2017;134:459–73.
14. Nasrabady SE, Rizvi B, Goldman JE, Brickman AM. White matter changes in Alzheimer's disease: a focus on myelin and oligodendrocytes. Acta Neuropathol Commun. 2018;6:22.
15. Love S, Miners JS. Cerebrovascular disease in ageing and Alzheimer's disease. Acta Neuropathol. 2016;131:645–58.
16. Wardlaw JM, Smith EE, Biessels GJ, et al. Neuroimaging standards for research into small vessel disease and its contribution to ageing and neurodegeneration. Lancet Neurol. 2013; 12:822–38.
17. Gouw AA, Seewann A, Van Der Flier WM, et al. Heterogeneity of small vessel disease: A systematic review of MRI and histopathology correlations. J Neurol Neurosurg Psychiatry 2011;82:126–35.
18. Ter Telgte A, Van Leijsen EMC, Wiegertjes K, Klijn CJM, Tuladhar AM, De Leeuw FE. Cerebral small vessel disease: From a focal to a global perspective. Nat Rev Neurol. 2018;14: 387–98.

19. Toledo JB, Arnold SE, Raible K, et al. Contribution of cerebrovascular disease in autopsy confirmed neurodegenerative disease cases in the National Alzheimer's Coordinating Centre. Brain. 2013;136:2697–706.
20. McKhann G, Drachman D, Folstein M, Katzman R, Price D, Stadlan EM. Clinical diagnosis of Alzheimer's disease: Report of the NINCDS-ADRDA Work Group* under the auspices of Department of Health and Human Services Task Force on Alzheimer's Disease. Neurology. 1984;34:939–44.
21. Roman GC, Tatemichi TK, Erkinjuntti T, et al. Vascular dementia: Diagnostic criteria for research studies: Report of the NINDS-AIREN International Workshop. Neurology. 1993; 43:250–60.
22. Jack CR, Bennett DA, Blennow K, et al. NIA-AA Research Framework: Toward a biological definition of Alzheimer's disease. Alzheimer's Dement. 2018;14:535–62.
23. Aalten P, Ramakers IHGB, Biessels GJ, et al. The Dutch Parelsnoer Institute - Neurodegenerative diseases; methods, design and baseline results. BMC Neurol. 2014;14:254.
24. de Wilde A, van Maurik IS, Kunneman M, et al. Alzheimer's biomarkers in daily practice (ABIDE) project: Rationale and design. Alzheimer's Dement Diagnosis. 2017;6:143–51.
25. Reijmer YD, Brundel M, De Bresser J, Kappelle LJ, Leemans A, Biessels GJ. Microstructural white matter abnormalities and cognitive functioning in type 2 diabetes: A diffusion tensor imaging study. Diabetes Care. 2013;36:137–44.
26. Dutch National Institue for Public Health and the Environment (RIVM). Diabetes Mellitus, Cijfers en Context. Huidige Situatie. [online]. Accessed at: www.volksgezondheidenzorg.nl.
27. Zwan M, van Harten A, Ossenkoppele R, et al. Concordance between cerebrospinal fluid biomarkers and [11C]PIB PET in a memory clinic cohort. J Alzheimers Dis. 2014;41:801–7.
28. Fazekas F, Chawluk JB, Alavi A. MR signal abnormalities at 1.5 T in Alzheimer's dementia and normal aging. Am J Neuroradiol. 1987;149:351–6.
29. Groeneveld O, Reijmer Y, Heinen R, et al. Brain imaging correlates of mild cognitive impairment and early dementia in patients with type 2 diabetes mellitus. Nutr Metab Cardiovasc Dis. 2018;28:1253–60.
30. Tax CMW, Otte WM, Viergever MA, Dijkhuizen RM, Leemans A. REKINDLE: Robust Extraction of Kurtosis INDices with Linear Estimation. Magn Reson Med. 2015;73:794–808.
31. Jeurissen B, Leemans A, Jones DK, Tournier JD, Sijbers J. Probabilistic fiber tracking using the residual bootstrap with constrained spherical deconvolution. Hum Brain Mapp. 2011;32:461–79.
32. Tzourio-Mazoyer N, Landeau B, Papathanassiou D, et al. Automated anatomical labeling of activations in SPM using a macroscopic anatomical parcellation of the MNI MRI single-subject brain. Neuroimage. 2002;15:273–89.
33. Dai Z, Yan C, Li K, et al. Identifying and mapping connectivity patterns of brain network hubs in Alzheimer's disease. Cereb Cortex. 2015;25:3723–42.
34. Lee WJ, Han CE, Aganj I, Seo SW, Seong JK. Distinct Patterns of Rich Club Organization in Alzheimer's Disease and Subcortical Vascular Dementia: A White Matter Network Study. J Alzheimer's Dis. 2018;63:977–87.
35. Fagerholm ED, Hellyer PJ, Scott G, Leech R, Sharp DJ. Disconnection of network hubs and cognitive impairment after traumatic brain injury. Brain. 2015;138:1696–709.
36. Rubinov M, Sporns O. Complex network measures of brain connectivity: Uses and interpretations. Neuroimage. 2010;52:1059–69.
37. Benjamini Y, Hochberg Y, Benjaminit Y. Controlling the False Discovery Rate: A Practical and Powerful Approach to Multiple Controlling the False Discovery Rate: a Practical and Powerful Approach to Multiple Testing. J R Stat Soc. 1995;57:289–300.
38. Iaccarino L, Tammewar G, Ayakta N, et al. Local and distant relationships between amyloid, tau and neurodegeneration in Alzheimer's Disease. NeuroImage Clin. 2018;17:452–64.

39. Hase Y, Horsburgh K, Ihara M, Kalaria RN. White matter degeneration in vascular and other ageing-related dementias. J Neurochem. 2018;144:617–33.
40. Sweeney MD, Sagare AP, Zlokovic BV. Blood-brain barrier breakdown in Alzheimer disease and other neurodegenerative disorders. Nat Rev Neurol. 2018;14:133–50.
41. Yan T, Wang W, Yang L, Chen K, Chen R, Han Y. Rich club disturbances of the human connectome from subjective cognitive decline to Alzheimer's disease. Theranostics. 2018;8: 3237–55.
42. Chen X, Wang J, Shan Y, et al. Cerebral small vessel disease: neuroimaging markers and clinical implication. J Neurol. 2018:10.1007/s00415-018-9077-3.
43. Buckner RL, Sepulcre J, Talukdar T, et al. Cortical Hubs Revealed by Intrinsic Functional Connectivity: Mapping, Assessment of Stability, and Relation to Alzheimer's Disease. J Neurosci. 2009;29:1860–73.
44. Hardy J, Selkoe DJ. The amyloid hypothesis of Alzheimer's disease: Progress and problems on the road to therapeutics. Science. 2002;297:353–6.
45. Jones DT, Knopman DS, Gunter JL, et al. Cascading network failure across the Alzheimer's disease spectrum. Brain. 2016;139:547–62.
46. Crossley NA, Mechelli A, Scott J, et al. The hubs of the human connectome are generally implicated in the anatomy of brain disorders. Brain. 2014;137:2382–95.
47. Fornito A, Zalesky A, Breakspear M. Graph analysis of the human connectome: Promise, progress, and pitfalls. Neuroimage. 2013;80:426–44.
48. Duering M, Finsterwalder S, Baykara E, et al. Free water determines diffusion alterations and clinical status in cerebral small vessel disease. Alzheimer's Dement. 2018;14:764–74.
49. Arab A, Wojna-Pelczar A, Khairnar A, Szabó N, Ruda-Kucerova J. Principles of diffusion kurtosis imaging and its role in early diagnosis of neurodegenerative disorders. Brain Res Bull. 2018;139:91–8.
50. Verhage F. Intelligentie en leeftijd: onderzoek bij Nederlanders van twaalf tot zevenzeventig jaar [Intelligence and Age: study with Dutch people aged 12 to 77]. Assen Van Gorcum. 1964.

Chapter 8

General discussion

This thesis focuses on changes in the gray and the white matter of the brain that extend beyond the visible lesions in patients with cerebral small vessel disease (SVD). As visible SVD lesions on conventional structural MRI do not fully capture the burden of SVD-related brain injury (representing only the tip of the iceberg), effects of SVD in the brain's gray and white matter beyond these visible lesions have gained increasing attention. In this thesis, I used different techniques to look at the effects of SVD beyond the visible lesions in both the gray and white matter of the brain in memory clinic patients and how these effects relate to different SVD lesion types as well as co-occurring Alzheimer's disease pathology. The main findings of this thesis are summarized in Box 8.1.

Box 8.1 | Main findings of this thesis

Chapter 2 and 3: when measuring brain and white matter hyperintensity (WMH) volumes in a multi-center dataset, performance of automated segmentation methods varies markedly. Yet, techniques are available that perform robustly across different datasets.
Chapter 4: although cortical cerebral microinfarcts (CMIs) cluster in highly interconnected brain regions, white matter (WM) connections projecting to these regions do not seem to be disproportionally affected in patients with CMIs.
Chapter 5: the cumulative effect of multiple SVD lesions is reflected in WM connectivity and relates to cognitive functioning.
Chapter 6: WMHs and lacunes but not cerebral microbleeds relate to brain atrophy and mainly in the absence of markers of amyloid-beta (amyloid-β) pathology.
Chapter 7: the occurrence and spatial pattern of impairments in WM connectivity differ between patients with primarily amyloid-β and SVD pathology.

SVD-related brain changes: what's in the name and how to measure them?

What exactly does one mean when talking about SVD-related brain changes and in particular those that occur beyond the visible SVD lesions? And how should these changes be measured? In the present thesis, I used two of the most obvious measures to systematically describe the changes that have occurred in the brain's gray and white matter in memory clinic patients and refer to these changes as 'effects beyond visible SVD lesions'. First, I used brain volumes (obtained with structural brain MRI) and compared them with the total intracranial volume to estimate (both the pattern and severity of) brain atrophy (i.e. a lower brain volume that is not related to a specific macroscopic focal injury such as trauma or infarction).[1] Second, I used brain network connectivity measures (obtained with diffusion based tensor imaging or DTI)[2] to look at changes that have occurred in the white matter (i.e. white matter connectivity). I used these measures since they are very sensitive to SVD-related processes and are more closely related to the functional impact

of SVD. Also, they can give more insight in possible underlying disease mechanisms in SVD, as will be discussed below.

In **chapter 6** I focused on the severity and pattern of brain atrophy in memory clinic patients and we showed that different SVD lesions are differentially related to brain atrophy. In particular WMHs and lacunes were related to brain atrophy. WMHs associated atrophy was most pronounced in frontal cortical gray matter regions. This suggests a ´distant´ effect of WMHs reflecting neurodegeneration through disconnection.

These findings have two important implications. First, the traditional concept of brain atrophy as a marker of neurodegenerative diseases (such as Alzheimer's disease) should be reconsidered, as brain atrophy in memory clinic patients with manifestations of SVD on MRI (e.g. WMHs) could also be secondary due to SVD. Second, it stresses the importance of including measures of more global effects instead of focusing on the visible lesions when investigating SVD-related brain changes.

Challenges in unravelling what causes SVD-related brain changes

Although it is clear that SVD is related to brain atrophy and impaired white matter connectivity, the question remains what processes actually underly these changes. It has been shown that the pathological changes underlying atrophy are heterogeneous and not necessarily indicative of neuronal loss.[3-5] Possible mechanisms suggested in SVD include secondary degeneration caused by the disruption of white matter fibers projecting towards cortical gray matter,[6] or direct trophic changes in the cortical gray matter due to cortical cerebral microinfarcts.[7] Unravelling which mechanisms underlie brain atrophy in SVD is difficult, since often co-occurring pathology is present (such as Alzheimer's disease) which can also result in brain atrophy. The findings from **chapter 6** suggest that secondary degeneration can indeed occur in memory clinic patients with SVD. Future longitudinal studies should try to clarify the temporal relation between the visible SVD lesions and brain atrophy, in order to confirm that secondary degeneration underlies brain atrophy in SVD.

What exactly underlies impairments in white matter connectivity is also unknown, as abnormal measures of FA and MD are assumed to indicate axonal loss and/or demyelination,[8] but have also been related to other forms of tissue injury (e.g. increased extracellular fluid)[9] as well as non-disease related variations in tissue structure.[10-12] A recent study compared histopathologic measures and DTI measures in patients with cerebral amyloid angiopathy (CAA), a common form of SVD, with elderly controls.[13] This study found that the major component underlying CAA-related alterations in DTI measures was overall

tissue loss (and in particular axonal loss and demyelination), suggesting that FA and MD reflect rather specific underlying microstructural changes in patients with CAA. As such, future studies should focus on investigating the underlying histopathology of white matter changes (measured with DTI) in memory clinic patients, as this is informative for inferring disease specific mechanisms using (longitudinal) DTI.

The interplay between SVD and Alzheimer's disease

An important challenge regarding SVD-related brain changes is the issue of mixed etiologies. It can be difficult to determine whether brain changes are in fact due to SVD or due to co-occurring pathology such as Alzheimer's disease. Most previous studies investigating SVD-related brain changes that have reported co-occurring Alzheimer's disease, used clinical criteria[14] rather than biomarker evidence of amyloid-β and tau pathologies.[15] This thesis systematically describes changes in both the gray and white matter of the brain in memory clinic patients with both SVD and co-occurring Alzheimer's disease pathology.

In **chapter 6**, we stratified patients with SVD lesions in those with and without evidence of co-occurring amyloid-β pathology in the cerebrospinal fluid. In this way, we could show that certain SVD lesions related differentially to brain atrophy, but mainly in the absence of co-occurring amyloid-β pathology. Vice versa, the relation between the presence of co-occurring amyloid-β pathology and brain atrophy was much stronger in patients with a low SVD burden. Apparently, both pathological processes contribute to brain atrophy, but for each this is most evident in the absence of the other. This could perhaps be explained by a ceiling effect of both diseases, possibly linked to disease stage. These results stress the importance to measure and correct for the possible confounding effect of co-occurring Alzheimer's disease pathology when investigating SVD-related brain changes.

The possible confounding effect of co-occurring pathological processes such as Alzheimer's disease can also be tackled by using highly specific patient samples from a relatively young age group (i.e. before the manifestation of co-occurring pathology), for instance in patients with genetic forms of SVD, such as CADASIL[16] (or in the case of Alzheimer's disease, autosomal dominant Alzheimer's disease).[17] Although several of such cohorts exist, the majority of patients in clinical care (e.g. memory clinics) have mixed pathologies. Furthermore, disease mechanisms causing SVD-related brain changes could differ from CADASIL patients, limiting the external validity. In **chapter 7**, we aimed to increase the homogeneity of the memory clinic patient sample by investigating selected patient groups with either a biomarker supported diagnosis of Alzheimer's disease or SVD pathology. We showed that the occurrence and spatial pattern of impairments in WM connectivity differ between patients with primarily Alzheimer's disease and SVD pathology, suggesting that

these pathologies affect the WM network through partly different mechanisms. Identifying these mechanisms in future studies is highly relevant since it may ultimately support development of treatment.

Functional impact of SVD-related brain changes

Nowadays, there is extensive literature regarding the functional impact of SVD-related brain changes.[18] While in the beginning, focus has been on cognitive decline, it has become clear that SVD also effects gait and balance,[19] and can lead to apathy,[20] depression[20,21] and extrapyramidal symptoms.[22] Part of these manifestations can be explained by strategic visible SVD lesions (e.g. a sudden cognitive deficit due to a infarct in the thalamus).[23] The field of voxel-based lesion-symptom mapping (VLSM), that investigates the relation between lesion location and symptoms/function, has given great insight into certain 'vulnerable' areas in patients with SVD.[24] Also, the functional impact depends on the total visible lesion burden (which can be taken together in a total SVD burden score, as was done in **chapter 5**).[25] However, there is growing evidence that effects of SVD that occur beyond the visible lesions, even though they are more subtle, also account for clinical symptoms. For instance, impairments in WM connectivity in the 'normal appearing white matter' relate to cognitive decline and dementia in patients with SVD, independently from visible SVD lesions.[26] Brain atrophy also independently relates to clinical status and disease progression.[27] These relations illustrate that if brain atrophy and impaired WM connectivity could be prevented, this could help to slow down the clinical manifestations of SVD. Furthermore, the functional impact of SVD-related brain changes underline the need to look at SVD as a global rather than a focal brain disease.

Implications for clinical practice

This thesis shows that focal SVD lesions relate to more global changes in the brain's gray and white matter. Furthermore, we show that the relation between SVD lesion load (when taking different SVD lesions together) and cognitive functioning in memory clinic patients is mediated by impairments in WM connectivity. Although the measures used to capture the effects of SVD beyond the visible lesions on conventional MRI are not specific for SVD, they are very sensitive to SVD-related processes and provide additional insight in the functional impact of SVD. In the near future, they could potentially be used to measure disease progression, which would help determine the prognosis of patients with SVD. Also, these measures could be beneficial in etiological research as well as be used as an outcome in future clinical trials. Unfortunately, the use of these measures in the clinical setting is still limited. My perspective on the future use of these measures in a memory clinic is the

following: a structural MRI is performed in every patient and includes diffusion tensor imaging (DTI). The physician receives a detailed MRI report containing brain volume and lesion volume measurements as well as several connectivity measures, compared to the mean value and standard deviation of a reference population. In this way, SVD lesion load can be evaluated in relation to changes that have occurred in both the gray and white matter of the brain. A physician can estimate whether the amount and pattern of lesional, but also more global, SVD-related brain changes are likely to explain the clinical symptoms sufficiently. Since mixed pathology often occurs in memory clinic patients, a panel of biomarkers for various neurodegenerative diseases such as Alzheimer's disease and synucleopathies (e.g. dementia with Lewy bodies) is also determined to evaluate the presence of co-occurring pathology. Furthermore, this report is combined with VLSM results, showing a patient specific vulnerability map for several clinical symptoms in SVD. In this way, physicians are given more tools to help explain patients and their caregivers where their clinical symptoms originate and what can be expected in the (near) future.

Directions for future research

Several challenges remain in unravelling the pathophysiology of SVD and developing SVD-specific treatment. Knowing that SVD can have effects beyond visible lesions on conventional structural MRI and that these effects can have a considerable functional impact, this thesis and recent literature provide leads for future studies.

First, most studies on SVD-related brain changes have been cross-sectional. Longitudinal research is important to elucidate the sequence of events that lead to SVD-related brain changes. Up to now, endothelial dysfunction (including blood-brain barrier dysfunction), impaired vasoreactivity, increased intracranial vascular pulsatility, (chronic) ischemia, demyelination and inflammation are some of the most important mechanisms proposed to underlie SVD-related brain changes.[28,29] However, the order of these events is yet to be determined and should the focus of ongoing research (for an example see the ongoing study SVDs@target; https://www.svds-at-target.eu/).

Second, how SVD-related brain changes behave over time is not yet clear. Recent studies have shown that visible SVD lesions might regress, remain stable, expand or develop into other lesions.[30,31] One of these studies found a difference in lesion progression between patients with mild WMHs and patients with severe WMHs, implying a difference in etiology of mild versus severe SVD.[31] The temporal dynamics of more global effects of SVD, how this relates to differences in progression of visible SVD lesions as well as the clinical consequences, should be investigated in future longitudinal studies.

Third, an important knowledge gap that remains and potentially hinders longitudinal and especially multicenter studies, is the reproducibility of measurements of SVD-related brain changes. A recent review identified several aspects that influence the reproducibility and provides recommendations regarding MRI acquisition and data processing.[32] Another important initiative is the harmonization of MRI methods to study SVD, such as the HARNESS initiative.[33] Such advancements are highly needed to help implement measures of SVD-related brain changes as a biomarker in future clinical trials.

Fourth, when investigating SVD-related brain changes, it is vital to combine visible SVD lesions with measurements of more global effects of SVD, instead of focusing on the visible lesions alone. This probably requires statistically more complex models that can deal with complex interactions (for a recent example see[34]). Furthermore, co-occurring pathology such as Alzheimer's disease should be measured and taken into account, to ensure that changes that occur in the brain are in fact due to SVD. This might also help to further unravel the complex interplay between SVD and Alzheimer's disease.

Fifth, focus should shift towards a younger study population (i.e. an earlier disease stage). Many of the previous studies have been performed in memory clinic patients, stroke clinic patients or elderly communities. By studying patients who exhibit manifestations of SVD on a young age, possibly representing a certain vulnerability for the effects of SVD, and in which other pathology (such as Alzheimer's disease pathology) has not occurred, changes and underlying mechanisms could be studied that are involved in the origin of SVD. An example of such a population is a hereditary form of SVD such as CADASIL, in which patients can even be studied in a presymptomatic disease stage. Also, less variety in patient selection (e.g. solely symptomatic lacunar infarcts) can help to compare results from studies.

Finally, and most importantly, biomarkers for specific disease mechanisms in SVD are needed. There have been some promising developments recently. An example is the development of a perfusion-based periventricular small vessel region of interest, marking a region with homogeneously reduced cerebral blood flow that is particularly susceptible to progressive ischemic injury in elderly subjects.[35]

Conclusion

SVD has effects in the brain's gray and white matter that extend well beyond the visible lesions on conventional structural MRI. These effects can better explain the impact of SVD on cognition than the visible SVD lesions. Effects beyond the visible SVD lesions seem to differ depending on the SVD lesion type, as these effects were shown to relate to WMHs and lacunes, but not other manifestations of SVD (suggesting different underlying disease

mechanisms). The pattern of SVD-related changes in the white matter seems different as compared to what is seen in Alzheimer's disease, suggesting partially different underlying disease mechanisms. This thesis suggests that the effects of SVD and Alzheimer's disease on brain atrophy are additive, which could be explained by a ceiling effect of both diseases, possibly linked to disease stage. Measuring and reporting more global effects of SVD should become part of clinical care in order to help to explain patients and their caregivers the functional impact of SVD. Understanding which mechanisms underly effects of SVD beyond the visible lesions should be the focus of future studies, since it is vital to understand the pathophysiology of SVD to help develop new treatments.

REFERENCES

1. Wardlaw JM, Smith EE, Biessels GJ, et al. Neuroimaging standards for research into small vessel disease and its contribution to ageing and neurodegeneration. Lancet Neurol. 2013;12: 822–38.
2. Rubinov, M., Sporns, O. Complex network measures of brain connectivity: uses and interpretations. NeuroImage. 2010;52:1059–69.
3. Jack CR Jr. Alliance for aging research AD biomarkers work group: structural MRI. Neurobiol Aging. 2011;32:S48–57.
4. Walters RJ, Fox NC, Crum WR, Taube D, Thomas DJ. Haemodialysis and cerebral oedema. Nephron. 2001;87:143–7.
5. Duning T, Kloska S, Steinstrater O, Kugel H, Heindel W, Knecht S. Dehydration confounds the assessment of brain atrophy. Neurology. 2005;64:548–50.
6. Seo SW, Lee JM, Im K, Park JS, Kim SH, et al. Cortical thinning related to periventricular and deep white matter hyperintensities. Neurobiol Aging. 2012;33:1156–67.
7. Launer LJ, Hughes TM, White LR. Microinfarcts, brain atrophy, and cognitive function: the Honolulu Asia Aging Study Autopsy Study. Ann Neurol. 2011;70:774–80.
8. Beaulieu C. The basis of anisotropic water diffusion in the nervous system—a technical review. NMR Biomed. 2002;15:435–55.
9. Duering M, Finsterwalder S, Baykara E, Tuladhar AM, Gesierich B, et al. Free water determines diffusion alterations and clinical status in cerebral small vessel disease. Alzheimers Dement. 2018;14:764–74.
10. Pierpaoli C, Basser PJ. Toward a quantitative assessment of diffusion anisotropy. Magn Reson Med. 1996;36:893–906.
11. Miller KL, Stagg CJ, Douaud G, et al. Diffusion imaging of whole, post-mortem human brains on a clinical MRI scanner. Neuroimage. 2011;57:167–81.
12. Vos SB, Jones DK, Viergever MA, Leemans A. Partial volume effect as a hidden covariate in DTI analyses. Neuroimage. 2011;55:1566–76.
13. van Veluw SJ, Reijmer YD, van der Kouwe AJ, Charidimou A, Riley GA, et al. Histopathology of diffusion imaging abnormalities in cerebral amyloid angiopathy. Neurology. 2019;92:e933–43.
14. McKhann G, Drachman D, Folstein M, Katzman R, Price D, Stadlan EM. Clinical diagnosis of Alzheimer's disease: Report of the NINCDS-ADRDA Work Group* under the auspices of Department of Health and Human Services Task Force on Alzheimer's Disease. Neurology. 1984;34:939–44.
15. Jack CR, Bennett DA, Blennow K, Carrillo MC, Dunn B, Haeberlein SB, et al. NIA-AA Research Framework: Toward a biological definition of Alzheimer's disease. Alzheimer's Dement. 2018;14:535–62.
16. Di Donato I, Bianchi S, De Stefano N, Dichgans M, Dotti MT, Duering M, et al. Cerebral Autosomal Dominant Arteriopathy with Subcortical Infarcts and Leukoencephalopathy (CADASIL) as a model of small vessel disease: update on clinical, diagnostic, and management aspects. BMC Med. 2017;15:41.
17. Moulder KL, Snider BJ, Mills SL, Buckles VD, Santacruz AM, Bateman RJ, et al. Dominantly Inherited Alzheimer Network: facilitating research and clinical trials. Alzheimers Res Ther. 2013;5:48.
18. Rensma SP, van Sloten TT, Launer LJ, Stehouwer CDA. Cerebral small vessel disease and risk of incident stroke, dementia and depression, and all-cause mortality: a systematic review and meta-analysis. Neurosci Biobehav Rev. 2018;90:164–73.
19. Kim YJ, Kwon HK, Lee JM, Cho H, Kim HJ, Park HK, et al. Gray and white matter changes linking cerebral small vessel disease to gait disturbances. Neurology. 2016;86:1199–207.

20. Hollocks MJ, Lawrence AJ, Brookes RL, Barrick TR, Morris RG, Husain M, et al. Differential relationships between apathy and depression with white matter microstructural changes and functional outcomes. Brain. 2015;138:3803–15.
21. van Agtmaal MJM, Houben A, Pouwer F, Stehouwer CDA, Schram MT. Association of microvascular dysfunction with late-life depression: a systematic review and meta-analysis. JAMA Psychiatry. 2017;74:729–39.
22. van der Holst HM, van Uden IW, Tuladhar AM, de Laat KF, van Norden AG, Norris DG, et al. Cerebral small vessel disease and incident parkinsonism: the RUN DMC study. Neurology. 2015;85:1569–77.
23. Valdés Hernández MC, Maconick LC, Muñoz Maniega S, Wang X, Wiseman S, Armitage PA, et al. A comparison of location of acute symptomatic versus 'silent' small vessel lesions. Int J Stroke. 2015;10:1044–50.
24. de Haan B, Karnath HO. A hitchhiker's guide to lesion-behaviour mapping. Neuropsychologia. 2018;115:5–16.
25. Ter Telgte A, Van Leijsen EMC, Wiegertjes K, Klijn CJM, Tuladhar AM, De Leeuw FE. Cerebral small vessel disease: From a focal to a global perspective. Nat Rev Neurol. 2018;14: 387–98.
26. Wardlaw JM, Smith C, Dichgans M. Small vessel disease: mechanisms and clinical implications. Lancet Neurol. 2019;18:684–96.
27. Staals J, Makin S, Doubal F, Dennis M, Wardlaw JM. Stroke subtype, vascular risk factors and total MRI brain small-vessel disease burden. Neurology. 2014;83:1228–34.
28. Lawrence AJ, Chung AW, Morris RG, Markus HS, Barrick TR. Structural network efficiency is associated with cognitive impairment in small-vessel disease. Neurology. 2014;83:304–11.
29. Chabriat H, Hervé D, Duering M, Godin O, Jouvent E, Opherk C, et al. Predictors of clinical worsening in cerebral autosomal dominant arteriopathy with subcortical infarcts and leukoencephalopathy: prospective cohort study. Stroke. 2016;47:4–11.
30. Wardlaw JM, Chappell FM, Valdés Hernández MDC, Makin SDJ, Staals J, Shuler K, et al. White matter hyperintensity reduction and outcomes after minor stroke. Neurology. 2017;89: 1003–10.
31. van Leijsen EMC, van Uden IWM, Ghafoorian M, Bergkamp MI, Lohner V, Kooijmans ECM, et al. Nonlinear temporal dynamics of cerebral small vessel disease: the RUN DMC study. Neurology. 2017;89:1569–77.
32. De Guio F, Jouvent E, Biessels GJ, Black SE, Brayne C, Chen C, et al. Reproducibility and variability of quantitative magnetic resonance imaging markers in cerebral small vessel disease. J Cereb Blood Flow Metab. 2016;36:1319–37.
33. Smith EE, Biessels GJ, de Guio F, de Leeuw FE, Duchesne S, During M. Harmonizing brain magnetic resonance imaging methods for vascular contributions to neurodegeneration. Alzheimer's Dement. 2019;11:191–204.
34. Jaarsma-Coes MG, Ghaznawi R, Hendrikse J, Slum C, Witkamp TD, van der Graaf Y, et al. MRI phenotypes of the brain are related to future stroke and mortality in patients with manifest arterial disease: the SMART-MR study. J Cereb Blood Flow Metab. 2018: 271678X18818918.
35. Dolui S, Tisdall D, Vidoretta M, Jacobs Jr DR, Nasrallah IM. Characterizing a perfusion-based periventricular small vessel region of interest. NeuroImage: Clinical. 2019;23:101897.

Appendices

Summary
Nederlandse samenvatting
About the author
Publications
Dankwoord

SUMMARY

Cerebral small vessel disease (SVD) is an umbrella term describing heterogeneous pathological processes that affect the smallest vessels of the brain, including the perforating arterioles, capillaries, and venules. SVD is a major cause of cognitive decline, dementia and stroke. Various SVD lesions can be detected using conventional structural brain MRI and include white matter hyperintensities (WMHs), lacunes, cerebral microbleeds, recent small subcortical infarcts and perivascular spaces. These different lesion types can reflect different disease processes affecting different vessels, in different parts of the brain. However, visible SVD lesions do not seem to fully capture the total burden of SVD-related brain changes. In addition, previous studies have suggested that SVD-related changes occur beyond these visible lesions in the brain's gray and white matter. These 'effects of SVD beyond the visible lesions' provide a new framework to look at the impact of SVD. These effects can be used to better understand the functional impact of SVD than visible SVD lesions alone, as they have been shown to relate to cognitive decline and dementia. However, there are still some open questions regarding the effects of SVD beyond the visible lesions. For instance, are these effects similar for different types and manifestations of SVD? Do these effects also occur in patients with cortical cerebral microinfarcts (a relatively new MRI marker of SVD)? Do these effects have specific patterns? Is there an interplay with Alzheimer's disease, a common co-morbidity of SVD?

- *The overarching aim of the work described in this thesis was to examine changes in the gray and white matter of the brain that extend beyond the visible lesions in patients with SVD.*

Until now, changes in the gray and white matter of the brain that extend beyond the visible lesions have not been systematically investigated in memory clinic patients with SVD, often with co-occurring Alzheimer's disease pathology. In this thesis, we used two different techniques to measure changes in both the gray and white matter of the brain in memory clinic patients. First, we used brain volumes (obtained with structural brain MRI) and compared them with the total intracranial volume to estimate brain atrophy. Second, we used brain network connectivity measures (obtained with diffusion based tensor imaging or DTI) to look at changes that have occurred in the white matter (i.e. white matter connectivity). We investigated in memory clinic patients with SVD, some with co-occurring Alzheimer's disease pathology: the severity and pattern of changes in both the gray and white matter of the brain, how these changes relate to visible SVD lesions and whether this differed between lesion types, the impact of these changes on cognition, and the interplay with co-occurring Alzheimer's disease pathology.

The first part of this thesis deals with some of the technical challenges regarding automated brain and lesion segmentation in a multicenter dataset (**part 1**). The second part of this thesis looks at the effects of SVD beyond the visible lesions and the interplay with co-occurring Alzheimer's disease (**part 2**).

Part 1: Challenges when measuring SVD-related brain changes

Measurements of SVD-related changes on MRI can be obtained using various qualitative and (semi)quantitative techniques, where the quantitative techniques in particular depend on brain segmentation. Several automated segmentation methods have been developed to measure the volume of the SVD lesion of interest, such as WMHs. These measurements can be influenced by several factors, such as the burden of pathology, including presence of SVD lesions, motion artifacts, and technical issues (e.g. field strength or MRI scan protocol). Dealing with technical issues is of great importance when pooling multicenter brain MRI data, which has become a trend in various research fields (e.g. age-related brain diseases such as SVD). In **part 1** of this thesis, we performed two studies in which we compared the performance of several automated segmentation methods for WMH and brain volumes to support segmentation in a multicenter setting.

In **chapter 2**, we looked at the performance of three widely used automated methods for brain volume measurements (SPM, Freesurfer and FSL) across different MRI field strengths. We assessed robustness (i.e. whether measured volumes on scans with different acquisition techniques in the same subjects were similar) of these three methods using ten subjects with ageing related brain changes, but without a known primary cerebral disease. These subjects were scanned on 1.5 Tesla and 3 Tesla MRI on the same day. As a frame of reference, we also looked at accuracy (i.e., whether measured volumes correspond with expert-defined reference volumes) of the three methods by comparing their brain volume measurements of 20 additional functionally independent elderly subjects with manually segmented brain volume measurements. Brain volumes and total intracranial volumes could be measured quite robustly in scans acquired at different field strengths, but performance of the methods varied depending on which volume was assessed (e.g. total brain volume or total intracranial volume). The same was seen for accuracy. These findings illustrate that selecting an appropriate method for automated brain segmentation in a multicenter dataset depends on the volume of interest.

In **chapter 3**, we evaluated the performance of five freely available and fully-automated WMH segmentation methods (Cascade, kNN-TTP, Lesion-TOADS, LST-LGA and LST-LPA), using sixty subjects with WMHs from the TRACE-VCI study (a multicenter study on subjects with vascular cognitive impairment that were scanned using six different MRI

scanner vendors). We compared automated WMH segmentations with manual WMH segmentations as a reference and looked at performance of each method both within and across the different MRI scanners. We found the best performance, both within and across scanners, for kNN-TTP, followed by LST-LPA and LST-LGA, with worse performance for Lesion-TOADS and Cascade. These findings can serve as a guide for choosing a method for automated WMH segmentation in a multicenter dataset. It also highlights the importance to further improve and evaluate consistency of automated WMH segmentation methods in a multicenter setting in future studies.

Part 2: Effects of SVD beyond the visible lesions and the interplay with Alzheimer's disease

The relation between visible SVD lesions and changes in the brain occurring beyond these lesions

Different SVD lesion types (such as WMHs and lacunes) can reflect different disease processes affecting different vessels, in different parts of the brain. As such, the different lesion types and distributions can be used to study the effects of different types of SVD in the brain. Effects of SVD beyond the visible lesions have been shown for several SVD lesion types (e.g. WMHs, lacunes). However, previous studies have often focused on a single lesion type (such as WMHs). Also, for some lesion types (such as cortical cerebral microinfarcts or CMIs) it is unknown whether more global effects occur in the brain. Furthermore, it has become a trend in SVD research to use a SVD burden score to capture multiple types of vascular brain injury in a single measure. The rationale behind this "lumping" is creating a single measure of vascular brain injury that relies on more than just a single SVD lesion, is easy to use and could serve as a surrogate endpoint in clinical research. Therefore, in **part 2** of this thesis, we looked at the relation between visible SVD lesions and effects of SVD beyond these lesions in both the gray and the white matter of the brain (using either measures of brain volumes or white matter connectivity). We also investigated possible effects of SVD on white matter connectivity in patients with CMIs. Finally, we also looked at the impact of SVD on white matter connectivity and cognition by using a SVD burden score.

In **chapter 4**, we investigated the spatial distribution of cortical CMIs in 164 memory clinic patients with vascular brain injury on MRI. More than 70% of the cortical CMIs were located in the superior frontal, middle frontal, and pre- and postcentral brain regions (covering 16% of the cortical surface). We then looked at the relation between presence of cortical CMIs in these regions and WM connectivity in the entire brain as well as directly underneath the cortical surface. WM connectivity did not differ between patients with

and without cortical CMIs. In the high CMI burden regions, presence of cortical CMIs was not associated with WM connectivity after correction for visible SVD lesions such as WMHs. So despite the fact that cortical CMIs displayed a strong local clustering in highly interconnected brain regions, WM connections projecting to these regions were not disproportionally impaired in patients with CMIs compared to those without cortical CMIs. This suggests that alternative mechanisms, such as focal disturbances in cortical structure and functioning, may better explain CMI associated cognitive impairment instead of SVD-related effects beyond the visible lesions.

In **chapter 5**, we investigated the impact of effects of SVD beyond visible lesions on the brain's white matter. We used a SVD burden score to capture multiple types of vascular brain injury in a single measure and looked at the relation between the SVD burden score, WM connectivity (by measuring the global network efficiency) and cognition in 173 memory clinic patients with vascular brain injury on MRI. Each increase in the SVD burden score was associated with a decrease in global network efficiency, which in turn was related to worse cognitive performance (information processing speed and attention and executive functioning). Global network efficiency also mediated the relation between the SVD burden score and information processing speed. This shows that network metrics such as global network efficiency are sensitive to the cumulative effect of multiple manifestations of SVD on WM connectivity. Furthermore, it demonstrates the impact of SVD-related brain changes beyond visible lesions on cognition in memory clinic patients.

In **chapter 6**, we investigated the relation between visible SVD lesions and brain atrophy and assessed whether these relations differ between lesion types (such as WMHs, lacunes and cerebral microbleeds) in 725 memory clinic patients with vascular brain injury on MRI. We compared brain volumes (total brain volume, gray matter volume and white matter volume) between patients with each lesion type (moderate/severe WMHs, lacunes and cerebral microbleeds) and a reference group (mild WMHs but no lacunes or cerebral microbleeds). Different SVD lesions related differentially to brain atrophy as only patients with moderate/severe WMHs had a smaller gray matter volume compared to the reference group. Patients with cerebral microbleeds or lacunes had no significant brain volume differences compared to the reference group. Furthermore, the relation between WMHs and brain atrophy was most evident in the frontal (cortical) gray matter. This may reflect secondary neurodegeneration through disconnection of WM fibers projecting towards frontal brain regions. In other words, brain atrophy, which is often considered to be a manifestation of a neurodegenerative disease (such as Alzheimer's disease), can also be secondary to (manifestations of) SVD.

The interplay between SVD and co-occurring Alzheimer's disease pathology

When investigating SVD-related brain changes, it is important to consider common co-occurring pathologic processes that can also lead to changes in the gray and white matter, such as Alzheimer's disease. SVD and Alzheimer's disease pathology often co-occur in memory clinic patients. Therefore, in **part 2** of this thesis we also investigated the interplay between SVD and Alzheimer's disease on changes in the gray and white matter beyond visible SVD lesions.

In **chapter 6**, we also looked at the relation between different SVD lesions and brain atrophy after stratifying patients in those with and without evidence of co-occurring amyloid-β pathology in the cerebrospinal fluid (CSF). Significant associations between SVD lesion type and brain volumes were only seen in patients without CSF evidence of co-occurring amyloid-β pathology: those with moderate/severe WMHs had smaller gray matter volumes and those with lacunes had smaller total brain and gray matter volumes. Thus, certain SVD lesion types related differentially to brain atrophy, but mainly in the absence of co-occurring amyloid-β pathology. Vice versa, the relation between the presence of co-occurring amyloid-β pathology and brain atrophy was much stronger in patients with a low SVD burden. Apparently, both pathological processes contribute to brain atrophy, but for each this is most evident in the absence of the other, which could perhaps be explained by a ceiling effect of each disease, possibly linked to disease stage. All in all, it stresses the importance to measure and correct for the possible confounding effect of co-occurring Alzheimer's disease pathology when investigating SVD-related brain changes.

Because it is difficult to examine which brain changes are actually due to SVD and which are due to co-occurring pathologies such as Alzheimer's disease, we chose a different approach in **chapter 7**. We aimed to increase the homogeneity of a memory clinic patient sample by investigating selected patient groups with either Alzheimer's disease or SVD pathology based on CSF or PET-scan biomarker status and the presence of SVD on MRI. We compared fractional anisotropy (FA)- and mean diffusivity (MD)-weighted connectivity strength of the WM network between patients that were amyloid-β (Aβ) positive/SVD negative with patients that were Aβ negative/SVD positive and compared both patient group with control subjects. The occurrence and spatial pattern of impairments in WM connectivity differed between patients with primarily Alzheimer's disease and SVD pathology. Patients with primarily SVD pathology showed both impaired FA- and MD-weighted WM connectivity compared to controls (predominantly in frontal brain regions), while patients with primarily Alzheimer's disease pathology only showed impaired MD-weighted connectivity (predominantly in medial and parietal-occipital brain regions). We also assessed which type of WM connections were more severely affected, and found that

in both patient groups, relatively long WM connections and WM connections between so called 'hub' regions were more severely affected than all other WM connections. These findings suggest that these pathologies affect the WM network through partly different mechanisms. Which mechanisms this could be and how they are linked should be the focus of future studies.

In conclusion, SVD has effects in the brain's gray and white matter that extend well beyond the visible lesions on conventional structural MRI. These effects can better explain the impact of SVD on cognition than the visible SVD lesions. We have shown that effects beyond the visible SVD lesions seem to differ depending on the SVD lesion type, as these effects were shown to relate to WMHs and lacunes, but not other manifestations of SVD (suggesting different underlying disease mechanisms). The pattern of SVD-related changes in the white matter seems different as compared to what is seen in Alzheimer's disease, suggesting partially different underlying disease mechanisms. The work described in this thesis suggests that the effects of SVD and Alzheimer's disease on brain atrophy are additive, which could be explained by a ceiling effect of both diseases, possibly linked to disease stage. Measuring and reporting more global effects of SVD should become part of clinical care in order to help to explain patients and their caregivers the functional impact of SVD. Understanding which mechanisms underlie effects of SVD beyond the visible lesions should be the focus of future studies, since it is vital to understand the pathophysiology of SVD to help develop new treatments.

NEDERLANDSE SAMENVATTING

Ziekten van de kleine bloedvaten in de hersenen, in het Engels *cerebral small vessel disease* (SVD) genoemd, komen veel voor. SVD is een van de belangrijkste oorzaken van een beroerte, dat wil zeggen een herseninfarct of een hersenbloeding. Daarnaast is SVD óók een belangrijke oorzaak van dementie, waarbij het hogere verstandelijke vermogen (cognitie) achteruit gaat. Ondanks dat SVD veel voorkomt en ernstige gevolgen kan hebben, zijn er tot op heden geen behandelmogelijkheden die specifiek gericht zijn op de ziekteprocessen die de kleine bloedvaten in de hersenen beschadigen.

Met behulp van een MRI-scan kan hersenschade als gevolg van SVD in kaart worden gebracht. Voorbeelden van *zichtbare* schade als gevolg van SVD op een normale hersenscan zijn *witte stof afwijkingen*, kleine infarcten (lacunes) en hele kleine bloedingen (*microbloedingen*). In Figuur 1 zijn voorbeelden van enkele vormen van zichtbare schade weergegeven.

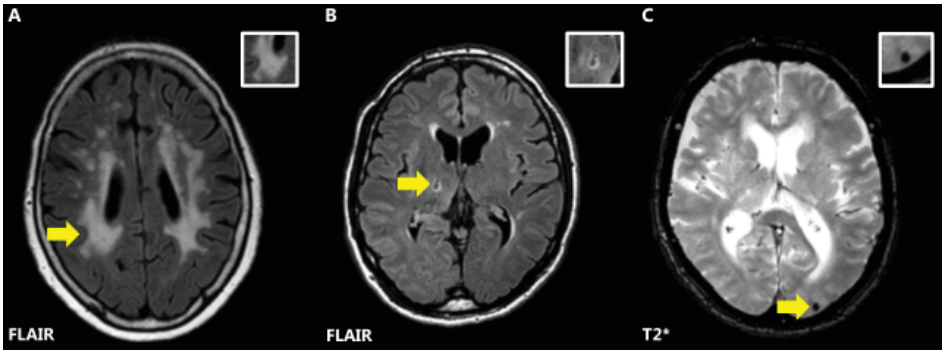

Figuur 1 | Voorbeelden van zichtbare schade ten gevolge van SVD op een normale hersenscan. De gele pijlen geven witte stof afwijkingen (A), kleine infarcten ofwel lacunes (B) en hele kleine bloedingen ofwel microbloedingen (C) aan.

Deze zichtbare afwijkingen kunnen door verschillende ziekteprocessen ontstaan en kunnen op verschillende locaties in de hersenen worden gezien. Zichtbare hersenschade als gevolg van SVD hangt samen met dementie, maar de relatie wisselt per persoon. Het lijkt erop dat SVD meer doet op de hersenen dan wat we met het blote oog kunnen zien op een normale hersenscan. Deze '*onzichtbare*' hersenschade als gevolg van SVD kunnen we meten met geavanceerde technieken. Onzichtbare hersenschade als gevolg van SVD kan zowel in de *grijze stof* als in de *witte stof* van de hersenen optreden. De grijze stof bestaat uit hersencellen die informatie verwerken, terwijl de witte stof bestaat uit vezelbanen die delen van de hersenen met elkaar verbinden en zo voor communicatie tussen de hersencellen zorgen. De witte stof wordt ook wel vaak het '*hersennetwerk*' genoemd. Een voorbeeld

van onzichtbare hersenschade ten gevolge van SVD zijn afwijkingen in de witte stof die gevonden kunnen worden in de directe (op een MRI-scan normaal uitziende) omgeving van witte stof afwijkingen (zogenaamde *perilesionele effecten van SVD*). Een ander voorbeeld is het krimpen van de grijze stof van de buitenste laag van de hersenen (hersenschors) in gebieden die ver weg liggen van een nieuw herseninfarct, waarschijnlijk doordat de verbindingen tussen het infarct en de hersenschors beschadigd raken (zogenaamde *effecten van SVD op afstand*). De gedachte is dat deze schade op afstand waarschijnlijk secundair ontstaat aan de zichtbare hersenschade. Ook kan er meer globale schade, deels onafhankelijk van de zichtbare hersenschade, optreden (zogenaamde *globale effecten van SVD*).

Het detecteren van onzichtbare hersenschade ten gevolge van SVD biedt de mogelijkheid om op een andere manier naar het ziekteproces SVD te kijken. Zo kunnen we de functionele impact van SVD mogelijk beter begrijpen dan op basis van alleen de zichtbare hersenschade. De klachten waarmee patiënten zich presenteren op een geheugenpolikliniek zijn namelijk vaak veel uitgebreider/ernstiger dan op basis van de zichtbare hersenschade op de MRI-scan te verwachten zou zijn.

Er zijn nog wel de nodige vragen die beantwoord moeten worden om de onzichtbare hersenschade als gevolg van SVD beter te begrijpen. Bijvoorbeeld: gaan alle vormen van SVD gepaard met onzichtbare hersenschade (dus zowel witte stof afwijkingen als kleine bloedingen)? Treedt onzichtbare hersenschade ook op bij patiënten met kleine herseninfarcten in de hersenschors (zogenaamde corticale cerebrale micro-infarcten, een relatief recent ontdekte manifestatie van SVD die op een MRI-scan gezien kan worden)? Is er een specifiek patroon van deze onzichtbare hersenschade te herkennen? Is er een wisselwerking met bijkomende ziektes zoals de ziekte van Alzheimer?

Het overkoepelende doel van dit proefschrift was om veranderingen in de grijze en de witte stof van de hersenen die niet op normale hersenscans zichtbaar zijn bij patiënten met SVD te onderzoeken.

In dit proefschrift heb ik twee verschillende technieken gebruikt om veranderingen in de grijze stof en de witte stof van de hersenen zeer gevoelig te meten. Allereerst gebruiken we MRI-scans waarmee met behulp van geautomatiseerde methoden *hersenvolumes* gemeten kunnen worden. Door deze volumes te vergelijken met de totale inhoud van de schedel kan een schatting worden gemaakt in welke mate er sprake is van verlies van hersenweefsel oftewel hersenkrimp ('*hersenatrofie*'). Anderzijds gebruiken we *diffusie tensor imaging* (DTI), een geavanceerde MRI-techniek om schade te meten aan de witte stof verbindingen, ook wel het hersennetwerk genoemd. Hiermee kun je bepalen of er sprake is van een 'gestoorde hersenconnectiviteit'.

De studies in het eerste deel van mijn proefschrift onderzochten enkele technische uitdagingen die komen kijken bij het meten van hersenvolumes en zichtbare hersenschade. In het tweede deel van het proefschrift onderzochten we de relatie tussen zichtbare en onzichtbare hersenschade ten gevolge van SVD en de impact hiervan op het cognitief functioneren. Ook keken we naar de wisselwerking tussen SVD en de ziekte van Alzheimer, aangezien deze ziekten vaak samen voorkomen bij patiënten op een geheugenpolikliniek.

Deel 1: uitdagingen bij het meten van SVD-gerelateerde veranderingen in de hersenen

Er bestaan verschillende technieken om SVD-gerelateerde veranderingen in de hersenen te meten. Dit kan zowel kwalitatief als (semi)kwantitatief. Kwantitatieve technieken maken over het algemeen gebruik van *hersensegmentatie*: het onderverdelen (segmenteren) van een MRI-scan van de hersenen in de verschillende onderdelen van de hersenen (zoals witte stof en grijze stof en witte stof afwijkingen). Er bestaan verschillende automatische methoden om hersenvolumes te meten. Die metingen kunnen beïnvloed worden door verschillende factoren, waaronder de mate van hersenschade, bewegingsartefacten en technische variatie (zoals het gebruik van verschillende MRI-scanners, met een andere magnetische veldsterkte of een ander scanprotocol). Het kunnen omgaan met variatie in technische factoren is erg belangrijk als MRI-data uit meerdere centra worden gecombineerd. Dit is de laatste jaren een trend geworden in verschillende onderzoeksgebieden, waaronder onderzoek naar SVD. In het eerste deel van mijn proefschrift onderzochten we hoe verschillende automatische segmentatiemethoden voor het meten van hersenvolumes en witte stof afwijkingen presteren onder verschillende technische omstandigheden, om zo het combineren van MRI-data uit meerdere centra of van verschillende scanners te ondersteunen.

In **hoofdstuk 2** hebben we de prestatie vergeleken van drie veelgebruikte automatische methoden voor hersensegmentatie (SPM, Freesurfer en FSL). Tien personen van oudere leeftijd, zonder een bekende primaire hersenaandoening, werden op dezelfde dag twee keer gescand: eenmaal met een MRI-scanner met een veldsterkte van 1,5 Tesla en eenmaal met een MRI-scanner met een veldsterkte van 3 Tesla. We gebruikten vervolgens de automatische methoden om de MRI-scans van beide veldsterkten te segmenteren en volumes te meten van de totale schedel, de hersenen als geheel, alsook van onderdelen van de hersenen. Vervolgens keken we hoe robuust de methoden waren, dat wil zeggen of de volumes van dezelfde persoon zoals gemeten door de automatisch methode voor de twee scans hetzelfde waren. We keken daarnaast hoe accuraat de methoden waren, dat wil zeggen of de volumes van dezelfde persoon zoals gemeten door de automatische methode overeenkwamen met de volumes zoals die door een expert waren gedefinieerd door de

MRI-scan met de hand te segmenteren. We vonden in deze studie dat hersenvolumes en schedelvolumes robuust konden worden gemeten ondanks het gebruik van scans vervaardigd op een verschillende veldsterkte, maar er waren aanzienlijke verschillen tussen de methoden afhankelijk van welk deel van de hersenen werd bekeken (bijvoorbeeld totaal hersenvolume of schedelvolume). Hetzelfde vonden we voor de accuratesse. Deze studie geeft inzicht in welke methode het beste gekozen kan worden afhankelijk van welk volume gemeten moet worden bij hersensegmentatie van gecombineerde MRI-data vanuit meerdere centra of van verschillende scanners. Zo kan het beste FSL worden gebruikt als een totaal hersenvolume of schedelvolume moet worden gemeten, terwijl SPM beter kan worden gebruikt als onderscheid moet worden gemaakt tussen grijze stof en witte stof volumes.

In **hoofdstuk 3** hebben we vijf vrij beschikbare en volledig automatische methoden voor segmentatie van witte stof afwijkingen vergeleken (Cascade, kNN-TTP, Lesion-TOADS, LST-LGA en LST-LPA). We gebruikten hiervoor scans van zestig patiënten met witte stof afwijkingen uit de TRACE-VCI studie, een grote multicenter studie bij patiënten met cognitieve klachten en zichtbare schade op de MRI-scan van de hersenen. In deze studie werden zes verschillende MRI-scanners gebruikt. We vergeleken de volumes van de witte stof afwijkingen zoals gemeten door de automatische methoden met de volumes zoals die door een expert waren gedefinieerd door de witte stof afwijkingen met de hand te segmenteren. De methoden werden per scanner en over de gehele groep vergeleken. We zagen dat kNN-TTP het beste presteerde, gevolgd door LST-LPA en LST-LGA en dat Lesion-TOADS en Cascade het slechtst presteerden. Deze studie kan fungeren als een leidraad bij het kiezen van een methode voor automatische segmentatie van witte stof afwijkingen in een gecombineerde dataset van verschillende scanners. Op basis van de resultaten van deze studie besloten we kNN-TTP te gebruiken voor de analyse van onze eigen gecombineerde dataset in de studies in het tweede deel van mijn proefschrift. De studie laat ook zien hoe belangrijk het is om dit soort methoden verder te ontwikkelen en te evalueren hoe consistent ze zijn in gecombineerde datasets.

Deel 2: Onzichtbare hersenschade ten gevolge van SVD

In het tweede deel van mijn proefschrift hebben we gekeken naar de relatie tussen zichtbare en onzichtbare schade in zowel de grijze stof als de witte stof van de hersenen. We keken daarbij naar verschillende vormen van zichtbare schade op een normale hersenscan, zoals witte stofafwijkingen, lacunes en hele kleine bloedingen. Daarnaast gebruikten we geavanceerde technieken om onzichtbare hersenschade, niet met het blote oog op een normale hersenscan te zien, te meten, zoals hersenkrimp of een gestoorde hersenconnectiviteit. Daarnaast onderzochten we de impact op cognitie van zowel zichtbare als onzichtbare

hersenschade als gevolg van SVD, in de vorm van een gestoorde connectiviteit in de witte stof.

Corticale cerebrale micro-infarcten, ofwel hele kleine infarcten in de hersenschors, zijn een relatief nieuwe vorm van zichtbare schade als gevolg van SVD op een normale hersenscan. Het voorkomen van zulke kleine infarcten hangt samen met dementie. Echter, het is nog onduidelijk of al die kleine infarcten samen tot problemen in het hersennetwerk leiden. In **hoofdstuk 4** onderzochten we daarom waar corticale cerebrale micro-infarcten in de hersenen voorkomen en of er een relatie was met een verstoring van het hersennetwerk. We onderzochten dit bij 164 patiënten die zich op een geheugenpolikliniek presenteerden en zichtbare vaatschade hadden op de MRI-scan van de hersenen. We zagen dat meer dan 70% van de micro-infarcten zich bevonden in slechts enkele, meer naar voren gelegen (frontale) hersengebieden. Dit suggereert dat deze gebieden een bepaalde kwetsbaarheid hebben voor het ontstaan van deze kleine infarcten. Hoe en waarom deze kleine infarcten vooral in deze gebieden ontstaan is nog niet duidelijk en zal in de toekomst verder moeten worden onderzocht. We vonden geen verschillen in de connectiviteit in de witte stof tussen patiënten met en zonder corticale cerebrale micro-infarcten, zelfs niet in gebieden waar zich de meeste corticale cerebrale micro-infarcten bevonden. Dus ondanks dat corticale cerebrale micro-infarcten zich lijken te concentreren in hersengebieden die sterk onderling met elkaar verbonden zijn, zijn de witte stof banen die deze verbindingen vormen niet meer aangedaan bij patiënten met corticale cerebrale micro-infarcten dan patiënten zonder deze micro-infarcten. Dit suggereert dat andere mechanismen, zoals lokale verstoringen in de hersenschors, mogelijk een betere verklaring vormen voor de cognitieve klachten die patiënten met corticale cerebrale micro-infarcten hebben dan (onzichtbare) schade aan de witte stof. Het kan, mede gezien de andere resultaten in mijn proefschrift, ook de vraag oproepen of deze kleine infarcten wel een uiting zijn van SVD of juist vaker van andere bijkomende ziekteprocessen en/of risicofactoren.

In **hoofdstuk 5** keken we naar de functionele impact van onzichtbare hersenschade ten gevolge van SVD in de witte stof. We gebruikten een SVD somscore als maat voor de ernst van de zichtbare hersenschade ten gevolge van SVD. Het gebruik van een dergelijke score, waarbij meerdere vormen van zichtbare schade ten gevolge van SVD op een MRI in één maat worden gecombineerd, is een trend geworden in onderzoek naar SVD. Het idee hierachter is dat deze score een breed spectrum van aandoeningen representeert die de kleine bloedvaten in de hersenen aandoen. Daarnaast is zo'n score makkelijk te gebruiken, bijvoorbeeld als een uitkomstmaat in onderzoek bij patiënten. We keken vervolgens naar de relatie tussen de SVD somscore, de connectiviteit in de witte stof, en cognitie bij 173 patiënten die zich presenteerden op een geheugenpolikliniek en waarbij vaatschade

zichtbaar was op de normale MRI-scan van de hersenen. Elke punt toename van de SVD somscore was geassocieerd met afname in de connectiviteit in de witte stof. Een afname in de connectiviteit was weer gerelateerd aan een slechtere cognitie, in het bijzonder op de gebieden 'informatie verwerkingssnelheid' en 'aandacht en executief functioneren'. De verstoorde connectiviteit medieerde zelfs de relatie tussen de SVD somscore en de informatie verwerkingssnelheid, wat betekent dat het effect van de hersenschade bij SVD op cognitie zich manifesteert via verstoringen in het hersennetwerk. Met deze studie tonen we aan dat er een duidelijke relatie is tussen zowel zichtbare en onzichtbare hersenschade als gevolg van SVD en cognitie. Ook laat het zien dat maten van verstoringen van het hersennetwerk gevoelig zijn voor het cumulatieve effect van schade als gevolg van SVD op de connectiviteit van de witte stof. Dit soort maten zou daarom goed gebruikt kunnen worden om de ziekteprogressie van SVD te volgen of als uitkomstmaat in onderzoek naar de behandeling van SVD.

In **hoofdstuk 6** onderzochten we de relatie tussen zichtbare hersenschade en hersenkrimp. We keken daarbij of die relatie anders was voor verschillende vormen van zichtbare schade op een normale hersenscan, zoals witte stof afwijkingen, lacunes en hele kleine bloedingen. Als die relatie verschilt voor verschillende vormen van hersenschade, zou dat kunnen wijzen op andere onderliggende ziekteprocessen. We gebruikten in deze studie 725 patiënten die zich presenteerden op een geheugenpolikliniek en waarbij er zichtbare schade was op de normale hersenscan. We vergeleken totaal hersenvolume, grijze stof volume en witte stof volume tussen patiënten met een bepaalde vorm van zichtbare hersenschade, zoals matig/ernstige witte stof afwijkingen, lacunes en kleine bloedingen, en een referentiegroep met milde witte stof afwijkingen maar geen lacunes of kleine bloedingen. Witte stof afwijkingen en lacunes waren gerelateerd aan hersenkrimp, in het bijzonder van de grijze stof. Voor witte stof afwijkingen werd de meest uitgesproken krimp gezien in de hersenschors van meer naar voren gelegen (frontale) hersengebieden. Daarmee suggereert deze studie dat krimp van de hersenschors mogelijk ontstaat doordat witte stof banen die naar de (frontale) hersengebieden lopen beschadigd raken. Dit wordt ook wel secundaire degeneratie genoemd, in tegenstelling tot primaire degeneratie van de hersenschors zoals bij de ziekte van Alzheimer, waarbij de schade direct in de hersenschors optreedt. Hersenkrimp wordt nu nog vaak gezien als een manifestatie van een neurodegeneratieve ziekte zoals de ziekte van Alzheimer. Als hersenkrimp inderdaad ook secundair kan zijn aan (manifestaties van) SVD, biedt dit mogelijkheden om hersenkrimp te gebruiken om de ziekteprogressie van SVD te volgen of als uitkomstmaat in onderzoek naar de behandeling van SVD.

De wisselwerking tussen SVD en de ziekte van Alzheimer

Bij het onderzoeken van SVD-gerelateerde veranderingen in de hersenen is het belangrijk om andere ziekteprocessen die tot soortgelijke veranderingen kunnen leiden in ogenschouw te nemen, zoals de ziekte van Alzheimer. SVD en de ziekte van Alzheimer komen vaak samen voor bij patiënten die zich presenteren op een geheugenpolikliniek. Dat was ook zo in de patiënten die meededen aan ons onderzoek. Daarom hebben we in het tweede deel van mijn proefschrift ook gekeken naar de wisselwerking tussen SVD en de ziekte van Alzheimer als het gaat om veranderingen in de grijze stof en de witte stof die niet met het blote oog zichtbaar zijn.

In **hoofdstuk 6** keken we ook hoe de relatie tussen zichtbare hersenschade als gevolg van SVD en hersenkrimp beïnvloed werd door bijkomende ziekte van Alzheimer. We zagen vooral een relatie tussen zichtbare vaatschade als gevolg van SVD en hersenkrimp bij patiënten zonder bijkomende ziekte van Alzheimer. Andersom was de relatie tussen de ziekte van Alzheimer en hersenkrimp veel sterker bij patiënten die weinig zichtbare schade ten gevolge van SVD op de normale hersenscan hadden. Blijkbaar dragen beide ziekten bij aan hersenkrimp, maar voor zowel SVD als de ziekte van Alzheimer is dit het meest uitgesproken in de afwezigheid van de ander. Dit kan wellicht verklaard worden doordat er een bepaald plafond zit aan de mate van hersenkrimp die kan optreden, waarbij de bijdrage van eventueel bijkomende ziekteprocessen beperkt is als deze limiet reeds is overschreden. Mogelijk is dit ook gerelateerd aan het stadium van ziekte waarin een patiënt zich bevindt. Al met al laat deze studie zien hoe belangrijk het is om aanwezigheid van andere ziekteprocessen, zoals de ziekte van Alzheimer, te meten en zo nodig hiervoor te corrigeren als SVD-gerelateerde veranderingen in de hersenen worden onderzocht.

Omdat SVD en de ziekte van Alzheimer vaak samen voorkomen en kunnen leiden tot soortgelijke veranderingen in de hersenen, is het lastig te onderzoeken welke veranderingen in de hersenen daadwerkelijk het gevolg zijn van SVD en welke door bijkomende ziekteprocessen, zoals de ziekte van Alzheimer. Daarom kozen we in **hoofdstuk 7** voor een andere aanpak. We wilden de homogeniteit van onze groep patiënten vergroten door alleen te kijken naar patiënten met ofwel de ziekte van Alzheimer ofwel SVD. We vergeleken de connectiviteit in de witte stof tussen patiënten met de ziekte van Alzheimer, patiënten met SVD en gezonde controles. Ten opzichte van gezonde controles hadden patiënten met SVD afwijkende witte stof connectiviteit in de meer naar voren gelegen (frontale) hersengebieden. Daarentegen hadden patiënten met de ziekte van Alzheimer een abnormale witte stof connectiviteit ten opzichte van de gezonde controles in de centrale en meer naar achter gelegen (pariëto-occipitale) hersengebieden. We vonden ook dat zowel bij patiënten met SVD als bij patiënten met de ziekte van Alzheimer relatief langere

witte stof banen en witte stof banen die onderdeel uitmaken van de kern van het hersennetwerk, zogenaamde knooppunten of 'hubs', ernstiger waren aangedaan dan alle andere witte stof banen. Deze bevindingen suggereren dat SVD en de ziekte van Alzheimer deels via andere mechanismen de witte stof beschadigen. Welke mechanismen dat zijn en hoe deze invloed hebben op elkaar moet in toekomstige studies verder onderzocht worden. Dit is belangrijk omdat een beter begrip van deze mechanismen uiteindelijk kan helpen in het ontwikkelen van nieuwe behandelingen voor SVD.

Conclusie

In dit proefschrift hebben we laten zien dat patiënten met SVD meer hersenschade hebben dan in eerste instantie zichtbaar is op een normale MRI-scan, namelijk hersenkrimp en een verstoring van het hersennetwerk. Deze 'onzichtbare' schade kan de impact die SVD heeft op het functioneren van patiënten beter verklaren dan alleen de zichtbare schade. Het nauwkeurig meten en rapporteren van de totale hoeveelheid hersenschade ten gevolge van SVD kan van toegevoegde waarde zijn op een geheugenpolikliniek, omdat het patiënten en hun omgeving kan helpen om beter te begrijpen wat voor impact SVD heeft op hun functioneren. Dit geldt zeker wanneer een normale hersenscan weinig tot geen zichtbare schade laat zien en er twijfel kan bestaan over de mogelijke oorzaken van de klachten. Welke ziekteprocessen precies leiden tot zowel zichtbare als onzichtbare hersenschade ten gevolge van SVD moet verder onderzocht worden. Als we namelijk beter begrijpen hoe SVD ontstaat, kan dit uiteindelijk leiden tot de ontwikkeling van nieuwe behandeling.

ABOUT THE AUTHOR

Rutger Heinen was born on the 29th of August, 1988 in Hilvarenbeek, the Netherlands. In 2006, he graduated from secondary school (VWO) with honors at the Sint Odulphus Lyceum in Tilburg. He started his medical training at the University of Utrecht in 2006. Between 2008 and 2009 he took place in the study association board MSFU "Sams" of the Faculty of Medicine at the University of Utrecht, where he led the student book sales and created a new accountancy. In 2009 he started his first scientific research on 'Symptomatic Carotid Occlusion' at the department of neurology of the University Medical Center Utrecht. In the final year of his medical training, after doing his clinical rotation in neurology at the University Medical Center Utrecht, his interest for cognitive disorders and in particular cerebral small vessel disease and Alzheimer's disease grew, and he decided to switch his research focus towards advanced structural brain imaging in memory clinic patients. In that same year, he also did an educational internship at the Faculty of Medicine at the University of Utrecht. After obtaining his medical degree in 2013, graduating with honors, he started his neurology residency program at the University Medical Center Utrecht under supervision of prof. dr. J.H.J. Wokke, dr. T. Seute and prof. dr. G.J. Biessels, which he plans to complete in 2022. In 2014, he started his PhD on effects of cerebral small vessel disease beyond visible lesions in memory clinic patients under supervision of prof. dr. G.J. Biessels (promotor), dr. Y.D. Reijmer and dr. J.H.J.M. de Bresser (co-promotors). 2019 marked a special year as he moved to 's-Hertogenbosch and married Lieke Savelkouls-Heinen in Italy.

PUBLICATIONS

* These authors contributed equally to this work.

Included in this thesis

Heinen R, Bouvy WH, Mendrik AM, Viergever MA, Biessels GJ, de Bresser J. Robustness of Automated Methods for Brain Volume Measurements across Different MRI Field Strengths. PLoS One. 2016;11:e0165719.

Ferro D*, **Heinen R***, de Brito Robalo B, Kuijf HJ, Biessels GJ, Reijmer Y. Cortical microinfarcts and white matter connectivity in memory clinic patients. Front Neurol. 2019;10:571.

Heinen R*, Vlegels N*, de Bresser J, Leemans A, Biessels GJ, Reijmer Y. The cumulative effect of small vessel disease lesions is reflected in structural brain networks of memory clinic patients. Neuroimage Clin. 2018;19:963–9.

Not included in this thesis

Jolink WM, **Heinen R**, Persoon S, van der Zwan A, Kappelle LJ, Klijn CJ. Transcranial Doppler CO2-reactivity does not predict recurrent ischemic stroke in patients with symptomatic carotid artery occlusion. Cerebrovasc Dis. 2014;37:30–7.

Boomsma JMF, Exalto LG, Barkhof F, van den Berg E, de Bresser J, **Heinen R**, et al. Vascular Cognitive Impairment in a Memory Clinic Population: Rationale and Design of the "Utrecht-Amsterdam Clinical Features and Prognosis in Vascular Cognitive Impairment" (TRACE-VCI) Study. JMIR Res Protoc. 2017;6:e60.

Verwer JH, Biessels GJ, **Heinen R**, Exalto LG, Emmelot-Vonk MH, Koek HL; Utrecht Vascular Cognitive Impairment (VCI) study group. Occurrence of Impaired Physical Performance in Memory Clinic Patients With Cerebral Small Vessel Disease. Alzheimer Dis Assoc Disord. 2018;32:214–19.

Van der Stigchel S, de Bresser J, **Heinen R**, Koek HL, Reijmer YD, Biessels GJ, et al. Parietal involvement in constructional apraxia as measured using the pentagon copying task. Dement Geriatr Cogn Disord. 2018;46:50–9.

Reijmer YD, van den Heerik MS, **Heinen R**, Leemans A, Hendrikse J, de Vis JB, et al. Microstructural white matter abnormalities and cognitive impairment after aneurysmal subarachnoid hemorrhage. Stroke. 2018;49:2040–5.

Groeneveld O, Reijmer Y, **Heinen R**, Kuijf H, Koekkoek P, Janssen J, et al. Brain imaging correlates of mild cognitive impairment and early dementia in patients with type 2 diabetes. Nutr Metab Cardiovasc Dis. 2018;28:1253–60.

Groeneveld ON, Moneti C, **Heinen R**, de Bresser J, Kuijf HJ, Exalto LG, et al. The clinical phenotype of vascular cognitive impairment in patients with type 2 diabetes mellitus. Journal of Alzheimer's Disease. 2019;68:311–22.

Boomsma JMF, Exalto LG, Barkhof F, van den Berg E, de Bresser J, **Heinen R**, et al. How do different forms of vascular brain injury relate to cognition in a memory clinic population: the TRACE-VCI study. J Alzheimers Dis. 2019;68:1273–86.

Kuijf HJ, Biesbroek JM, de Bresser J, **Heinen R**, Andermatt S, Bento M, et al. Standardized assessment of automatic segmentation of white matter hyperintensities; results of the WMH segmentation challenge. IEEE Trans Med Imaging. 2019;2905770.

Submitted /in revision

Heinen R, Steenwijk MD, Barkhof F, Biesbroek JM, van der Flier WM, Kuijf HJ, et al. Performance of five automated white matter hyperintensity segmentation methods in a multicenter dataset. *In revision*.

Heinen R, Groeneveld ON, Barkhof F, de Bresser J, Exalto LG, Kuijf HJ, et al. Amyloid status modifies the relation between small vessel disease lesion type and brain atrophy. *Submitted*.

Heinen R, de Brito Robalo BM, Koek HL, Vlegels N, de Wilde A, Biessels GJ, et al. Pattern of impaired white matter connectivity in Alzheimer's disease versus small vessel disease. *Submitted*.

DANKWOORD

Er is maar één woord dat in mij opkomt als ik denk aan de afgelopen vijf jaar: perseverance. Zonder zwaarmoedig te willen klinken denk ik dat veel promovendi (en inmiddels ook de mensen in mijn directe omgeving) direct begrijpen wat ik daarmee bedoel. Hoewel onderzoek nooit af is, markeert dit proefschrift wel degelijk een einde van een bijzonder traject. In de laatste fase van mijn promotie heb ik daarom vaak gedacht aan de volgende uitspraak:

> "*Every day you may make progress. Every step may be fruitful. Yet there will stretch out before you an ever-lengthening, ever-ascending, ever-improving path. You know you will never get to the end of the journey. But this, so far from discouraging, only adds to the joy and glory of the climb.*" (Winston S. Churchill)

Ik wil iedereen ontzettend bedanken die mij heeft vergezeld tijdens deze klim en die heeft bijgedragen bij het tot stand komen van dit proefschrift. Hieronder richt ik me tot een aantal mensen in het bijzonder.

Allereerst, prof. dr. Biessels, beste **Geert Jan**, bedankt voor jouw tomeloze inzet en begeleiding. Je beloofde me monnikenwerk toen we voor het eerst spraken over dit project, maar eenzaam (het woord monnik komt van het Griekse 'monos') heb ik me tijdens dit project nooit gevoeld. Altijd was je bereid me te helpen en net wanneer ik dacht dat er geen oplossing voor een probleem kon worden gevonden, verraste je me met een nieuw inzicht. Ik bewonder de manier waarop jij tot de essentie van iets kan doordringen, zowel binnen de wetenschap als in de dagelijkse patiëntenzorg. Ik hoop de komende jaren daar nog veel van te mogen blijven opsteken.

Dr. Reijmer, beste **Yael**, ik weet nog goed dat jouw promotie de eerste was die ik ooit meemaakte. Als jonge wetenschapsstudent was ik toen al onder de indruk van jouw manier van werken. Wat ik altijd bijzonder heb gewaardeerd aan jou is dat je mensen vanuit hun eigen waarden benaderd. Ik was dan ook maar wat blij dat je periode in Boston niet het einde betekende van onze samenwerking. Maar boven alles heb ik respect voor het pad wat jij uiteindelijk hebt gekozen en de manier waarop je mij daarin betrok. Ik wens je het allerbeste in de nieuwe uitdagingen die je gaat opzoeken.

Dr. De Bresser, beste **Jeroen**, jij wakkerde mijn fascinatie voor techniek, waarvan ik had gedacht dat die naar de achtergrond was verdwenen toen ik geneeskunde ging studeren, vanaf het eerste moment aan. Mede daardoor is dit proefschrift geworden wat het nu is. Ons eerste gezamenlijke artikel, hoe lang het ook leek te duren voordat het klaar was, werd geroemd op internationale congressen en wordt nog altijd frequent aangehaald door andere studies. Ik waardeer jouw precisie, in je manier van werken, schrijven en het aanpakken van

problemen. Leiden heeft het maar getroffen met je. Ik blijf in ieder geval met belangstelling jouw stappen binnen de neuroradiologie en de onderzoekswereld volgen.

Alle collega's van de VCI onderzoeksgroep, zowel in Utrecht als daarbuiten, ontzettend bedankt voor al die koffiemomenten, lunches, barbecues, bowlavonden, borrels en congressen. **Jurre** en **Onno**, zonder jullie was geen enkel van de studies in dit boekje afgekomen. Ik ga jullie droge humor en gesprekken over gitaren (inclusief pingelgeluiden) missen. **Willem**, in mijn eerste jaar fungeerde jij als mijn mentor en vooral de karaoke-avond in Tokyo ga ik nooit vergeten. **Matthijs**, je bent een gewaardeerde collega zowel binnen het onderzoek, de neurologie als erbuiten. Ik was vereerd om paranimf te zijn bij jouw promotie. **Doeschka** en **Sanne**, toen ik voor de derde keer moest verhuizen van plek in vier jaar tijd was ik er wel klaar mee, maar wat was het fijn die laatste maanden weggestopt bij de Psychiatrie in de VCI psycho room. Ik hoop dat iemand anders tegenwoordig de hitjes op vrijdagmiddag verzorgt. **Naomi**, ik heb er echt mijn best voor gedaan zo lang mogelijk geen student te begeleiden omdat ik een student een mooi project wilde geven en geen 'onzinklusjes'. Nu weet ik niet waar al die uren Freesurfer segmentaties bijwerken precies onder vallen, maar ik heb genoten van onze samenwerking. **Angela**, ik kan met niemand (behalve misschien met mijn vrouw) zo goed praten over eten als met jou. Ik zal zorgen dat ik je op de hoogte houd van mijn culinaire avonturen en geplande trips naar Italië, als jij belooft hetzelfde te blijven doen. **Hilde**, **Chloë**, **Manja**, **Bruno** (sorry this is all in Dutch), **Nick**, **Hugo** en **Hugo**, **Laurien** en **Lieza**, ik heb genoten van onze samenwerking en het vele lachen.

Alle collega's van de neurologie in het UMC Utrecht, en in het bijzonder de arts-assistenten. Hoe wij het toch allemaal voor elkaar krijgen om negen jaar (opleiding + promotie) rond te blijven lopen in hetzelfde ziekenhuis is me soms een raadsel, tot ik weer eens een tweede vrijdag van de maand borrel of assistentenweekend bezoek. Ik kijk ernaar uit nog twee jaar met jullie door te brengen en hoop nog velen van jullie te overtuigen dat tequila op de Biemond over tien jaar nog steeds een goed idee is.

Lieve vrienden, wat fijn dat ik jullie daartoe mag rekenen. **Jodine**, **Barbara**, **Rosalie**, **Renée** en **Wilmar**, wij hebben een unieke vriendschap. Ieder van ons heeft zijn uitdagingen gehad de afgelopen jaren en de steun die onze groep elkaar daarbij geeft is ontroerend. De avondjes en weekenden zijn wellicht schaarser geworden, maar als we elkaar zien (gelukkig ook met kouwe kant tegenwoordig) is het als vanouds. Viva la vida! **Maarten**, jij was de eerste vriend en daarmee de oudste vriend die ik in Utrecht heb leren kennen. Zonder jou was ik nooit actief geworden binnen de studievereniging en had ik talloze vriendschappen niet gehad. Ook andere vrienden van de studie kan ik niet genoeg bedanken voor de gezelligheid de afgelopen jaren. **Rob**, **Thomas**, **Wouter**, Bazige Bourgondiërs, laten we vooral heerlijke avondjes blijven plannen.

Mijn dierbare vriend en paranimf **Wouter**. Misschien was je enigszins verrast dat ik je vroeg voor deze functie, maar voor mij was het vanaf de eerste minuut duidelijk. De vele gesprekken die wij door de jaren heen voerden over onderzoek doen, en het enthousiasme waarmee jij over onderzoek bleef praten (zelfs als ik net een uur had geklaagd over mijn onderzoek), hebben in belangrijke mate bijgedragen aan de voltooiing van dit proefschrift. Ik vind het onwijs knap dat je ervoor hebt gekozen je hart te volgen en je witte jas aan de wilgen hebt gehangen. Je bent de beste onderzoeker die ik ken en een goede vriend.

My brother from another mother, beste vriend, getuige en paranimf **Wilmar**. Ik weet nog goed dat we na ons bestuursjaar besloten onderzoek te gaan doen bij de neurologie in het UMC Utrecht. Die beslissing heeft me, mede dankzij jou, gebracht tot waar ik nu ben. Ik weet dat ik tegenwoordig niet meer om de hoek woon, maar ik hoop je in de komende twee jaar alsnog te overtuigen om af te zakken naar de mooiste stad van het land. En zo niet, dan weet ik dat ik altijd op onze vriendschap kan blijven rekenen. We gaan ze, als jij straks ook je proefschrift hebt afgerond, eens laten zien hoe je een feestje viert.

Mijn familie, in het bijzonder mijn moeder **Els** en twee zussen **Eefje** en **Wieske**. Ik had graag ook mijn vader in dit rijtje genoemd. Ik ben ontzettend trots dat ik straks dezelfde titel mag dragen als mijn vader ooit deed. Ik kan me weinig meer herinneren van zijn promotie, maar ik weet wel hoe trots hij was toen ik vertelde dat ik ook aan een promotietraject ging beginnen. Zijn overlijden was het zwaarste punt in mijn promotietraject. Jullie steun en liefde hebben mij gebracht tot de dag van vandaag. Ik ben jullie daarvoor eeuwig dankbaar en ontzettend trots op eenieder van jullie.

Tot slot, **Lieke**, mijn alles. Wat kan ik nog tegen je zeggen wat ik niet al heb gezegd op die prachtige heuvel op een zonovergoten namiddag in Gambassi Terme. Laat me een poging wagen. Ik had zonder jou nooit het doorzettingsvermogen gevonden om dit proefschrift te voltooien. Jij bent er altijd voor me geweest en je haalt het beste in mij naar boven. Het maakte niet uit of het ging om een teleurstellend resultaat (soms voor mijn gevoel elke dag), een afwijzingsmail van een tijdschrift na een half jaar wachten (wat niet één maar twee keer gebeurde) of het doorvoeren van wijzigingen in een artikel (vooral als het ging om versie nummer twintig). Ook al kon mijn stemming soms slechter zijn dan na het verlies van PSV, jij luisterde geduldig en zette me weer op het juiste pad als ik dreigde af te dwalen. Onze culinaire avondjes (binnens- of buitenshuis), onze reizen (eigenlijk altijd naar Italië) en zo veel andere mooie momenten deden mij altijd weer beseffen dat ik moest genieten van de reis in plaats van me druk te maken over waar die heen ging. Dat ik die reis samen met jou mag maken is het beste wat mij ooit is overkomen.

UMC Utrecht

Universiteit Utrecht

ISBN 978-90-393-7191-6